



Durham E-Theses

An esca investigation of low energy electron beam modification and formation of polymers

Brennan, William James

How to cite:

Brennan, William James (1984) *An esca investigation of low energy electron beam modification and formation of polymers*, Durham theses, Durham University. Available at Durham E-Theses Online: <http://etheses.dur.ac.uk/7203/>

Use policy

The full-text may be used and/or reproduced, and given to third parties in any format or medium, without prior permission or charge, for personal research or study, educational, or not-for-profit purposes provided that:

- a full bibliographic reference is made to the original source
- a [link](#) is made to the metadata record in Durham E-Theses
- the full-text is not changed in any way

The full-text must not be sold in any format or medium without the formal permission of the copyright holders.

Please consult the [full Durham E-Theses policy](#) for further details.

AN ESCA INVESTIGATION OF
LOW ENERGY ELECTRON BEAM MODIFICATION
AND FORMATION OF POLYMERS

by

The copyright of this thesis rests with the author.
No quotation from it should be published without
his prior written consent and information derived
from it should be acknowledged.

William James Brennan, B.Sc. (Hons.)
(Dunelm)

A Candidate for the Degree of Doctor of Philosophy

Hatfield College,
University of Durham

January 1984



13. APR. 1984

To
My Parents
and
Barbara

AN ESCA INVESTIGATION OF LOW ENERGY ELECTRON BEAM MODIFICATION AND
FORMATION OF POLYMERS

by
WILLIAM JAMES BRENNAN

ABSTRACT

Physical and chemical aspects of the interaction of low energy electrons with organic polymers and polymer precursors have been investigated using X-ray photoelectron spectroscopy (XPS or ESCA).

Electron mean free paths have been determined over a substantial kinetic energy range using $TiK\alpha$ and $CuL\alpha$ excitation sources employing the substrate overlayer technique for poly(paraxylylene) films on gold substrates. The ability of the Ti source to probe deep lying core levels in conjunction with the use of a $CuL\alpha$ source enabled a square root dependence of mean free path on kinetic energy to be formulated over the energy range 0.5→4.4 keV such that at 4.4 keV mean free path is $\sim 40\text{\AA}$.

In view of technological interest in the radiation modification of polymers the interaction of low energy electron beams with fluoropolymers, specifically PTFE and PVF_2 , has been investigated. In both cases defluorination of the surface regions has been shown to take place which increases with radiation dose and dose rate leading to the formation of an unsaturated carbonaceous network. The reaction is, however, independent of electron beam energy.

In the initial states of irradiation inhomogeneities in the surface region occur in the case of PTFE but not PVF_2 , but the depth of modification in both cases being beyond the ESCA sampling depth using $MgK\alpha$ radiation.

The irradiation of condensed fluorobenzenes results in the formation of films of involatile polymeric material whose composition is a function of starting material and shows greater defluorination with applied dose. Under controlled conditions the films closely resemble those obtained by plasma polymerisation illustrating the similarity in electron beam and plasma processes.

As an extension to this idea MNDO-SCF-MO calculations have been carried out on the structural isomers of the perfluorodiazabenzene in an attempt to interpret previous experimental observations relating to their plasma polymerisation, which may also be relevant to their electron beam polymerisation.

MEMORANDUM

The work described in this thesis was carried out at the University of Durham between October 1980 and November 1983. It has not been submitted for any other degree and is the original work of the author except where acknowledged by reference.

Part of the work in this thesis has formed the subject matter of the following publications:

- (i) Electron Mean Free Paths as a Function of Genetic Energy, a Substrate Overlayer Investigation of Polyparaxylylene Films on Gold using a $TiK\alpha$ X-ray Source.

D.T. Clark, M.M. Abu-Shbak and W.J. Brennan,
J. Electron Spectrosc., Rel Phenom, 28, 11 (1982).

- (ii) An MNDO SCF MO Investigation of some Structural Isomers of the Perfluoro Diazines (Pyrimidine, Pyrazine and Pyridazine) of Relevance to their Plasma Polymerisation.

D.T. Clark, S.A. Johnson and W.J. Brennan,
submitted to J. Polym. Sci., Polym. Chem.

ACKNOWLEDGEMENTS

I would like to express my thanks to the many people from whom I have gained assistance during the course of this research. Firstly, I would like to thank my supervisor, Professor Dave Clark for his help, guidance, encouragement and patience over the past three and a half years.

I would also like to thank my colleagues for their comradeship, help and laughing at my dreadful jokes, *viz.* Mohammed Abu-Shbak, Rob Allaker, Jeff Eaves, Andy Fowler, Alan Harrison, Dick Hutton, Steve Johnson, Hugh Munro, Pete Stephenson, Rosemary Wilson and Zaki.

Thanks are also due to the technical back-up received from Jim Coulson and George Rowe, and assistance in computing from Bob Sheehan at Numac and Lascelles Williams at UMRCC.

I am indebted to the SERC for the provision of a research studentship and equipment and to Mullard Southampton for their help towards the completion of this work.

Finally, great thanks go to Mrs. Marion Wilson for her great secretarial skill and even greater patience in typing this manuscript.

CONTENTS

	<u>Page No.</u>
CHAPTER ONE -	
ELECTRON SPECTROSCOPY FOR CHEMICAL APPLICATIONS (ESCA)	1
1.1 Introduction	2
1.2 Processes involved in ESCA	3
1.2.1 Photoionisation	3
1.2.2 Processes accompanying photoionisation	6
(i) Relaxation	6
(ii) Shake-up and Shake-off processes	8
1.2.3 De-excitation processes	11
1.2.4 Energy loss processes	14
1.3 Features of ESCA Spectra	14
1.3.1 Binding Energies	14
1.3.2 Chemical shifts	17
1.3.3 Fine structure	20
(i) Spin orbit splitting	21
(ii) Electrostatic splitting	21
(iii) Multiplet splitting	22
1.3.4 Signal intensities	23
(i) Fixed angle studies	23
(ii) Angular dependence and depth profiling	29
1.3.5 Line widths	31
1.3.6 Line shape analysis	32
1.3.7 Sample charging	33
1.4 ESCA Instrumentation	36
1.4.1 Components of the ES300 used in this thesis	37
(i) Sample analysis chamber	38
(ii) Sample preparation chamber	38
1.4.2 X-ray sources	39
1.4.3 Electron energy analyser	41
1.4.4 Electron detection and data acquisition	42
1.5 Sample Handling	43
1.5.1 Solids	43
1.5.2 Liquids	44
1.5.3 Gases	45
1.6 General Aspects of ESCA	45

CHAPTER TWO -

FUNDAMENTAL ASPECTS OF ELECTRON BEAM IRRADIATION	49
2.1 Introduction	50
2.2 Fundamental Aspects of Low Energy Electron Beam Interactions with Molecules and Solids	51
2.2.1 Characteristic structure of an electron energy distribution	51
(i) Plasmon loss peaks	53
(ii) Ionisation losses	54
(iii) Auger electrons	55
(iv) 'True' secondary electrons	61
2.2.2 Electronic processes occurring in electron bombardment	64
(i) Introduction	64
(ii) Ionisation by electron impact	65
(iii) Excitation by electrons	67
(iv) Electron attachment	70
2.2.3 Primary damage processes resulting from excitation, ionisation and electron attachment	72
(i) Electron stimulated desorption (ESD)	72
(ii) Electron stimulated adsorption (ESA)	75
(iii) Beam effects observed in Auger electron spectroscopy	75
2.3 Pathlengths of Electrons	77
2.4 Electron Interactions with Polymers	79
2.4.1 Introduction	79
2.4.2 Chemical changes due to high energy irradiation of polymers	80
2.4.3 Crosslinking	82
2.4.4 Degradation by main chain scission	84
2.4.5 Unsaturation formation and decay	86
2.4.6 Low energy electron irradiation of polymers	87

CHAPTER THREE -

ELECTRON MEAN FREE PATHS AS A FUNCTION OF KINETIC ENERGY: A SUBSTRATE OVERLAYER INVESTIGATION USING A $TiK\alpha_{1,2}$ X-RAY SOURCE	88
3.1 Introduction	89
3.2 Experimental	93

	<u>Page No.</u>
3.3 Results and Discussion	98
3.3.1 Introduction	98
3.3.2 Evaluation of mean free paths	102
(i) TiK α excited Au4f (KE 4430)	103
(ii) Au4d levels	105
(iii) Au4p ^{3/2}	106
(iv) Au3d levels	107
(v) Au3p ^{3/2}	109
(vi) Cu L α excited Au4f and Au4d levels	111
3.3.3 A brief note on photoionisation cross sections with the Ti anode	114
3.3.4 The dependence of electron mean free paths on KE	116
Conclusions	121
CHAPTER FOUR -	
THE ELECTRON BEAM BOMBARDMENT OF FLUOROPOLYMER SURFACES	122
4.1 Introduction	123
4.2 Experimental	124
4.2.1 Electron source	124
4.2.2 Samples	129
4.2.3 ESCA Instrumentation	130
4.2.4 Experimental procedure	131
4.3 Results and Discussion	133
4.3.1 Electron beam effects on PTFE	133
(i) Preliminary observations	133
(ii) Electron beam damage as a function of dose rate and the abstraction of kinetic data	152
(iii) Energy dependence of beam damage in PTFE	165
4.3.2 Electron beam bombardment of PVF ₂	167
(i) Preliminary observations	167
(ii) Electron energy and dose rate dependence of damage in PVF ₂	173
4.3.3 Mechanistic aspects of electron beam degradation of PVF ₂ and PTFE	178

CHAPTER FIVE -

AN ESCA INVESTIGATION OF THE LOW ENERGY ELECTRON
BEAM POLYMERISATION OF THE FLUOROBENZENES 185

5.1 Introduction 186

5.1.1 Previous studies of polymers produced by
low energy electron beams 187

5.2 Experimental 193

5.3 Results and Discussion 197

5.3.1 Electron beam polymer composition and gross
chemical structure as a function of
starting material 197

(a) Hexafluorobenzene 197

(b) Pentafluorobenzene 204

(c) Tetrafluorobenzene 208

(d) Trifluorobenzene 210

(e) Difluorobenzene 212

(f) Monofluorobenzene 214

(g) Overall comparison of polymers produced 216

5.3.2 The effect of bombardment time on final
polymer structure 220

CHAPTER SIX - AN MNDO SCF MO INVESTIGATION OF SOME
STRUCTURAL ISOMERS OF THE PERFLUORO
DIAZINES (PYRIMIDINE, PYRAZINE AND PYRID-
AZINE) OF RELEVANCE TO THEIR PLASMA
POLYMERISATION 231

6.1 Introduction 232

6.2 Computational Details 234

6.3 Results and Discussion 236

6.3.1 Ground states 236

(i) Parent perfluoro heteroaromatics 236

(ii) Diazafulvenes 237

(iii) Diazadienynes 237

(iv) Diaza Dewar benzenes 239

(v) Diazabenzvalenes 240

(vi) Diazaprismanes 241

(vii) Summary 241

Page No.

6.3	Results and Discussion (contd.)	
6.3.2	Excited states	242
	(i) Cations	242
	(ii) Singlet and triplet states	244
6.3.3	Application to plasma polymerisation of these compounds	246
	(i) Interconversion of parent isomers	247
	(ii) Polymerisation	250
	(iii) Elimination	251
	APPENDIX ONE - PLATES SHOWING THE ES300 SPECTROMETER	253
	APPENDIX TWO - RESEARCH COLLOQUIA, SEMINARS, LECTURES AND CONFERENCES	258
	REFERENCES	261

CHAPTER ONE

ELECTRON SPECTROSCOPY FOR
CHEMICAL APPLICATIONS (ESCA)



1.1 Introduction

The ESCA experiment involves the measurement of the electron number distribution with kinetic energy of photoelectrons emitted from the sample (solid, liquid or gas) by irradiation with a beam of nearly monoenergetic soft X-rays. Development of the technique has taken place over the past three decades to an extent where it is routinely employed in studies of structure, bonding and reactivity in the fields of organic, inorganic and physical chemistry.¹

The photoelectric effect was discovered by Hertz in 1887² by observing that an electric discharge occurred more readily between two electrodes when the cathode was exposed to ultraviolet light. The results of subsequent experiments³⁻⁶ led to Einstein's formulation of the photoelectric effect in terms of photons.⁷ X-ray induced photoelectron emission from a variety of materials was investigated by Robinson,⁸ de Broglie⁹ and others¹⁰ until the early 1930s. Although the measurement of binding energies was possible from these studies, the severe experimental difficulties concerning electron detection and energy resolution concealed the potential of electron spectroscopy.

Significant progress in the technique, however, was made during the 1950s and 1960s, mainly as a result of the pioneering work by Siegbahn and co-workers at Uppsala University. With a background experience in nuclear spectroscopy this group developed an iron-free magnetic double focussing electron analyser capable of resolution of a few parts in 10^4 over a wide energy range up to several hundred keV, but suitable for electrons in the keV range. Using a $\text{CuK}\alpha$ X-ray source

($h\nu = 8048.04$ eV) the Uppsala group found that sharp, essentially symmetric photoelectron lines could be resolved from the edge of the electron continuum. The observed lines are due to electrons which have not undergone any energy loss and are therefore related to the binding energy of the atomic level from which photoemission has occurred. The observation that core electron binding energies exhibited chemically-induced shifts by Siegbahn,^{12,13,14} allied with the earlier observation by Steinhardt^{15,16} and co-workers that core photoelectron peak intensities could be used for analysis clearly demonstrated the utility of the technique. Much of the early work by the Uppsala group was extensively documented in 1968 in "ESCA, Atomic, Molecular and Solid State Structure Studied by means of Electron Spectroscopy",¹⁷ and in 1969 in "ESCA Applied to Free Molecules".¹⁸ An historical account of the work at Uppsala was given by Siegbahn in his Nobel lecture,¹⁹ and the development of ESCA prior to Siegbahn can be found in the comprehensive reviews by Jenkin *et al.*²⁰

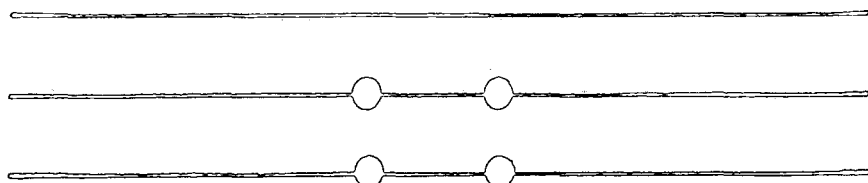
ESCA is also widely known as X-ray Photoelectron Spectroscopy (XPS). The technique has also been known by the terms High Energy Photoelectron Spectroscopy (HEPS), Induced Electron Emission Spectroscopy (IEES) and Photoelectron Spectroscopy of the Inner Shell (PESIS) although these are not in common usage.

1.2 Processes involved in ESCA

1.2.1 Photoionisation

Irradiation of atoms, in either molecules or a lattice, by soft X-rays causes the photoejection of electrons

Valence
Orbitals



Core
Orbitals

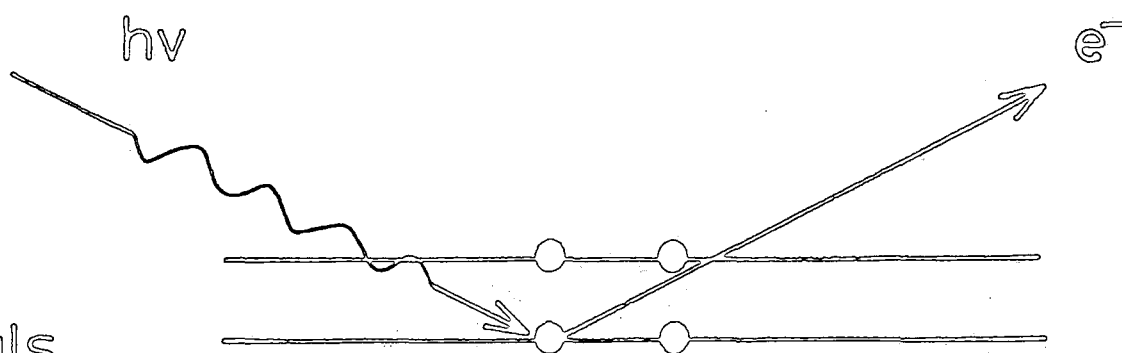


Figure 1.1 Schematic of photoionisation

with specific energies¹⁷ as shown schematically in Figure 1.1. The ejected electrons may originate from either the core or valence levels, however, with soft X-rays (typically $h\nu > 1\text{kV}$) the relative probabilities of photoionisation greatly favour core emission.²¹

The most commonly used X-ray sources are $\text{AlK}\alpha_{1,2}$ ($h\nu = 1486.6\text{ eV}$) and $\text{MgK}\alpha_{1,2}$ ($h\nu = 1253.7\text{ eV}$) although the use of harder sources (*e.g.* $\text{TiK}\alpha_{1,2}$, $h\nu = 4510\text{ eV}$) is becoming widespread. Chapter Three will deal with this point in more detail. Using $\text{MgK}\alpha_{1,2}$ excitation, the relative probabilities

of core and valence photoionisation in carbon, as determined by consideration of photoionisation cross sections for the 1s level and the 2s and 2p levels is 20:1 Ultraviolet Photoelectron Spectroscopy (UPS) using less energetic photons (*e.g.* He(I), $h\nu = 21.22$ eV; He(II), $h\nu = 40.8$ eV) is used to probe valence levels of molecules in greater detail.²²

The kinetic energy, KE, of an electron photoemitted from an isolated molecule or atom is given by

$$KE = h\nu - BE - E_r \quad (1.1)$$

where BE is the binding energy of the photoemitted electron, and E_r is the recoil energy of the atom or molecule. The recoil energy has been calculated to decrease with increasing atomic number and for typical photon sources used in ESCA it may be considered negligible.¹⁷ For very high photon energies, for example $AgK\alpha$ (22 keV) the recoil energy for light elements has been shown to be significant and must be taken into account.²³ However neglect of recoil energy is acceptable for commonly used X-ray sources and so equation 1.1 reduces to

$$KE = h\nu - BE \quad (1.2)$$

For a solid, binding energies are referred to the Fermi level, defined for a metal as being the highest occupied level at absolute zero.²⁴ This interpretation of the Fermi level is also very nearly true for metals at normal temperatures. For semiconductors and insulators however it is not so simple to locate the Fermi level, which lies somewhere between the filled valence bands and the empty conduction bands. If photoionisation is simply the ejection of an electron with no other effects on the atom or molecule then the binding energy is, by definition, simply the energy of the orbital from which the

electron is removed. That is

$$BE = -\epsilon_i \quad (1.3)$$

This relationship is straightforwardly derived and is known as Koopmans' theorem.²⁵ However the "frozen" final state binding energies as given by Koopmans' theorem are generally higher than those observed experimentally. This discrepancy is due to the effects of ionisation on the electronic structure of the atom or molecule. These processes occur over the same time scale as the photoionisation process, and may therefore be thought to accompany photoionisation and thus contributing to the observed binding energy and are dealt with in the next section.

1.2.2 Processes accompanying photoionisation

(i) Relaxation

Removal of a core electron, which is effectively completely shielding, exposes the valence electrons to a sudden increase in effective nuclear charge. The result is a contraction of the valence shell in space therefore imparting a stabilisation energy to the final core hole state. This reorganisation of the valence electronic structure is termed relaxation²⁶⁻²⁹ and results in modification of equation 1.3 to

$$BE = -\epsilon_i - R.E. \quad (1.4)$$

where R.E. is the relaxation energy accompanying photoionisation.

Before proceeding further it is worthwhile to point out that equation 1.4 does not represent the exact binding energy. A small error is introduced by the neglect of relativistic effects, which can be substantial however for deep levels in heavier elements. The Δ SCF method also ignores the change in

electron correlation energy on going from the initial state to the final core hole state. The Hartree-Fock method used in Δ SCF methods assumes an electron moves in the presence of an average potential created by the other electrons, and so neglects instantaneous repulsions between pairs of electrons. The contribution to the total energy due to instantaneous repulsions is the correlation energy which is usually a small proportion of the total energy of the molecule or atom but significant in terms of energies associated with physical and chemical phenomena.

The relaxation energy is found to be a sensitive function of the electronic environment of a molecule or atom²⁹⁻³⁴ and for core ionisation of first row atoms can result in a substantial correction to Koopmans' theorem (~ 13 eV)^{33,35} in the calculation of the absolute binding energy. Calculation of relaxation energy involves performing separate analyses of both the neutral species and the core ionised state.^{27,29,33} Differences in relaxation energy for closely related molecules are small and so cause only minor changes to shifts in binding energy.³³

Relaxation energies for valence electron photoionisation are typically an order of magnitude smaller than for core ionisation since the change in nuclear potential is larger on removal of a core electron due to its greater screening coefficient.³³

Figure 1.2 shows a schematic of photoionisation and relaxation processes and also the closely related phenomenon of shake-up which again occurs over a time scale fast enough as to be considered simultaneous with photoionisation.

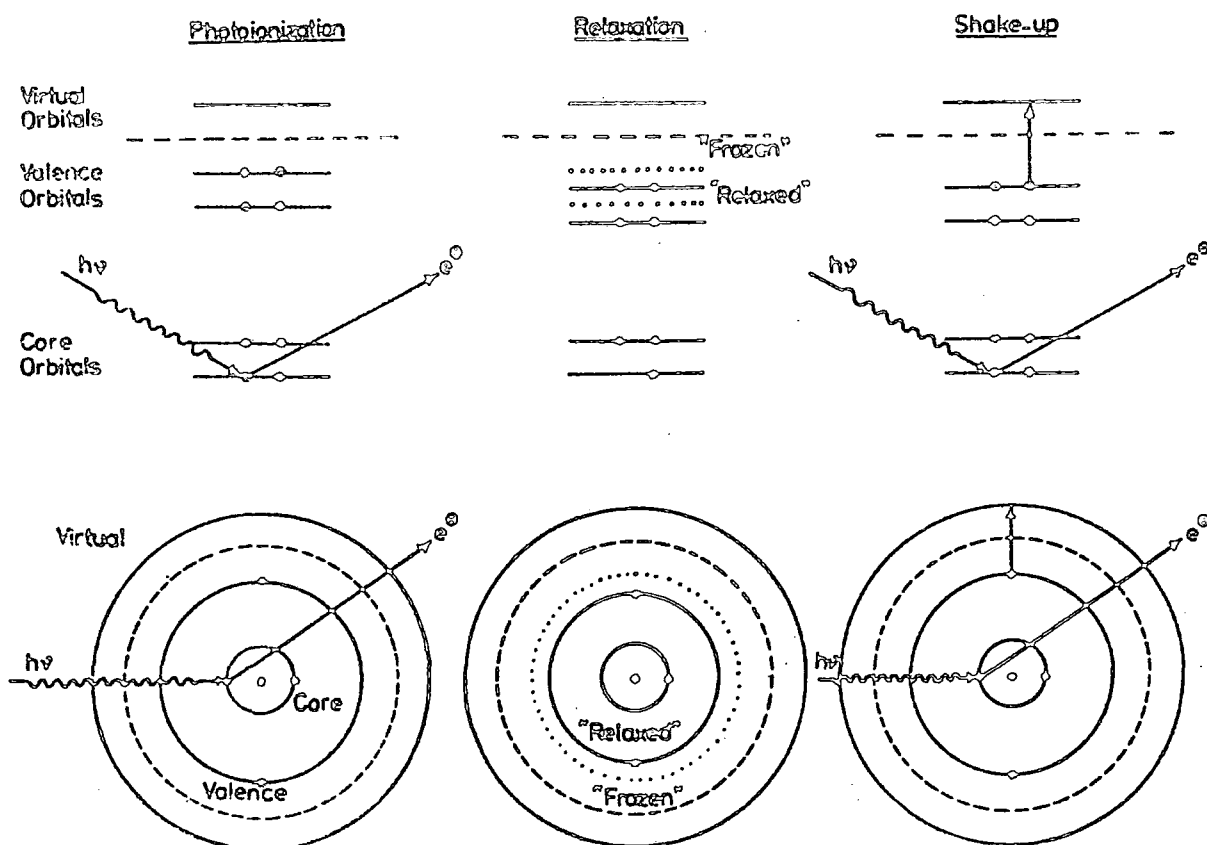


Figure 1.2 Photoionisation, relaxation and shake-up

(ii) Shake-up and Shake-off processes

Core electrons contribute a substantial proportion of the total electronic energy of an atom or molecule but are essentially localised in the proximity of the nucleus. Although they do not take an active role in bonding, the core electrons closely monitor the valence electron distribution.¹⁸ The sudden perturbation to the valence electron cloud accompanying core ionisation gives rise to a finite probability for

photoionisation to be accompanied by simultaneous excitation of a valence electron as well as the relaxation described in the previous section. The valence electron in the shake-up process is simultaneously excited to a virtual orbital and shake-off involves simultaneous emission of a valence electron from an occupied orbital to the vacuum level. Evidence has been presented for shake-down processes³⁶ (photoionisation of an excited state accompanied by de-excitation of the electron initially in a virtual orbital).

Shake-up and shake-off processes result in excited states of the core ionised species and because they are essentially simultaneous with photoionisation result in modification of the observed kinetic energy to

$$KE = h\nu - (BE + \bar{E}) \quad (1.5)$$

where \bar{E} is the energy of the multielectron transition. Thus satellite peaks to the low kinetic energy side of the direct photoionisation peak are observed as shown in Figure 1.3.

The shake-up process to a first approximation obeys monopole selection rules ($\Delta J = \Delta L = \Delta S = \Delta M_j = \Delta M_L = \Delta M_s = 0$) and may be viewed as the ESCA analogue of ultraviolet spectroscopy. Gaseous species spectra clearly³⁷ show a large number of peaks to the high binding energy side of the direct photoionisation peak, most of which are due to shake-up processes because the transition probabilities for shake-off tend to be relatively small. However for solids most shake-up and shake-off peaks are lost in the broad inelastic tail (see later) extending from ~ 20 eV to higher BE of the direct photoionisation. For organic materials in the condensed phase shake-up peaks may be observed if the transition energy is low enough. This occurs

in species which contain π bonding systems and identification of shake-up peaks has been shown to provide information regarding unsaturation in polymeric materials.³⁸⁻⁴⁰ Shake-up structure has also been observed in a variety of solid inorganic materials.^{41,42,43} In metals, and conductors in general, the form of the density of states curve above the Fermi level provides a continuous range of core electron excitation energies, rather than the discrete set observed in atoms and molecules. Thus shake-up processes result in an asymmetric tailing to high BE of the main peak rather than a sharp set of lines at discrete energies from the main peak.⁴⁴⁻⁴⁷

Manne and Åberg⁴⁸ have shown theoretically that the first moment of the satellite spectra with respect to the main photoionisation peak is equal to the relaxation energy, as shown schematically in Figure 1.3.

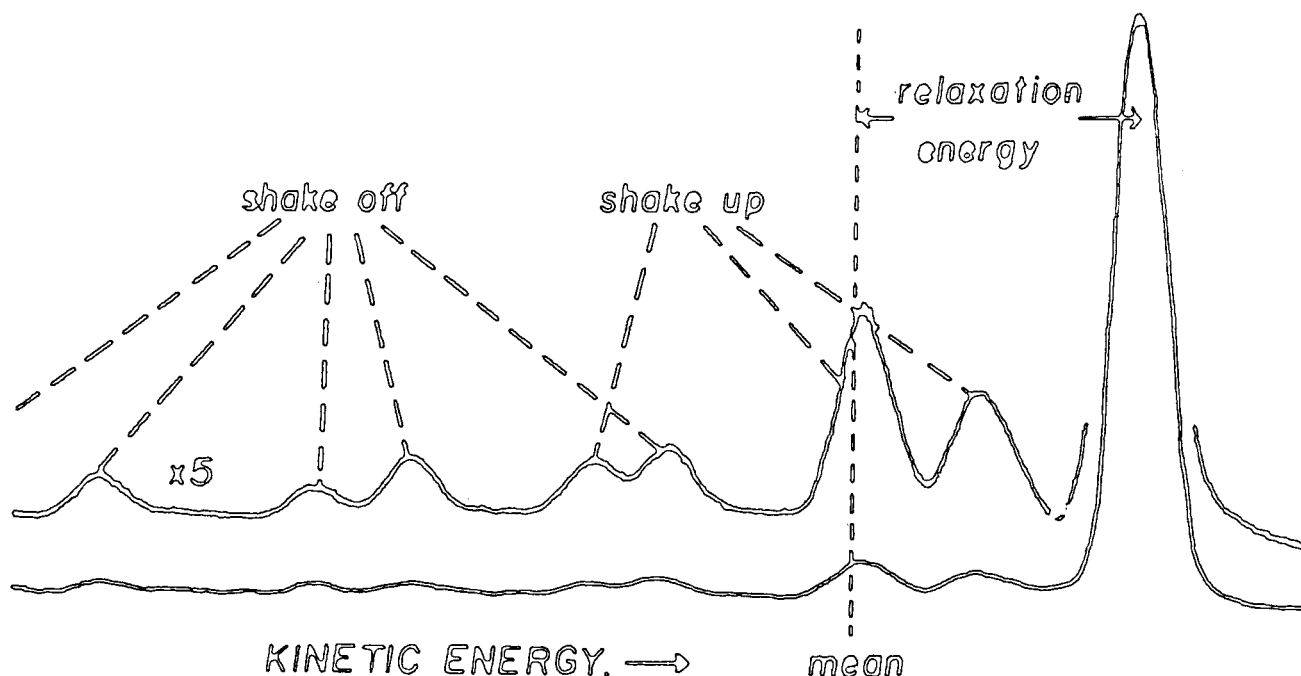


Figure 1.3 Relationship between Koopmans' theorem, relaxation energy, and the relative intensities of direct photoionisation, shake-up and shake-off

1.2.3 De-excitation processes

These processes are illustrated in Figure 1.4.

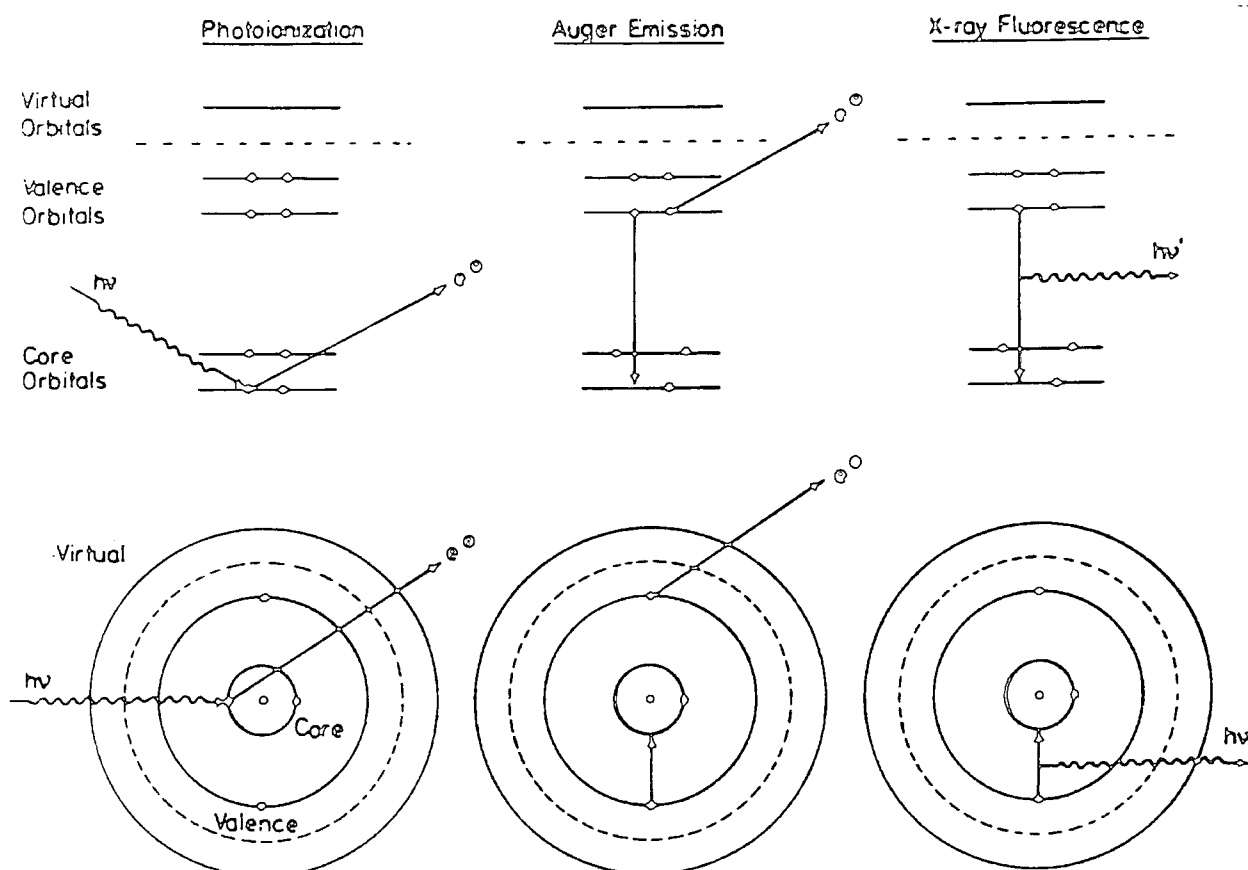


Figure 1.4 De-excitation by Auger emission and X-ray fluorescence

Briefly these processes involve filling of the core hole vacancy by an electron from a higher occupied level. The energy released by such a process results in simultaneous emission of either another electron from the high level, *viz* the Auger process,⁴⁹⁻⁵¹ or emission of a quantum of X-radiation, *i.e.* X-ray fluorescence.⁶⁰

The time scale for de-excitation processes of the core hole are generally much slower than photoionisation and have no effect on the observed KE of the photoelectron.

Figure 1.5 indicates that for de-excitation of a K shell vacancy (*i.e.* 1s core hole) Auger emission is the predominant process for elements of low atomic¹⁸ number while K shell fluorescence is dominant for heavier elements.

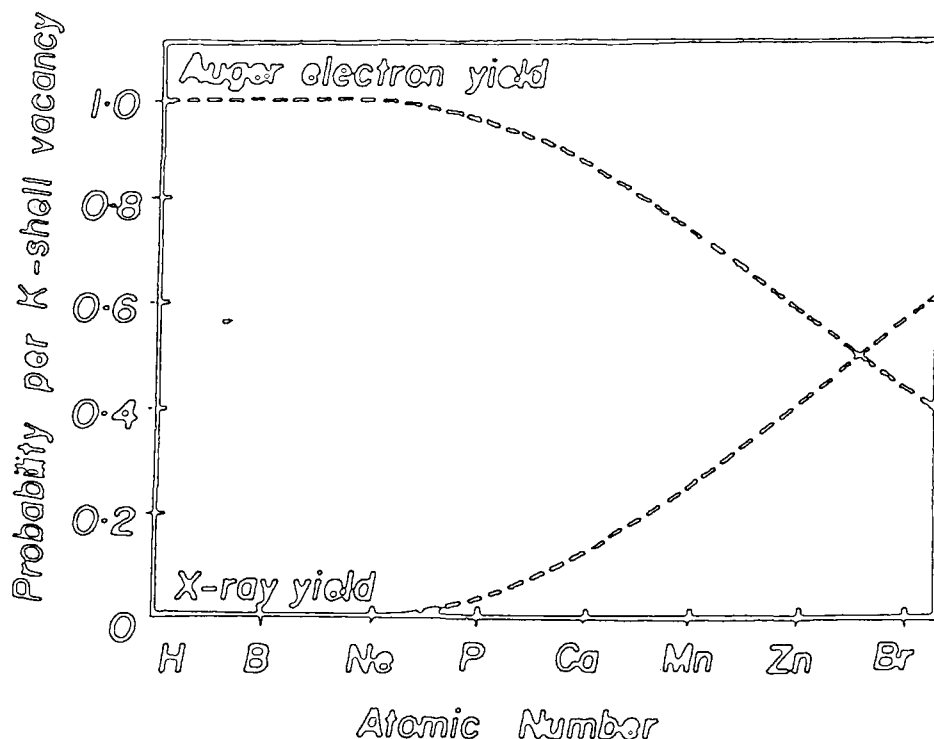


Figure 1.5 Relative probabilities of X-ray fluorescence and Auger emission for a K shell core hole

Auger electron spectroscopy^{52,53} is an established surface analytical technique and will be discussed in Chapter Two. Some mention will however be made here on the role of Auger lines in XPS. The concept of the Auger parameter has been developed,⁵⁴⁻⁵⁹ chiefly by Wagner, for the identification of chemical states. The parameter, α , is given by

$$\alpha = KE_A - KE_P, \quad (1.6)$$

where the Auger line chosen is generally the most intense and is recorded virtually simultaneously with the photoemission peak. Thus the parameter is independent of sample charging effects, and once obtained the parameter may be compared to

2 dimensional chemical state plots⁵⁹ on which photoelectron and Auger Data are represented and the oxidation state of the element estimated.

X-ray fluorescence spectroscopy is a means of qualitative analysis for elements of atomic number greater than 8 (as a consequence of the probabilities shown in Figure 1.5). Concentrations down to 0.01% for first row transition metals and 0.1% for most elements have been detected. A recent review of the technique has recently been published.⁶¹

The relative sensitivities of ESCA, Aes and X-ray fluorescence spectroscopy are shown in Table 1.1 together with other familiar analytical techniques.

TABLE 1.1 Relative sensitivities of ESCA compared to other analytical techniques

<u>Bulk Techniques</u>	<u>Minimum Detectable Quantity (g)</u>
Infrared absorption	10^{-6}
Atomic absorption	10^{-9} - 10^{-2}
Vapour phase chromatography	10^{-3} - 10^{-7}
High performance liquid chromatography	10^{-6} - 10^{-9}
Mass spectroscopy	10^{-9} - 10^{-15}
 <u>Surface Techniques</u>	
ESCA	10^{-10}
Neutron activation analysis	10^{-12}
Ion scattering spectrometry	10^{-15}
X-ray fluorescence	10^{-7}
Auger emission spectroscopy	10^{-14}
Secondary ion mass spectrometry	10^{-13}

1.2.4 Energy loss processes

In gas phase studies it is found that some of the features to the high binding energy side of the primary photoionisation peak increase with increasing pressure, whereas shake-up and shake-off peaks remain essentially the same. These features are due to discrete energy losses and in a solid phase spectrum they effectively drown most shake-up and shake-off peaks. The energy losses that occur are independent of the initial photoionisation event and may therefore be thought of as extrinsic. However some structure can be observed and 'plasmon' peaks are observed in the case of metals ~ 20 eV to the high binding energy side of the primary photoionisation peak,³¹⁴ and are due to photoelectrons having undergone one inelastic loss on exit from the sample,⁹⁷ and are therefore extrinsic to the photoionisation process.

1.3 Features of ESCA Spectra

1.3.1 Binding Energies

Since the core electrons are essentially localised on atoms their binding energies are characteristic for a given element.⁶³ Table 1.2 gives approximate core binding energies for first and second row elements and it can be seen from this that the binding energies are sufficiently separated that identification of the gross elemental composition of the sample is possible from the B.Es. of signals detected. With conventional sources ($\text{MgK}\alpha_{1,2}$ at 1253.6 eV and $\text{AlK}\alpha_{1,2}$ at 1486.7 eV) it is possible to probe down to the 1s levels for all first row elements, 2s or 2p for second row elements and so on. The

TABLE 1.2 Approximate core binding energies of first and second row elements

	Li	Be	B	C	N	O	F	Ne
1s	55	111	188	284	399	352	686	867
	Na	Mg	Al	Si	P	S	Cl	Ar
1s	1072	1305	1560	1839	2149	2472	2823	3203
2s	63	89	118	149	189	229	270	320
2p _{1/2}	31	52	74	100	136	165	202	247
2p _{3/2}	31	52	73	99	135	164	200	245

2s and 2p levels are effectively core like (*i.e.* shielding, localised on an atomic centre and non-participatory in bonding) for second row elements, as are the 3s, 3p, 3d for third row elements and so on.

It is worthwhile at this stage to clarify the relationship between the experimentally observed binding energy for a solid or liquid as opposed to a free atom or molecule. The following discussion does not include charging of the sample which will be dealt with later (Section 1.3.7), *i.e.* the sample is assumed to be conducting and in electrical contact with the spectrometer. As stated in Section 1.2.1 the Fermi level in a metal is defined as the highest occupied level. With the sample in electrical contact with the spectrometer the Fermi levels of both will line up and a contact potential will be established (see Figure 1.6).

The work function ϕ is defined as the energy gap between the vacuum level and the Fermi level. However the work function for the sample (ϕ_s) may not be the same as that for the spectrometer (ϕ_{spec}).⁶³ Thus the value of the contact potential will be $(\phi_s - \phi_{spec})$ and so the observed KE is related to the vacuum

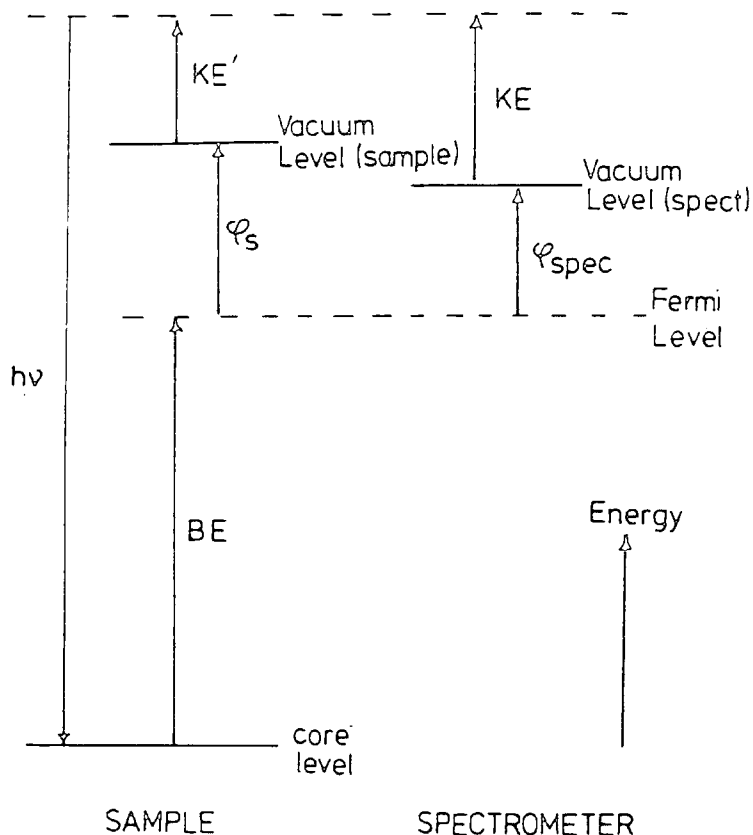


Figure 1.6 Energy level diagram for a sample in electrical contact with the spectrometer

level KE , KE^V

$$KE = E_k^V + (\phi_s - \phi_{spec}) \quad (1.7)$$

and so equation 1.2 now becomes

$$KE = h\nu - BE^V + \phi_s - \phi_{spec}.$$

Referencing the binding energy to the Fermi level then gives

$$KE = h\nu - BE - \phi_{spec}. \quad (1.8)$$

The binding energy referenced to the Fermi level therefore is independent of the work function of the sample. This is convenient since it gives a constant correction to all binding

energies. The measurement of absolute binding energies is circumvented by the use of reference standards⁶⁴ for calibration, although a recent ASTM report demonstrated the need for improved calibration methods and operating procedures amongst the U.S. ESCA community.⁶⁵

1.3.2 Chemical shifts

The energies of core levels in molecules are sensitive to their electronic environment,^{18,19} that is the valence electron charge distribution. Since they are localised, on the other hand, the shape of the core orbitals is essentially unchanged on chemical transformation. Thus differences in core binding energies occur depending on chemical environment, but the photoelectron cross section remains essentially constant, but intensities of chemically shifted peaks within the same core level envelope are directly related to the relative numbers of atoms in different environments. These points are illustrated in the C_{1s} spectrum of ethyl trifluoroacetate (Figure 1.7).

Some typical values for chemical shifts are given in Figure 1.8.

The interpretation of chemical shifts theoretically in general have been carried out using the following methods:

- (i) Koopmans' Theorem²⁵
- (ii) Δ SCF methods^{26,33,67}
- (iii) Equivalent cores model⁶⁸⁻⁷¹
- (iv) Charge potential model¹⁹
- (v) Quantum mechanical potential model⁷²⁻⁷⁴
- (vi) Transition state model^{75,76}
- (vii) Greens Function formalism¹⁰⁹

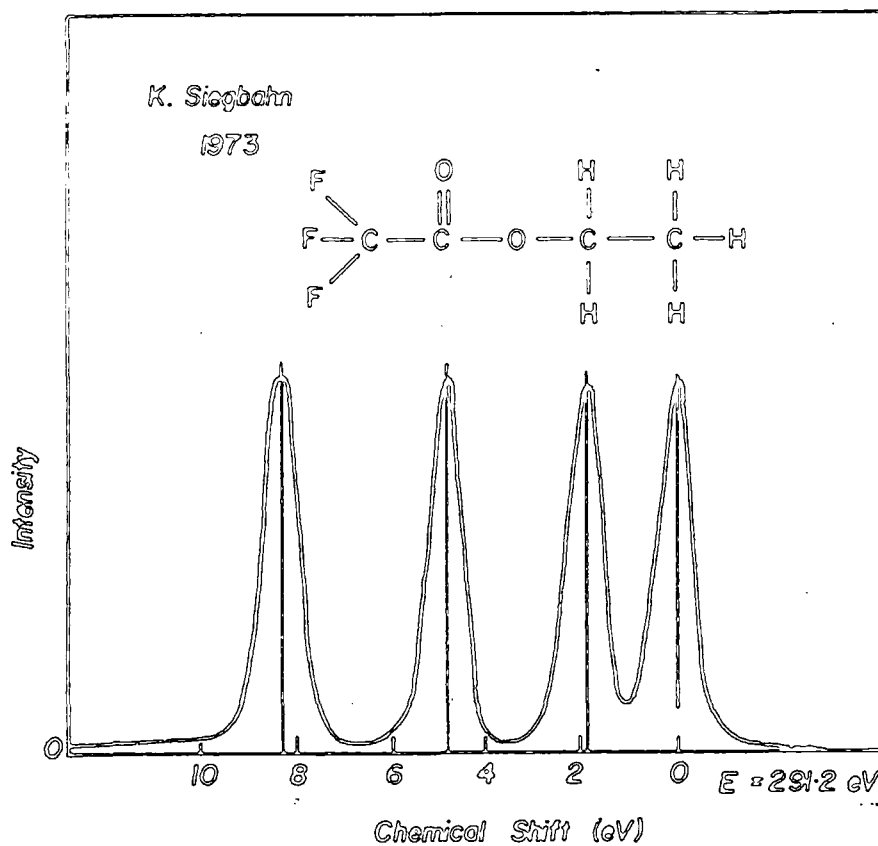


Figure 1.7 High resolution core level spectrum of ethyl trifluoroacetate

There are several recent accounts of the physical processes in photoionisation from a theoretical viewpoint.^{66,77}

1.3.3 Fine Structure

Fine structure in core hole spectra can arise as a consequence of the pseudo monopole selection rules in photoionisation. The types of splitting encountered for each shell are shown in Figure 1.9. Orbital 'splitting' is simply a manifestation of the different binding energies of the 2s and 2p levels and will not be considered any further. It is worthwhile to briefly discuss the remainder individually.

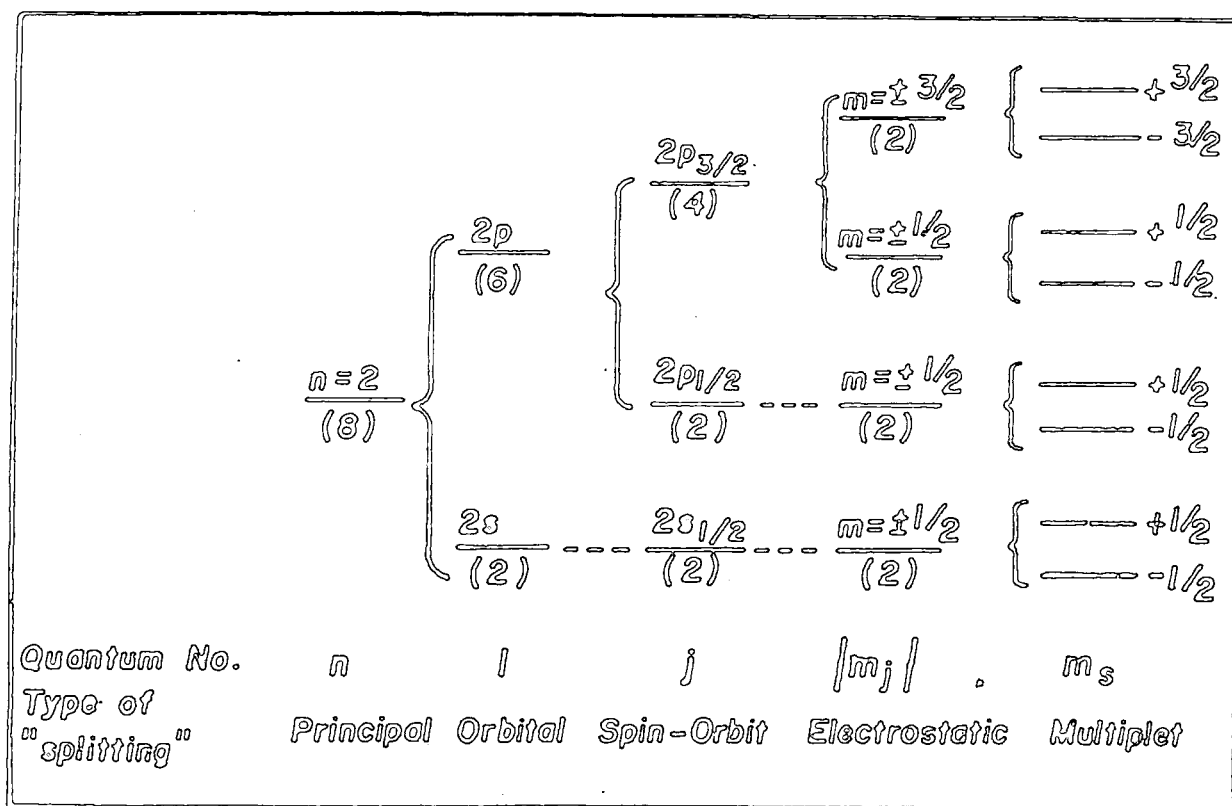


Figure 1.9 Schematic of types of splittings encountered in ESCA

(i) Spin orbit splitting

A doublet is observed in the ESCA spectrum when photo-ionisation occurs from an orbital with orbital quantum number (ℓ) greater than 1¹⁷ (*i.e.* p, d or f orbitals). The doublet is observed due to coupling between the spin (S) and orbital angular momentum L to yield a total momentum (J):

$$J = S + L \quad (1.9)$$

The doublet occurs because for any value of L, S can be $\pm\frac{1}{2}$. The relative intensities of the component peaks within the doublet are proportional to the degeneracies of the states, *viz.* $2J+1$. These intensities are shown in Table 1.3 for s, p, d, and f orbitals and typical spectra are shown in Figure 1.10.

TABLE 1.3 Spin orbit splitting degeneracies and intensities

<u>Orbital</u>	<u>Orbital Quantum No.</u>	<u>Total Quantum No.</u>	<u>Intensity Ratio</u>
	ℓ	$J = (\ell \pm S)$	$(2J + 1) : (2J - 1)$
s	0	$1/2$	singlet
p	1	$1/2, 3/2$	1 : 2
d	2	$3/2, 5/2$	2 : 3
f	3	$5/2, 7/2$	3 : 4

(ii) Electrostatic Splitting

This occurs in a number of spectra *e.g.* in the $5p^{3/2}$ levels of uranium and thorium and some compounds of gold,^{78,79} and is due to the differential interaction between the internal electrostatic field and the spin states of the core level being investigated. Such splittings are highly unlikely even in appropriately substituted organic polymers on account of their inherently amorphous structure.

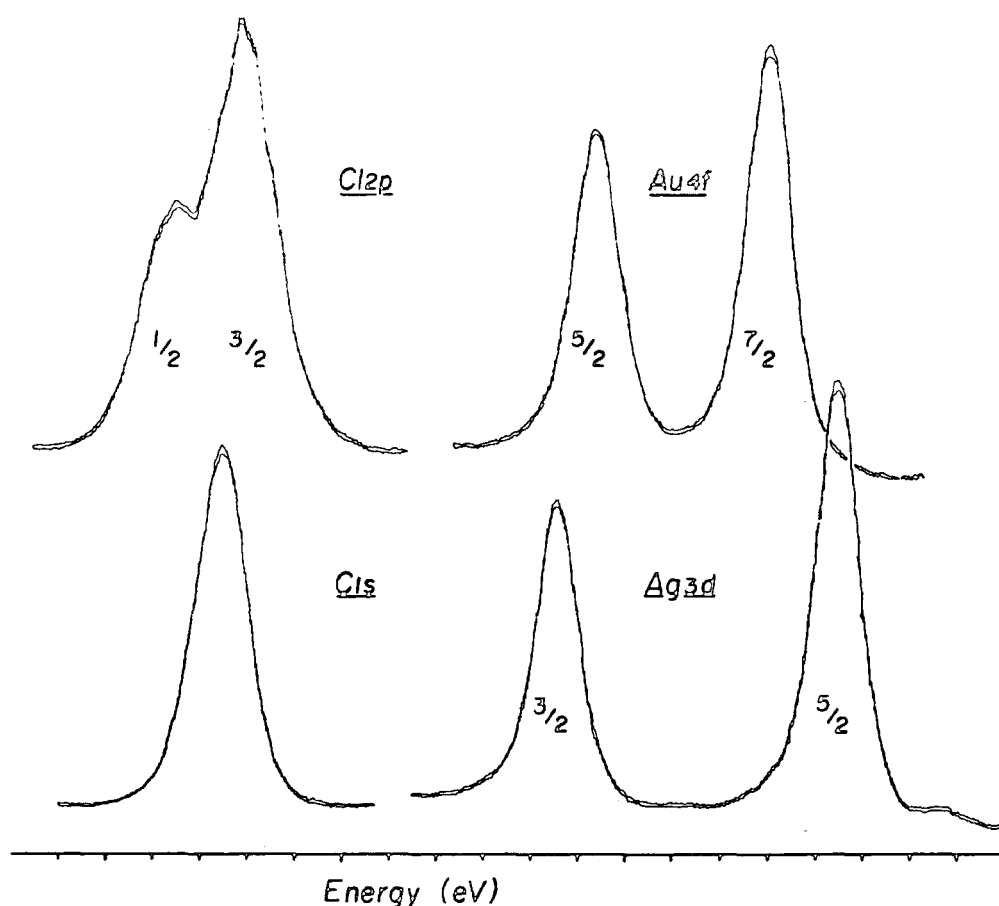


Figure 1.10 Spin orbit splittings in Cl_{1s} , Cl_{2p} , Ag_{3d} and Au_{4f} core levels

(iii) Multiplet splittings

Multiplet splitting occurs in paramagnetic systems and arises from coupling between unpaired electrons present in the system and the unpaired core orbital electrons remaining after photoionisation.^{80,81} A simple example may be seen in the spectra of O_2 , and NO , (see Figure 1.11).¹⁹ For the NO case greater splitting is observed in the N_{1s} spectrum than the O_{1s} spectrum. It may be shown theoretically that the greater the unpaired spin density on an atom, then the greater the splitting. Thus the spectra for NO indicate that there most of the unpaired spin density is on the nitrogen.

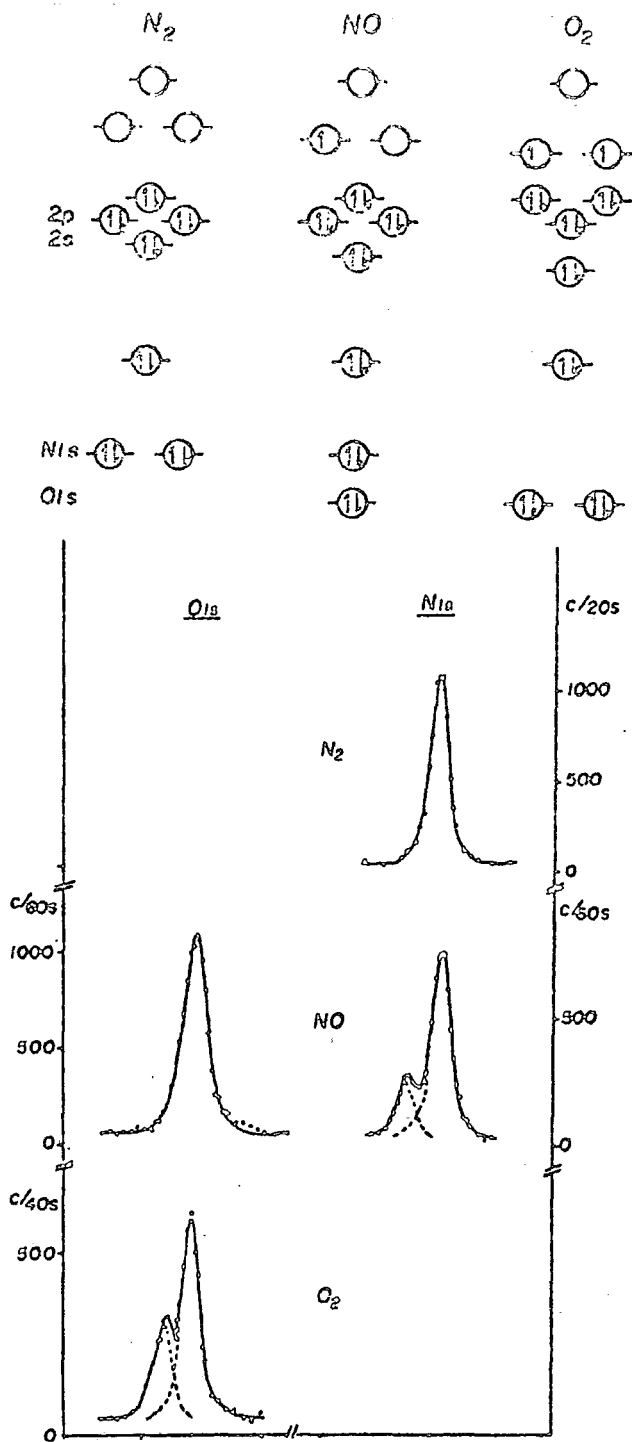


Figure 1.11 Core hole spectra of N_2 , NO and O_2 illustrating multiplet splitting

1.3.4 Signal intensities

(i) Fixed Angle studies

The quantitative or semi qualitative interpretation of ESCA peak intensities requires developing a model for predicting their values from various properties of the photon source, specimen, electron energy analyser and detection system. The idealised geometry for the ESCA experiment involving a fixed

arrangement of analyser and X-ray source is shown in Figure 1.12. Thus X-rays enter the sample at an angle $\phi - \theta$ and detected electrons emerge from the sample at an angle θ .

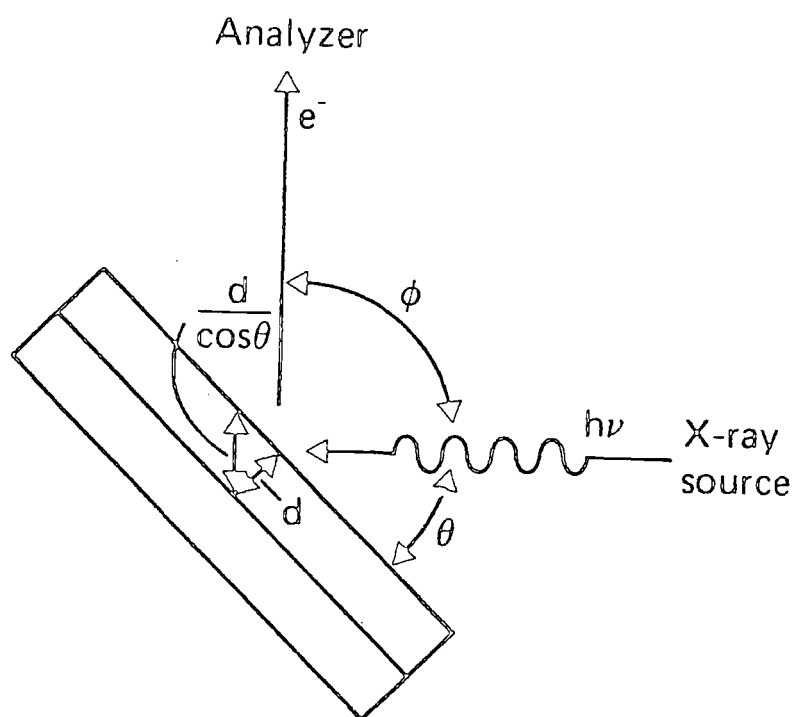


Figure 1.12 Sample geometry with respect to the analyser and photon source

If the photoelectrons are emitted from a depth, d , inside the sample then the only electrons actually detected will have travelled a distance d' through the sample, where d' remains

$$d' = d \cos \theta \quad (1.10)$$

essentially constant so by varying the angle the depth sampled can be varied. Thus at high angles less depth is sampled, a

point which will be expanded on in Section 1.3.4.(ii).

For an infinitely thick homogeneous sample the intensity (I_i) of photoelectrons arising from core level i which have not undergone any energy loss is given by the differential equation

$$dI_i = F\alpha_i N_i k_i e^{-x/\lambda_i} dx \quad (1.11)$$

where:

F is the X-ray flux

α_i is the photoionisation cross section

N_i is the number of atoms per unit volume on which the core level i is localised

k_i is a spectrometer factor

λ_i is the electron mean free path

x is the depth of photoionisation of core level i .

The integration of this equation is straightforward since for a homogeneous sample F , α_i , N_i , k_i and λ_i are independent of x . Thus,

$$I_i = \int_0^{\infty} F\alpha_i N_i k_i e^{-x/\lambda_i} dx \quad (1.12a)$$

$$= F\alpha_i N_i k_i \lambda_i \quad (1.12b)$$

A fuller explanation of each of the parameters will be given below:

The X-ray flux, F , is dependent primarily on the power applied to and the efficiency of the X-ray gun. It is important to note that the flux may be assumed constant at any depth x sampled by ESCA since the attenuation of X-rays occurs over a much greater depth when compared to the electron mean free path. Refraction of the collimated X-rays in the outermost surface layers can occur for X-rays nearly parallel to an optically flat surface causing an increase in signal intensity.⁸² However for the instrumentation used in this study this is not applicable.

The photoionisation cross section, α_i , of a core level is a measure of the probability of the level being ionised by irradiation of photons of known energy, with the incident photo-electron emission angle being favourable for the electron detection.

α_i is a function of both the core level, and the incident photon energy. The radial distribution of photoelectrons is not uniform and α_i is a function of ϕ (see Figure 1.12). α_i is given by^{23,84}

$$\alpha_i = \alpha_i^{\text{TOT}} / 4\pi [1 - \frac{1}{4} \beta_i (3\cos^2\phi - 1)] \quad (1.13)$$

α_i^{TOT} is the total cross section for photoionisation from core level, i , and may be calculated quantum mechanically^{21,85} or found experimentally.¹⁹ β_i is termed the asymmetry parameter and has also been determined theoretically.⁸⁶ For conventional spectrometers, where ϕ is kept constant then α_i may be considered constant for particular level. It should be noted that cross sections for photoionisation of core levels using conventional X-ray sources for most elements are within two orders of magnitude of that for the C_{1s} levels,²¹ emphasising the sensitivity range for most elements. Using harder X-ray sources (*e.g.* $TiK\alpha$), the cross sections of levels observable by conventional sources⁸⁵ is decreased by several orders of magnitude, a point elaborated on in Chapter Three.

The spectrometer factor k_i includes contributions due to detector efficiencies and analyser transmission characteristics, which are both dependent on the kinetic energy of the core electrons being analysed, geometric factors such as the solid angle of acceptance of the analyser. The mean free path,

λ_i , is defined as the distance through which electrons will travel before $1/e$ of them have not suffered energy loss. Chapter Three is a study of the variation of mean free paths over the kinetic energy range 0-4400 eV using a TiK α source. The various determinations of mean free paths indicate that for conventional sources mean free paths vary in proportion to the square root of kinetic energies for energies greater than ~ 100 eV, such that for 1170 eV electrons the mean free path has a value $\sim 22\text{\AA}$, and at 4400 eV about 40\AA . The variation of mean free paths with kinetic energy is illustrated in Figure 1.13.

The sampling depth is typically taken as the depth from which 95% of the signal for a given core level originates and is $\sim 3\lambda_i$. It should be noted that the exponential drop off in relative signal intensity with depth is exponential such that 67% of the signal derives from a depth λ_i , and 90% from $2\lambda_i$.

The surface sensitivity of ESCA is a consequence of the very short distances of the mean free path.

The number density, N_i , is not directly related to the density of the sample. For similar materials the ESCA signal for a given core level has been shown to be more intense for the higher density material.⁸⁷ The overall stoichiometry of a material giving signals from core levels i and j may therefore be written

$$\frac{N_j}{N_i} = \frac{I_j}{I_i} \times \text{S.F.} \quad (1.14)$$

where $\text{S.F.} = \frac{\alpha_j k_j \lambda_j}{\alpha_i k_i \lambda_i}$ is known as the instrumental sensitivity factor and can be determined experimentally using standard

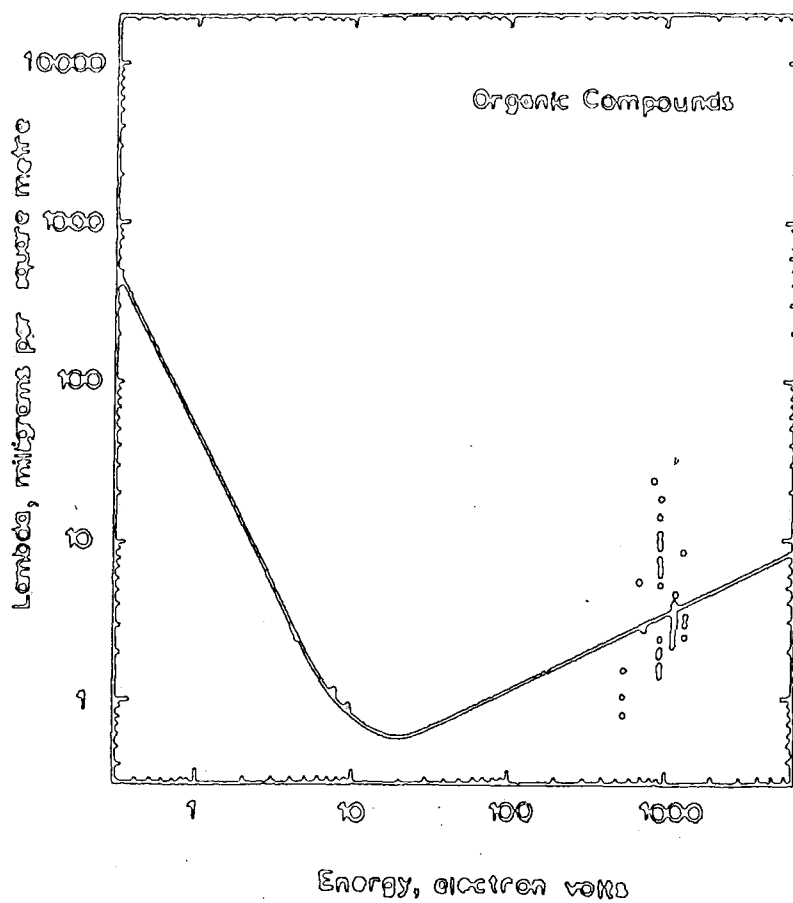


Figure 1.13 Variation of experimentally determined mean free paths for organic compounds

samples of known stoichiometry containing i and j .

When i and j correspond to the same core in different chemical environments then,

$$k_i \alpha_i \lambda_i = k_j \alpha_j \lambda_j \quad (1.15)$$

therefore,

$$\frac{N_1}{N_2} = \frac{I_1}{I_2} \quad (1.16)$$

(ii) Angular dependence and Depth profiling

A unique feature of ESCA is the capability to elaborate features of structure and bonding in vertically inhomogeneous samples on the tens of Angstroms scale. There are two methods by which depth profiling may be achieved, non-destructively, the first is to investigate signal intensities of sample levels having differing escape dependencies and the second is by monitoring intensities as a function of electron take off angle θ .

To illustrate these two points it is worthwhile to consider an idealised example of a single homogeneous overlayer of thickness d and a homogeneous substrate which may be considered infinitely thick as shown in Figure 1.14

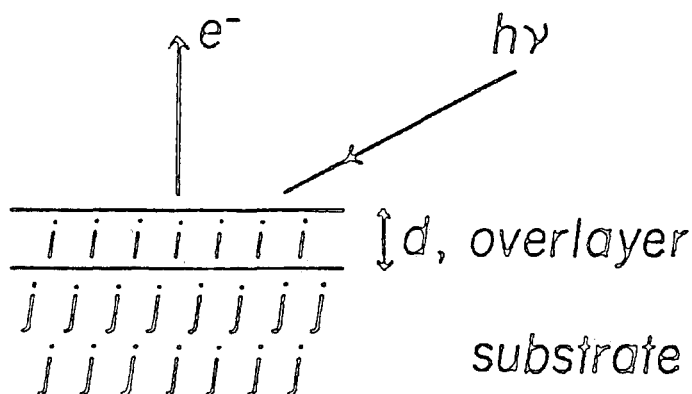


Figure 1.14 The substrate overlayer model

The intensity of the signal arising from the overlayer I_i^O can be obtained by integrating equation 1.11 between $x = 0$ and $x = d$,

$$I_i^O = F\alpha_i N_i K_i \lambda_i (1 - e^{-d/\lambda_i \cos\theta}) \quad (1.17)$$

The intensity of signal arising from the substrate I_j^S is similarly given by integration between $x = d$ and $x = \infty$.

$$I_j^S = F\alpha_j N_j K_j \lambda_j e^{-d/\lambda_j \cos\theta} \quad (1.18)$$

If $j=i$ then it can be clearly seen from these equations that the intensity of the overlayer relative to the substrate increases for larger values of θ , up to 90° , *i.e.* surface features are enhanced at larger take off angle. Also evident from equations 1.17 and 1.18 is the dependence of signal intensity on the mean free path of the core level under study. As mentioned earlier and as will become clear in Chapter Three electron mean free paths show a dependence on kinetic energy. In the region of interest for most ESCA studies *i.e.* at $KE > 100$ eV the mean free path increases with kinetic energy. Thus the attenuation of a signal arising from a core level in a substrate by an overlayer coverage will depend strongly on the kinetic energy of the photoelectrons. This may be exploited in two ways. With a single photon source, *e.g.* $MgK\alpha_{1,2}$ the same element may have two core levels with largely differing BE, for example the F_{1s} and F_{2s} levels. With an $MgK\alpha_{1,2}$ source these levels will have kinetic energies of ~ 560 eV and 1220 eV, hence the mean free paths will differ by a substantial proportion.

Thus monitoring of the F_{1s}/F_{2s} intensity ratio will give information on the relative vertical homogeneity, with large values corresponding to greater fluorination at the surface

(since $\lambda_{F_{1s}} = \sim 7\text{\AA}$, $\lambda_{F_{2s}} = \sim 20\text{\AA}$), and smaller values indicating lower fluorine content at the absolute surface.

When two photon sources are available such as Mg and $TiK\alpha_{1,2}$ at 4510 eV the depth profiled may be greatly extended, a point which will be further covered in Chapter Three.

1.3.5 Line Widths

One of the major disadvantages of ESCA in comparison to other spectroscopies is the relatively large linewidth, as measured by the Full Width at Half Maximum, compared to chemical shifts.¹⁸ There are several contributory factors which determine the total observed line width, ΔE_m , summarised in equation 1.19 for Gaussian lineshapes.

$$(\Delta E_m)^2 = (\Delta E_x)^2 + (\Delta E_{cl})^2 + (\Delta E_s)^2 + (\Delta E_{ss})^2 \quad (1.19)$$

where ΔE_x is the broadening due to the non-monochromatic nature of the X-ray source.

ΔE_{cl} is natural line width of the core level under investigation,

ΔE_s is the effective resolution of the electron analyser and ΔE_{ss} is the broadening due to solid state effects.

The natural linewidths of the core level under investigation (ΔE_{cl}) and that of the incident radiation (ΔE_x) depend on the uncertainty principle

$$\Delta E \cdot \Delta t = h/2\pi \quad (1.20)$$

where t is the lifetime of the state and h is Planck's constant. Thus a line width of 1 eV corresponds to a lifetime of approximately 6.6×10^{-16} s. Table 1.4 displays some line widths of core levels derived from X-ray spectroscopic studies: it also indicates the variation of the natural line widths for the 1s

TABLE 1.4 Linewidths of core levels

Level	S	Ar	Ti	Mn	Cu	Mo	Ag	Au
1s	0.35	0.5	0.8	1.05	1.5	5.0	7.5	54
2p _{3/2}	0.10	-	0.25	0.35	0.5	1.7	2.2	4.4

and 2p_{3/2} levels for various elements and shows that there is no particular virtue in studying the most tightly bound core levels, since for example in Au the 54 eV FWHM would swamp any chemical shift.

The broadening due to ΔE_x and ΔE_{Cl} is essentially Lorentzian, although when monochromatisation of the X-ray source is used the X-ray broadening is Gaussian and also no longer directly depends on the lifetime of the X-ray fluorescing state.

The broadening due to spectrometer aberrations ΔE_s is essentially Gaussian and its value depends on the type of analyser, the slit widths and the photoelectron energy. Thus the observed photoelectron spectrum is a convolution of Lorentzian and Gaussian distributions such that the line shape is predominantly Gaussian with Lorentzian character to the tails.

1.3.6 Line Shape Analysis

The resolution of complex line shapes in ESCA may be achieved by two methods. The first involves mathematical manipulation of the raw data to try to unfold or deconvolute the effects of the instrument function on the observed spectrum, whilst the second involves curve fitting techniques in either analogue or digital fashion.

Deconvolution by mathematical methods is usually by Fourier analysis or iterative procedures such as van Cittert's

deconvolution procedure.⁸⁸ These methods rely on a suitable choice of the instrumental function and experimental data where the signal to noise ratio is very high. The use of mathematical deconvolution can bring about an improvement in resolution comparable to that obtained by the use of a monochromator⁸⁹ although considerable caution must be exercised to prevent the interpretation of spurious structures as experimentally observed peaks.⁹⁰

Curve fitting techniques involve the simulation of the observed core level line shape using a digital or analogue computer. The binding energies, line widths and peak heights of the component peaks are under close control of the operator. For polymeric materials it is found that only small errors are introduced by the use of Gaussian component lineshapes.¹⁹ The underlying philosophy behind line shape analysis is best illustrated in the flow chart in Table 1.5.

1.3.7 Sample Charging

The loss of electrons occurring in a solid due to the emission of photoelectrons, Auger electrons and secondary electrons constitutes a net loss of negative charge from the surface of the material during an ESCA experiment. For conductors in electrical contact with the spectrometer no positive potential increase occurs due to electron replacement predominantly by normal conduction processes. Thus the Fermi levels of the sample and spectrometer remain lined up and energy referencing presents no problems. In an insulating sample or a conducting sample not in electrical contact with the spectrometer replacement of electrons by straightforward conduction is

General background knowledge of the system to be studied



From model compounds establish (i) binding energies

(ii) FWHM and line shapes of likely structural features

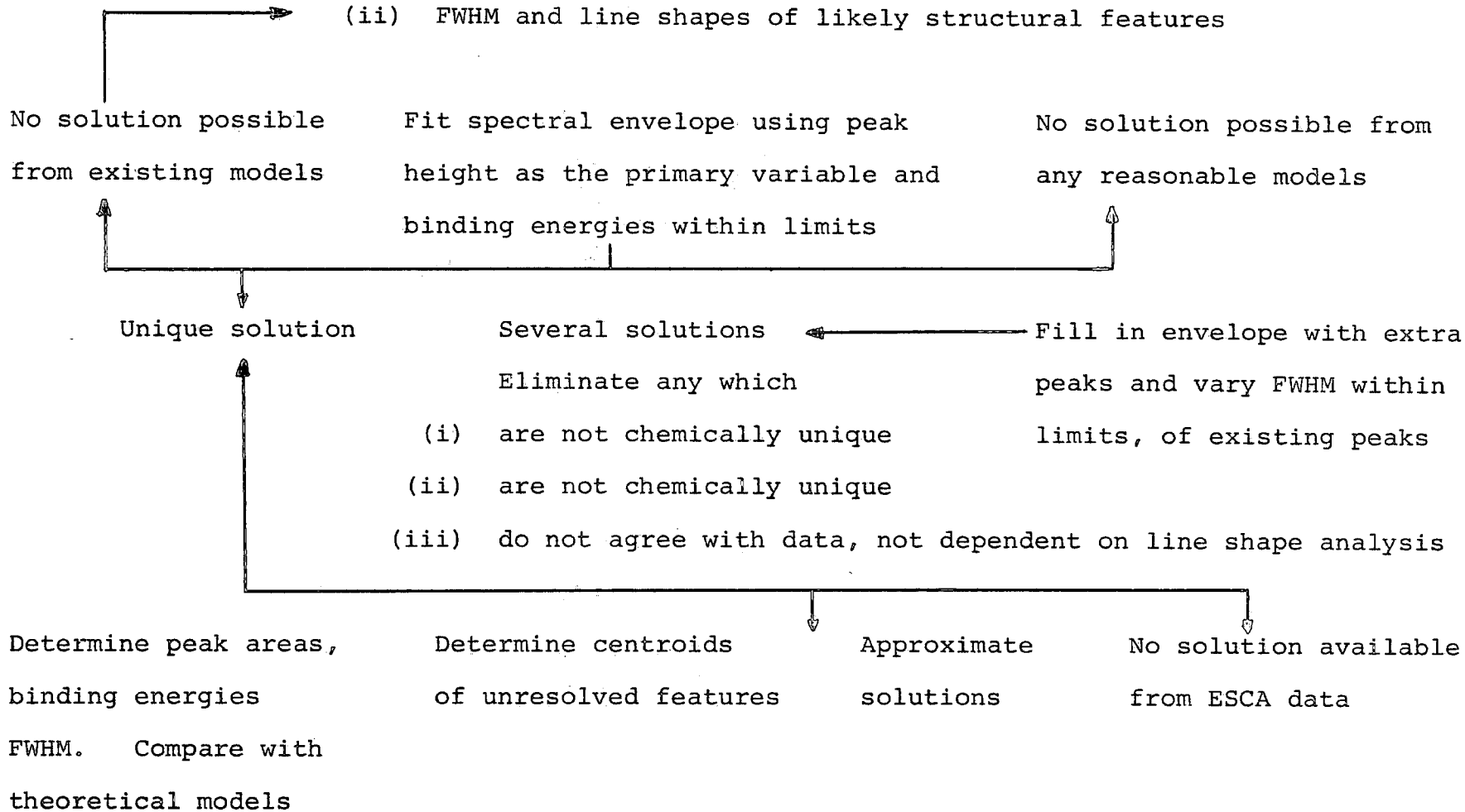


TABLE 1.5 Schematic of the peak fitting procedure

not possible but the build up of positive charge is decreased by the flux of secondary electrons,^{97,98} originating either from the sample or parts of the spectrometer, at the surface of the sample. For insulating samples these secondary electrons have been shown to amount typically to 99% of the total photoelectron flux⁹⁸ and play an important role in the establishment of an electrical equilibrium at the sample surface, but in general a small net positive potential occurs. Thus photoemitted electrons leaving the surface therefore experience a net retardation voltage and so the observed KE is

$$KE = h\nu - BE - \phi_{\text{spec}} - \Delta$$

where Δ is the net positive charge of the sample. Charging may be overcome by increasing the number of low energy electrons in the sample chamber. A simple method for achieving this is the use of a low energy electron flood gun.⁹⁹ Alternatively illumination of the sample region with u.v. radiation from a low pressure, low power mercury lamp produces sufficient low energy electrons, by direct photoemission from the walls of the spectrometer, to neutralise sample charging.¹⁰⁰

With monochromatised X-ray sources sample charging can be of the order of 100s of eV, since the absence of Bremsstrahlung severely decreases the number of low energy secondaries. With monochromatic sources however it is rarely greater than ~20 eV. The most convenient method of sample referencing when charging is present is to monitor a suitable reference peak. A correction factor (*i.e.* Δ) calculated from the observed kinetic energy of the reference signal is then used to find the binding energies of the other peaks present. The two most commonly used calibration peaks are the hydrocarbon C_{1s} peak at 285 eV, which may be either inherent in the sample or arising from hydrocarbon contam-

ination within the spectrometer, or the Au $4f_{7/2}$ peak at 84.0 eV if the sample has been deposited on a gold substrated.

The phenomenon of sample charging has often been treated as a nuisance in ESCA but it has been shown that sample charging can be of importance as an information level in its own right.¹⁰¹ For samples studied insulated from the probe tip under a variety of operating conditions sample charging is characteristic of the sample and is related to the total photoionisation cross-section. The surface sensitivity of charging has been demonstrated by monitoring the change in charge shift as a function of thin film thickness. Changes in surface composition of polymers may be monitored by sample charging measurements as was shown by extensive studies¹⁰²⁻¹⁰⁵ on the inert gas plasma modification of an ethylene-tetrafluoro ethylene copolymer. The surface defluorination demonstrated by core and valence level ESCA studies could be monitored also by the changes in charging, on going from a surface high in fluorine to an essentially cross linked surface low in fluorine content.

1.4 ESCA Instrumentation

The majority of the work in this thesis was carried out on a custom designed Kratos ES 300 electron spectrometer. Figure 1.15 shows the essential components of an electron spectrometer and Plate 1.1* is a photograph of the vacuum regions of the ES 300 used, with a key to indicate the nature of the various equipment attached to the spectrometer. It is worthwhile at this stage to discuss these components in greater detail, followed by discussion of the essential ESCA equipment.

* see Appendix One

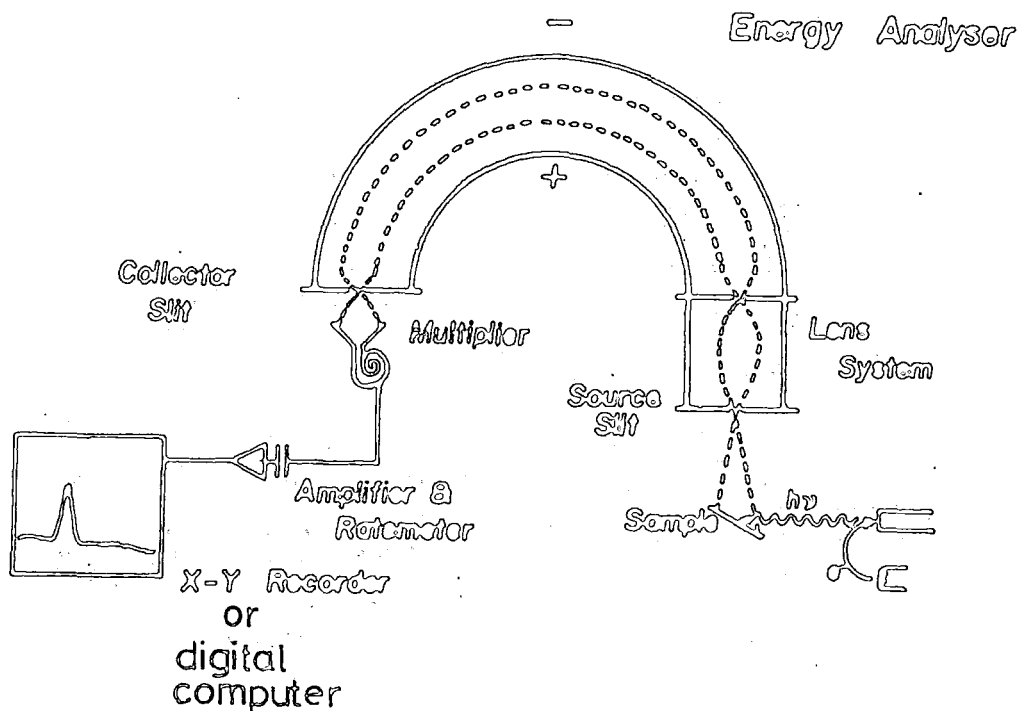


Figure 1.15 Essential components of an ESCA spectrometer

1.4.1 Components of the ES 300 used in this thesis

The ES 300 is custom designed to allow a multitude of *in situ* pretreatments of samples in addition to ESCA analysis. The spectrometer may be divided into two sections, the sample analysis chamber and the sample preparation chamber, whose names are self explanatory and are indicated on the key to Plates 1.1. (Appendix One).

(i) Sample analysis chamber

The sample analysis chamber is of tubular design which allows the attachment of various equipment as well as that necessary for ESCA analysis. Pumping for the system is achieved by independently pumping the source and analyser regions using electrically driven, turbomolecular pumps of nominal pumping speeds 350 l s^{-1} and 140 l s^{-1} respectively. The base pressure is typically $\approx 2 \times 10^{-9}$ torr. There are two fast entry insertion locks on the sample analysis chamber, insertion lock (1) is the normal mode of entry for solids on a probe whereas lock (2) allows introduction of volatiles, using a reservoir shaft, for condensation onto a cooled substrate. Purpose built reaction chambers may also be attached to the source chamber *via* insertion lock (1) thus providing great flexibility for *in situ* treatment of samples.

Plate 1.1 also indicates the position of a differentially pumped ion gun (Vacuum Generators type AGS) for either cleaning of metallic samples or treatment of polymers. The ions used may be mass selected by means of a Wien filter.

There are two X-ray guns, one a Ti/Mg dual anode and the other an $\text{AlK}\alpha_{1,2}$ source equipped with a monochromator. These and the electron energy analyser will be discussed in greater detail in Sections 1.4.2 and 1.4.3 respectively.

(ii) Sample Preparation Chamber

The sample preparation chamber allows the *in situ* treatment of samples with a vacuum system independent of the sample analysis chamber. Normal sample entry is through insertion lock (3) with deposition facilities available *via* insertion locks (4) and

(5). The key to Plate 1.1 indicates the position of the electron gun (Vacuum Generators type LEG 31) used for the work described in Chapters Four and Five. U.v. irradiation of samples is possible through the sapphire window fitted to the preparation chamber. Once treated the sample may be moved into the analysis chamber *via* an inter-connecting insertion port. The preparation chamber is pumped by a 600 l s^{-1} diffusion pump, and typical base pressures are 10^{-10} torr.

1.4.2 X-ray Sources

The X-ray beam is produced by bombardment of an anode with high energy electrons. The characteristic X-ray emission lines thus produced will be superimposed on a continuous background of Bremsstrahlung radiation, as indicated by the X-ray spectrum of tungsten in Figure 1.16.⁹¹ The shape of the Bremsstrahlung is governed by the energy of the incident electrons on the anode, and is independent of anode material. Increasing Bremsstrahlung to characteristic emission decreases the signal to background in the ESCA spectra so there are optimum operating conditions in terms of incident electron energy. For soft X-ray sources, *e.g.* $\text{MgK}\alpha$ ($h\nu = 1253.7 \text{ eV}$) and $\text{AlK}\alpha$ ($h\nu = 1486.6 \text{ eV}$) typical acceleration voltages which give excellent signal to background are 12kV and 15kV respectively.

Both the dual anode Mg/Ti source⁹² and the $\text{AlK}\alpha_{1,2}$ X-ray sources on the ES 300 are based on the Henke hidden filament design.⁹³ The risk of contamination of the anode material by evaporated tungsten from the filament is considerably reduced by this design since the filament is out of line of sight of

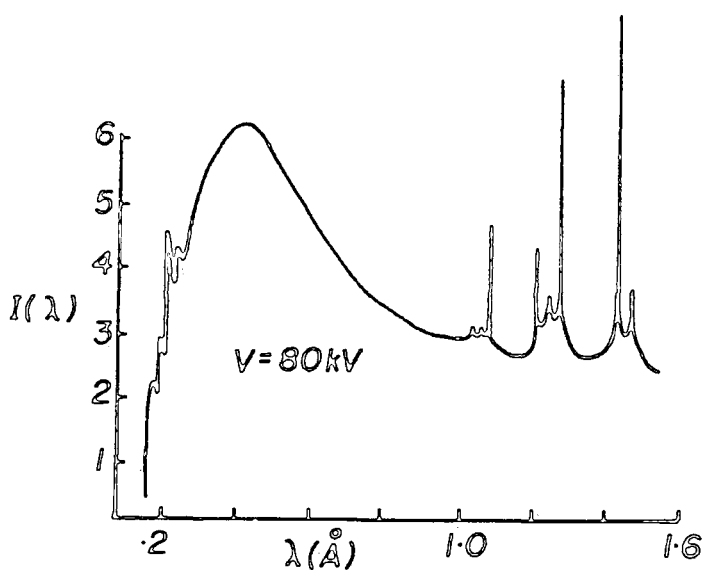


Figure 1.16 X-ray spectrum of tungsten

the target. The risk of target contamination from the sample being investigated is prevented by a thin aluminium window which isolates the area from the sample, the window also prevents interference due to electrons from the filament. Excitation of X-rays from the aluminium window is curtailed by operating the filament at near ground potential and the anode at high voltage.

The $\text{AlK}\alpha_{1,2}$ source is monochromatised using slit filtering and diffraction from the (100) plane of quartz at the Bragg angle of 78.3° . The use of dispersion compensation¹⁷ or rotating anodes improves the observed signal intensity.

1.4.3 Electron Energy Analyser

The analyser on the ES 300 is a hemispherical double focussing dispersive analyser based on the principle first proposed by Purcell.⁹⁴ The analyser is screened from external magnetic fields by means of two Mu metal shields. For ESCA studies a resolution of 1 in 10^4 is desirable. The resolution of this form of analyser is given by

$$\Delta E/E = W/R$$

where E is the energy of the electron, R is the mean radius of the hemispheres and W is the combined width of the entrance and exit slits.

The resolution may therefore be improved by

- (1) reducing the slit width, which reduces the signal intensity,
- (2) increasing the radius of the hemispheres; this increases engineering costs in manufacture and requires greater pumping,
- (3) retarding the electrons before entry into the analyser.

On the ES 300 a compromise is made on the slit widths to obtain sufficient signal intensity and the size of the hemispheres so as to keep costs down and prevent mechanical distortion. Preretardation of the electrons is carried out by a lens system which, as well as decreasing the resolution requirements of the analyser, also allows the analyser to be located at a convenient distance physically from the sample chamber. This latter feature allows maximum flexibility in sample handling and is especially important in gas phase studies where the gas load in the analyser is reduced by the greater distance between sample and analyser.

Electrons entering the analyser at the desired kinetic energy may be focussed at the detector slit by one of two methods,

- (1) scanning the retarding potential applied at the lens keeping the hemispheres potential constant: *i.e.* Fixed Analyser Transmission (FAT) mode,
- (2) simultaneously scanning the retarding potential and the potential between the analyser hemispheres, maintaining a constant ratio between the two, *i.e.* in Fixed Retardation Ratio mode (FRR).

Greater sensitivity is achieved using FAT mode at low kinetic energies (<500 eV) whereas FRR mode is more sensitive at higher kinetic energies. Castle has recently published a comparison of the two modes.³¹⁵

1.4.4 Electron detection and data acquisition.

Electrons of pre-selected energy pass from the analyser into an electron multiplier *via* the collector slit. The ES 300 employs a single channeltron electron multiplier, which gives an amplification of the signal by a factor of $\sim 10^7$. The use of multichannel detectors is now becoming prevalent in commercial spectrometers. The increase in rate of data acquisition afforded by multichannel detection will have a dramatic effect on the use of ESCA in the future.

In the single detector system on the ES 300 pulses from the multiplier are preamplified and fed into a rate meter. Spectra may be generated by two methods,

- (1) the continuous scan, where the electrostatic field is increased continuously at a known rate from a starting kinetic energy. The electron count from the ratemeter

versus the kinetic energy may be recorded on an X-Y plotter;

(2) the step scan, where the analyser voltage is increased by preset increments (*e.g.* 0.1 eV), and at each increment

(a) the counts may be measured for a fixed length of time, or (b) a fixed number of counts may be timed. The data so obtained may be stored in a multichannel analyser or onto floppy disc *via* a minicomputer.

The ES 300 is now mainly used in the step scan mode, with data acquisition under the control of a Kratos DS-300 data system. This system consists of an LSI 11/2 central processor unit interfaced to the spectrometer with control over excitation source, scan speed and kinetic energy. Data is dumped onto floppy discs for subsequent manipulation. A display package allows inspection of the data on disc and various treatments of the raw data, including background subtraction, smoothing, peak synthesis, spectra subtraction and addition, differentiation and so on.

1.5 Sample handling

1.5.1 Solids

Solids may be mounted on the probe tip in several ways, depending on the form of the sample *e.g.* for powders pressing onto either a soft metal backing, such as lead or indium or a wire mesh backing. Films or sheets may be clipped or screwed down onto the probe tip. Thin films may be deposited on an inert substrate, usually gold, by sublimation or evaporation from a suitable solvent. Alternatively sheet or powdered samples may be mounted onto double sided adhesive tape. Sample

charging effects will occur using this method but with suitable referencing these effects can be compensated for.

The ES 300 probes have facilities for use in the temperature range -178°C to $\sim 600^{\circ}\text{C}$. Cooling is carried out by pumping liquid nitrogen through the probe and heating is achieved by resistance heating. Both heating and cooling are thermostatically controlled, using a thermocouple to monitor the temperature. The provision of cooling enables solids which are slightly volatile to be studied. More volatile solids are usually sublimed from a capillary tube onto a cooled probe tip.

1.5.2 Liquids

The handling of liquids and solutions poses particular problems not encountered with solids or gases.⁶⁶ Heavy differential pumping is required to overcome the vapour pressures encountered and the liquid sample must be renewed continuously, particularly if solutions are investigated.

Siegbahn has developed three techniques for the study of liquids, where samples are studied in the form of submillimetre beams,¹⁰⁷ or as a wetted surface on either a wire¹⁰⁸ or a rotating cone.¹⁰⁹

The only technique for studying liquids on commercially available spectrometers involves the injection of the liquid into a heatable, evacuated reservoir shaft followed by diffusion of the vapour through a metrosil leak and subsequent condensation of the vapour onto a cooled gold substrate in UHV. Under these conditions the sample surface is continually reviewed thereby reducing contamination and radiation damage to a minimum.

1.5.3 Gases

Gas may be studied by confining the gas to a small volume in the spectrometer by the use of gas cells. Alternatively the gas may be studied in the solid phase by condensation onto a cooled substrate. Gas phase studies are not complicated¹⁹ by processes occurring in solids such as solid state broadening, inelastic losses and variable work functions, and so offer simpler comparison with theoretical calculations and the opportunity to observe shake-up and shake-off structure at energies further removed from the primary photoionisation peak.

1.6 General Aspects of ESCA

ESCA is an extremely powerful technique which provides a large number of information levels from a single experiment. These may be summarised as follows:

- (1) absolute binding energies, relative peak intensities shifts in binding energies. Elemental mapping for solids analytical depth profiling, identification of structural features, *etc.* Short range effects directly, longer range indirectly;
- (2) shake-up-shake-off satellites. Monopole excited states, energy separation with respect to direct photoionisation peaks and relative intensities of components of singlet and triplet origin. Short and longer range effects directly. (Analogue of U.V.):
- (3) multiplet effects. For paramagnetic systems, spin-state, distribution of unpaired electrons (analogue of e.s.r.):
- (4) valence energy levels, longer range effects directly:

(5) angular dependent studies. For solids with fixed arrangement of analyser and X-ray source, varying take off angle between sample and analyser provides means of differentiating surface from subsurface and bulk effects. For gases with variable angle between analyser and X-ray source, angular dependence of cross sections, asymmetry parameter β , symmetries of levels.

The wealth of information available from ESCA as outlined above is coupled with some general advantages of the technique. The sample requirements are minimal, the technique being capable of studying gases, liquids or solids with sample sizes being ~ 1 mg. of solid, $0.1 \mu\text{l}$ of liquid and $\sim 0.5 \text{ cm}^3$ of gas (at STP). These represent convenient sizes for sample handling, the technique has the sensitivity of detecting fractional monolayer coverage. Samples studied do not require elaborate preparation and may therefore be studied in their working environment. This has been found to be especially advantageous when ESCA is used in a 'trouble shooting' role. In the majority of cases sample damage is minimal since the X-ray flux is small ($0.1 \text{ millirad sec}^{-1}$). ESCA may be used to study any element in the periodic table with the exception of hydrogen and helium. This is in contrast to, for example, n.m.r. and n.q.r. whose application is dependent on the spin properties of the nucleus. A unique capability of ESCA is the ability to perform non-destructive analytical depth profiling enabling differentiation between surface, subsurface and bulk phenomena. Where depth profiling indicates homogeneity of the sample, data obtained from ESCA is often complementary for that obtained by other techniques.

Information obtained from ESCA is directly related to the molecular structure and bonding. Investigation of the valence and core levels of the molecule enables a thorough investigation of the electronic structure of the molecule. This has enabled a thorough understanding of processes occurring from a theoretical basis, and full advantage of the technique often requires a high level of theoretical competence.

The advantages listed above however should be compared with some disadvantages of the technique. The major drawback is the relatively poor overall chemical shift to linewidth ratio for core levels as a function of chemical environment. For example, for the C_{1s} levels the differences observed in binding energies between sp^3 , sp^2 and sp hybridised species is virtually swamped by the linewidth using a non-monochromatized photon source whereas in ^{13}C n.m.r. the shift linewidth ratio would be $\sim 10^3$. Although the depth resolution in ESCA is excellent over the range 0 to $\sim 120 \text{ \AA}$, the lateral resolution is poor, with an area of $\sim 0.3 \text{ cm}^2$ normally being sampled. The use of finely focussed X-rays in conjunction with multidetector systems will undoubtedly improve this, but for the spectrometer used in this thesis the spatial resolution is poor. The surface sensitivity of the technique does have the drawback when information about the bulk structure of a material is required but the surface differs from the bulk. However sectioning of the sample can overcome this problem and *in situ* fracture stages are now available commercially.

The vacuum system of an ESCA instrument, like any vacuum system, does require cautious attention. For clean metal surface studies the vacuum requirements are generally better than

10^{-10} , since monolayer oxygen coverage of a metal occurs over a very small time scale at higher pressures. For polymers the sticking coefficients are generally far lower, and 10^{-8} T is an acceptable working pressure. The use of vacuum interlocks is therefore feasible and these allow sample introduction and withdrawal over a matter of minutes.

The overall costs of ESCA instrumentation are comparable to a ^{13}C n.m.r. or standard mass spectrometer. The trend at present is to have multi-purpose surface science instruments which are capable of multiphoton XPS, ISS, SIMS, ACS and scanning auger microprobe analysis of samples where suitable. These systems are usually under minicomputer control and offer great flexibility in surface analysis.

CHAPTER TWO

FUNDAMENTAL ASPECTS OF
ELECTRON BEAM IRRADIATION

2.1 Introduction

This chapter introduces some of the processes involved in the bombardment of a solid by a beam of low energy electrons. The study of electron beam interactions with organic materials in particular originates from several sources. Technologically high energy ionising radiation has been a mode of polymer modification for over 30 years now, and although there is an extensive literature on the study of radiation effects in polymers it is true to say that progress in the elucidation of the fundamental processes involved has been slow and that many of the conclusions drawn from scattered experimental data over twenty years ago are just as valid today. The use of lower energy electron beams as tools in micro-electronic device manufacture had been advanced twenty-five years ago. With the development in electron beam resists technological interest in the physics of electron beam damage is widespread. However investigation of chemical processes involved have been somewhat neglected.

The degradation of organic materials, particularly bio-organic materials by electron beams has been of considerable interest to electron microscopists, although the chemical interactions have been neglected to some extent. Finally processes occurring during the electron beam excited acquisition of Auger spectra are of growing interest, with the problems of sample damage now being dealt with in a systemised fashion.

2.2 Fundamental aspects of low energy electron beam interactions with molecules and solids

2.2.1 Characteristic structure of an electron energy distribution

Some idea of the number of processes occurring on exposure of a solid to an electron beam may be ascertained by investigation of the energy distribution of electrons leaving a solid surface during bombardment by a primary beam of electrons. Such a distribution is shown in Figure 2.1(a) for bombardment of 1 keV and 1.25 keV electrons on Gallium Phosphide¹¹⁰ plus the electronically differentiated secondary electron distributions in Fig. 2.1(b).¹¹⁰ It should be noted

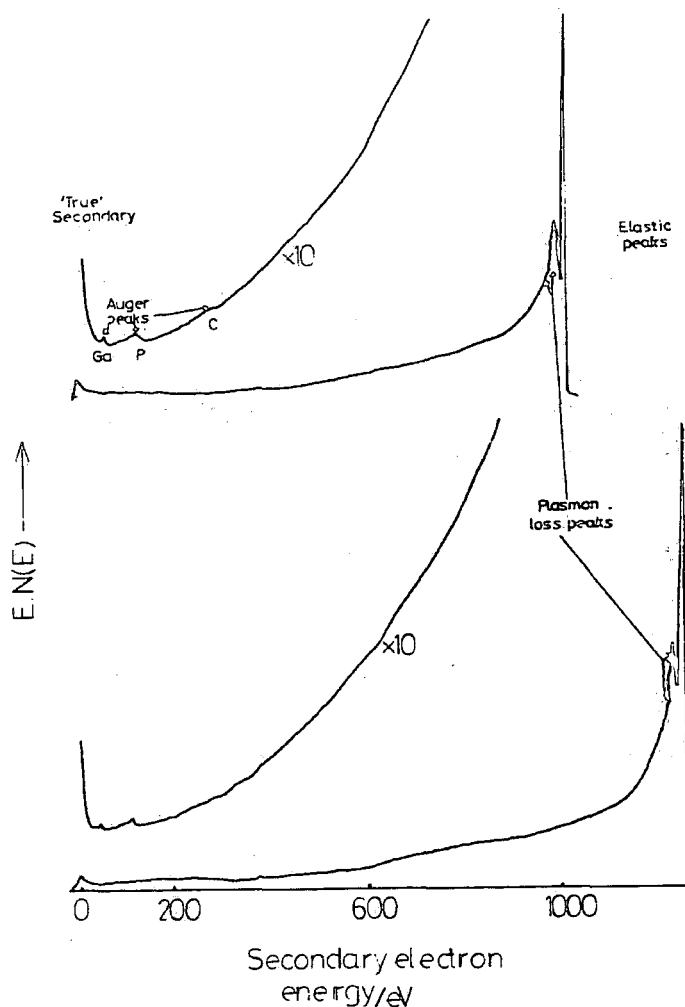


Figure 2.1(a) Secondary emission spectra from GaP for primary electron energies 1.25 keV and 1.0 keV

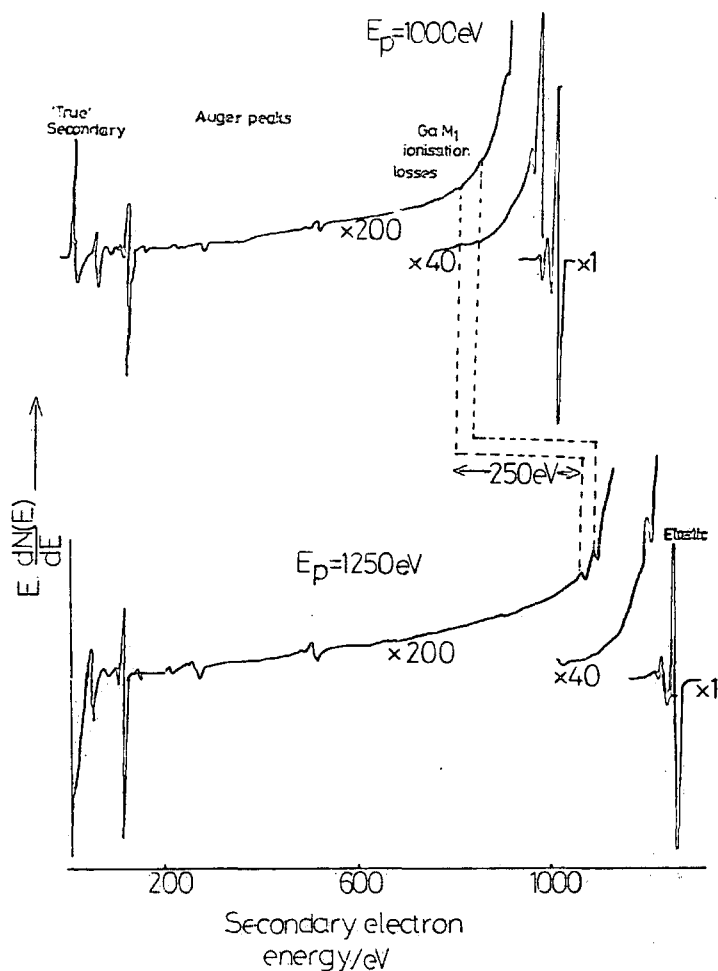


Figure 2.1(b) Electronically differentiated secondary emission spectra from GaP at primary electron energies 1.25 keV and 1.0 keV

that the distribution shown in Fig. 2.1(a) is such that the intensity at the lower kinetic energy end is strongly attenuated. However, Fig. 2.1(a) reveals that the most conspicuous feature is the elastic peak at the primary energy which corresponds to those electrons which have not lost any energy and have simply elastically rebounded from an ion core. These electrons cause little, if any, damage to the surface directly although the phonon energy imparted by them can cause heating at high doses.

It can be seen from Fig.2.1 that there are peaks whose absolute energy varies with E_p , the primary electron energy, but remain constantly shifted in energy from E_p . These are discrete energy loss peaks and can be classified under two headings, (i) Plasmon Loss Peaks and (ii) Ionisation Loss Peaks.

(i) Plasmon Loss Peaks

The movement of an electron through a solid causes a perturbation of the potential which normally influences the valence band electrons. The valence electrons respond to this change in potential by collectively oscillating at the so-called plasmon frequency, which corresponds to the point at which the dielectric function is a minimum and the system responds with a polarisation equal in magnitude but opposite in sign to the field applied by the primary electron. There is a finite probability that the primary electron will lose an amount of energy since the response is moderately long-lived compared to the primary electron transit time. Since the valence electrons respond most strongly at the plasmon frequency then the energy loss is equal to the plasmon energy given by equation 2.1.

$$\hbar\omega_p = \hbar(4\pi ne^2/M_e)^{1/2} \quad \text{eqn. 2.1}$$

where n is the electron density, e is the electron charge, and M_e the electron mass

Plasmon excitations are a collective response and so correspond to a "classical" free electron gas model. In polymers plasmon peaks are also observed in, for example, ESCA¹¹¹ and Electron Energy Loss Spectroscopy (EELS).¹¹²

Plasmon loss peaks in electron spectroscopies exhibit further structure due to surface and bulk excitations, where the surface plasmon frequency is $\frac{1}{\sqrt{2}}$ that of the bulk plasmon. Also present in the EELS spectra of polymeric systems are peaks which may be adequately described within a one electron model, namely excitations of a single electron to an unoccupied level. Thus for polystyrene $\pi \rightarrow \pi^*$ peaks are clearly observed, and excitations of deeper lying levels, e.g. $6 \rightarrow 6^*$ etc. are also present, but obscured by the collective plasmon excitation peaks. ¹¹³

(ii) Ionisation Losses

Ionisation of either a core or valence electron will cause the primary electron to lose some of its initial energy. For a primary energy E_p and binding energy of the level which has been ionised E_B the final state of the system following ionisation will contain an ion of energy D_B and two electrons whose kinetic energy is $E_p - E_B$ in total. This energy may be partitioned in any between the two electrons, with an extreme leaving one electron at the Fermi level and the other with energy $E_p - E_B$. Thus the electron distribution measured contains loss 'peaks' in the region $0 - E_p - E_B$ and are so blurred that electronic manipulation of the spectrum, by differentiation can reveal the ionisation loss peak at $E_p - E_B$.

Peaks in Figs.2.1 which are independent of the primary electron energy are due to processes which happen over a time scale long enough that they essentially lose 'memory' of the primary event. These peaks may be separated into two groups: (i) those arising from Auger processes and (ii) those due to 'true' secondary electrons.

(iii) Auger Electrons

Auger peaks may be observed in Fig.2.1(a) as slight features residing on a very large background. As mentioned in Chapter One Auger electrons are a result of de-excitation of a core hole state by an electron in a higher level filling the core hole and a concomitant elimination of an electron from an upper level. The process of Auger emission is slow compared to the primary ionisation process and so the Auger electrons have energies independent of the primary electron energy. The Auger peaks observed in Figs.2.1(a) and 2.1(b) are due to electrons which have not undergone any energy loss after the Auger event. Unobservable Auger electrons which have undergone energy losses will make up part of the background in the kinetic energy range $0-E_A$ where E_A is the kinetic energy of the Auger electron. Enhancement of the Auger signal by electronic differentiation of the electron distribution was first carried out by Harris¹¹⁴ in 1968 after Lander¹¹⁵ and Hagstrum¹¹⁶ had pointed out the presence of Auger peaks in electron and ion excited secondary electron distributions respectively.

Shortly after Harris's achievement Weber and Peria¹¹⁷ showed that LEED systems could provide suitable electron detection for derivative Auger analysis. With the development of the cylindrical mirror analyser system¹¹⁸ a real upturn in Auger electron spectroscopy occurred. Although mainly used for elemental analysis in 1971 the possibility of obtaining information on a molecular level from Aes was demonstrated.¹¹⁹

Further indications of the potential of molecular Auger spectroscopy particularly for organic systems have come

from the work at the Sandia Laboratories in the U.S.A., which has been the subject of several recent reviews.^{130,185,186,187} The Auger lineshape obtained is in principle sensitive to the local electronic environment since the initial core hole is spatially localised. Thus for core-valence valence (KVV) transitions the Auger lineshape should reveal general "fingerprint" structures containing information about the local symmetry and hybridisation of the atom with the initial core hole.¹⁸⁷ This has been illustrated in the series of alkanes from methane up to n-hexane where general features corresponding to an sp^3 hybridised system can be deduced (Fig. 2.2).¹⁸⁸ Using methane as a model system it can be deduced that the large main peak at ~ 250 eV is due to two final hole states in 2p type molecular orbitals, those at ~ 230 eV are due to a double hole in the 2s levels and features in between correspond to one hole in a 2s and one hole in a 2p level. The complexity of the Auger process however makes complete theoretical analysis of more complex systems infeasible since the number of Auger transitions in a system with N filled valence orbitals is N^2 (although some may lead to degenerate final states). Thus in methane (4 valence levels) a maximum of 16 Auger transitions are possible but in n-hexane (19 filled valence levels) the possible 361 Auger states would preclude a treatment based on, say, Δ SCF methods. However general features may be dealt with semi-quantitatively using several theoretical models. The sensitivity of Auger lineshapes to hybridisation may be amply demonstrated by comparison of the spectra obtained for methane, ethylene and acetylene shown in Fig. 2.3. It is worthwhile contrasting the difference with the similarities obtained for the core hole ESCA spectra of these molecules which do not significantly change in position and the only difference will

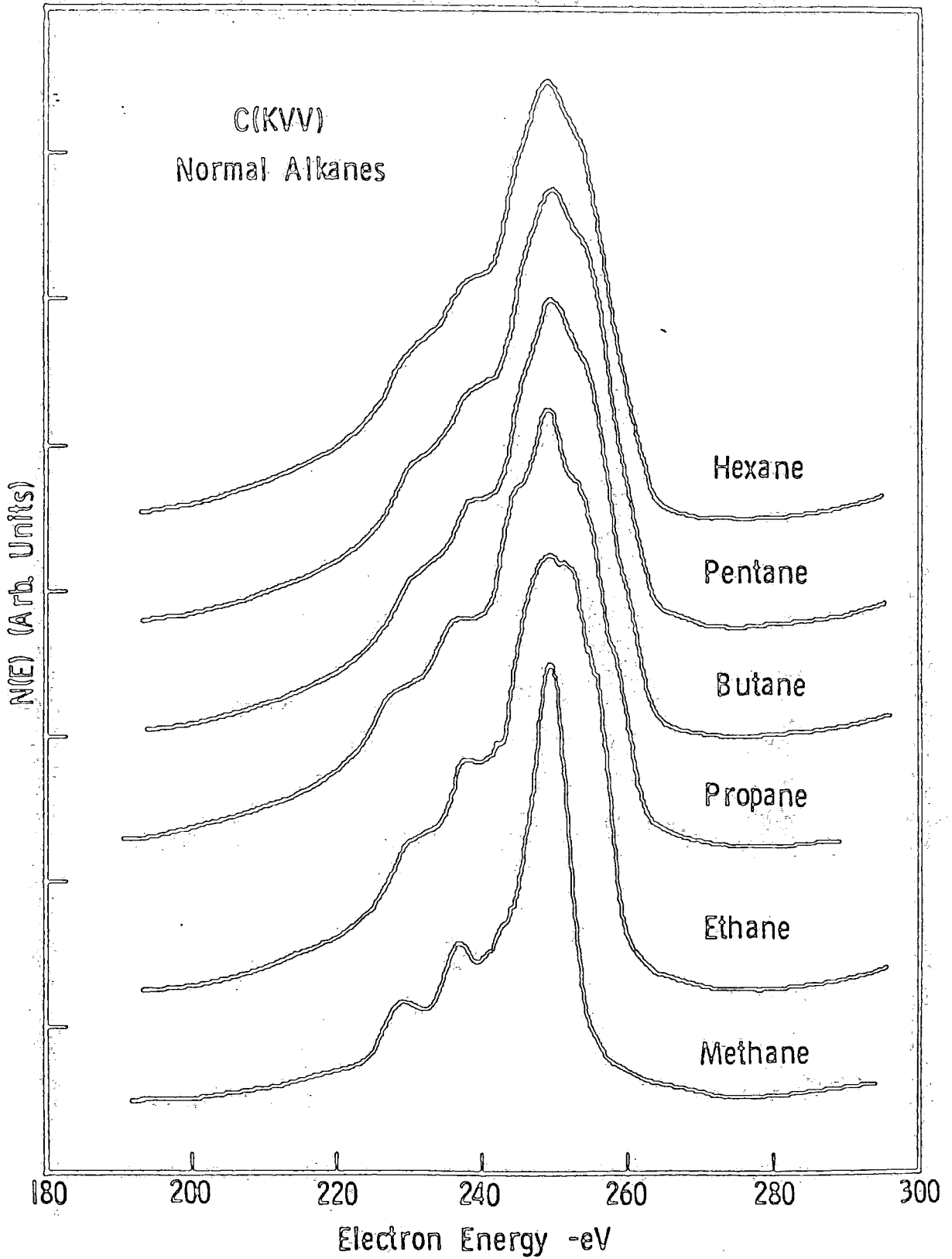


Figure 2.2 C KVV Auger spectra of a series of gaseous alkanes

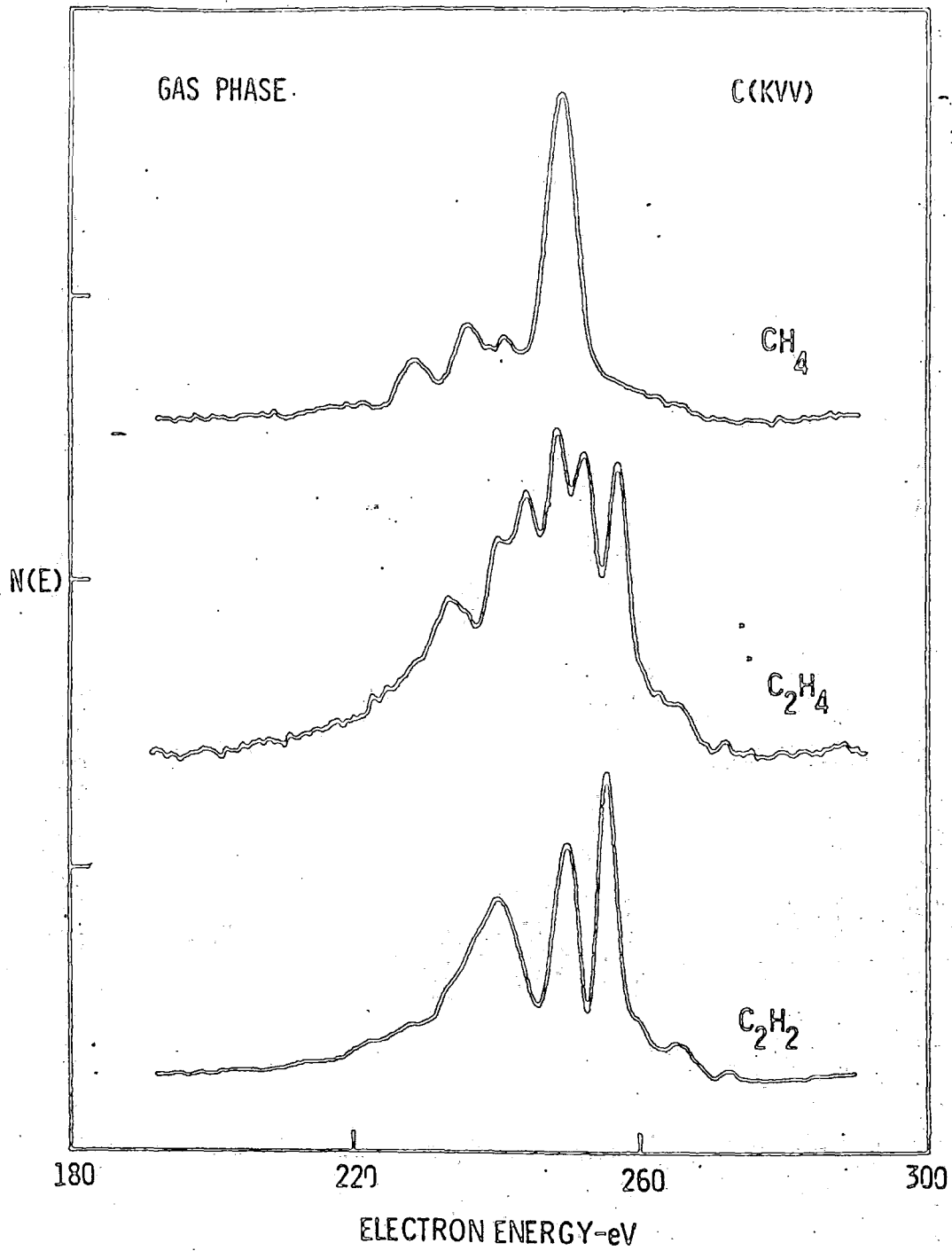


Figure 2.3 C KVV Auger spectra of methane, ethylene and acetylene

be the change in the features due to shake-up transitions.

The lack of any significant shift in the series of alkane spectra implies that the relative coulomb interaction between the final state holes, U_{eff} remains the same, since the KE of the Auger electrons is given by the relationship

$$\text{KE} = I_{\text{c}} - I_{\text{j}} - I_{\text{k}} - U_{\text{eff}} \quad ^{187}$$

where the I 's are the valence (j, k) and core (c) are electron energies. Thus the pair of holes is confined or localised to approximately the same spatial extent in the alkanes as in methane.¹⁸⁸ The same behaviour is shown by polyethylene¹⁸⁹ and the cycloalkanes¹⁹⁰ whereas the Auger spectrum of benzene indicates¹⁸⁷ that spectral contributions arising from the σ backbone structure are essentially the same as ethylene, *i.e.* a localised final z hole whereas those from the π system indicate the double hole is delocalised. Such delocalisation in the upper valence orbitals of the higher alkanes are shown by subtle differences in the high energy regions of the spectra in Fig. 2.2.

The relative intensities of transitions within a KVV envelope can also give information on the relative electron density of an orbital on an atom. Thus the nitrogen carbon KVV spectra of methylcyanide¹⁸⁷ when shifted to the same relative energy scale show transitions of the same relative energy but differing intensities (Fig. 2.4). The dramatic difference is the extra peak in the carbon KVV spectrum which is due to a transition involving final holes in the methyl group which has little density on the nitrogen atom. This effect is seen, but to a lesser extent, in most heteroatomic molecules.

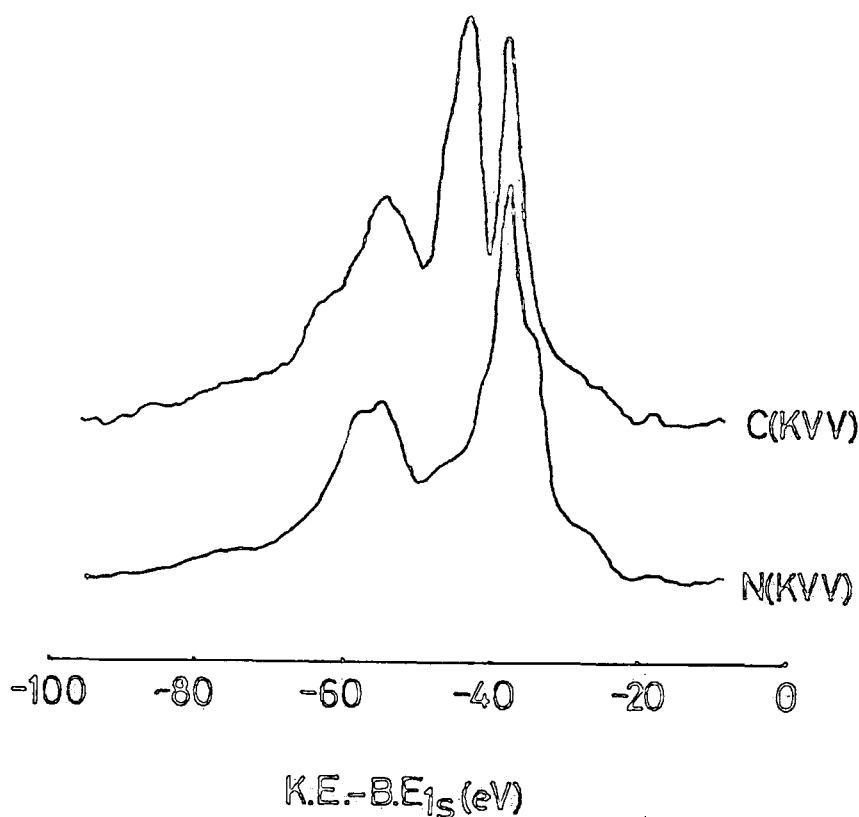


Figure 2.4 N KVV and C KVV Auger spectra of methyl cyanide (CH₃CN)

Solid phase Auger spectra are complicated by broadening, background and energy loss processes but with sufficient data manipulation these effects can be reduced to give spectra of sufficient integrity to compare with calculated or measured electronic structures.^{185,186} Thus fingerprint spectra of several condensed phase organic compounds and polymers have been published. However the extreme complexity of the KVV spectra of polyethylene¹⁸⁹ and poly(methylene oxide)¹⁸⁹ makes direct interpretation of features present in the Auger line-shapes very difficult. An interesting approach has been used by Gaarenstroom¹⁹¹ for the interpretation of the C KVV spectra of a series of n-alkyl methacrylates, based on factor analysis

of the Fourier transformed spectra. Gaarenstroom found that reasonable correlation could be found between the contributions from alkane chain and methacrylate components with the expected values from the structure of the polymers.

(iv) 'True' secondary electrons

The electrons found at the low energy end of the secondary electron distribution constitute the majority of the current leaving the sample during bombardment.¹¹⁰ Electrons of 100 eV kinetic energy or less result from pair production cascade processes in which the primary beam excites electrons from the valence band which, in turn, may have enough energy to excite other valence band electrons and so on. The net effect is to build up an energy distribution in the solid of slow electrons which has its peak below the vacuum level. The observed secondary electron distribution is a convolution of this internal energy distribution and an escape function which is dependent mainly on electron energy and depth below the surface.

Secondary emission was first observed in 1902¹²⁰ and since that time the phenomenon has been extensively investigated for a whole range of materials.^{121,122,123} The secondary electron yield δ is defined as

$$\delta = \frac{I_s}{I_p} = \frac{n_s}{n_p}$$

where I_s and I_p are the respective secondary electron and primary electron currents and n_s, n_p are the numbers of secondary and primary electrons.

Several theories have been developed to explain the

secondary yield *versus* primary energy curves obtained, examples of which are shown in Fig. 2.5.¹²² It can be seen that the yield increases from 0eV primary energy, reaches a maximum value and then gradually decreases. For metals and semiconductors the maximum yield is typically between 0.5 and 1.8,¹²² for insulators values of over 20 have been reported. Polymers have maximum yields at ~ 250 eV which have values between 1.7 and 2.5. 124,125

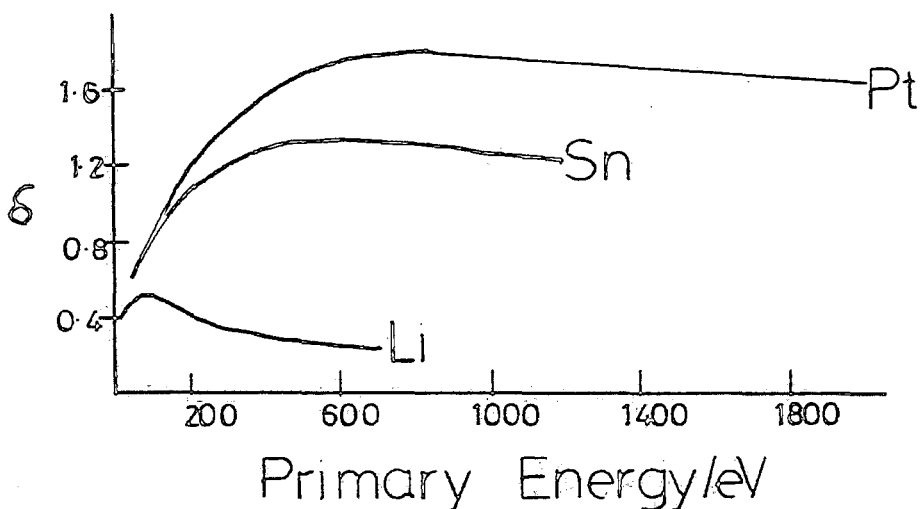


Figure 2.5 Variation of the secondary electron yield, δ , with primary electron energy

Semiempirical secondary electron emission theory is based on the assumption that the secondary yield δ as a function of the energy E_0 of the incident primaries may be written in the form¹²⁶

$$\delta = \int n(x, E_0) f(x) dx \quad \text{eqn. 2.2}$$

where $n(x, E_0) dx$ represents the average number of secondaries produced per incident primary in a layer thickness dx , at a

depth x below the surface; $f(x)$ represents the probability of escape of the secondary electron. $f(x)$ may be assumed to follow an exponential absorption law, *viz.*

$$f(x) = Be^{-\alpha x} \quad \text{eqn. 2.3}$$

and $n(x, E_0)$ is proportional to the average energy loss per unit path length, $\frac{-dE}{dx}$, per incident primary.

$$\text{Thus } \delta = -\left(\frac{B}{\epsilon}\right) \int \left(\frac{dE}{dx}\right) e^{-\alpha x} dx \quad \text{eqn. 2.4}$$

Equation 2.4 does not take any account of the energy distribution of secondaries, and the escape function is assumed to be exponential, with suitable choice of the form of the primary loss function, $\frac{dE}{dx}$, good agreement between experiment and theory is found in the case of polymers.¹²⁴

It should be emphasised that the secondary emission distribution is not the same as the secondary electron distribution in the solid, since the probability of escape for lower energy electrons, especially those between the Fermi level and the vacuum level of the solid is very low. However there is a very large number of these electrons, as is illustrated in Fig. 2.6,¹¹⁰ and a significant proportion of the effects of electron beam irradiation is due to these electrons. In a conductor these electrons would occupy a conduction band and cause minimal damage. In an insulator however such low energy electrons have favourable cross sections for excitation and attachment, points which will be discussed later.

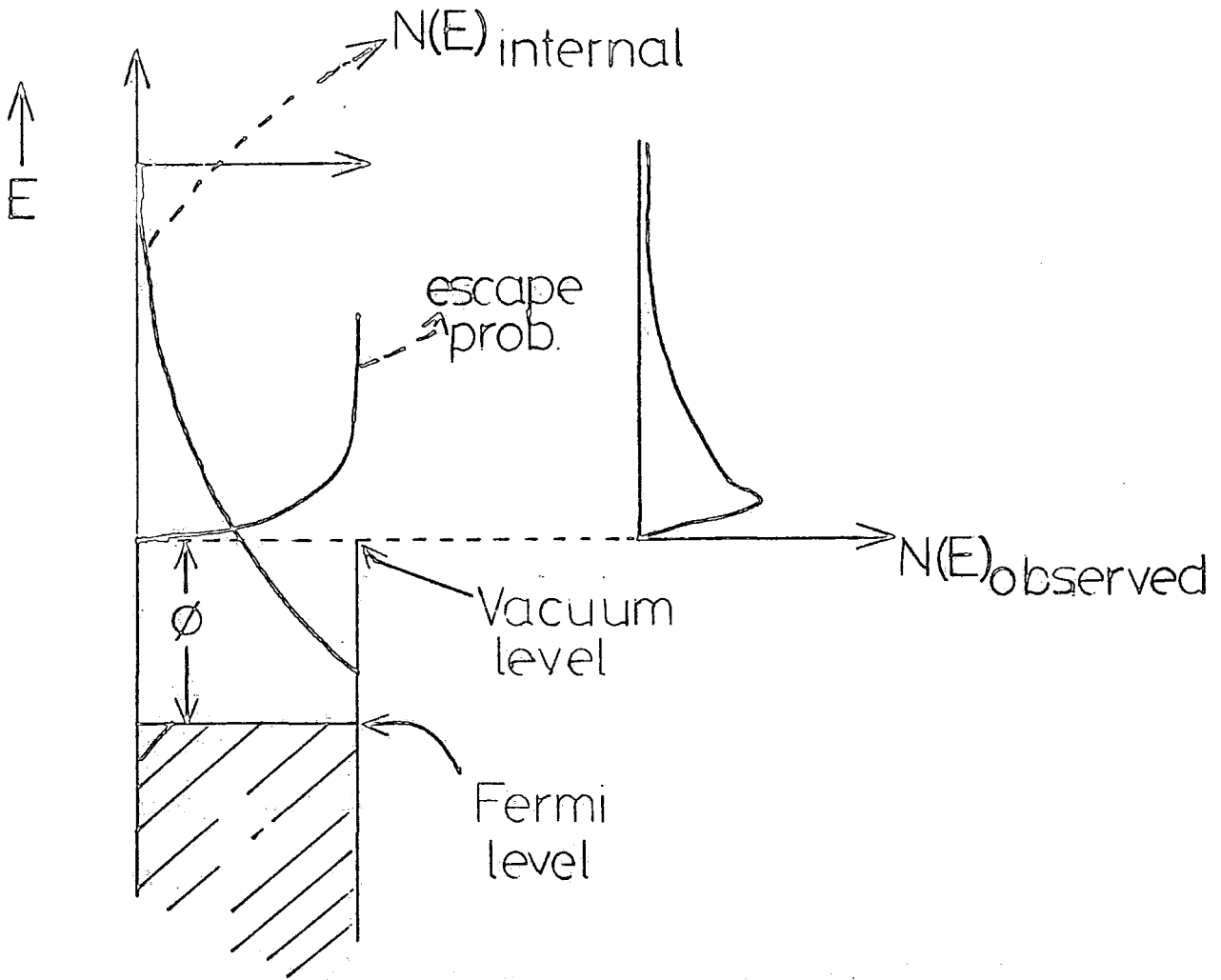


Figure 2.6 Schematic of the variation of escape probability, internal electron energy distribution and its convolutive effect on the observed secondary electron emission distribution

2.2.2 Electronic processes occurring in electron bombardment

(i) Introduction

Section 2 briefly detailed the form of the energy distribution of electrons leaving a sample. The features observed in such a distribution give an indication of the pro-

cesses occurring in a solid. It is worthwhile to take a closer look at these processes in the light of the discussion in Section 2.2.1. Ionisation and excitation are apparent from the secondary distribution. The large number of slow electrons will undoubtedly cause some degree of electron attachment to occur. Excited, ionised or attached species will cause chemical changes in the irradiated material and in the remainder of this section a discussion will be presented on the three processes.

(ii) Ionisation by electron impact

Electrons with energy greater than the binding energy of a bound electron have a finite probability of causing ionisation of the bound electron. The cross sections of ionisation by electron impact are not fully tabulated although Gryzinski¹²⁷ has derived a semiempirical relation for the cross section relating the binding energy of a level with the incident electron energy, as shown in eqn. 2.5

$$\sigma = \left(\frac{N \times 6.56 \times 10^{-18}}{\text{B.E.}^2} \right) \frac{1}{x} \left(\frac{x-1}{x+1} \right) \left\{ 1 + \frac{2}{3} \left(1 - \frac{1}{2x} \right) \ln(2.7 + (x-1)^{\frac{1}{2}}) \right\}$$

eqn. 2.5

where $x = \frac{\text{incident electron energy}}{\text{B.E.}}$

Figure 2.7 shows the variation of this cross section for electron energies 0→2500eV of levels corresponding to the Carbon 1s (BE=285), the fluorine 1s (BE=690) and a level with BE=20, *i.e.* corresponding to the middle of typical valence bands. It can clearly be seen from Fig. 2.7 that the cross section is substantially larger for the 20eV level compared to C_{1s} and F_{1s} ionisation, by a factor of ~10²-10³. Valence level excitation is therefore significantly favoured, especially since a large

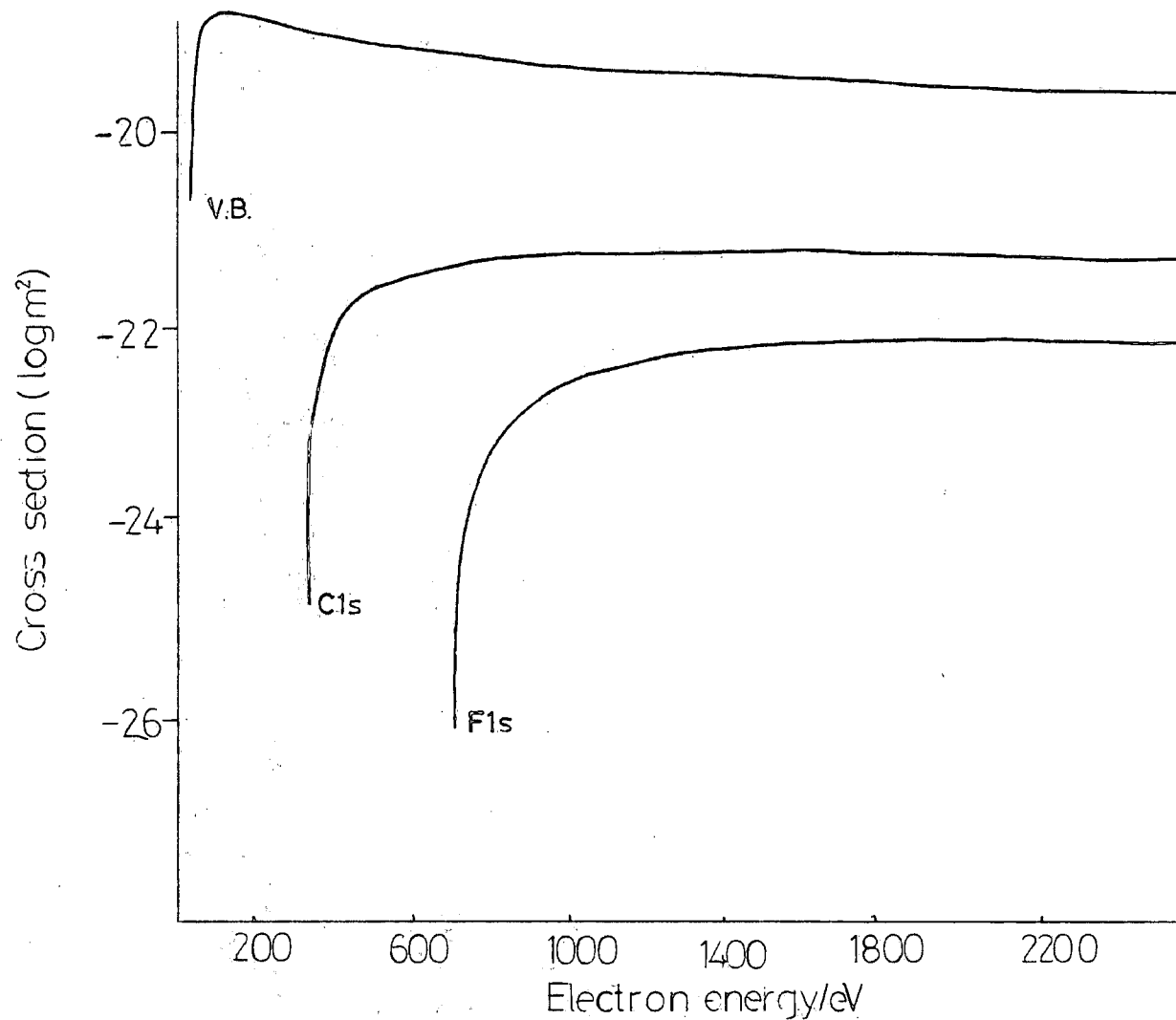


Figure 2.7 Grysinski cross sections as a function of primary electron energy for binding energies appropriate to F_{1s}, C_{1s} and valence band ionisation

proportion of secondary electrons are at energies below the core level binding energies. Ionisation by low energy electrons is, of course, the means of ion production in conventional mass spectroscopy, and there is growing interest in the use of electron beams for the generation of ions at surfaces^{128,129} in order to perform analogous analysis to that obtained from Secondary Ion Mass Spectrometry utilising the Electron Stimulated Desorption (ESD) process. It is also worth pointing out at this stage that core excitation by soft X-rays (e.g. $Mg_{K\alpha_{1,2}}$) has about the same order of magnitude cross section as electron excitation,¹³⁰ although valence ionisation is considerably less probable in the photon case. In metals ionised species are quickly neutralised by free conduction electrons, however in insulators no such neutralisation is possible and the system may eliminate a positive ion accompanied by rearrangement or crosslinking.

(iii) Excitation by electrons

Excitation induced by light is a result of the radiation's electromagnetic field on the molecular electrons. Analogously the force induced on molecular electrons by an incident electron of relatively high energy is of similar electromagnetic origin, mainly as a result of coulombic interaction between these electrons. The selection rules will be analogous to those for optical excitations because of the similarity of the processes involved.¹³⁴ However when the incident electron is of relatively low energy, of the order of a few tens of electron volts, then exchange interactions between the incident and molecular electrons can occur.¹³⁵

The result is an electronic transition in which the spin angular momentum changes by one, so that if the initial state is a singlet then the final state will be a triplet as a result of spin exchange. The cross section for such a process is still lower than for an optically allowed excitation, but by a factor of typically 10^{-2} ¹³² compared to a factor of 10^{-6} observed in optical excitation.

Studies of electron induced excitation of molecules have been carried out using several methods. ^{131,132} The most adaptable technique involves measurement of the energies of an initially constant energy electron beam scattered by the material under study and is known as Electron Energy Loss Spectroscopy. The excitation cross sections are found to follow the Born approximation ¹³¹ for higher energy ($\sim 200\text{eV}$) bombardment, *viz.* for optically allowed transitions

$$\sigma \propto \frac{\ln E_p}{E_p}$$

and for disallowed transitions

$$\sigma \propto 1/E_p$$

Thus the cross sections falls off faster in the disallowed case. Measurement of absolute cross sections of molecules by EELS is rare, but theoretically determined cross sections for various states of benzene ¹³⁶ are shown in Fig. 2.8. As can be seen from Fig. 2.8 the triplet excitations cross sections fall faster than those for the singlet with increasing incident electron energy. The electron energy region where the cross section is highest for all states considered is from ~ 5 to 10eV , *i.e.* at energies where there is a large secondary electron distribution in a solid bombarded by an electron beam.

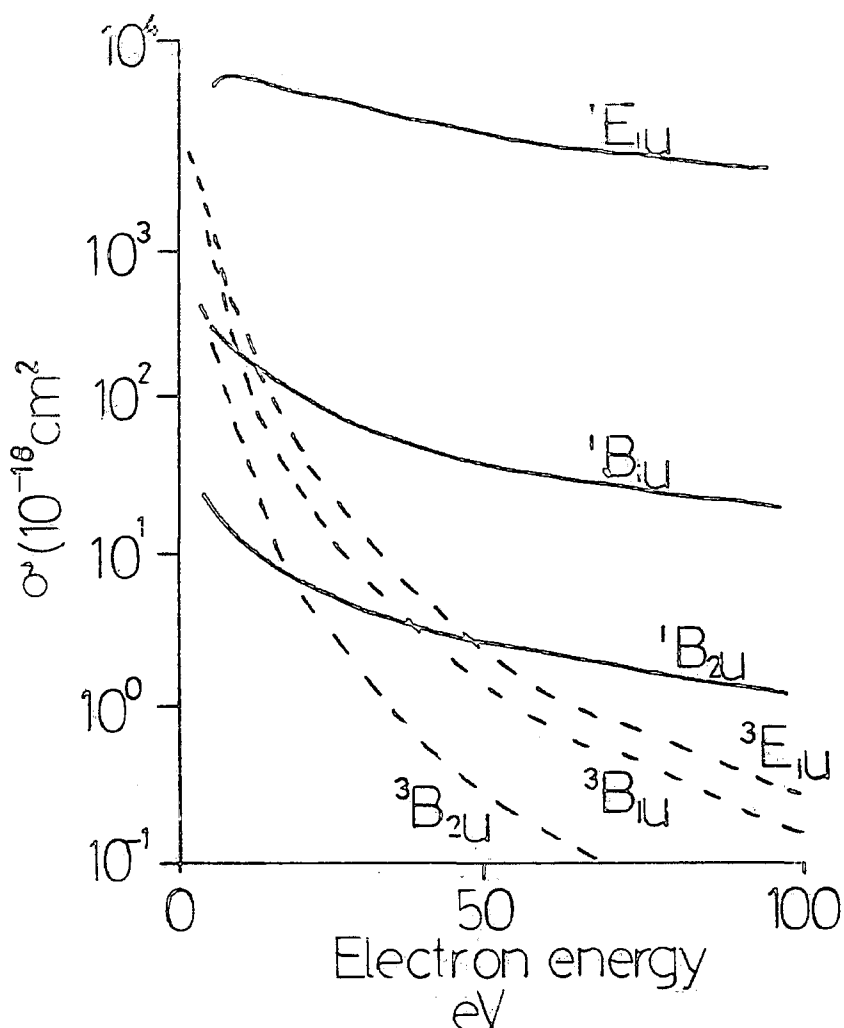


Figure 2.8 Excitation cross sections for various final states in benzene over the electron energy range 0-100eV (The dotted lines are optically forbidden)

It is also worthwhile to compare the data in Fig.2.8 with Fig.2.7. The cross sections for ionisation from a level of BE=20eV is seen to be of the same order of magnitude as excitation to the 1E_u state in benzene for electrons in the energy range 0-100eV. Electron impact ionisation cross sections calculated for benzene by Seu and Basu¹³⁷ also indicate that π electron ionisation cross sections are within the same order of magnitude as excitation.

EELS studies of polymer films have been performed by several workers,¹³⁸⁻¹⁴² generally using higher energy electrons. Earlier investigations¹³⁸ were hampered by electron

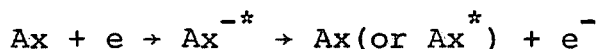
beam induced damage and contamination of the samples but recent studies have shown that with suitable control of the beam effects data obtained from EELS can be complementary with results of optical experiments.^{139,140} Also evident in the EELS spectra of poly(methylmethacrylate)¹⁴⁰ poly(styrene)¹³⁹ and poly(vinylpyridine)¹³⁹ are core electron excitations to unfilled molecular orbitals, although the relative intensities of the exciton spectra are not reported.

(iv) Electron Attachment

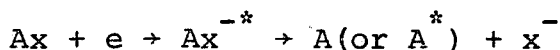
Negative ions of atoms or molecules may be generally considered to have been formed when the incoming electron is associated with the atom or molecule for a time longer than the transit time of the electron. Electron attachment to numerous molecules has been studied extensively by Christophorou and co-workers¹⁴³ using very low energy (0-10eV) electrons, with particular emphasis on benzene and the benzene derivatives.

The lifetimes of negative ions formed by electron attachment can vary from 10^{-15} s to greater than 10^{-6} s.¹³¹ The transient molecular ion can decay through one of three competing processes:

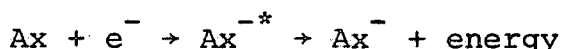
(a) Autoionization



(b) Dissociative detachment



(c) Radiative or collisionally stabilisation



Electron attachment cross sections have been reported for hexafluorobenzene¹⁴⁴ and benzene¹⁴⁵ for the latter molecule

a very large value ($\sim 10^{-14}$ cm) is seen at electron energies close to 0eV. The attachment cross section for benzene over a limited energy range is shown in Fig. 2.9 which corresponds to the attached electron occupying the highest virtual π orbital.

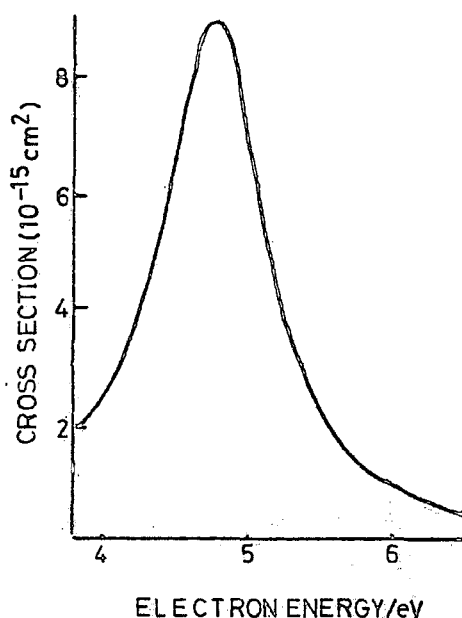


Figure 2.9 Cross sections for electron attachment to Benzene

It can be seen from Fig. 2.9 that the cross sections are larger than cross sections found for ionisation and excitation, but the electron attachment cross section does fall off dramatically outside of a small energy range. Cross sections for dissociative electron attachment have also been reported by Christophorou and coworkers for a series of halobenzenes,³⁹ as shown in Fig. 2.10. The absolute values are similar to values found for ionisation and excitation, the major difference again being that the dissociative attachment cross sections

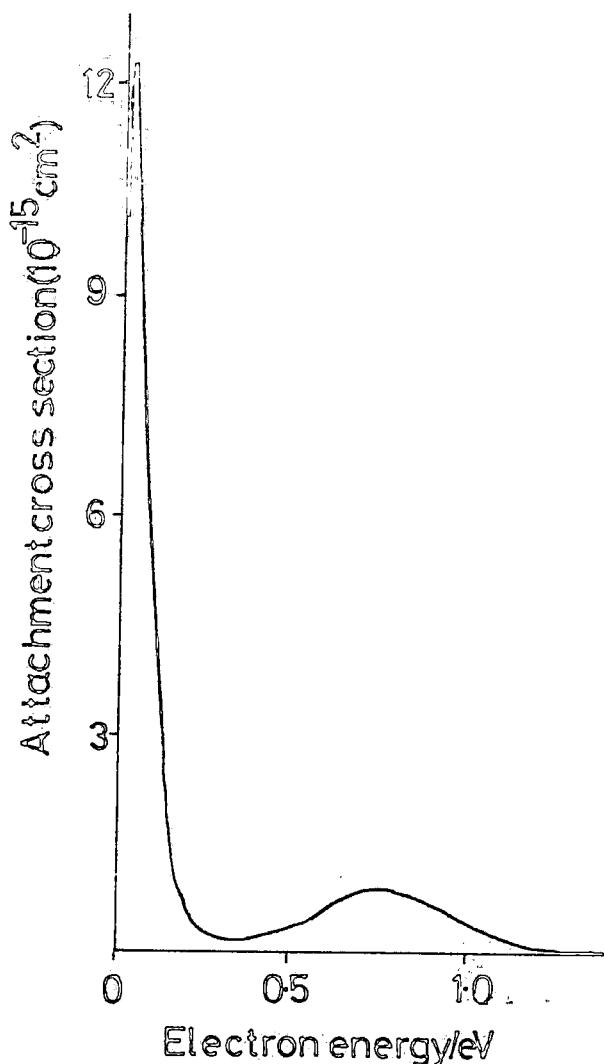


Figure 2.10 Cross sections for electron attachment for perfluorobenzene

are significant over a very small electron energy range in which excitation and ionisation are not possible. Detachment will be thermodynamically favoured even for attachment by 0eV electrons if the electron affinity of the halogen is greater than the bond dissociation energy of the halogen substituent. 131

2.2.3 Primary damage processes resulting from excitation, ionisation and electron attachment

(i) Electron Stimulated Desorption (ESD)

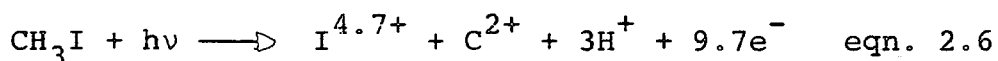
ESD was a term originally applied to desorption of

adsorbed molecules on surfaces under the action of an electron beam¹⁴⁶ but is now generally applied to desorption of ions or neutral fragments from ionic and covalent surfaces undergoing electron irradiation.

Ionic desorption from the surface is usually discussed in the context of two different models. In the Menzel-Gauer-Redhead (MGR)^{147,148} model the initiating process to desorption is valence ionisation or excitation. The Knotek-Feibelman¹⁴⁸ model indicates that core ionisation by the impinging electron beam is a primary process. It is worthwhile to discuss these models in somewhat greater detail. The MGR model assumes that the primary event is a Frank-Condon excitation or ionisation to a repulsive neutral or ionic state, therefore leaving a one hole-one electron state and a one hole excited state respectively. The repulsive nature of the states formed causes dissociation or desorption of the species involved. Evidence for the MGR model is supplied by the observation of desorption thresholds in the valence region¹⁴⁹ and by the dominance of the neutral yield over the ion yield, with neutrals contributing 95% of the total yield in some cases.¹⁴⁹

The Knotek-Feibelman model,¹⁴⁸ which is particularly applicable to highly ionic, *i.e.* maximal valency, systems, involves initial ionisation of a core level followed by Auger decay of the core hole to a state containing at least two holes. The expulsion of a positive ion takes place from the effective reversal of the Madelung potential. The so-called 'Coulomb explosion',¹⁵¹ is an extreme example of such a process. In methyl iodide, for example, ionisation of a deep lying core level of the iodine atom causes a multiple Auger vacancy cascade to occur, and when the vacancies reach the valence shell elect-

rons are transferred from the other atoms leaving a collection of multiply charged ions in close proximity to each other. The ions then recoil from one another due to the Coulombic repulsion, gaining considerable recoil energy. This process has been studied experimentally^{152,153} and for methyl iodide the results indicated the process occurring could be summarised as in eq. 2.6



Recent work has shown that the KF and MGR mechanisms may both be operable to some extent in certain systems.¹⁵⁴ ESD of molecule ions from¹⁵⁵ condensed phase neopentane, methylsilane and other branched alkanes suggest that multi-electron, or rather 'multihole' states may be involved in the dissociation of large molecules. Thus in a comparison of threshold energies for production of H^+ from alkanes and F^+ from fluoroalkanes,¹⁵⁶ in the latter case ionisation of the C_{2s} levels was close to the thresholds obtained, whereas for F^+ a threshold at $\sim 40\text{eV}$ electron energy corresponding to F_{2s} ionisation (when a work function correction for the incoming electron is applied). No ionic desorption of any ions was observed in the region appropriate to F_{2p} or C_{2p} ionisation thus the mechanism of ionic desorption was attributed to initial deep valence ionisation followed by decay of this state to multi hole upper valence states.^{155,156} Increased yields were also observed at 55eV ¹⁵⁶ electron energies, and this was again taken as being indicative of the role of multiply ionised/excited states in desorption processes.^{156,155}

(ii) Electron Stimulated Adsorption (ESA)

Electron stimulated adsorption is usually caused by electronic excitation and/or dissociation of a molecule in the gas phase above the surface, or of a molecule weakly bound to a surface. Interaction of the electronically excited molecule or atom with the surface can lead to adsorption and surface reaction.

This process is the first step in the polymerisation of residual pump oil vapours on surfaces and has been observed in electron microscopy investigations since the 1930s. The introduction to Chapter Five of this thesis contains a thorough review of such 'polymerisation' processes.

In electron excited Auger electron spectroscopy electron stimulated adsorption has been observed on various substrates,¹⁵⁷ chiefly clean metals and silicon, where enhanced reaction and adsorption is observed during simultaneous electron irradiation and gas exposure, and are dealt with in the next section.

(iii) Beam effects observed in Auger electron spectroscopy

ESD and ESA are frequently observed in Aes studies of inorganic and semiconducting materials. The subject has recently been reviewed by Pantano and Madey,¹⁵⁷ who define a damage threshold as being the dose required to cause a 10% change in concentration of the particular system investigated. Most inorganic and organic solids are found to exhibit critical doses in the range 10^{-4} - 10^{-2} C/cm²,¹⁵⁷ which corresponds to a 0.5 μ A beam, .5mm in diameter exposure time of between .4 and

40s. There have to date been few reports of solid phase electron excited Aes studies of polymers and organic materials, mainly as a result of the expected high degree of beam damage, and charging of the polymer giving poor peak resolution. One exception is the Aes study of condensed multilayers of $(\text{CH}_3)_2\text{O}$, CH_3OH and H_2O ,¹⁵⁸ where detectable changes in the Auger and ESCA lineshapes were observed after a dose of only $5 \times 10^{-4} \text{C/cm}^2$. Water and hydrocarbons were found in the irradiated system by thermal desorption spectroscopy and these were assumed to have been formed in the irradiation process.

Charging of insulators in Aes can cause migration of mobile ions present in the surface region.¹⁵⁷ When the secondary electron yield is greater than unity a positive charge develops on the surface of the sample. Localised accumulation of electrons in the subsurface can also result in a deeper net negative charge. The resultant electric field can cause migration of anions to the surface and cations to the subsurface,¹⁵⁹ as shown in Fig.2.11. A final effect observed in Aes is due

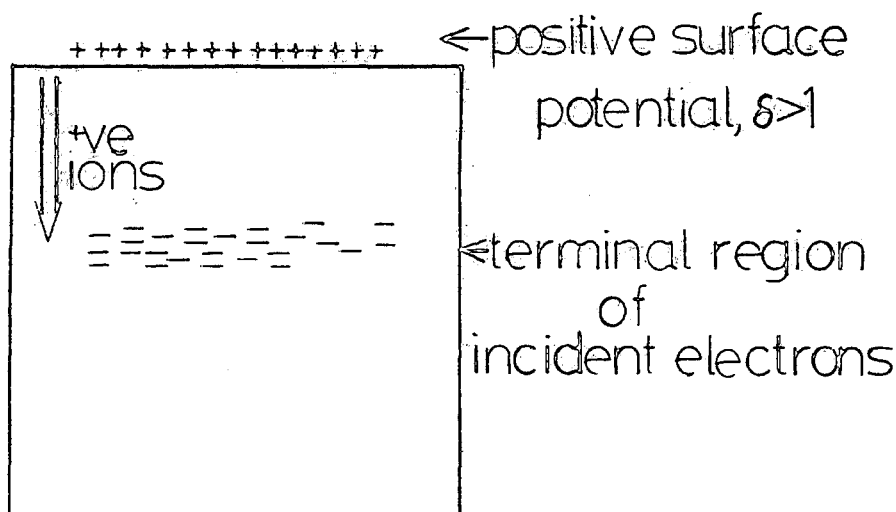


Fig. 2.11 Charge induced migration of ions

to beam heating.¹⁶⁰ When finely focussed, high current electron beams are used temperatures higher than 500°C can occur in insulators. For a current density of 1mA/cm² temperatures of ~250°C have been reported.¹⁶¹ For the typical current densities used in this thesis heating may be assumed to be negligible however.

2.3 Pathlengths of Electrons

Although the mean free path of, for example, 2keV electrons is approximately 30Å, the total pathlength for a 2keV electron in a solid can be significantly larger, depending on the inelastic scattering events which occur. Bethe¹⁶² derived a continuous loss relationship which considers pathlength, $\frac{dE}{dx}$ is given by

$$\frac{dE}{dx} = -Z\pi e^4 N_{AV} \frac{Z_P}{AE_m} \ln(1.166E_m/J) \quad \text{eqn. 2.7}$$

where e , N_{AV} , Z , P have their usual meanings, E_m is the electron energy and J is the mean ionisation energy of the material.

The range of the electron is therefore given by

$$R = \int_{E=E_0}^{E=0} \frac{1}{dE/dx} dE \quad \text{eqn. 2.8}$$

which for 5keV electrons in aluminium gives a value of 5600Å.¹⁶³ This represents a straight line range where no elastic scattering has occurred and overestimates maximum values obtained by SEM by about 15%.¹⁶⁴ The calculation of range including the effects of elastic and inelastic scattering

is complex although Kanaya and Okayana¹⁶⁵ have derived an expression which is closer to the actual depth an electron can penetrate:

$$R = 0.0276 AE^{1.67}/Z^{.889} \text{ } \mu\text{m} \quad \text{eqn. 2.9}$$

This gives a corresponding value of 4100Å for 5keV electrons in aluminium.

In a number of recent publications Ashley and coworkers have calculated stopping powers,¹⁶⁶⁻¹⁶⁹

$$S = \frac{1}{\rho} \frac{dE}{dx} \quad \text{eqn. 2.10}$$

for several organic and polymeric materials taking account of valence electron interactions using a model insulator theory and K shell interactions from atomic, general oscillator strengths. For polystyrene the ranges for electrons from 10eV to 10keV are plotted in Fig.2.12.¹⁶⁷ The great difference between the mean free path and the path length can be

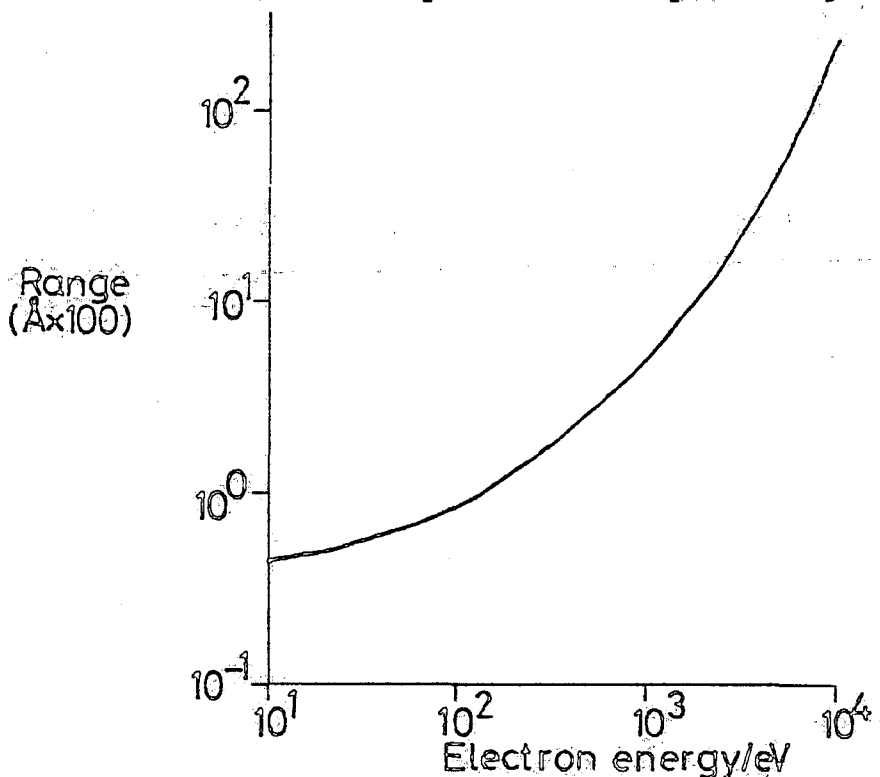


Figure 2.12 Path ranges for 10-10000 eV electrons in polystyrene as calculated by Ashley

justified in terms of the Gryzinski cross sections¹²⁷ mentioned in Section 2.2.2. Valence ionisation by, say a 2keV electron is distinctly more probable than core ionisation so that the energy loss for each collision will be $\sim 20\text{eV}$ rather than energies corresponding to core binding energies.

2.4 Electron Interactions with Polymers

2.4.1 Introduction

Although the use of low energy (2kV to 10kV) electron beams for polymer treatment is of increasing technological importance in the realm of electronic device manufacture there are very few examples in the literature of investigations of the chemical effects of the process. One reason for this absence of data is the nature of the treatment process which could typically be expected to modify the top 5000\AA of a sample hence rendering bulk sensitive analytical techniques insensitive. However the early treatments of polymers by high energy ionising radiations had been extensively studied in the 1950s^{170,171} and it is worthwhile to briefly discuss the main conclusions reached from these studies concerning mechanisms of modification. The radiation damage to organic compounds is an effect not so much of the incident radiations, *i.e.* α -rays, β -rays, slow neutrons, etc., but of the secondary electrons liberated by them in their passage through the material.²³¹ Indeed the energy distributions of secondary electrons arising from primary electrons of energies 1meV and 1keV calculated by Bethe¹⁶² are remarkably similar, as can be observed from Table 2.1. Thus the processes of excitation, ionisation and electron attach-

ment will also be occurring in high energy irradiation, the greatest difference will be the depth to which modification of a solid occurs.

TABLE 2.1 Energy distributions of secondary electrons from 1 kV and 1 MeV energy primary electron beams

Energy Range of Secondary Electrons	% of electrons	
	EP = 10^3 eV	10^6 eV
0 - 3.39	33	38.9
3.39 - 6.77	17.9	19.5
6.77 - 13.55	17.9	17.7
13.55 - 27.1	13.7	11.7
27.1 - 40.6	5.3	4.0
40.6 - 67.7	5.5	3.5
67.7 - 135.4	4.1	2.5
>135.4	2.5	2.2

2.4.2 Chemical changes due to high energy irradiation of polymers

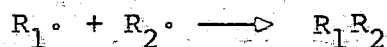
The major chemical changes observed induced by ionising radiation are main chain scission and crosslink formation. The formation of volatile products, formation and decay of unsaturation and cyclisation processes have also been observed.

Crosslinking and degradation by main chain scission often occur simultaneously with one process predominant. An empirical rule first proposed by Miller¹⁷² states that vinyl polymers in which there is more than one side chain attached to a carbon, *i.e.* $\langle \text{CH}_2 - \text{CR}_1\text{R}_2 \rangle_n$ will degrade by main chain scission while those with a single or no side chain will

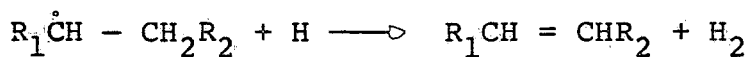
predominantly crosslink. The presence of a tetra-substituted carbon atom in the chain causes a strain due to steric repulsion so that main chain scission is favoured on irradiation.¹⁷¹

The mechanisms for crosslinking and degradation are very complex, and although since the pioneering work of Charlesby¹⁷⁰ and Chapiro¹⁷¹ the use of modern techniques, such as n.m.r.¹⁷³ and e.s.r.¹⁷⁴ spectroscopies, has become prevalent the original guidelines summarised by the above authors are still accepted. A series of reactions may be envisaged which can be expected to occur in a long chain hydrocarbon and possibly other polymers, as follows:¹⁷⁰

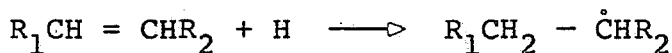
- (1) Ionisation and Excitation;
- (2) Decomposition of ionised or excited molecules to give radicals and ions;
- (3) Recapture of an electron by an ion;
- (4) Molecular rearrangement within a molecule;
- (5) Migration of a radical along a chain and possibly transfer between chains;
- (6) Combination of two radicals to give a crosslink,



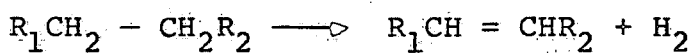
- (7) Abstraction of hydrogen from a radical molecule by means of another radical (*e.g.* hydrogen) giving unsaturation,



- (8) Elimination of a double bond, leaving a radical



- (9) Direct formation of unsaturation by removal of molecular hydrogen

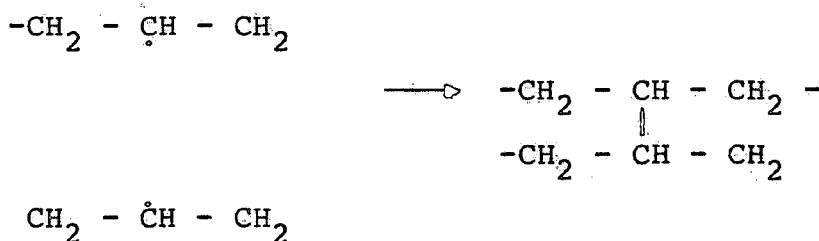


The above are based mainly assuming free radical mechanisms although there is evidence for ionic mechanisms. One of the great problems with studying the radiation chemistry of polymeric systems is the complexity of processes involved.^{170,175} Studies of short-lived excited states in polymers are difficult, and ionic intermediates are usually speculated when there is a reasonable case for excluding free radical reactions.¹⁷⁵ The next sections deal with the observed chemical effects of crosslinking, degradation and unsaturation formation and decrease in a general manner, although for specific polymer systems the radiation chemistry can be exceptional.

2.4.3 Crosslinking

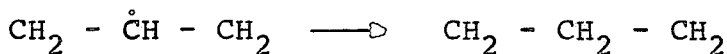
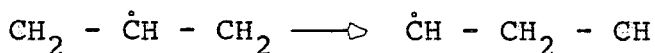
Crosslinking is the joining together of two macromolecules by a chemical band which ultimately results in an insoluble network. Mechanistic studies of radiation induced crosslinking have concentrated to a large extent on the polyethylene system.^{170,171,175,176,177}

The 'concensus' opinion^{175,176} is that crosslinking occurs by recombination of two adjacent free radicals in different chains

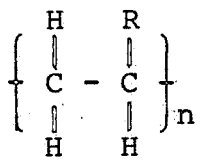


The low rates of diffusion in a solid polymer necessitate migration of radicals along the chain¹⁷¹ or even between chains for the above process to be valid, and such migration may occur *via* a series of hydrogen abstraction re-

actions either intra- or intermolecularly.¹⁷⁶

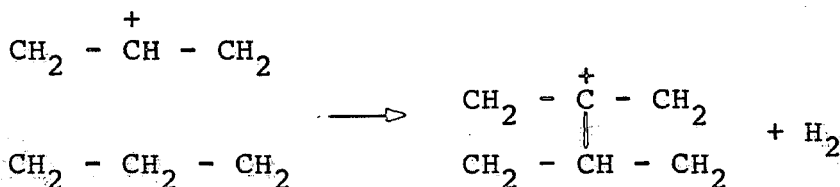


The events leading to radical formation undoubtedly involve ions and highly excited states but e.s.r. evidence does indicate that at 77K virtually all radicals present are alkyl radicals and there is evidence to suggest that the number of crosslinks is about half the number of alkyl radicals produced.¹⁷⁶ Polymers which, according to the Miller rule,¹⁷² should predominantly crosslink are of the type -



and include polyethylene, polypropylene, polystyrene and polyvinylhalides. Polymers of the fluorinated ethylenes¹⁷⁸ also show greater crosslinking than degradation on exposure to radiation, except for poly(tetrafluoroethylene).

Justification for the Miller rule has been attempted in terms of resonance stabilisation,¹⁷⁰ heats of polymerisation of the original monomers,^{170,171} and semiempirical MO calculations¹⁷⁹ although the idea of steric effects already mentioned is simplest to envisage. Crosslinking could also occur by ionic processes,¹⁸⁰ e.g.



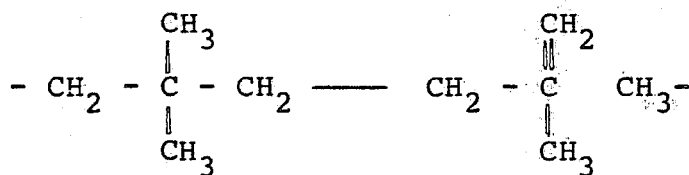
or other free radical processes involving a repeated process of fracture of the main chain of carbon atoms followed by

branding to yield trifunctional crosslinks, or addition of radicals to double bonds formed during radiolysis¹⁷⁵ (see later).

2.4.4 Degradation by main chain scission

Degradation is a process where the molecular weight of a polymer decreases upon irradiation due to fracture of bonds in the main chain of the polymer. Typical polymers^{170,171} which degrade include polyisobutylene, polymethylmethacrylate, PTFE, Kel-F and cellulose. Justification for the Miller rule is again evident in predicting that these polymers will degrade. Degradable polymers are suitable for use as negative electron beam resists since a lowering of molecular weight renders exposed portions of the rest more soluble.¹⁸¹

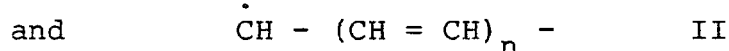
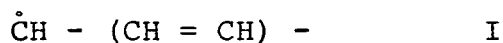
The mechanisms of degradation proposed in the literature are again mainly based on free radical processes, although they have not been studied to the same extent as polyethylene. Thus for polyisobutylene, for example, several mechanisms have been proposed. For a permanent break in the main chain it has been suggested that two stable molecules should be given from rearrangement of the activated polymer:¹⁷¹



However the steric requirements about the free^{171,172} radical do discourage recombination and crosslinking, as for example in PMMA,

2.4.5 Unsaturation formation and decay

Unsaturation occurs in irradiation of polymers of either crosslinking or degrading types. The presence of unsaturation in irradiated polymers has been demonstrated using i.r. and u.v. spectroscopies. In polyethylene, a simple polymer of the crosslinking type, early studies¹⁸³ demonstrated that initial vinyl and vinylidene unsaturation present in the polymer disappeared very quickly, while trans-vinylene increased steadily. The radicals



have been detected by e.s.r. at above 320K irradiation temperature. The presence of II may also explain the darkening in colour observed in irradiated polyethylene. The formation of polyene structures is also supported by u.v. spectroscopy and by the EELS data of Ritsko.¹¹³ Backbone unsaturation was also found by Ritsko¹¹³ during the acquisition of EELS spectra of polystyrene, *i.e.* by a beam of electrons of 60 keV energy.

The mechanism of unsaturation formation is again unclear, the 'consensus' opinion being that it involves an intramolecular process of hydrogen abstraction.^{170,171}

Polymers which are initially largely unsaturated upon irradiation tend to lose unsaturation,¹⁸³ however benzene rings tend to 'protect' polymers against high energy radiation, thus polystyrene was thought to only crosslink at a low rate.^{170,171}

2.4.6 Low energy electron irradiation of polymers

The relatively short range of low energy electrons in materials in general and polymers in particular has precluded the study of chemical effects by familiar, bulk analytical techniques. There is therefore a paucity of data available. The study by Hiraoka¹⁸⁴ of changes in polyacrylonitrile, as revealed by ESCA, is an exception. His overall conclusion is that a graphitic structure is formed by electron bombardment, and also that thermal and u.v. treatments had similar effects on the ESCA spectra.

Briggs and Wootton¹²⁸ briefly mentioned that no changes were observed in the C_{1s} and F_{1s} spectra of polytetrafluoroethylene after 700eV electron beam bombardment at a dose (20nA) sufficient to give a good signal to noise positive ion ESD spectrum. The ESD spectrum obtained was dominated by CF_3^+ ions, with less intense peaks corresponding to other fluorocarbon ions.

CHAPTER THREE

ELECTRON MEAN FREE PATHS

AS A FUNCTION OF KINETIC ENERGY:

A SUBSTRATE OVERLAYER INVESTIGATION

USING A $\text{TiK}\alpha_{1,2}$ X-RAY SOURCE

3.1 Introduction

The surface sensitivity of ESCA arises from the short path length of the probe, namely photoemitted electrons which have undergone no energy loss collisions on exit from the surface under examination. A measure of this distance is the inelastic mean free path which is defined as the distance in a solid through which electrons will travel before $1/e$ of their number have not suffered energy loss due to inelastic collisions. The sampling depth, defined typically as the depth from which 95%¹⁹² of the photoelectron signal is derived is related to the mean free path λ , by

$$\text{Sampling depth} = -\lambda \ln\left(\frac{100-95}{100}\right) \approx 3\lambda.$$

Thus for the quantification of ESCA studies of structure, bonding and reactivity of solids in general and polymers in particular an accurate knowledge of mean free paths as a function of kinetic energy is crucial.¹⁹³ To this end a data bank now exists at NPL and is updated by M.P. Seah of all determinations of mean free paths¹⁹⁴ reported in the literature. However although very useful the non-discretionary nature of the data bank's accumulation entails some erroneous data are included. The methods available for the determination of mean free paths fall into two categories:¹⁹⁵

- (i) The substrate-overlayer technique, and
 - (ii) measurement of relative absolute intensities with a knowledge of photoionisation cross sections.
- Method (i), involves in its most complete form the measurement of the attenuation of photoelectron signals due to the substrate, and the concomitant increase in the overlayer signal on pro-

gressive deposition on to a substrate a uniform film of overlayer of known thickness. Determination of mean free paths assumes an exponential dependence of path length of the photoemitted electron and the intensity of its signal. Thus for the overlayer

$$I_o = I_o^\infty (1 - e^{-d/\lambda \cos \theta}) \quad (\text{eqn. 3.1})$$

and the substrate,

$$I_s = I_s^o (e^{-d/\lambda \cos \theta}) \quad (\text{eqn. 3.2})$$

as discussed in Chapter One.

The second method also makes use of the integrated form of the differential intensity relationship (eqn. 1.11) but between limits of $d=0$, and $d=\infty$, *i.e.*

$$I = F \alpha_i N_i k_i \lambda_i \quad (\text{eqn. 3.3})$$

Comparison of intensities of homogeneous samples can lead to ratios of mean free paths provided the X-ray F , the photoionisation cross section α_i , the Number density N_i and the relative efficiency of the spectrometer k_i for each sample can be related. In addition comparisons with a sample whose mean free path is known can yield absolute values of unknown mean free paths. However when used in practice the method can produce surprising results,¹⁹⁵ probably due to incomplete consideration of all the factors involved.

The available data show that there is little dependence of structure on mean free path in polymers,^{195,196} and indeed when the experimental accuracy of $\pm 20\%$ is taken into account the mean free paths of metals, semiconductors and polymers are similar. Notable exceptions to this behaviour are the mean

free paths of highly ordered organic overlayers.^{17,197,198}
The simplicity of successively building up a Langmuir Blodgett film for a substrate overlayer experiment has long been recognised but the unusually large mean free paths obtained result from specific channeling phenomena travelling parallel to the order chains of overlayer and also the lower packing density of Langmuir Blodgett films as opposed to other solid materials.

Most determinations of mean free paths have in the past centred on the use of conventional $MgK\alpha$ and $AlK\alpha$ X-ray sources, with one or two exceptions.^{199,200} There is now however growing interest within the surface science community on the use of harder X-ray sources for a number of reasons. The first is ease of use since there has been a large increase in the number of commercially available ESCA instruments fitted with a dual anode X-ray gun, thus allowing the user a change of anode at the flick of a switch, rather than having to physically change the anode increasing downtime on the instrument. The arrival of the quadranode, *i.e.* four targets, is an interesting²⁰¹ extension of this idea.

The probing of chemical states *via* the Auger parameter⁵⁵ is becoming increasingly routine, and for some elements this necessitates the use of harder X-ray sources in order to create the initial hole for an intense Auger transition.⁵⁹ The greatest potential for the use of harder X-ray sources however is in analytical depth profiling by ESCA.²⁰²

As mentioned in Chapter One there are three methods of depth profiling, namely argon ion etching, angular dependence

and the monitoring of two core levels of the same element but at differing kinetic energies (*e.g.* the F_{1s} and essentially core like F_{2s}). Of these argon ion etching is not applicable to any organic system,²⁰³ angular dependent studies are inappropriate for powders and fibrous samples and the latter is fortuitous and inapplicable in a large number of systems.

With harder X-ray sources the sampling depth is increased regardless of whether the sample is flat, fibrous or powdered, and the use of such sources will be of increasing importance in the study of polymeric systems by ESCA. The ability of harder X-rays to probe core levels out of range of conventional sources (*e.g.* the 1st levels of 2nd row elements) also increases methods of intermediate depth profiling.

The energies and some of the linewidths of some of the more feasible X-ray sources for use in XPS⁶⁶ are shown in Table 3.1. The linewidths of most of these sources preclude the possibility of detailed lineshape analysis, but this is not a serious problem when elemental ratios alone are desirable which is usually the case in depth profiling. The ability of monochromatising the AgL α source has recently been reported²⁰⁴ - this should greatly decrease the linewidth but the concomitant loss of intensity could be a serious problem without the use of a rotating anode¹⁸ and/or position sensitive detection.

Of harder X-ray sources actually in use Castle has reported various applications of SiK $\alpha_{1,2}$ ⁹⁵ and ZrL α sources.²⁰⁵ The TiK $\alpha_{1,2}$ source at Durham has proved immensely useful in studies of, *inter alia*, the nitration-denitration of cellulosic materials,²⁰⁸ the photooxidation of polymer surfaces,²⁰⁶ and the surface modification²⁰⁷ and formation²²⁰ of polymers by

TABLE 3.1 Feasible harder X-ray sources

<u>Source</u>	<u>Photon Energy (eV)</u>	<u>Width (eV)</u>
MgK α	1253.6	0.68
AlK α	1486.6	{.83 {.165 (mono)
SiK α	1739.4	
ZrL α	2024	
AgL α	2984.4	
ScK $\beta_{1,3}$	4460.5	
TiK α	6510	
CrK α	5414.9	2.1
MnK α	5898.9	
CuK α	8048.4	2.55

inductively coupled R.F. "cool" plasmas. Quantification of the results from these studies may only be achieved by a detailed knowledge of the sampling depth using a TiK α source. It is the purpose of this chapter, therefore, to present results of the measurement of electron mean free paths over the kinetic energy range 545-4400eV.

3.2 Experimental

The study reported here involved the use of *in situ* produced poly(p-xylylene) films as overlayer and gold as a substrate. Measurement of film thickness was achieved by monitoring MgK α excited Au4f and C_{1s} levels.

The poly(p-xylylene) was produced by sublimation followed by pyrolysis of [2.2] p-cyclophane and room temperature depos-

ition of the resulting p-xylylene precursor onto the substrate in a flow system. A schematic of the process is shown in Figure 3.1.

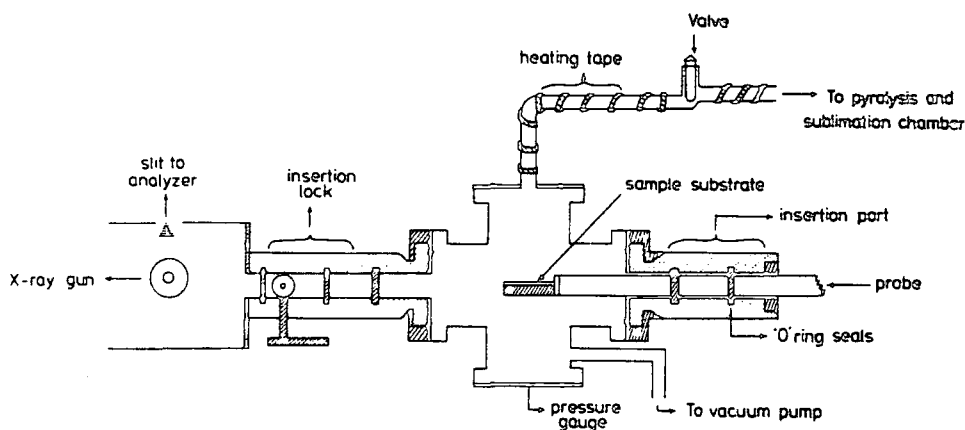


Figure 3.1 Schematic of the deposition chamber attached to the spectrometer sample chamber

This route has several advantages for our interests since additive free films are given in quantitative yields,²⁰⁹ and facile production of uniform thin films may be achieved because of the fine control available over the rate of generation and deposition of the p-xylylene intermediates.

The *in situ* production of these films by having the apparatus directly attached to the spectrometer greatly decreases the chances of contamination, surface oxidation and hydrolysis, possible if the samples had to be transferred to the spectrometer.

An important attribute of the thin films produced is that they will not be "crystalline" in the sense that single crystals are, hence channeling phenomena will not arise and the system studied resembles normal polymer samples.

Gold was chosen as a substrate for a number of reasons. In the determination of mean free paths using a $MgK\alpha^{195}$ source it was found that sticking coefficients of paraxylylene onto a gold substrate provide a convenient time scale for initial deposition. The chemical inertness of gold is advantageous in two ways, since once cleaned in a standard manner it will not form an oxide layer *etc.* prior to deposition and secondly no reaction will take place with the deposited poly(p-xylylene) film. Our thickness measurements were based mainly on the attenuation of the $MgK\alpha$ excited $Au4f$ signal, the mean free path for which is accurately known in paraxylylene from a previous detailed study in these laboratories.¹⁹⁵

Finally inspection of a wide scan spectrum of gold reveals that the heavier $TiK\alpha$ source opens the possibility of examining deeper lying core levels which encompass a wide range of kinetic energies.

The pyrolysis and sublimation chambers consisted of a 24" long $\frac{1}{2}$ " diameter quartz tube sealed at one end and with a ground glass joint at the other.

This was connected *via* greaseless couplings, flexible steel tubing and a greaseless isolation valve to the deposition chamber shown attached to the spectrometer in Figure 3.3.

The deposition chamber was a 70 mm flanged four-way adaptor which could be mounted onto the insertion lock of the spectrometer by means of a double-sided flange fitted between the insertion lock edge and the deposition chamber, and sealed by Viton O rings. The insertion port on the deposition chamber sealed onto the probe using two Teflon omniseal 'O' rings. The system was pumped by an Edwards ED50 two-stage rotary pump, and pressures were monitored on a Pirani gauge. The starting material [2.2] paracyclophane (Union Carbide Corporation, Bound Brook, U.S.A.) was recrystallised three times from xylene, and characterised by standard techniques.

Typically about 2g of sample were loaded into the closed sublimation end of the quartz tube and the system assembled pumped down.

A Lindberg furnace, Type 55035A, was used to set up a pyrolysis region over a length of ~ 12 " starting 6" from the sublimation end of the tube. Tubing between the pyrolysis zone and the deposition chamber was maintained at $\sim 80^{\circ}\text{C}$ using electrical heating tape.

The optimum temperatures for sublimation and pyrolysis were determined with the apparatus not attached to the spectrometer by subliming the cyclophane into the pyrolysis zone using a temperature controllable electric heater placed over the quartz tube. These experiments gave a uniform rate of film formation as measured by weight increase on aluminium foil substrates,

at a convenient time scale with the furnace set at $\sim 600^{\circ}\text{C}$ and the sublimation heater at 180°C .

With the apparatus on the insertion lock of the spectrometer deposition was achieved by placing the sublimation heater over the closed end of the quartz tube having pumped the apparatus down to $\sim 5 \times 10^{-2}$ torr and closed the pyrolysis-deposition isolation valve. By opening this valve for a known time period deposition of the poly-paraxylylene films onto the gold substrate could be controlled sufficiently. When enough deposition, evident also by a pressure rise, had occurred the pyrolysis region was valved off and the sublimation heater removed. To minimise polymer deposition in the insertion lock roughing system of the spectrometer about five minutes were allowed to elapse prior to sample entry into the analysis position of the spectrometer *via* the ball valve.

An initial series of experiments involved recording the MgK α excited Au4f and C $_{1s}$ for the initial gold sample followed by a TiK α examination of the gold 4f, 4d, 4p, 3d $^{3/2}$, 3d $^{5/2}$, 3p and two doublets occurring at KE's 590eV and 845eV. After deposition of the polymer the spectra were rerecorded, with the MgK α excited C $_{1s}$ and Au4f levels being run both before and after TiK α radiation to monitor sample damage. In this series of experiments seven different gold substrates were used but only three deposition thicknesses per sample were possible because of signal attenuation at low kinetic energy. Changes in the MgK α C $_{1s}$ spectra after TiK α exposure prompted a separate series of experiments in which only one of the TiK α excited levels was investigated in a single run, but with ~ 5 depositions

for each. The C_{1s} levels here revealed little evidence of damage by the $TiK\alpha$ source.

The peaks at $\sim 490\text{eV}$ and $\sim 845\text{eV}$ were at first thought to be due to Auger transitions resulting from initial excitation of a 3p level in gold, but were subsequently found to be due to photoemission peaks resulting from $CuL\alpha$ X-rays ($h\nu = 929.7\text{eV}$) excited $Au4p$ and $Au4f$ peaks respectively, however signal attenuation of these peaks was monitored to give an even better KE range of mean free path investigations.

The spectrometer used for this work was the customised Kratos ES300 spectrometer which at the time had two Alcatel air bearing air turbine turbomolecular pumps of nominal pumping speeds 450ls^{-1} and 120ls^{-1} pumping the source region and analyser respectively, giving a base pressure of the system during data acquisition of $\sim 10^{-9}$ torr. Spectra were recorded in analogue mode on an X-Y plotter with the analyser scanned continuously with a fixed retardation ratio.

Area measurements were made using both a Dupont 310 curve resolver and an Apple II microcomputer equipped with a graphics tablet.

3.3 Results and Discussion

3.3.1 Introduction

The data reported here concentrates solely on the attenuation of the substrate signal on deposition of layers of polyparaxylylene, since initial experiments showed that the $TiK\alpha$ excited C_{1s} signal was very weak for all but the thickest depositions, as can be seen from the wide scan $TiK\alpha$ excited

spectrum of Figure 3.2. This arises due to the low cross section for photoemission of a C_{1s} level with X-rays of 4510eV energy and also because most depths of overlayer studied were below the mean free path of photoelectrons emitted from C_{1s} levels (KE ~ 4325). A qualitative discussion of relative cross sections using Mg and Ti X-ray sources appears later. The lack of a mean free path measurement for the overlayer is greatly compensated for however by the ability of the harder X-ray source to probe deep lying levels of the gold substrate, as is clearly evident from Fig. 3.2. Thus core level spectra for the Au 3p, 3d, 4p, 4d and 4f levels may be monitored to provide direct estimates of mean free paths at kinetic energies 1768, 2220, 3970, 4177 and 4430 eV respectively. The CuLa excited Au4d and Au4f levels at ~ 590 and 845eV extend the range of kinetic energies over which mean free paths have been determined. Thus in conjunction with the earlier work from these laboratories using $MgK\alpha_{1,2}$ and $AlK\alpha_{1,2}$ photon sources the data presented here represent the most complete study of electron mean free paths as a function of kinetic energy for a given material over such a wide kinetic energy range.

A qualitative inspection of the high resolution core level spectra of Fig. 3.3 allows considerable insight into the strong dependence of mean free path on kinetic energy. Deposition of a 70 \AA overlayer of polyparaxylylene results in the $MgK\alpha_{1,2}$ excited Au4f level signal at 1170 K.E. undergoing attenuation by a factor of ~ 50 . The signal at KE ~ 4430 eV, arising from $TiK\alpha$ excitation of the Au4f levels, however, has a corresponding attenuation factor of ~ 5 . The $TiK\alpha$ excited Au $3d^{5/2}$ signal at an intermediate kinetic energy (2330eV) is

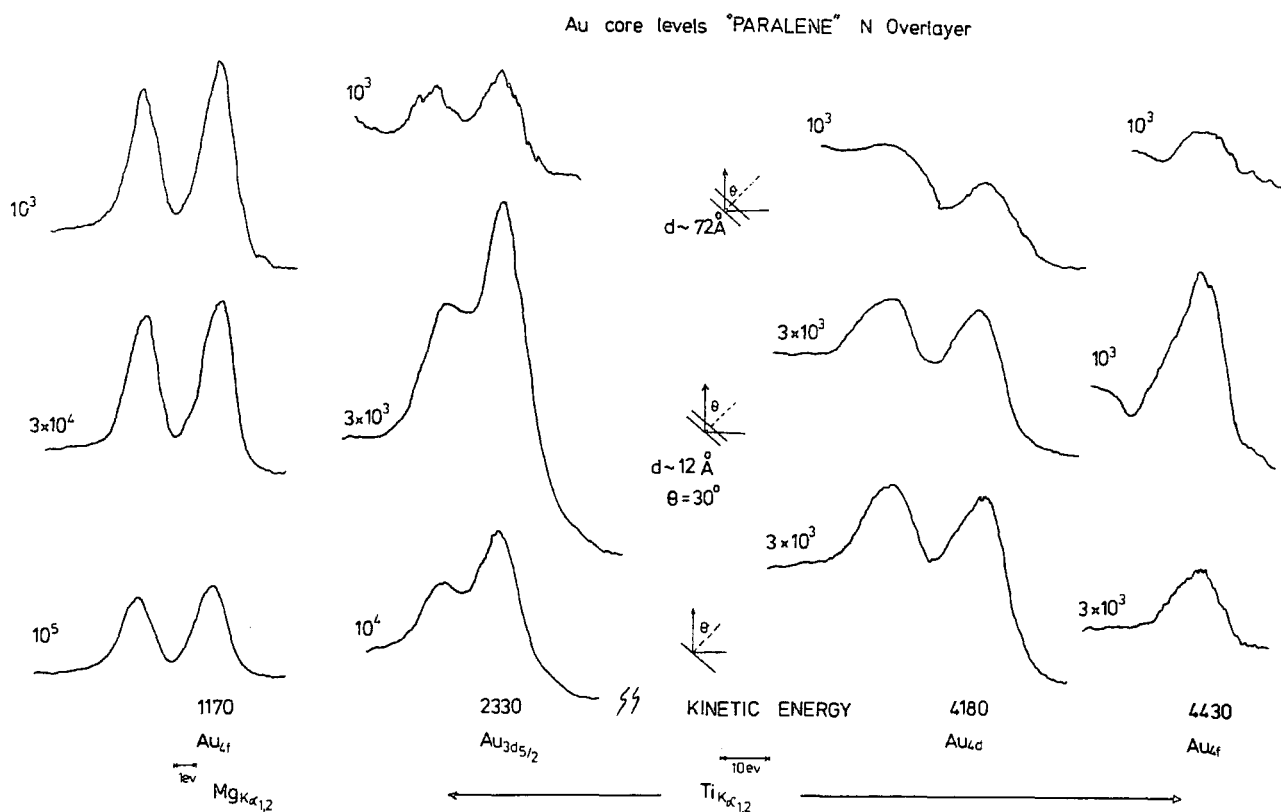


Figure 3.3 High resolution MgK $\alpha_{1,2}$ excited Au4f and TiK $\alpha_{1,2}$ excited Au 3d $^{5/2}$, Au 4d and Au4f core level spectra recorded at 30 $^{\circ}$ take-off angle for a gold substrate with differing thickness of polyparaxylylene overlayer.

attenuated by a factor of ~ 15 , also intermediate of the attenuation factors for the signals at 1170eV and 4430eV. Also evident from Fig.3.3 is the comparable attenuation of the TiK α excited Au4f and 4d signals, which arises from the relative proximity of their kinetic energies.

Figure 3.3 illustrates also the complexity of line shape which can occur using the TiK $\alpha_{1,2}$ source compared to



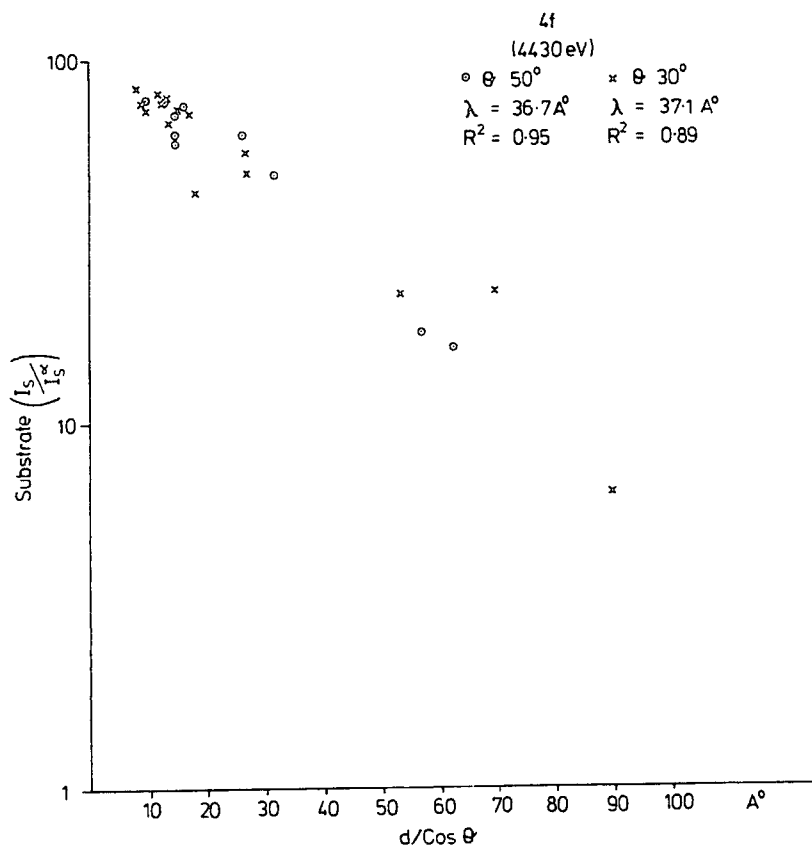
MgK $\alpha_{1,2}$ spectra. This results from spin-orbit splitting of the TiK $\alpha_{1,2}$ giving a doublet of intensity ratio 1:2 and separation $\sim 6\text{eV}$. The characteristic shape of the doublet is clearly seen in the Au $3d^{5/2}$ spectra in Fig. 3.3, whereas in the case of the TiK α excited Au 4_f and Au 4_d spectra convolution of the spin-orbit split components of the core level with the components excited by the TiK $\alpha_{1,2}$ doublet leads to a complex line shape. However since the splittings and relative intensities for both the core level concerned and the X-ray source are known detailed analysis of these lineshapes is straightforward, but time consuming. Such detailed line shape analysis was not necessary for this work since determination of electron mean free paths is achieved by an investigation of the attenuation of substrate core level intensities with increasing film thickness. This only requires the total integrated intensity for each core level envelope. Component analysis for the TiK $\alpha_{1,2}$ excited Au $3d^{5/2}$ peak nevertheless gave a FWHM of 2.4eV, compared to the value of 1.2eV for the Au $4f_{7/2}$ level excited by MgK $\alpha_{1,2}$ radiation. Hence under our instrumental conditions FWHM values for TiK $\alpha_{1,2}$ excited spectra are dominated by the inherent width of the X-ray source to a far greater extent than MgK $\alpha_{1,2}$ excited spectra.

3.3.2 Evaluation of mean free paths

The results are summarised in Table 3.2, together with the relevant statistical correlations of the data (r^2). A brief discussion for each core level will now be presented.

(i) TiK α excited Au4f (KE 4430)

The plot of $\ln\left(\frac{I}{I_0}\right)$ versus $d/\cos\theta$ is shown in Fig. 3.4. For this series of results and all subsequent results for the other substrate core levels the film thickness d has been calibrated using the mean free path value obtained from the previous work at the Durham laboratories investigating electron mean free paths as a function of kinetic energy in polyparaxylylene films employing MgK $\alpha_{1,2}$ and AlK $\alpha_{1,2}$ photon



N.B. In this and subsequent plots I_s is the substrate core level intensity at thickness $d/\cos\theta$ and I_s^0 is the initial intensity prior to deposition.

Figure 3.4 $\ln I/I_0$ versus $d/\cos\theta$ for the 4f levels of a Au substrate using the TiK $\alpha_{1,2}$ photon source

sources.¹⁹⁵ Thus 22\AA has been taken as a standard value for the mean free path for photoelectrons of kinetic energy 1170eV . This method of film thickness measurement has the advantages that it relates directly intensities obtained from one photon source to another and obviates the need for a deposition monitor. The use of a deposition monitor in such experiments entails extremely accurate and time consuming calibration since, depending on the apparatus used, the relationship between rates of deposition on the substrate and monitor head can be complex. Measurement of some of the film thicknesses used in this work using a deposition monitor would also involve pushing the monitor to the limits of its sensitivity hence increasing error greatly.

The low cross section for photoemission from the $4f$ levels under $\text{TiK}\alpha_{1,2}$ excitation evident from Figs. 3.2 and 3.3 manifests itself with low count rates with extensive coverage of polyparaxylylene film. However radiation damage precludes greatly extended counting times and so the statistical correlation of the data in Fig. 3.4 is poorer than for other levels studied. Despite the considerable scatter of the plots in Fig. 3.4 (also seen in the values of the correlation coefficients of 0.89 and 0.95 for respective take-off angles of 30° and 50°) the agreement of mean free paths determined from the slope of a least squares fit of the $\ln I/I_0$ versus $d/\cos\theta$ data are excellent, with values of 37\AA obtained for both 30° and 50° take-off angle. The proximity of the values determined at two angles suggests that islanding effects are not occurring but that the coverage of the overlayer was uniform. Non-uniform coverage would invalidate equation 3.1 since with a fractional

coverage f , the attenuation of the substrate levels would be given by

$$I = I_0(1-f) + I_0 e^{d/\lambda \cos \theta}$$

This would result in exponential behaviour of the $\ln I/I_0$ versus $d/\cos \theta$ plot, which is clearly not the case here.

(ii) Au4d levels

Although the intensities observed for the Au4d levels are higher than the 4f levels, the correlation coefficients and the plot of $\ln I/I_0$ versus $d/\cos \theta$ shows (Fig.3.5) more scatter

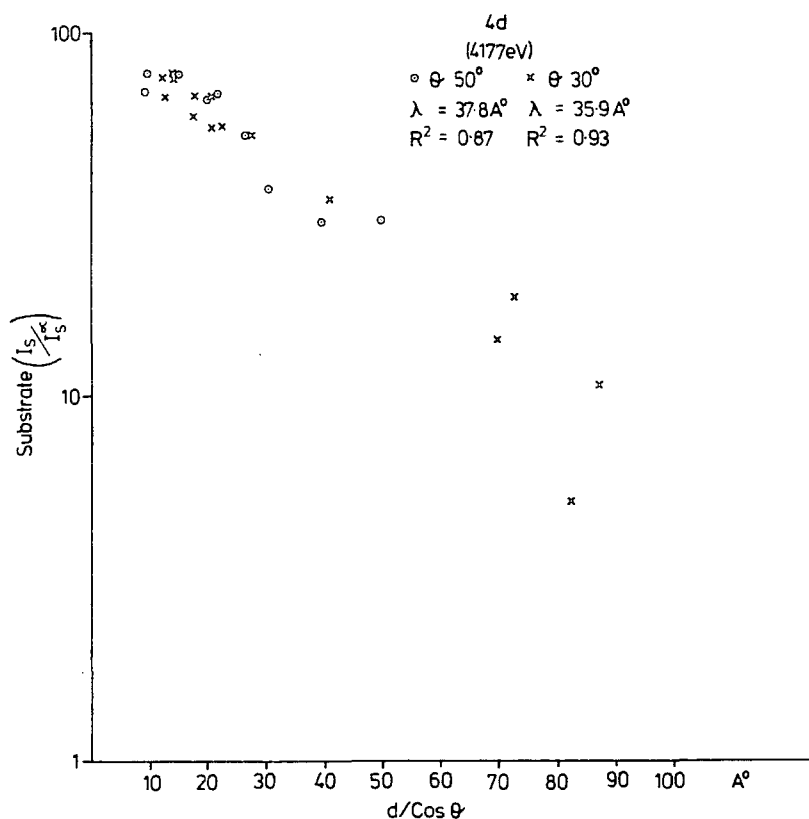


Figure 3.5 $\ln I/I_0$ versus $d/\cos \theta$ for the 4d levels of a Au substrate using the $\text{TiK}\alpha_{1,2}$ photon source

than the corresponding Au4f data. The major cause of this is the uncertainty in the position of the baseline over such a broad range, since the total envelope of the spin-orbit split components used here is much wider than for the 4f levels. However values of 38\AA and 36\AA evaluated for the mean free paths at two different take-off angles indicate consistency of results and uniform coverage.

(iii) Au4p^{3/2}

The splitting of the Au4p levels (98eV) is sufficient to allow examination of the individual spin-orbit split core level components. However the attenuation of the $4p^{1/2}$ component was not followed because of its low intensity compared to the $4p^{3/2}$ peak.

Fig. 3.2 indicates an increased cross section for TiK α excited Au4p photoemission compared to TiK α excited 4f and 4d photoionisation. This enables statistically good spectra to be taken for extensive overlayer coverage over periods of time short enough to inhibit appreciable radiation damage. The data shown in Fig. 3.6 show also that considerably less scatter is evident. Mean free paths obtained from these data for take-off angles of 30 and 50 are 34\AA and 33\AA , again in excellent agreement with each other indicating overlayer uniformity.

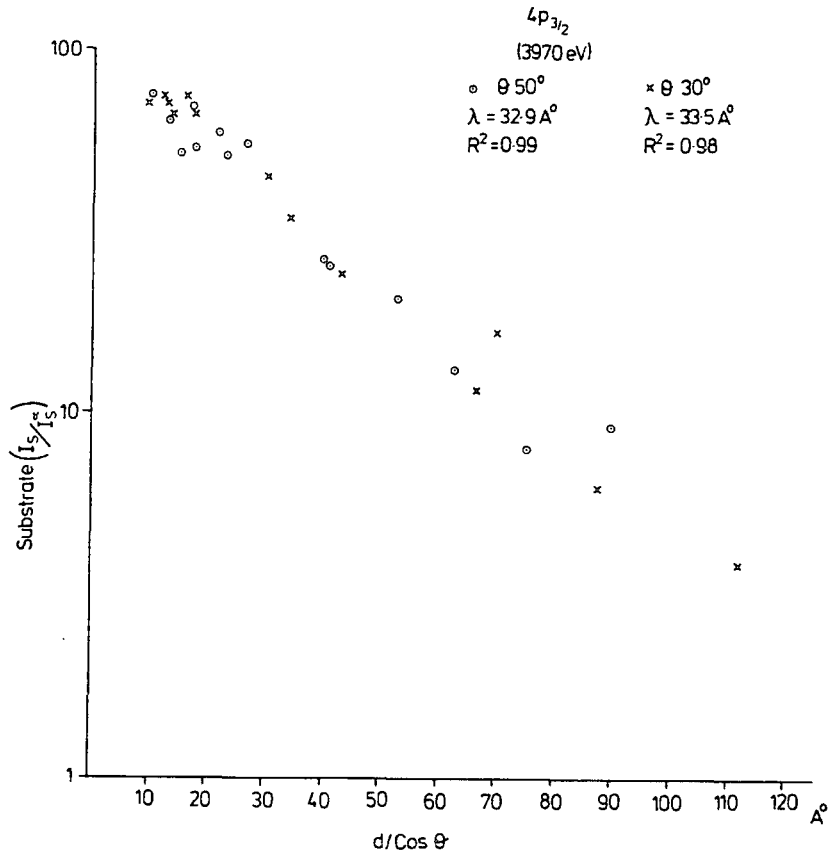


Figure 3.6 $\ln I/I_0$ versus $d/\cos\theta$ for the $4p^{3/2}$ levels of a gold substrate

(iv) Au 3d levels

The spin-orbit splitting of 85eV and the relative intensity ratio (2:3) enabled individual measurements of mean free path to be made for each component of the 3d level, and the data are shown in Fig.3.7 for the $3d^{5/2}$ level and Fig.3.8 for the $3d^{3/2}$ level. Both sets of results again indicate uniformity of coverage. The average value obtained for the $3d^{3/2}$

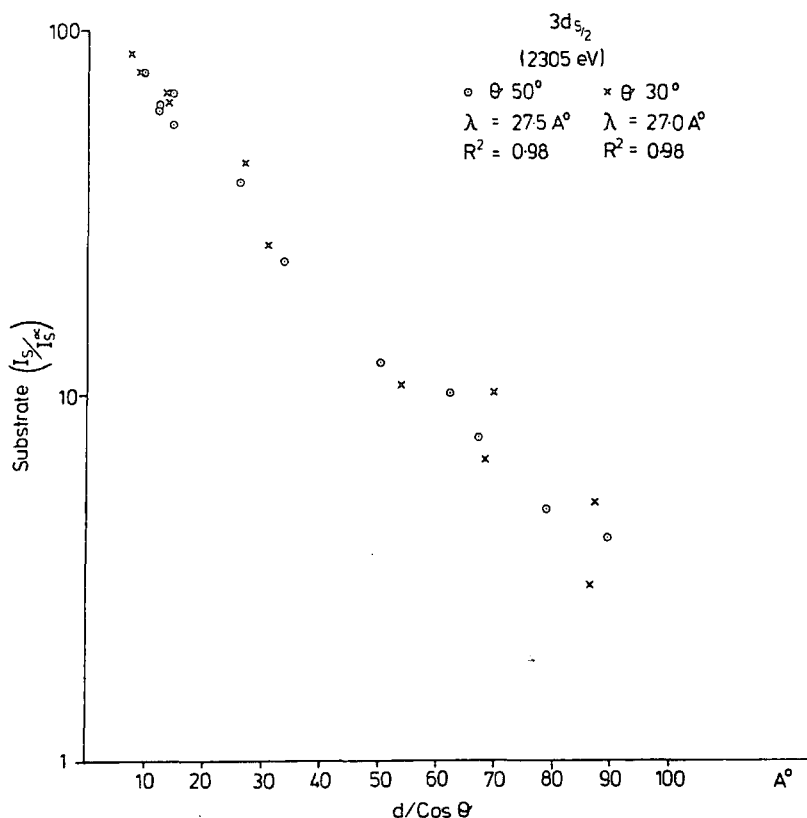


Figure 3.7 $\ln I/I_0$ versus $d/\cos\theta$ for the $3d^{5/2}$ gold substrate core levels.

level ($\sim 30\text{\AA}$) at kinetic energy 2220eV is within experimental error the same as that obtained for the $3d^{5/2}$ level (KE 2305eV). This is not unexpected since such a small energy difference (less than 100eV) at these kinetic energies will not affect the mean free paths between the two levels considering the square root dependence.

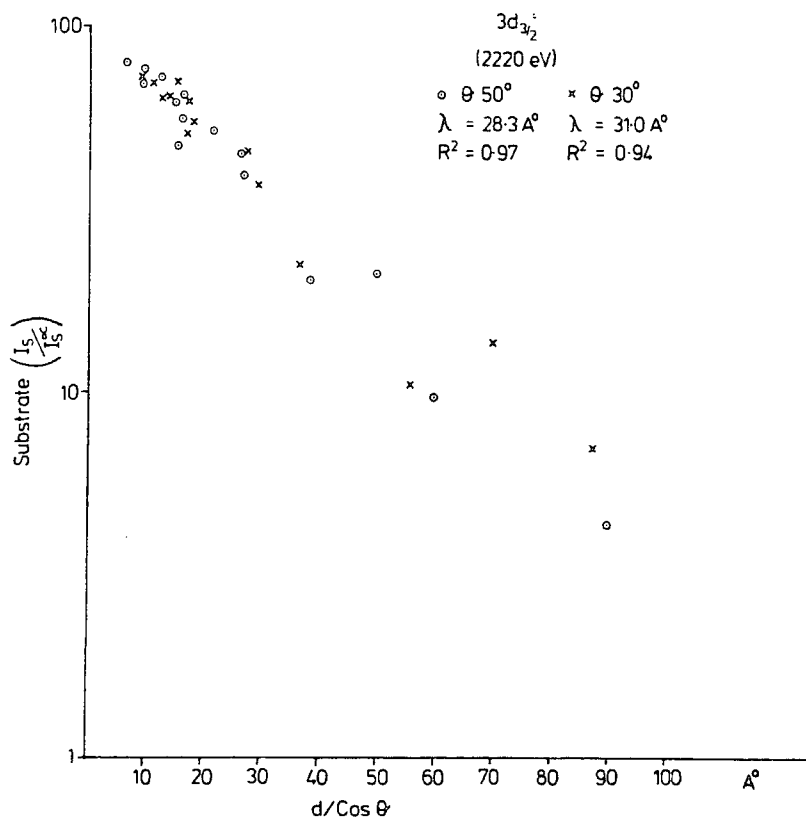


Figure 3.8 $\ln I/I_0$ versus $d/\cos\theta$ for the $3d^{3/2}$ levels of gold excited by $\text{TiK}\alpha_{1,2}$ X-rays

(v) Au $3p^{3/2}$

Although the Au $3p$ level gives signals of reasonable intensity, indicative of a large cross section the inner shell lifetime broadening of the peak is apparent. Although less data points were obtained for this level the statistical correlations for the data shown in Fig.3.9 are reasonable, with values

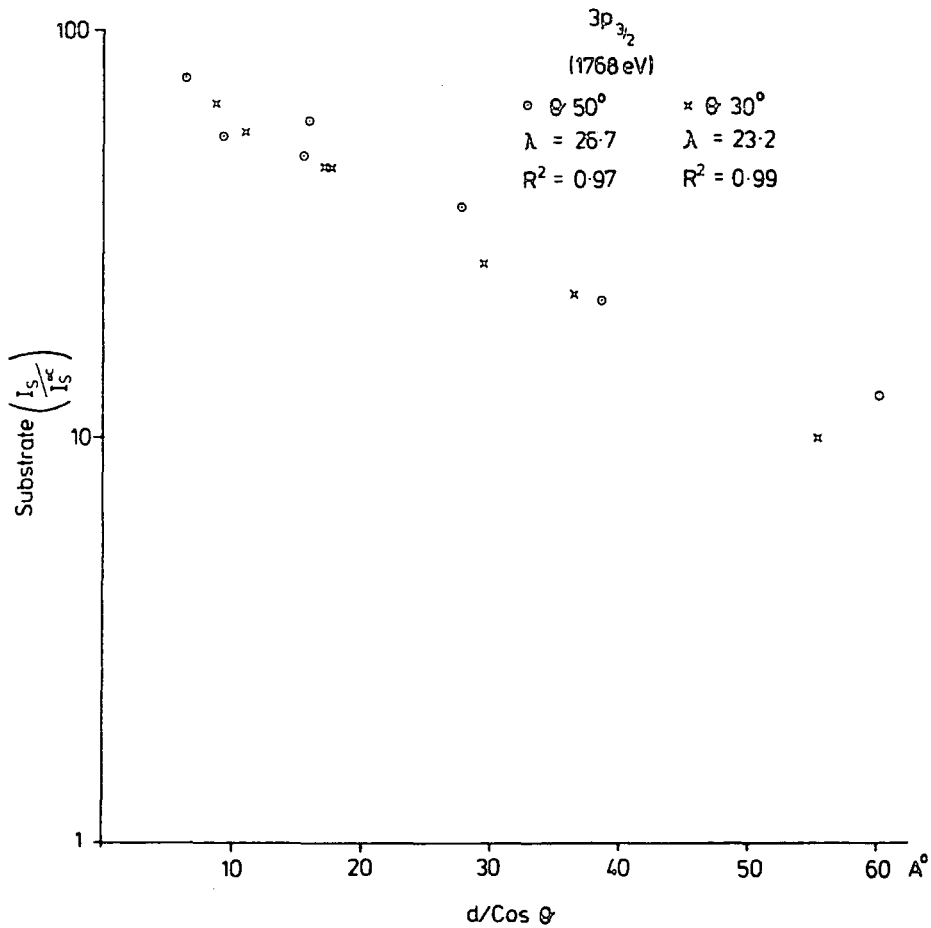


Figure 3.9 $\ln I/I_0$ versus $d/\cos\theta$ for $3p^{3/2}$ of gold

of 0.99 and 0.97 for take-off angles of 30° and 50° . The uniformity of the overlayer film is again confirmed by the proximity of calculated for the two take-off angles, viz 27\AA for 50° and 23\AA for 30° .

(vi) Cu L α excited Au4f and Au4d levels

The appearance of the peaks at KE 590eV and 845eV were at first thought to originate from decay of core holes originally excited by the TiK α source. However comparison of spectra run with the Ti anode of other materials eventually confirmed these peaks as being due to CuL α ($h\nu = 929.7\text{eV}$) excitation of the Au4f and 4d levels. The dual anode is constructed from a copper target coated with Mg on one level and Ti on the other as shown in Fig.3.10.

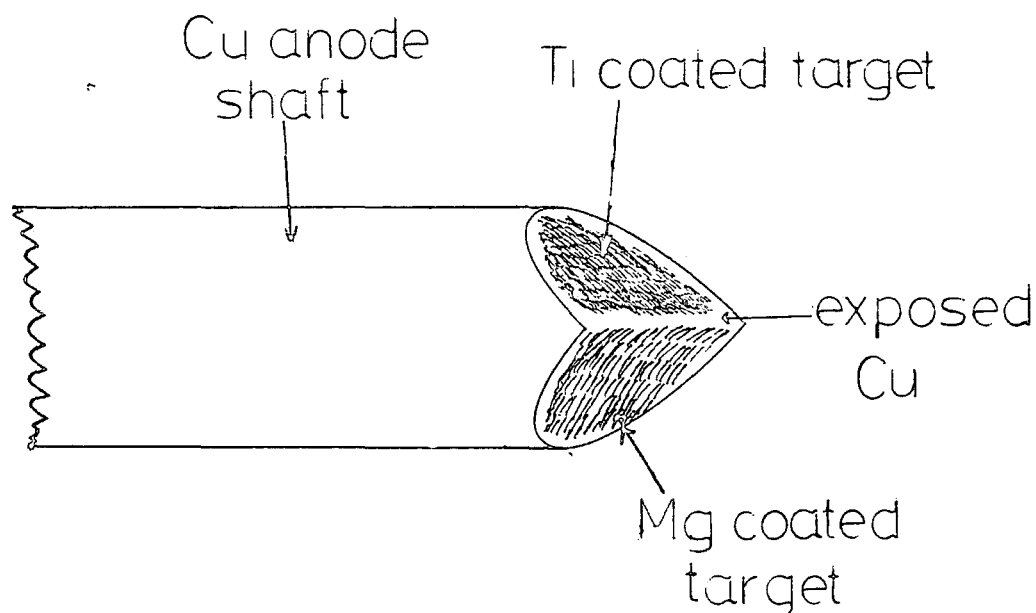


Figure 3.10 Schematic of the dual anode showing how a CuL α signal arises

Inspection of Fig.3.2 reveals that with the Ti source selected there is also some overlap with the Mg source. Thus the Cu X-rays must originate from electron bombardment of the region between the Mg and Ti coatings as shown in Fig.3.3.

The $\text{CuL}\alpha$ excited Au4f and Au4d peaks provide convenient energies for direct determination of mean free paths and the $\ln I/I_0$ versus $d/\cos\theta$ plots are shown in Figs.3.11 and 3.12 respectively.

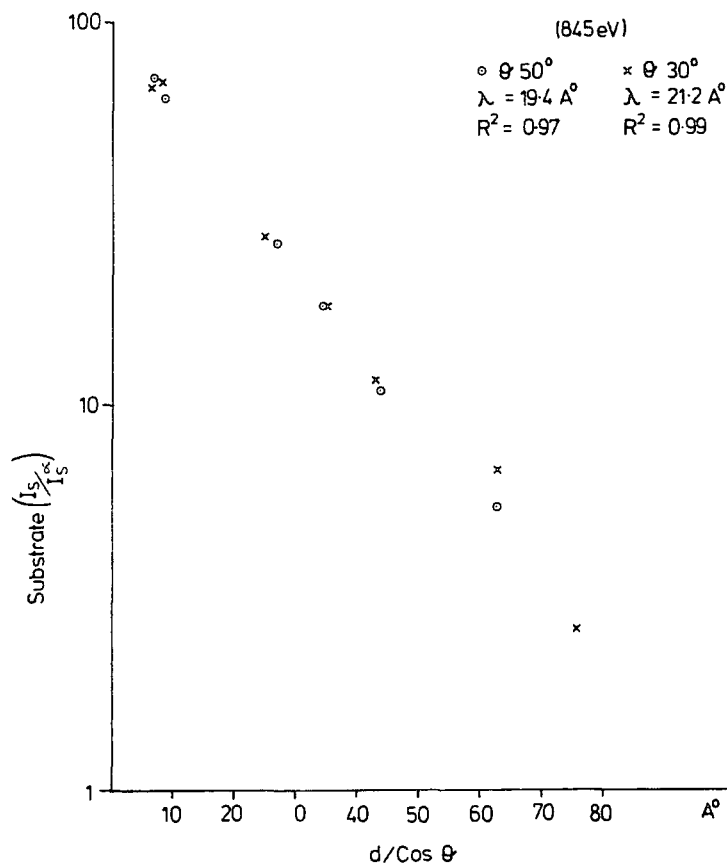


Figure 3.11 $\ln I/I_0$ versus $d/\cos\theta$ for Au4f levels excited using the $\text{CuL}\alpha$ X-rays

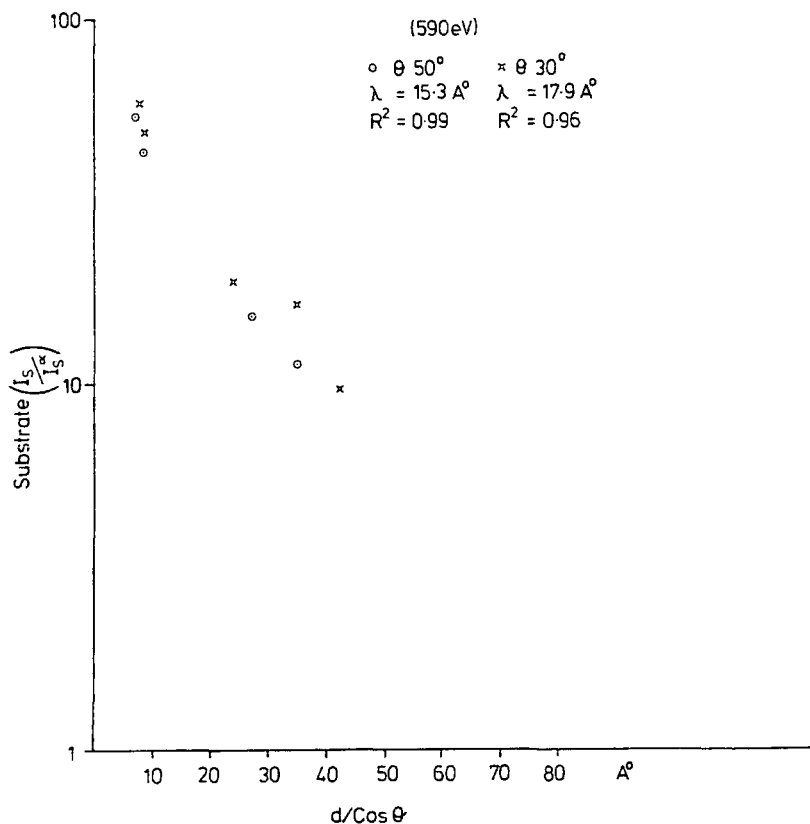


Figure 3.12 Log plot of the intensity variation of the Au4d levels with the CuL α source with increasing overlayer thickness

The 4f data provide estimates of mean free paths of 19 \AA (50 $^\circ$ take-off angle) and 21 \AA (30 $^\circ$) for 845eV electrons. The statistical correlations are very good although these values are very close to the AgK α excited Au4f mean free path of 22 \AA at 1170eV.

The CuL α excited Au4d peak at 545KE provides an average estimate for the mean free path of $\sim 17\text{\AA}$ which does seem high

compared with the MgK α excited F_{1s} level estimate (KE = 560eV) of about $7 \pm 3\text{\AA}$ from a substrate overlayer study of plasma polymerised 1,1 difluoroethylene on gold.¹⁹⁵

3.3.3 A brief note on photoionisation cross sections with the Ti anode

Brief mention has been made in the previous discussion of the relative photoionisation cross sections of the gold levels and it is appropriate to correlate those observations with known theoretical findings. Hence a series of plots has been compiled from Schofield's tables⁸⁵ showing the variation of the photoionisation cross section of the gold levels studied here over the photon energy range 1-6 keV. The results are shown in Fig.3.13 together with the variation of the C_{1s} cross section over the same range, for completeness. Comparison of these data with the wide scan spectra of Fig.3.2 clarifies several points which warrant further discussion. The most striking difference between the MgK $\alpha_{1,2}$ and TiK $\alpha_{1,2}$ spectra is the considerable fall off in intensity of the Au4f peak in the Ti excited spectrum. This is in qualitative agreement with the cross section in Fig.3.12 which indicates a decrease by a factor of ~ 80 for the Au4f level photoionisation cross section in going from MgK $\alpha_{1,2}$ photon energy to the TiK $\alpha_{1,2}$ energy.

The C_{1s} signal, observable on the Mg excited wide scan is lost in the noise on the Ti spectrum. The decrease may again be attributed to a much lower cross section; the theoretical decrease, as predicted by Schofield's numbers, being by a factor of $\sim 40x$.

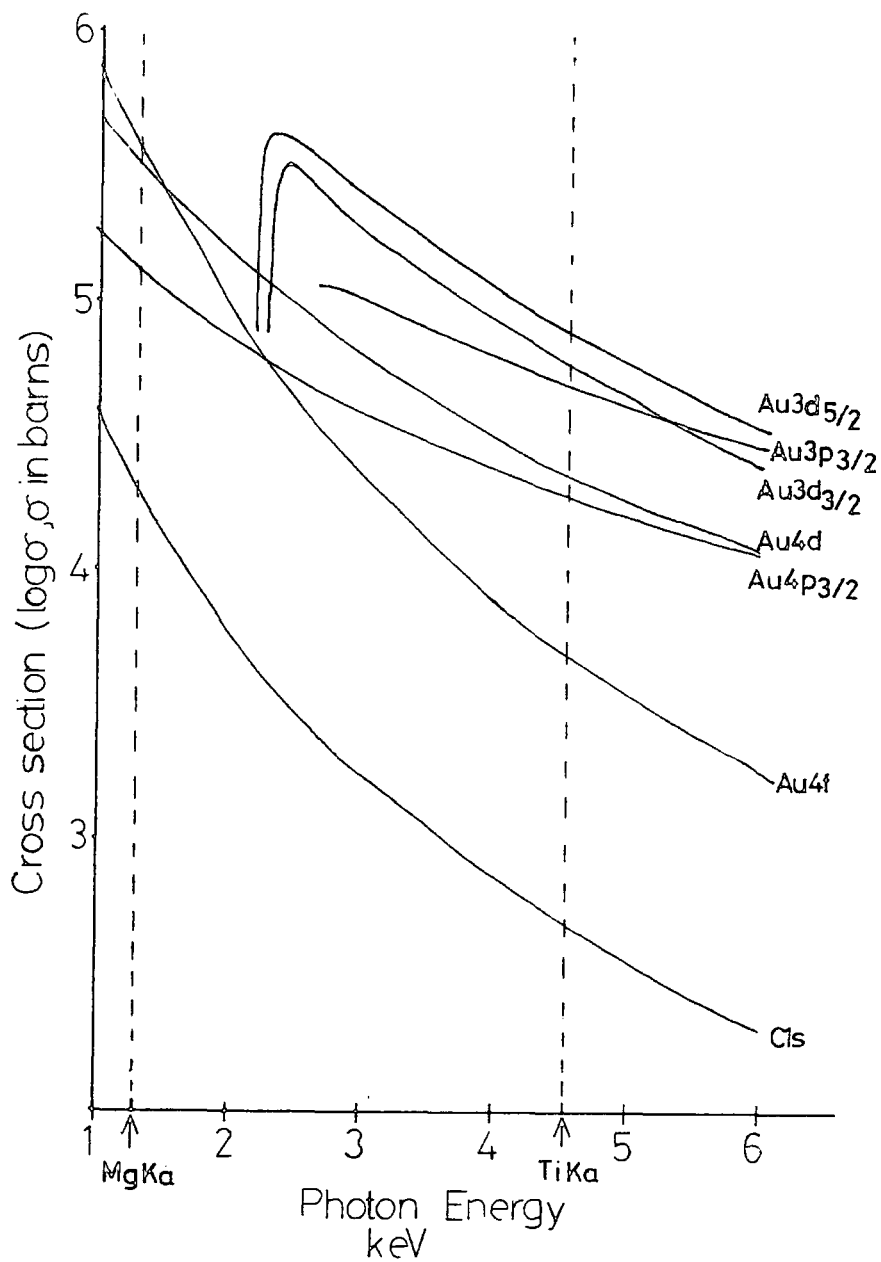


Figure 3.13 Theoretically determined photoionisation cross sections over the range 1000eV to 6000eV. N.B. For the 4f and 4d levels the total of the cross sections for the spin orbit split components has been used.

The cross section data of Fig.3.12 indicates that at 4510eV photon energy the cross section for the gold levels are in the order

$$4f \ll 4p^{3/2} < 4d^{1/2, 3/2} < 3p^{3/2} \approx 3d^{3/2} < 3d^{5/2}$$

The Ti wide scan spectrum of Fig.3.2 would suggest an ordering

$$4f \ll 4p^{3/2} \approx 4d < 3p^{3/2} \approx 3d^{3/2} < 3d^{5/2}.$$

Detailed intensity measurements of the gold levels do in fact give this same ordering, although a more thorough knowledge of the instrument response function at these energies and full angle dependence would be necessary in order to truly quantify these results.

However the foregoing treatment does show that Schofield's data is extremely useful explaining the differing intensities of the gold core level peaks excited by a TiK α anode.

Work is currently under way at Durham to further relate observed TiK α excited intensities with theoretically determined cross sections.

3.3.4 The Dependence of Electron mean free paths on KE

The major objective of this work has been the determination of electron inelastic mean free paths as a function of kinetic energy and the results are summarised in Table 3.2. It is appropriate therefore to consider the dependence of mean free path on kinetic energy in more detail and compare the results here with those previously obtained for polymer-metal systems by the substrate overlayer technique and results for organic systems in general.

TABLE 3.2 Summary of results obtained in this study, with values of r^2 for the least squares fit of plots and number of points used

Kinetic energy eV	Take-off angle(deg.)	λ (Å)	r^2	Average λ (Å)	No. of points
590 (Au 4d, CuL α)	30	17.9	0.96	16.6	5
	50	15.3	0.99		4
845 (Au 4f, CuL α)	30	21.3	0.99	20.4	7
	50	19.4	0.97		6
1768 (Au 3p ^{3/2} , TiK α)	30	23.2	0.99	25.0	7
	50	26.7	0.97		7
2220 (Au 3d ^{3/2} , TiK α)	30	31.1	0.94	29.7	14
	50	28.3	0.97		15
2305 (Au 3d ^{5/2} , TiK α)	30	27.0	0.98	27.2	11
	50	27.5	0.98		12
3970 (4p ^{3/2} , TiK α)	30	33.6	0.98	33.3	13
	50	32.9	0.99		14
4177 (Au 4d, TiK α)	30	35.6	0.93	36.7	15
	50	37.8	0.87		9
4430 (Au 4f, TiK α)	30	37.1	0.89	36.9	15
	50	36.6	0.95		10

Previous work in Durham employing $MgK\alpha$ and $AlK\alpha$ X-ray sources on polyparaxylylene¹⁹⁵ suggested an almost linear dependence of mean free path on kinetic energy over the range 970 to 1403eV. However the results reported here over the range up to 4400 eV indicates a square root dependence. This square root dependence is clearly evident from the plot of mean free path values determined here against the square root of kinetic energy displayed in Figure 3.14, together with data for $MgK\alpha$ source. Within the error limits involved the data are overall in very reasonable agreement.

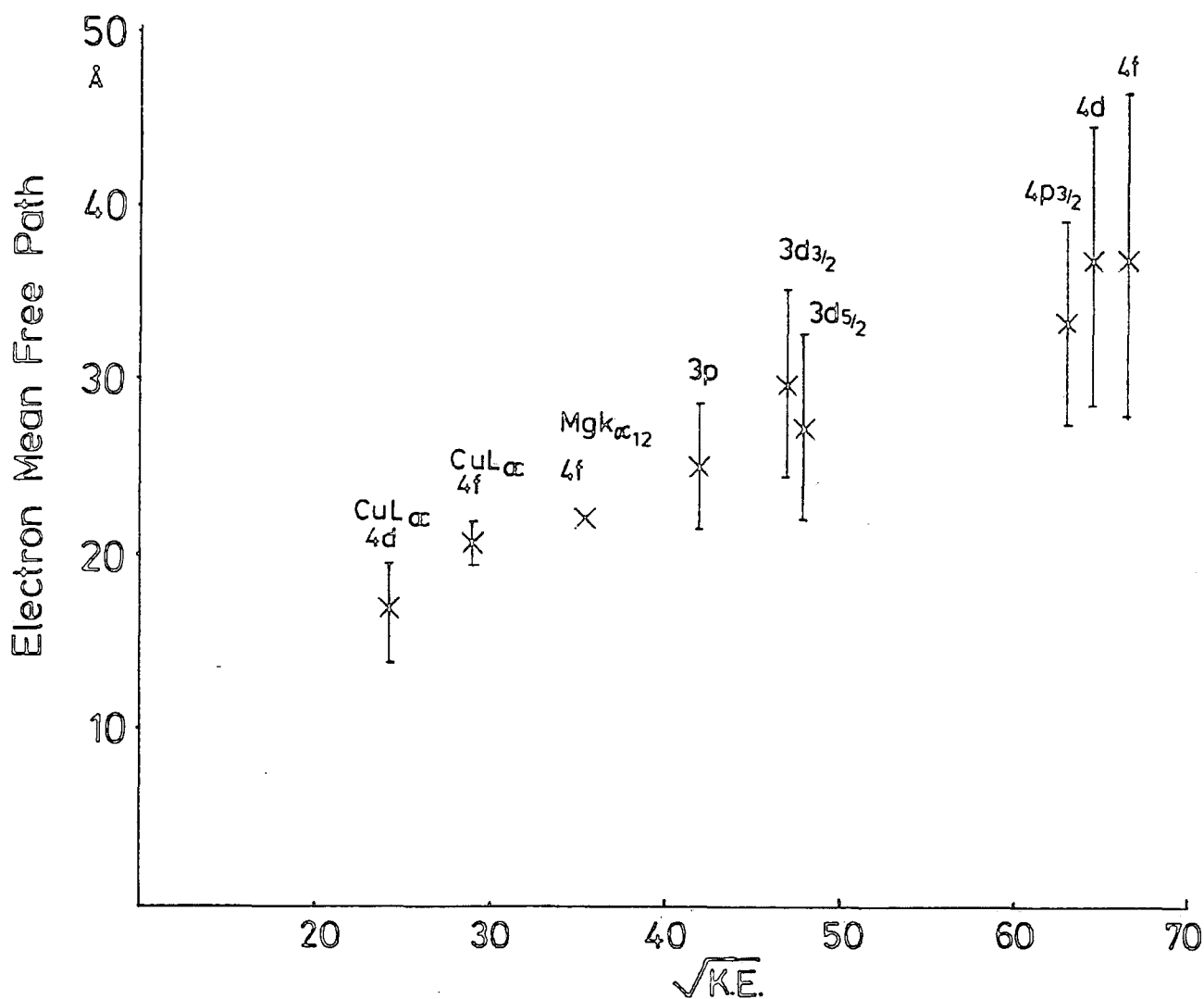


Figure 3.14 Electron mean free paths determined for the polyparaxylylene overlayers on gold substrates as a function of the square root of KE

The majority of mean free path investigations have concentrated on the 0-100eV range using synchrotron or vacuum UV sources or the 0-1480eV range using conventional X-ray sources (Al and Mg). One notable exception is the study of Nordling and co-workers¹⁹⁹ employing CrK $\alpha_{1,2}$ ($h\nu = 5414.7\text{eV}$) and AlK $\alpha_{1,2}$ X-ray sources of evaporated films on chromium substrates. It was found that the mean free path in gold doubles from 19 \AA to 37 \AA , going from 940eV kinetic energy to 3208eV. In conjunction with other results a square root dependence of mean free path on kinetic energy was evident over a $\sim 3\text{keV}$ range, in agreement with the results of this chapter.

There have been several attempts at estimating mean free paths from 'universal equations' derived theoretically,^{210,211} semi-empirically²¹² or empirically,¹⁹⁴ and it is instructive to look at one of these in the light of our results.

As already mentioned Seah has a data bank of all determinations of mean free path, and uses a least squares procedure to fit a universal curve of the form

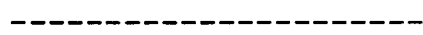
$$\lambda = \frac{a}{E^2} + bE^{\frac{1}{2}}$$

For organics, values of $a = 490$ and $b = 1.1$ are given for the fit. The results of applying this formula to the kinetic energies appropriate to this work are shown in Table 3.3, together with the data obtained experimentally.

The data show that Seah's equation gives results too high by a factor of between 1.4 \sim 2.1. This discrepancy is due to the original data to which the curve fit has been made, since a large proportion of Seah's data implies unusually large mean free paths. This arises for two reasons:

TABLE 3.3 Comparison of our results with values predicted by Seah's equation

Kinetic energy	λ calc. from Seah's eqn. (eqn.3.4) (Å)	λ observed (Å)
590	26.7	16.6
845	31.9	20.4
1768	46.2	25.0
2220	51.8	29.7
2305	52.8	27.2
3970	69.3	33.3
4177	71.0	36.7
4430	73.2	36.9



(i) Some of the measurements were made on Langmuir-Blodgett films^{17,213,197} which have large mean free paths as noted earlier.

(ii) The experimental method and treatment of results for some of Seah's data²¹³ has been shown to be erroneous,¹⁹⁵ giving overestimates of mean free path. Thus fitting eqn.3.4 to these large values will overestimate the value of b. A least squares fit of our data to the curve

$$\lambda = bE^{\frac{1}{2}}$$

does in fact give b a value of 0.45 significantly lower than Seahs. (The first term in eqn. 3.4 will be insignificant at these energies).

It is worthwhile noting that Seah's equation has been applied in a theoretical study of blurring due to secondary electrons at the surface of PMMA resists.²¹⁴ The results indicate a blurring of the order 10nm for 3000Å thick films, hence indicating a spacial resolution limit in electron beam

lithography. With the use of Seah's equation modified with a lower b value a better resolution limit could be envisaged.

Conclusions

The results presented in this chapter indicate that over a wide energy range mean free paths have a square root dependence on kinetic energy of photoemitted electrons. The great importance of the use of Ti X-ray sources is demonstrated, with the difference in sampling depth typically amounting to 50\AA . Mean free paths determined here provide the basis for semiquantitative interpretation of $\text{TiK}\alpha$ excited ESCA spectra.

CHAPTER FOUR

THE ELECTRON BEAM BOMBARDMENT
OF FLUOROPOLYMER SURFACES

4.1 Introduction

The modification of bulk properties of polymers by high energy ionising radiation has its origins in the 1940s²³⁴ but it was only after Charlesby reported²³⁵ that polyethylene extensively crosslinked by pile radiation had several desirable properties that commercial and academic interest really came to the forefront. The radiation treatment of polymers yields products with unique but very useful properties which have been exploited commercially,²³⁶ particularly in the field of heat shrinkable plastics. From the early studies it was found that, in spite of its chemical and thermal inertness, polytetrafluoroethylene rapidly showed a degradation in physical properties on irradiation.^{170,171} The irradiation of fluoropolymers¹⁷⁸ in general has shown that as a general rule those which contain hydrogen tend to predominantly crosslink, whereas when no hydrogen is present degradation in properties, that is chain scission, predominates.

Studies of the radiation chemistry of fluoropolymers were hampered by their insolubility in available solvents, thus measurement of sol and gel fractions^{170,171} of the irradiated material were not available to determine the degree of crosslinking.

Technological interest in lower energy electron beam treatments of polymers has been prevalent since the observation by Thornley and Sun²³⁷ that PMMA, which had been used as a photoresist in IC fabrication, could be degraded with good resolution by an electron beam and act as a positive acting resist. Since then other u.v. degradable resists had been tested as electron beam resists but optimisation of a *per se*

electron beam resist has only recently been investigated.²³⁸ The chemical effects of electron beam exposure have, however, been seriously neglected.

In this chapter, therefore, the results of an investigation of electron beam damage of polytetrafluoroethylene and polyvinylidene are presented.

4.2 Experimental

4.2.1 Electron Source

The electron gun used was an LEG31 (Vacuum Generators Ltd., Sussex) pentode, electrostatically focussed gun fitted with electrostatic X and Y deflection plates, as shown in Fig. 4.1. The cathode or filament is tantalum coated with thoria and provides the initial source of thermal electrons which are subsequently accelerated and focussed by the series of anodes A1, A2 and A3, and deflected using the X and Y plates shown in Fig. 4.1. The electron energy spread is quoted by the manufacturers as 0.2eV however the energy analysed elastic peak had a FWHM of typically 1.2eV. After continued use the elastic peak was found to be a doublet of variable splitting (between 5 and 0eV) depending on beam energy and current, (see Fig. 4.2). The doublet is due to the filament possessing two work functions, indicating either oxidation of some of the filament while the spectrometer was at atmospheric pressure or possibly thinning of thoria coating to reveal the tantalum. The doublet was a serious complication in the attempted measurement of electron energy loss spectra but may

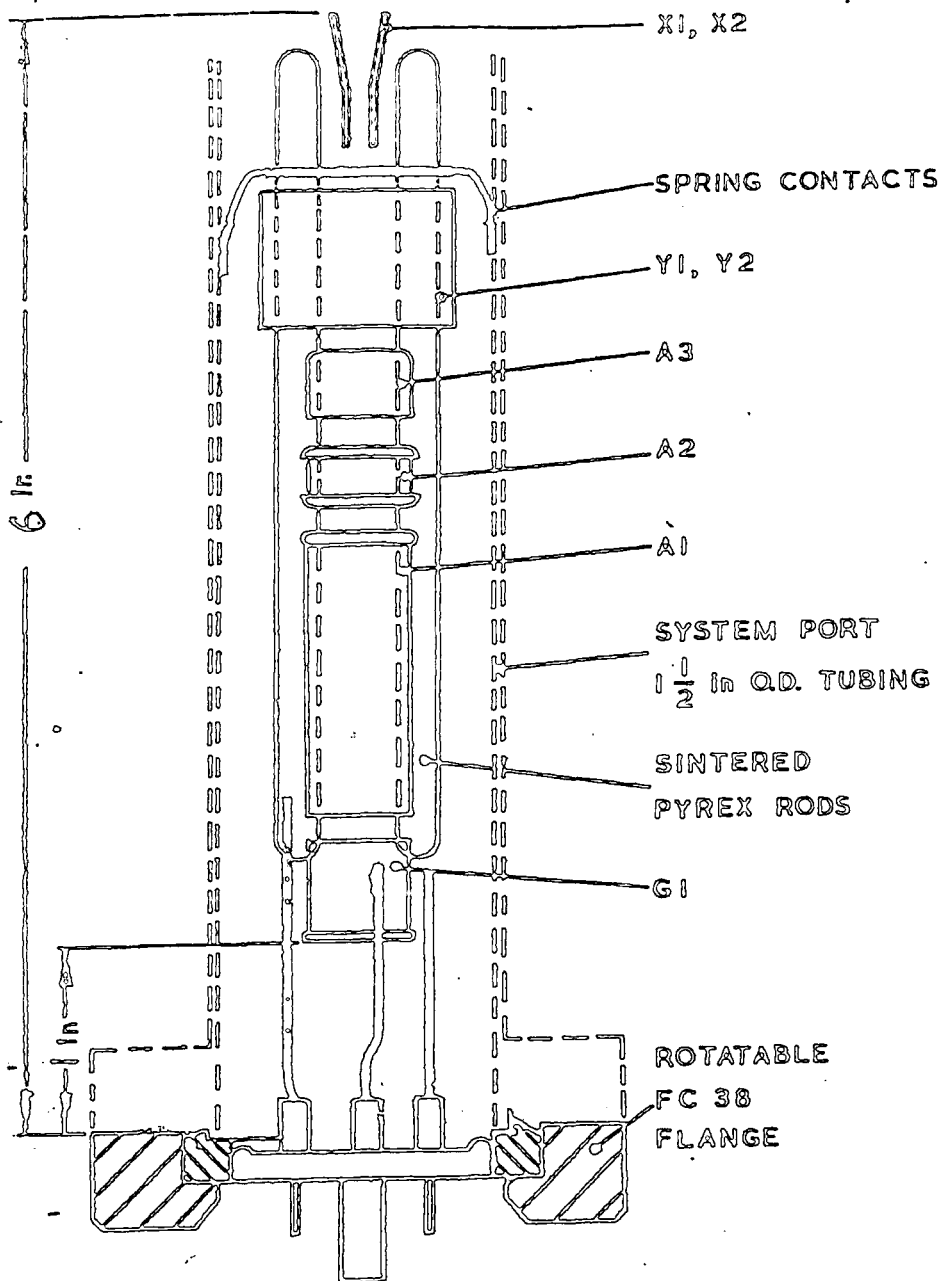


Figure 4.1 The LEG31 Electron Gun

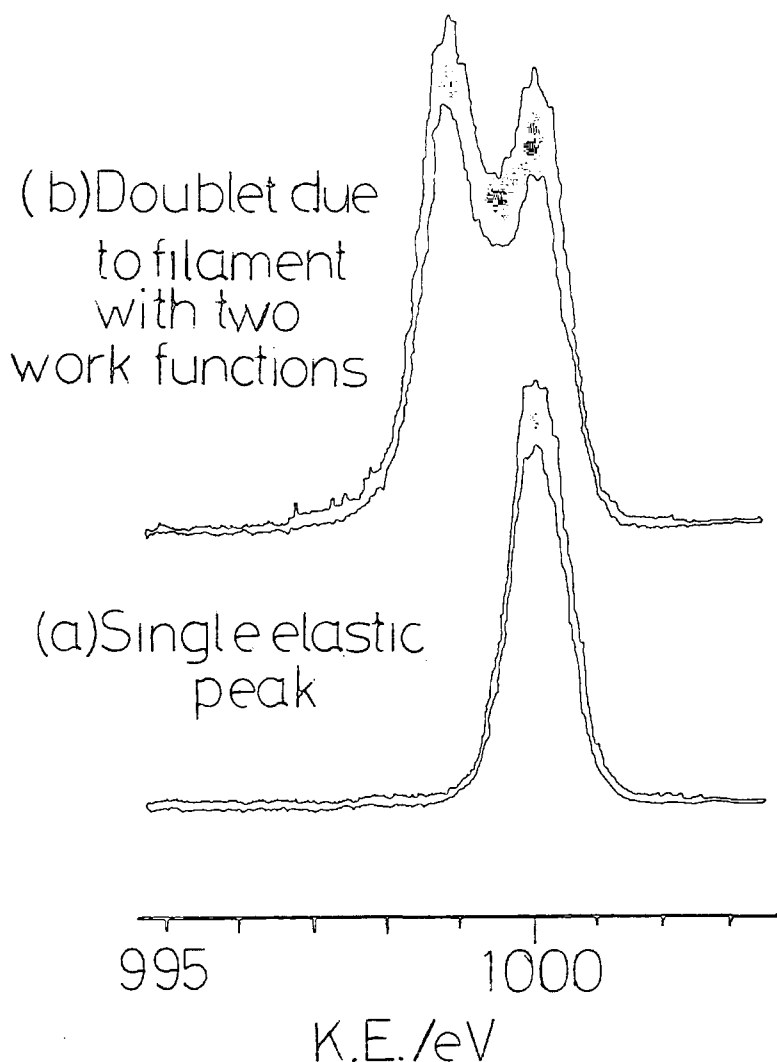


Figure 4.2 Elastic peaks measured at 1kV for 1kV electron energy
be neglected in the investigation of chemical effects on materials since the uncertainty introduced in the beam energy may be considered negligible.

The power supply for the gun was a model VG 326A multipurpose electron source power supply capable of supplying beam energies of 0-5keV. However the manufacturers do not advise use of the LEG31 gun below 1kV and considerable difficulty was found in operating the gun at beam energies greater

than 2.5keV because of electrical breakdown.

The gun has been used in two positions on the spectrometer. The first, on the sample analysis chamber itself was on the viewing port (1) position indicated on the key to plate 1.1 in Chapter One. This position allows use of the electron gun as an excitation source for Auger and EELS analysis, using the electron energy analyser usually used for XPS work. The angle of incidence of the beam onto the sample from this port ($\sim 20^\circ$) was however found to be a complication, in terms of alignment, when the chemical effects of beam irradiation were to be studied. Normal incidence onto a sample was thought to be desirable and this was achieved by moving the gun onto the sample preparation chamber as indicated in Plate 1.1. The sample preparation chamber also has reproducible ultra high vacuum conditions. Although the sample analysis chamber had base pressures in the 10^{-9} Torr range water contamination could be significant particularly when using a cooled probe. The sticking coefficients for polymers are such that ESCA analysis of polymers is not hampered by such contamination, however electron stimulated adsorption mentioned in Chapter Two would complicate the processes of beam irradiation if water was present.

Alignment of the electron beam onto the probe was attempted in several ways. Initially with the electron gun on the sample analysis chamber the elastic peak was optimised although this gave no indication of spot size. Composite samples of aluminium foil and Scotch Tape did not show great changes in the elastic peak. Prolonged exposure of the beam to polymer samples gave discolouration which could be used as an indication

of spot size. However alignment in this manner was extremely time consuming and somewhat haphazard. The use of phosphorescent materials was found to be the best method of alignment and measurement of spot size. Potassium bromide was a readily available reagent which could be mounted on the probe tip in either powder or disc form by means of double-sided adhesive tape. With the electron gun on the sample preparation chamber the phosphorescence could be readily observed through conveniently positioned view ports. For spots smaller than the total area of the probe tip, the relative position of the spot was found to be constant regardless of whether the sample was KBr or a polymer sample. Towards the end of this work a phosphorescent mineral, namely Wilhemite, Zn_2SiO_4 , was found to be a far brighter phosphor and was more convenient for lower dose electron beams.

Measurement of the beam current was carried out using a Keithley Instruments 621 electrometer by earthing one terminal to the spectrometer and attaching the other to the probe. Since the probe only touches the spectrometer *via* teflon omni seals very little leakage current is expected at low potential differences between the probe and spectrometer. The current measured was that due to the beam hitting a stainless steel face of the probe which is in a geometrically identical position to the polymer sample to be treated. At high beam energies (>1.5kV) the secondary electron yield for iron is low so the measured current will give a good indication of the electron beam current. For lower beam energies a positive current was measured which corresponds to more secondaries leaving the sample than primaries entering it. In order to gain comparable

measurements at differing energies the secondary yield must be taken into account. The simplest method would be to apply a positive bias to the probe of $\sim 15\text{V}$, since most secondaries have energies less than 15eV . However the leakage through the omni seal o rings was found to cause an electrical current which effectively swamped any effect due to the beam. The method finally chosen was to use a clean piece of gold as a standard for the secondary electron yield. Gold was chosen because its chemical inertness should make measurements here comparable to measurements of the secondary electron yield in the literature.²³⁹ The primary current I_p at a given voltage V could then be calculated from the measured current, I_m , with a knowledge of the secondary yield at voltage $V, \delta V$ since

$$I_m = I_p - I_s \quad (\text{eqn. 4.1})$$

and

$$\delta V = \frac{I_s}{I_p} \quad (\text{eqn. 4.2})$$

thus

$$I_p = \frac{I_m}{1 - \delta V} \quad (\text{eqn. 4.3})$$

Initial experiments were performed using a beam smaller than the size of the probe tip. However the problems of differential charging necessitated the use of larger beams which were only possible by interfacing the X and Y plates to a standard raster unit (Vacuum Generators):

4.2.2 Samples

The samples subjected to the most detailed scrutiny were poly(vinylidene fluoride) (PVF_2) and poly(tetrafluoroethylene) (PTFE). The PVF_2 was obtained from Kureha Chemical

Ind. Co. Ltd., Dusseldorf in the form of 300 μ sheet. The PTFE used was either skived film from Walkers Ltd., Woking, Surrey or 'polypenco' film from I.C.I. Ltd.

The fluoropolymers were chosen for several reasons. The shifts in binding energy for the C_{1s} levels for carbon in differing fluorine environments has been studied extensively over the past decade, and reference shifts are readily available from these studies of both model compounds,¹ polymers²⁴⁰ and theoretical investigations.²⁴¹ Changes in structure may therefore be monitored by both changes in the C_{1s} peak envelope and from F_{1s}/C_{1s} relative area ratios. The F_{1s} and F_{2s} levels span a substantial range in kinetic energy for the photoemitted electron and the monitoring of these levels should provide a convenient means of establishing the homogeneity or otherwise of the sample.

4.2.3 ESCA Instrumentation

Spectra were recorded on the Kratos ES300 described in Chapters One and Three. The excitation used was mainly $MgK\alpha_{1,2}$ although some studies have been performed using the harder $TiK\alpha_{1,2}$ X-ray source. Under the conditions used the $Au4f^{7/2}$ at 84eV peak excited by $MgK\alpha_{1,2}$ radiation had a FWHM of 1.2eV. Area ratios determined by curve fitting were carried out using the DS300 peak synthesis routine.

Electron bombardment was also carried out in the ES300, and although some initial experiments were performed where irradiation was carried out in the sample analysis chamber most of the work reported here was carried out with the electron gun on the sample preparation chamber previously described (Chapter One, section 8.3 and Appendix One).

4.2.4 Experimental Procedure

Before any exposure the electron beam was aligned onto a probe tip coated with either KBr or Wilhemite. The relative position of the probe was noted and the probe withdrawn and a polymer sample mounted onto the probe tip by means of double-sided adhesive tape. The probe was then re-entered into the sample preparation chamber, straight through to the sample analysis chamber and ESCA analysis carried out. The probe was then withdrawn to the position previously aligned with the beam and the probe turned through 120° to expose a clean surface of the stainless steel probe tip in a geometrically equivalent position to the polymer sample. The beam was then turned on and the filament current and gun current adjusted to give the required current measured on the probe tip by a Keithley Instruments 621 electrometer, using the circuit shown in Fig. 4.3. The potential difference between the probe and

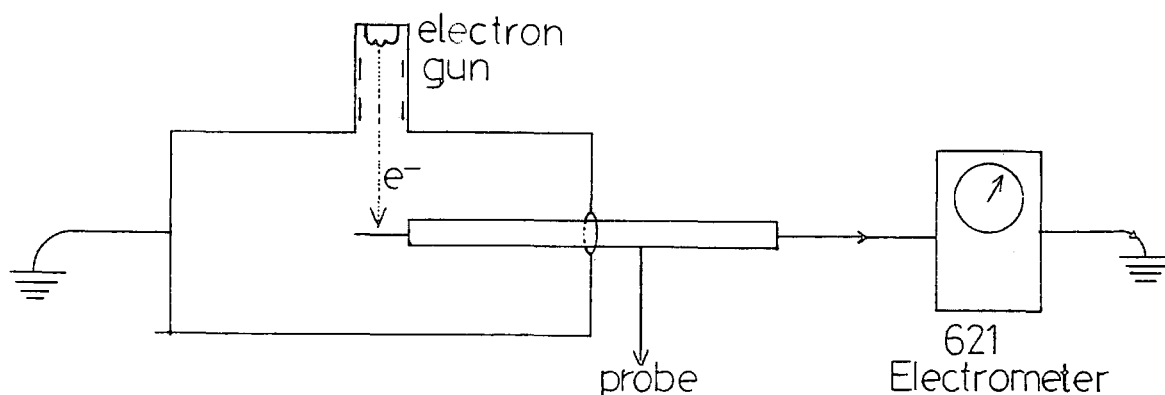


Figure 4.3 Schematic of circuit used to measure electron beam current

the spectrometer ($<1V$) coupled with the high resistance between the probe and spectrometer ($\sim 10^8 \Omega$) causes a negligible leakage current to be lost through the teflon omni seals which are the only direct contact which the probe has with the spectrometer. With the beam current stabilised the probe was turned through 120° to expose the polymer sample to the beam and after a timed period the electron gun was switched off. The sample was then re-analysed by ESCA by pushing the probe through to the sample analysis chamber. The electron irradiation and subsequent ESCA analysis was carried out with the sample maintained in high vacuum conditions: the spectrometer analysis chamber and the sample preparation chamber having typical base pressures of 10^{-9} T. During irradiation of the polymer the preparation chamber pressure showed a slight increase which is due to both the electron gun filament degassing and the sample losing gaseous products.

Initially a beam was defocussed to give a beam which irradiates the central 1cm^2 of the probe tip and leaves some of the sample therefore untouched. ESCA analysis of these samples however was severely hampered by differential charging between the treated area and the untreated area. A more satisfactory method of irradiation is to spread the beam over the entire probe tip area. Although it was found that the beam could not be defocussed over the entire probe tip, interfacing the X, Y plates of the electron gun to a scanning control unit, usually used for rastering the argon ion gun beam, does give an electron beam large enough to cover the whole probe tip. To ensure homogeneity the beam was defocussed as well as rastered.

Time dependence runs were performed by successive irradiation and ESCA analysis of the same sample with total irradiation times of 30s, 1 min, 2 min, 4 min, 10 min and 20 min for PTFE and 30s, 1 min, 2 min, 4 min, 8 min and 16 min for PVF₂ samples.

The possibility of hydrocarbon build up was investigated in two ways. The first checked for hydrocarbon contamination as a result of ESCA analysis by performing an identical experiment to a normal run but without turning the electron source on. Secondly a clean piece of gold was irradiated by the electron gun and the change in the C_{1s} and Au4f signals monitored.

4.3 Results and Discussion

4.3.1 Electron beam effects on PTFE

(i) Preliminary observations

As a starting point to the discussion of effects of electron irradiation on PTFE the results of an ESCA investigation of the changes in core level spectra of PTFE irradiated by a 6 μ A, 2kV electron beam shown in Fig. 4.4 will be presented.

Considering firstly the F_{1s} levels, a marked decrease in intensity is clearly evident as a function of bombardment time. As can be seen in Fig. 4.3 the total intensity decreases gradually with increasing bombardment time indicating that substantial fluorine loss has occurred, in fact, after 10 minutes bombardment the total integrated intensity is less than 30% of its initial value, however doubling the bombardment time to

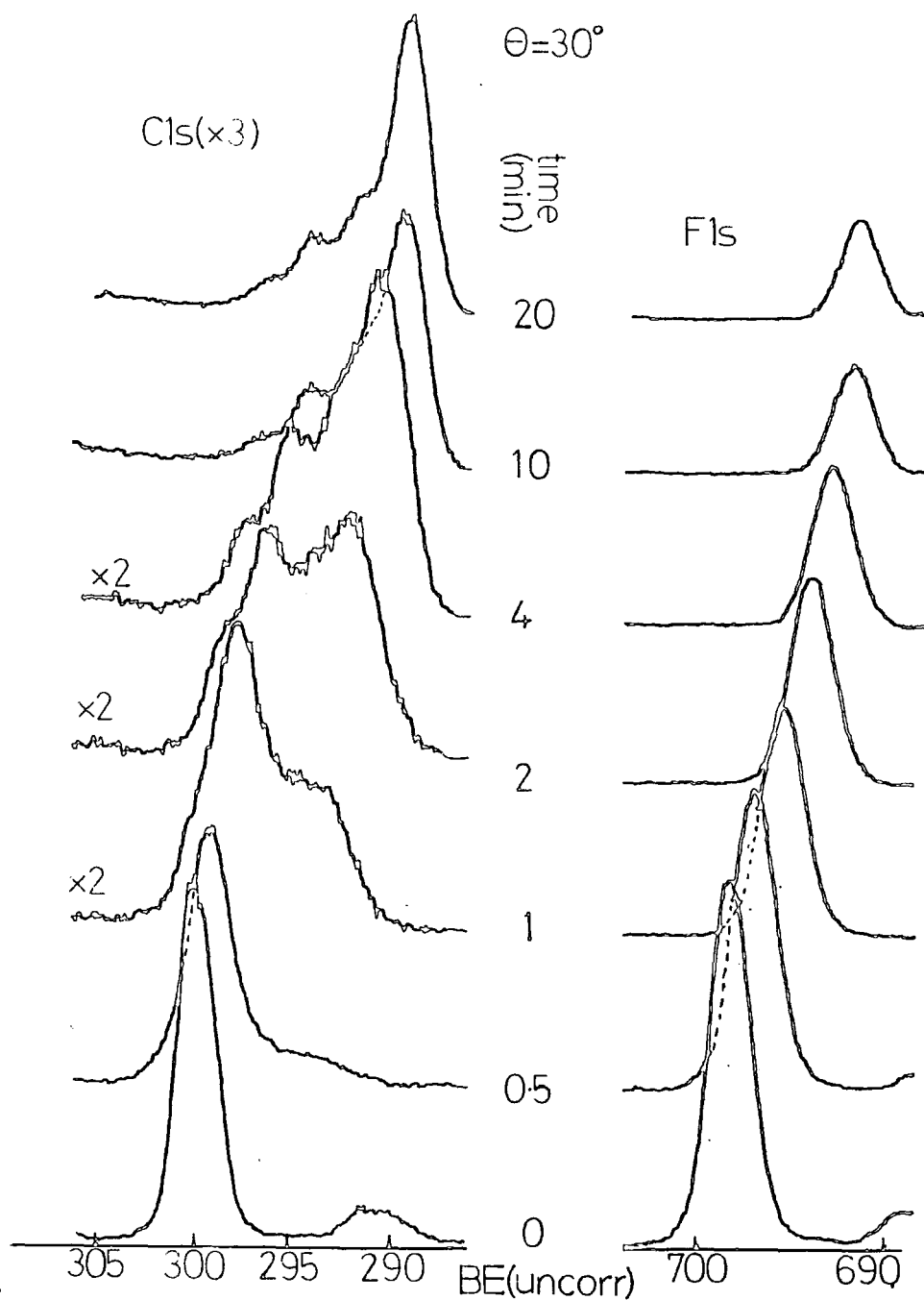


Figure 4.4 F_{1s} and C_{1s} spectra of PTFE as a function of time of bombardment by a 2kV 6 μ A electron beam. (N.B. C_{1s} spectra have had the $MgK\alpha_{3,4}$ satellite subtracted except for $t=0$)

twenty minutes does not cause such a great decrease in the F_{1s} intensity, which is an initial indication that the rate of reaction does fall off markedly with time. The other striking feature evident from the F_{1s} spectra of Fig. 4.4 is the apparent 'shift' to lower binding energy of the centroid of the F_{1s} peak with increasing bombardment time. The 'shift' observed between the F_{1s} level of the starting material and of the 20 minute bombarded material is 6.3eV which is far greater than the shift range typically observed in the F_{1s} levels of organic compounds and indeed most ionic, covalent compounds and is therefore due to a change in the surface charging characteristics with increasing bombardment time since the spectra are shown on an energy scale of X-ray photon energy minus observed kinetic energy. The sample charging of polymers and conductors not in electrical contact with the spectrometer has been studied in detail by Clark and coworkers and a significant finding of these investigations was that utility of sample charging as a probe of surface composition, particularly in polymers.^{100,101} In the latter a lesser degree of charging during XPS analysis has been shown to be indicative of decreased fluorine¹⁰¹ content and so the decrease in charging observed in the F_{1s} spectra of Fig. 4.4 is a second indication that defluorination is occurring in PTFE with increasing electron bombardment. Further evidence that the change in position of the F_{1s} signal was due to charging phenomena rather than a pure chemical shift was provided by experiments where less than the total area of the sample was irradiated by the beam. After long treatment times the F_{1s} level showed two peaks, one corresponding to untreated PTFE and the other arising from the treated

area of the sample. The appliance of a bias to the probe and measurement of the spectra was found to shift the two peaks in a differential manner, thus indicating that the initial splitting was due to varying electrical characteristics of the untreated and treated portions of the sample and not a true 'chemical' shift.

One further point worthy of discussion arising from the F_{1s} spectra of Fig.4.4 concerns the change in line-widths observed. The untreated sample F_{1s} spectrum consists of a single photoionisation peak at (corrected) binding energy 690.2eV, (the peak to ~ 8 eV to lower binding energy is a doublet caused by ionisation of the F_{1s} levels by $MgK\alpha_{3,4}$ satellite X-radiation and will not be considered further), and FWHM 2.0eV. Upon 30s irradiation the FWHM of the F_{1s} peak changes to ~ 2.2 eV. This broadening is indicative of a change in chemical environment of fluorine atoms present in the sample. Initially only fluorine in $(CF_2)_n$ environments was present and thus gave a relatively sharp photoelectron signal. The shift range of the F_{1s} level is small in comparison to its full width at half maximum and so the differing chemical environments manifests itself as a broadening in the F_{1s} spectra. The changes in chemical environment are more readily seen in the C_{1s} spectra where the shift range is far greater than the FWHM and these changes will now be discussed.

As can be seen from Fig. 4.4 the $6\mu A$ beam has a severe effect on the C_{1s} lineshape. The untreated sample shows a single C_{1s} photoelectron peak corresponding to carbon in polytetrafluoroethylene, $\langle CF_2 \rangle_n$. The $K\alpha_{3,4}$ satellite is again evident and on removal of this feature using the satellite subs-

traction procedure on the DS300 data system very little hydrocarbon contamination was evident as deduced from the peak at a (corrected) binding energy of 285eV. After 30 seconds bombardment time, which corresponds to a dose received by the sample of $\sim 8 \times 10^{14}$ electrons/cm², significant changes have occurred to the C_{1s} spectrum with the growth of features to the low binding energy side of the main CF₂ peak and significant broadening of the latter feature. This trend continues with increasing bombardment time with the initial growth of features to both the low and high binding energy of the main CF₂ peak. After two minutes bombardment time therefore the spectrum bears little resemblance to the starting material with features corresponding to CF₃, CF₂, CF, and C type carbons being clearly evident. Defluorination continues such that by 4 minutes bombardment time features corresponding to CF and C type carbons dominate the spectrum, and after twenty minutes the spectrum has mainly C type carbon with very little CF₂ and CF₃ evident.

Component analysis of the C_{1s} spectra allows close examination of the points introduced in the previous paragraph in somewhat greater detail. The chemical shifts for fluorine substitution on the C_{1s} binding energy has been previously studied for a large variety of systems allowing^{1,240} a generalised additive model to be adopted.²⁴² Fluorine substitution at an α position involves a shift of ~ 2.9 eV and substitution at a β position ~ 0.7 eV are acceptable values within the model and it is using these generalised values that peak fitting of the C_{1s} spectra has been undertaken. The complexities of the line-shapes given inhibited a totally unambiguous analysis but gross trends which occur are indicated. The results of such an analysis for the spectra in Fig.4.4 are shown in Fig. 4.5.

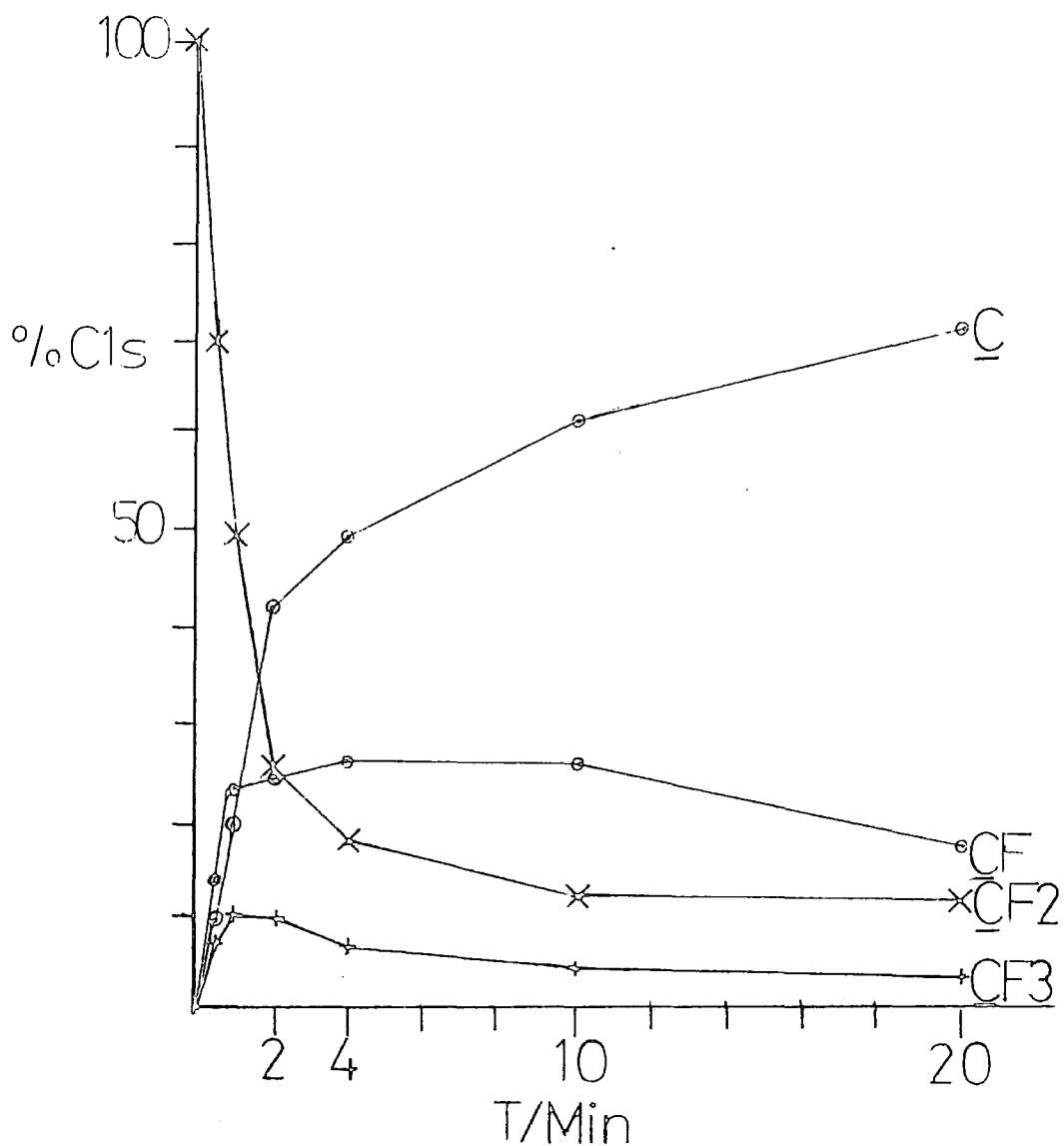


Figure 4.5 Variation in C_{1s} components with bombardment time (Current = 6μA, Energy = 2keV) for PTFE

The trends apparent by visual inspection of the C_{1s} spectra may clearly be seen from the component analysis. Initially there is a very fast decrease in the intensity of components arising from CF_2 functionalities such that after 2 minutes less than 25% of the total C_{1s} intensity is due to these features which initially comprised $\sim 100\%$ of the C_{1s} spectrum. This corresponds to 1.65 CF_2 groups lost per bombarding electron incident upon the sample assuming a mean free path for the C_{1s} levels of 14\AA (and an effective sampling depth of 3λ). However since the mean free path for 2kV electrons, from the data presented in Chapter Three can be extrapolated to be $\sim 30\text{\AA}$, the fraction of electrons incident upon the sample surface which have undergone any energy loss is in fact

$$\left(1 - e^{-\frac{14 \times \cos\theta \times 3}{30}} \right)$$

i.e. ~ 0.7 , thus for each electron which has undergone an unspecified energy loss a crude estimate tells that approximately 2.4 CF_2 groups have been lost per energy loss electron. Similar data at the other treatment times will be dealt with in a later section. Returning now to the component analysis it can be seen that accompanying the rapid decrease in intensity due to CF_2 functionalities is a rise in features corresponding to carbon not directly bonded to fluorine (C), carbon with one fluorine at the α position (CF) and some trifluoro substituted carbon atoms (CF_3). The relative proportion of the latter reaches a maximum of $\sim 9\%$ of the total C_{1s} envelope after 1 min. treatment times and then decreases. The presence of $-CF_3$ is an indication of chain end groups within the polymer, since PTFE is known to undergo main chain scission under the action of high energy

radiation source.^{170,171,243} However the proportion of $\underline{\text{CF}}_3$ groups after 1 min. irradiation implies that there is one $\underline{\text{CF}}_3$ for every 17 carbon atoms. It would seem likely therefore that $\underline{\text{CF}}_3$ groups are present also as branch end groups as well as long chain end groups. This is the first observation to imply that electron irradiation involves branching to some extent. The observation of $\underline{\text{CF}}_3$ groups in PTFE irradiated by high energy radiation has mainly rested on I.R. evidence, although the difficulty of assignment of structural features from I.R. has been highlighted by several conflicting accounts in the literature. Thus Slovoktova²⁴⁴ noted an increase in bands assigned to $-\text{CF}_3$ between $745-725 \text{ cm}^{-1}$ with heavy doses. A band at $\sim 980 \text{ cm}^{-1}$ was also observed to grow on irradiation which the authors assigned as being due to fluorocyclobutane structures but which has recently²⁴⁵ been assigned as indicative of CF_3 functionalities. The latter study however did not report any major changes in this band on irradiation but on post-irradiation annealing an increase in intensity was observed. The ESD spectrum of PTFE is dominated by the CF_3^+ peak, however, although quantification of the ion yield, particularly in relation to the neutrals desorbed, is complex. Mass spectra of any perfluoroalkane are generally dominated by CF_3^+ ions. Gases evolved from PTFE have been studied, with CF_4 being the major product,²⁴⁶ with some longer chain perfluoroalkanes.^{247,248} The origin of the $-\text{CF}_3$ functionalities observed in the ESCA spectra presented here could therefore be due to a chain fragment reacting with the polymer surface prior to desorption: the fragment in question being either a fluorine atom or ion, or a perfluoroalkyl radical or ion.

The initial rise in CF_3 functionalities in Fig. 4.5 is seen to drop and the general fluorine loss occurring in the polymer is reflected by a gradual decrease in the proportion of $-\text{CF}_3$ groups contributing to the C_{1s} envelope.

The evolution of $\underline{\text{CF}}$ functionalities is also rapid for short irradiation times but afterwards shows a decrease, again reflecting the overall fluorine loss of the system under investigation.

The initial increase in $-\underline{\text{CF}}$ groups is less than 50% of the initial decrease in $-\underline{\text{CF}}_2$ functionalities. Defluorination is therefore happening on such a scale that fluorine loss is also occurring from $-\underline{\text{CF}}$ functionalities themselves initially formed by loss of fluorine from CF_2 groups. Beyond treatment times of 1 minute the dominant features in the C_{1s} spectra are due to carbon atoms with no fluorine atom directly attached to fluorine. The lineshape analysis of this region of the spectra is particularly difficult, because of the appearance of features with a binding energy of less than 285eV. Charge referencing of the spectra is therefore difficult. The method of allowing a hydrocarbon overlayer to develop as a result of condensation extraneous vacuum²⁴⁹ vapours was not fruitful in this respect mainly as a result of the cleanliness of the spectrometer at the time. Referencing was therefore performed in a self-consistent manner, summarised in Fig. 4.6, using the centroid of the F_{1s} peak and approximating a binding energy of this peak from known values for model compounds and the fluorine to carbon stoichiometry ratio calculated from the $\text{F}_{1s}/\text{C}_{1s}$ relative area intensities. Using this procedure growth of features at B.E.s lower than 285eV is certainly implicit, indicating the presence

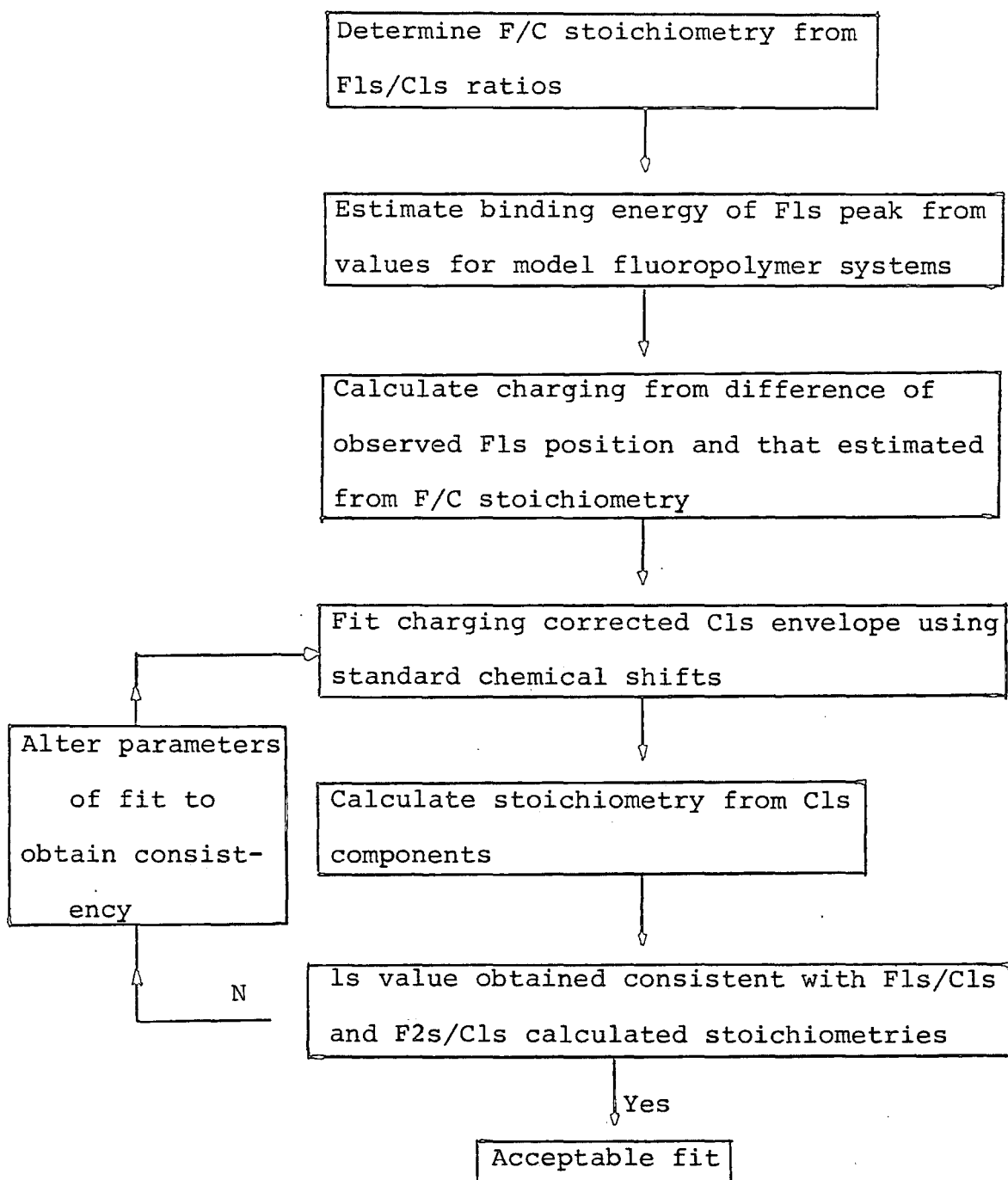


Figure 4.6 Schematic of analysis routine for ESCA data

of a graphitic and/or polyenic structure. For longer treatment times this feature dominates the C_{1s} spectrum, the sharpness of the peak indicating that the final structure is not in as wide a variety of chemical environments as initially. The formation of unsaturation in PTFE has been reported in high energy irradiated samples^{245,250} and the present results would tend to corroborate such an observation.

Further evidence of unsaturation in the final structure was established by a crude bromination experiment where the sample was allowed to stand in bromine vapour for several minutes and the spectra rerun. A Br 3d peak was detected after the treatment indicating that either trapped radicals and/or unsaturation was present. The initial untreated sample and the final sample showed a very small (<1% of the C_{1s} signal) O_{1s} peak, but on the latter's exposure to air the O_{1s} peak showed a marked increase. This could be due to oxygen trapping of surface free radicals or oxidation of a polyenic final structure. Oxygen uptake would occur in a disordered graphitic system provided prismatic edges were exposed at the surface since these have been shown to have sticking coefficients for oxygen far greater than basal plane edges.²⁵²

The emergence of shake-up features to the high binding energy side of the main photoionisation peak has been shown by Clark and coworkers^{38,39,40} to be a major information level in the ESCA spectra of polymers and organic monomers in general possessing double bonds. However no such peaks can be straightforwardly discerned in the spectra in Fig.4.3. However the baseline of the C_{1s} , F_{1s} and F_{2s} spectra is seen to rise with respect to the low binding energy region as can be seen in the expanded spectra of the 20 min. treated sample in Fig. 4.7

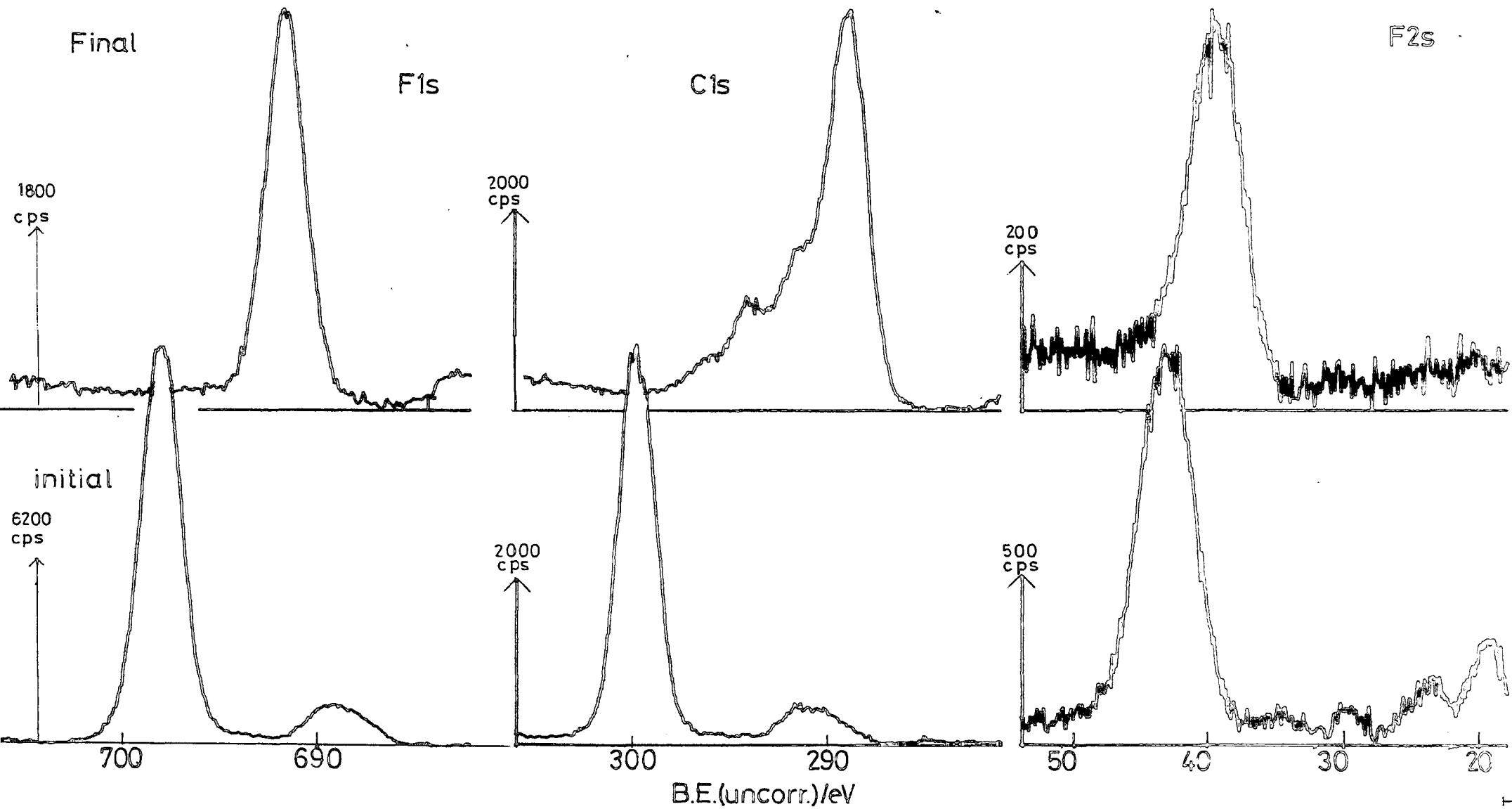


Figure 4.7 Comparison of initial C_{1s} , F_{1s} and F_{2s} spectra with spectra obtained after 20 min.

compared to those for the starting material. The asymmetrical baseline is indicative of a highly delocalised π system,²⁰³ such as a polyene or indeed graphite. The raising of the high energy baseline is a manifestation of the asymmetry of the main photoionisation peak. Such asymmetry is observed in materials which have a high density of states near the Fermi level,^{77,251,47} in general conductors, and may be thought in a crude manner as arising from a multitude of shake-up processes⁷⁷ whose transition energy \bar{E} (as defined by eqn. 1.5 in Chapter One) varies from 0eV upwards. The raising of the baseline of the upper spectra in Fig.4.7 can be seen to follow the trend

$$F_{1s} < C_{1s} < F_{2s}$$

The asymmetry of the F_{2s} level is greatest since valence excitation (shake-up processes) would be expected to have greatest overlap with the F_{2s} levels. However theoretical modelling of these processes is beyond the scope of this investigation.

The defluorination of the PTFE surface can be illustrated dramatically by consideration of the F_{1s}/C_{1s} ratios of the spectra in Fig. 4.8. Also included in Fig. 4.8 are the corresponding data for spectra run at 70° take-off angle which are therefore more indicative of the absolute surface of the system. It can be seen that in both cases substantial loss of the F_{1s} signal relative to the C_{1s} signal has occurred with the fastest drop occurring in the initial stages of the reaction. The reaction appears to be faster initially in the outermost surface region as evidenced by the greater F_{1s}/C_{1s} decrease in the 70° spectra, but in the latter periods of irradiation increasing homogeneity is evident by convergence of the ratios at the two take-off angles. Further insight into the homo-

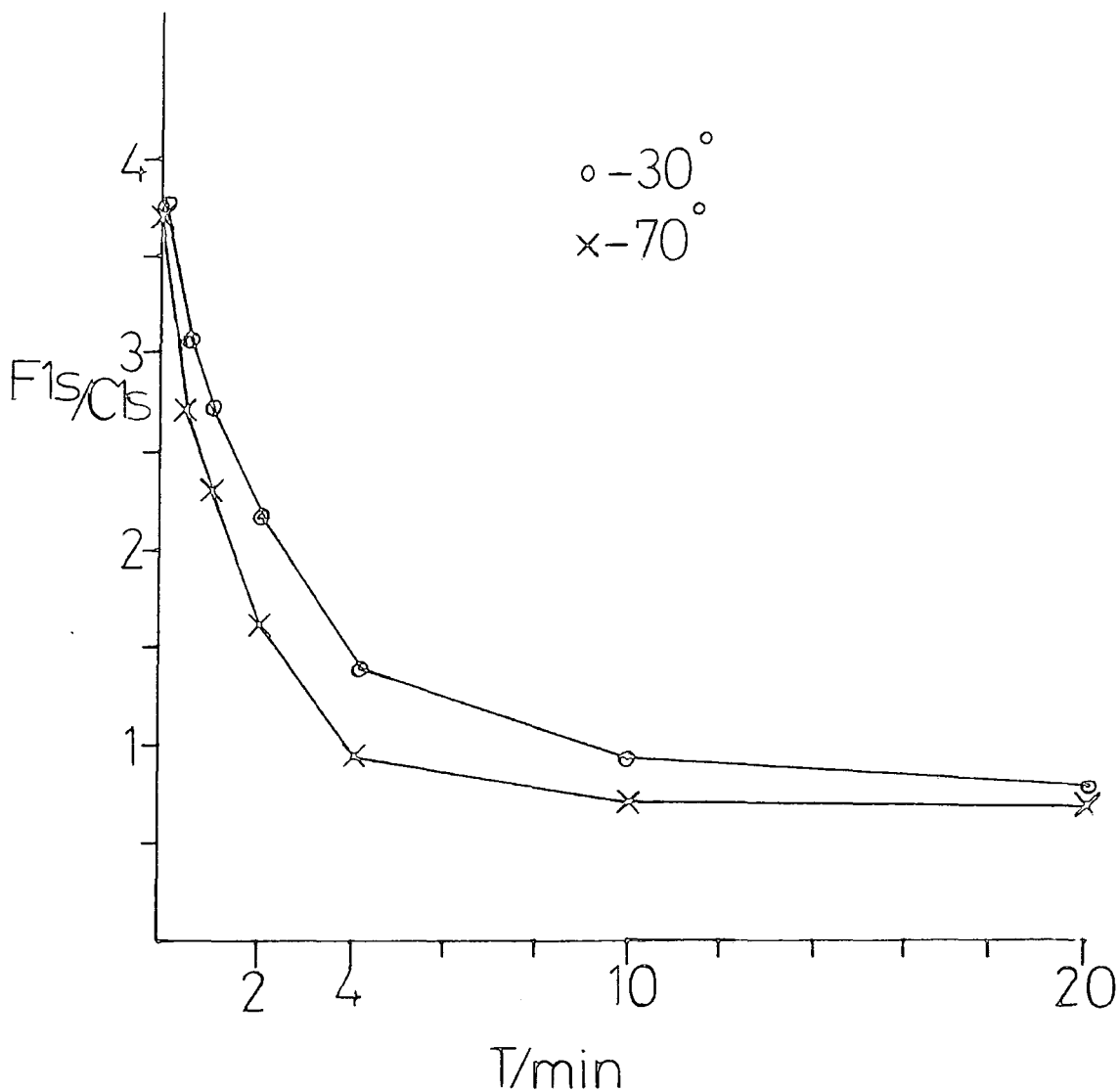


Figure 4.8 Variation in the F_{1s}/C_{1s} relative intensity ratio for $6\mu\text{A}$ bombarded PTFE

generality or otherwise is available by using the large difference in sampling depth between the F_{1s} and F_{2s} levels. A plot of the F_{1s}/F_{2s} relative intensity ratios is shown in Fig.4.9 and reveals that after an initial period the F_{1s}/F_{2s} ratios decrease indicating again that defluorination is more rapid in the surface regions of the sample since preferential attenuation of

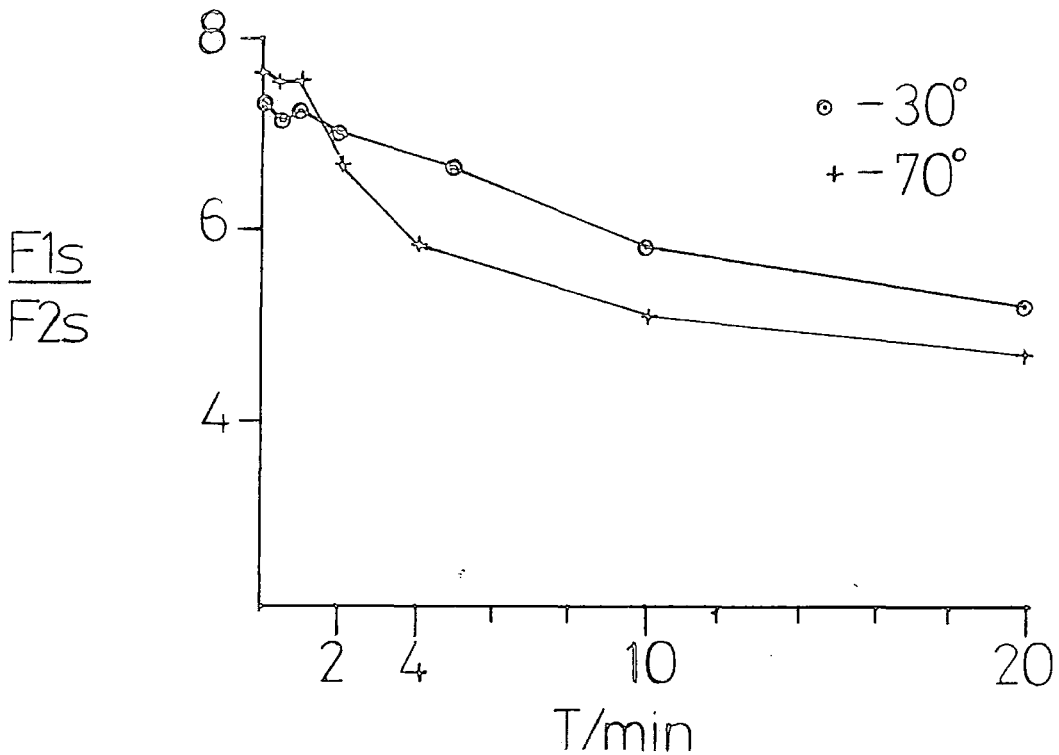


Figure 4.9 Variation in F_{1s}/F_{2s} ratio for $6\mu\text{A}$ bombarded PTFE

of the F_{1s} levels by a surface region low in fluorine occurs as a consequence of the lower mean free path (*viz* $\sim 7\text{\AA}$ versus $\sim 20\text{\AA}$ for the F_{2s} levels). Also evident is a slight difference in the F_{1s}/F_{2s} ratios at the two take-off angles indicating that the decrease in fluorine is greater in the surface regions of the sample.

The differences between 30 and 70° take-off angle may be seen by comparison of the spectra in Fig.4.10 with Fig.4.4.

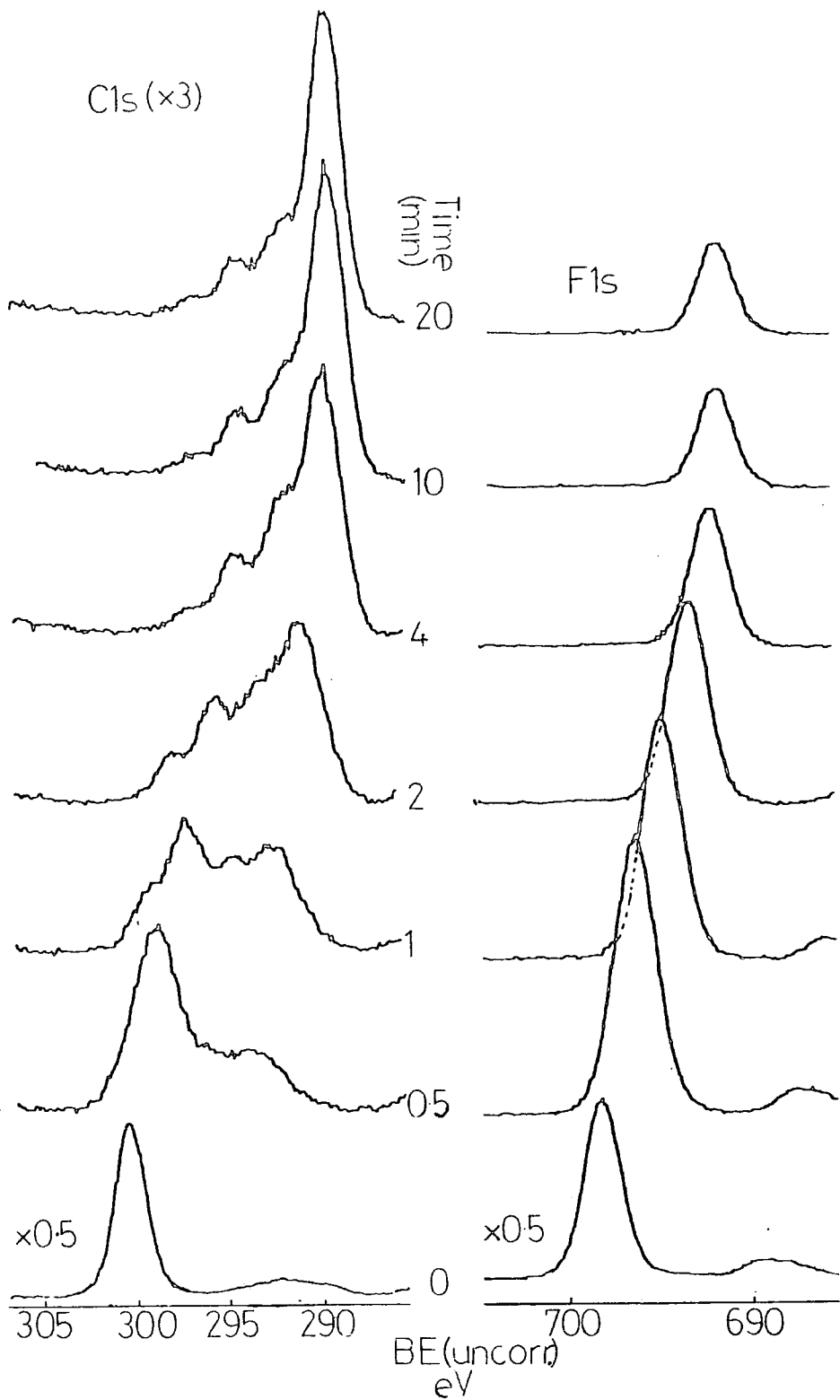


Figure 4.10 F_{1s} and C_{1s} spectra recorded at 70° take-off angle for PTFE bombarded by $6\mu A$ 2kV electrons

The component analysis for the 70° spectra is presented in Fig. 4.11 and shows that the decrease in the $\underline{\text{CF}}_2$ peak occurs much faster such that after 30s irradiation it only contributes 55% to the total C_{1s} signal. The increase in CF_3 functionalities is not as pronounced. In the surface region of the sample the fragment ion/radical mentioned earlier involved in the

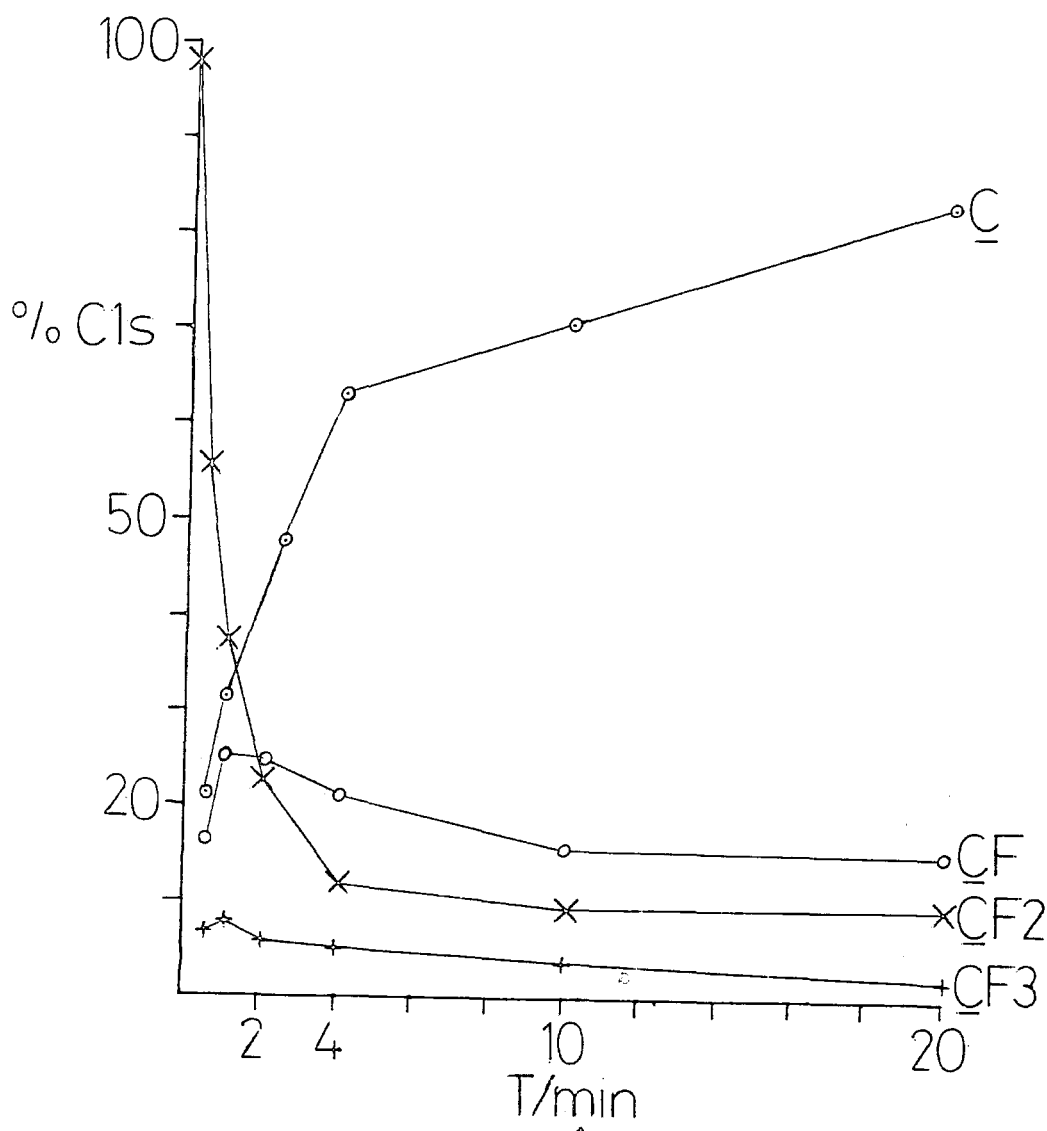


Figure 4.11 Variation of C_{1s} components at 70° take-off angle

formation of CF_3 groups has a greater probability of escape, defluorination competing with the favourable surface free energy of CF_3 groups over CF_2 ²⁹³. The decrease of CF functionalities is also more rapid after an initial increase to about the same proportion as that in the 30° spectra. This observation is also consistent with the idea that reactive species, in this case a fluorine radical or ion stands a greater chance of escape than in the subsurface region of the irradiated polymer.

The large differences in C_{1s} lineshape for identical treatment times between the 30° and 70° take-off angles are, in fact, revealed to be due to only small differences in the component analysis. For example after 2 minutes treatment the $\text{CF}_3:\text{CF}_2:\text{CF}:\text{C}$ ratios are 9:24:24:42 for the 30° spectra and 6:22:25:47 for the 70° spectra, indicating that in the more surface sensitive region greater defluorination has taken place. The effects reported at both 30° and 70° take-off angles indicate a variety of processes are occurring: the possibility of hydrocarbon contamination or adsorption being solely responsible for the changes observed may be partially discounted by the observation of CF_3 , and CF functionalities in the C_{1s} envelope. The possibility of electron stimulated adsorption of residual hydrocarbon contamination was also checked by bombardment of a gold sample for 20 minutes by a $1.5\mu\text{A}$ electron beam. The C_{1s} and $\text{Au}4f$ spectra before and after the electron treatment are shown in Fig.4.12 and reveal that there is an increase in C_{1s} intensity but that its effect on the $\text{Au}4f$ envelope intensity is negligible. Substrate/overlayer calculations on both the $\text{Au}4f$ intensity attenuation and the C_{1s} increase indicate that less than a monolayer deposition of 'carbonaceous' material has occurred due to

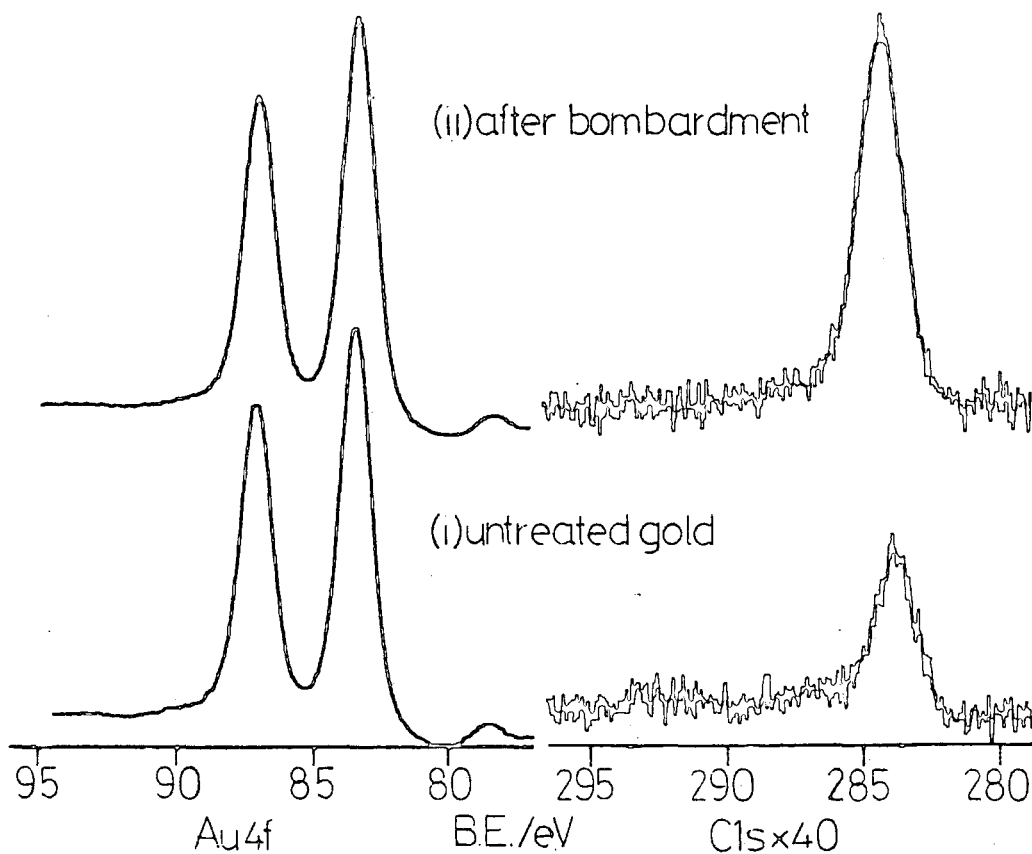


Figure 4.12 Au_{4f} and C_{1s} spectra of gold before and after 20 minute bombardment by a 2kV 1.5µA electron beam

beam treatment. The sticking coefficient of hydrocarbon for gold is, however, expected to be significantly higher than for a polymer. X-ray degradation during a run was investigated by leaving a sample under the X-ray beam for the appropriate time and the spectra recorded at similar intervals to those during a run revealed negligible changes in both lineshape, area ratios and binding energy.

4.3.1 (ii) Electron beam damage as a function of dose rate and the abstraction of kinetic data

The preceding section described the changes observed during irradiation by a current of $6\mu\text{A}$, which was the grossest treatment used in this study. A variety of runs were undertaken keeping the beam voltage constant (2kV) but varying the beam current over greater than an order of magnitude.

As a contrast to the data presented in the preceding section Fig.4.13 shows changes in the $\text{C}_{1\text{s}}$ spectra which occur to PTFE on receiving a dose of $0.15\mu\text{A}$, *i.e.* $\sim 6.7 \times 10^{11}$ electrons $\text{cm}^{-2} \text{s}^{-1}$. Changes in the spectra can be seen to be significantly less than at beam currents of 40 times greater presented in the preceding section. Again some degree of vertical inhomogeneity is apparent since changes in the $\text{C}_{1\text{s}}$ lineshape appear to be occurring faster at 70° than at 30° . This is revealed in the component analyses for the spectra as seen in Fig. 4.14 where the growth of $\underline{\text{C}}$ type features and the decay of the $\underline{\text{CF}}_2$ signal is greater in the surface regions than in sub-surface. Also shown in Fig.4.14 are contributions to the $\text{C}_{1\text{s}}$ envelope obtained after 30s treatment by a $6\mu\text{A}$ beam, which is the equivalent, in terms of dose, of 20 mins. at $0.15\mu\text{A}$. It is apparent that after the same dose at a higher current less defluorination had occurred as evidenced by greater contributions from $\underline{\text{CF}}_2$ and $\underline{\text{CF}}_3$ functionalities at the higher dose. It would appear therefore, as will become more apparent later, that overall damage caused to the sample is not a linear function of beam current. However since defluorination may be envisaged as the initial loss of a fluorine atom or ion from the main chain, the concentration of free fluorine moieties at the greater dose rate

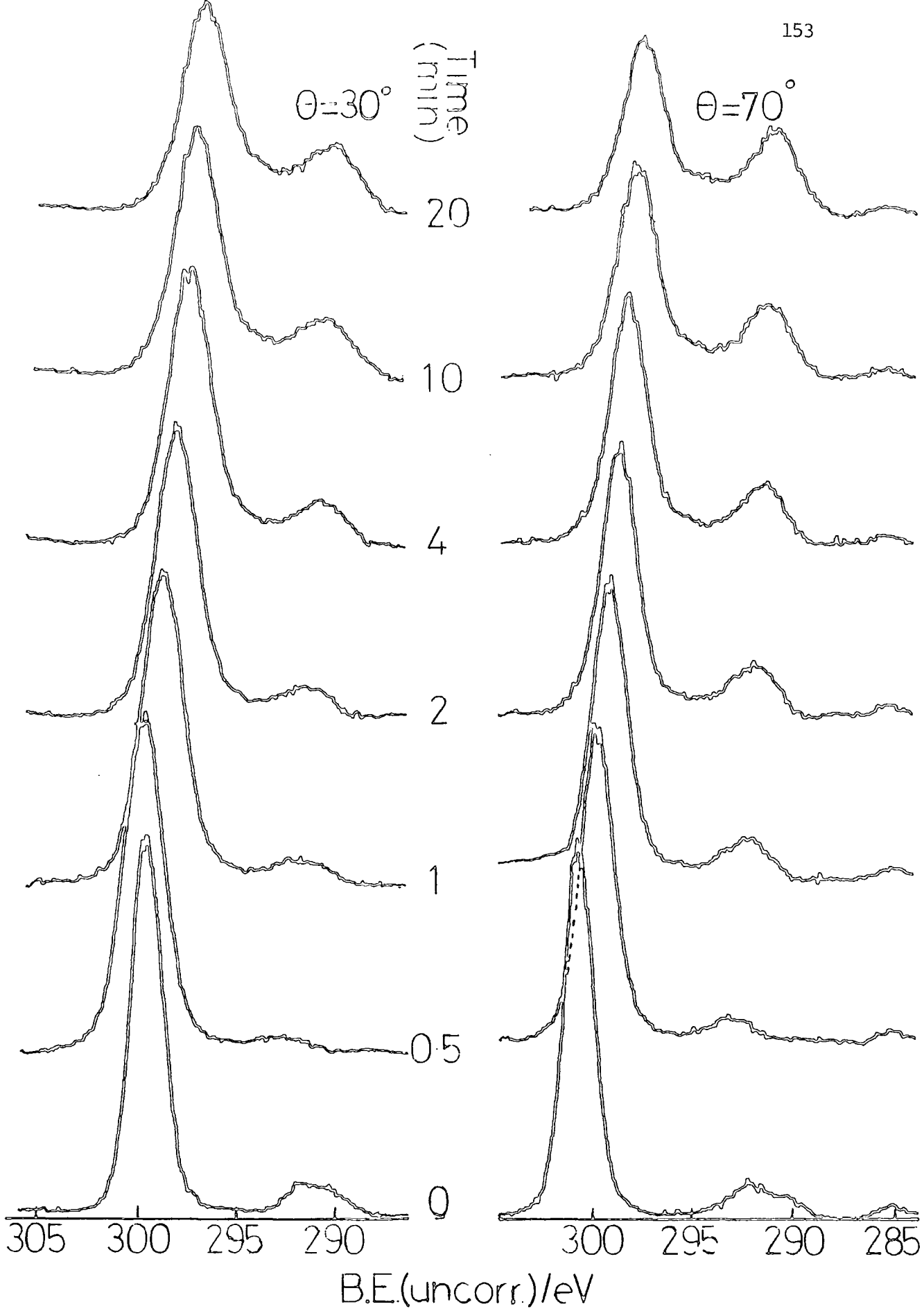


Figure 4.13 C_{1s} spectra at two take-off angles of PTFE
bombarded by a $0.15\mu A$ electron beam

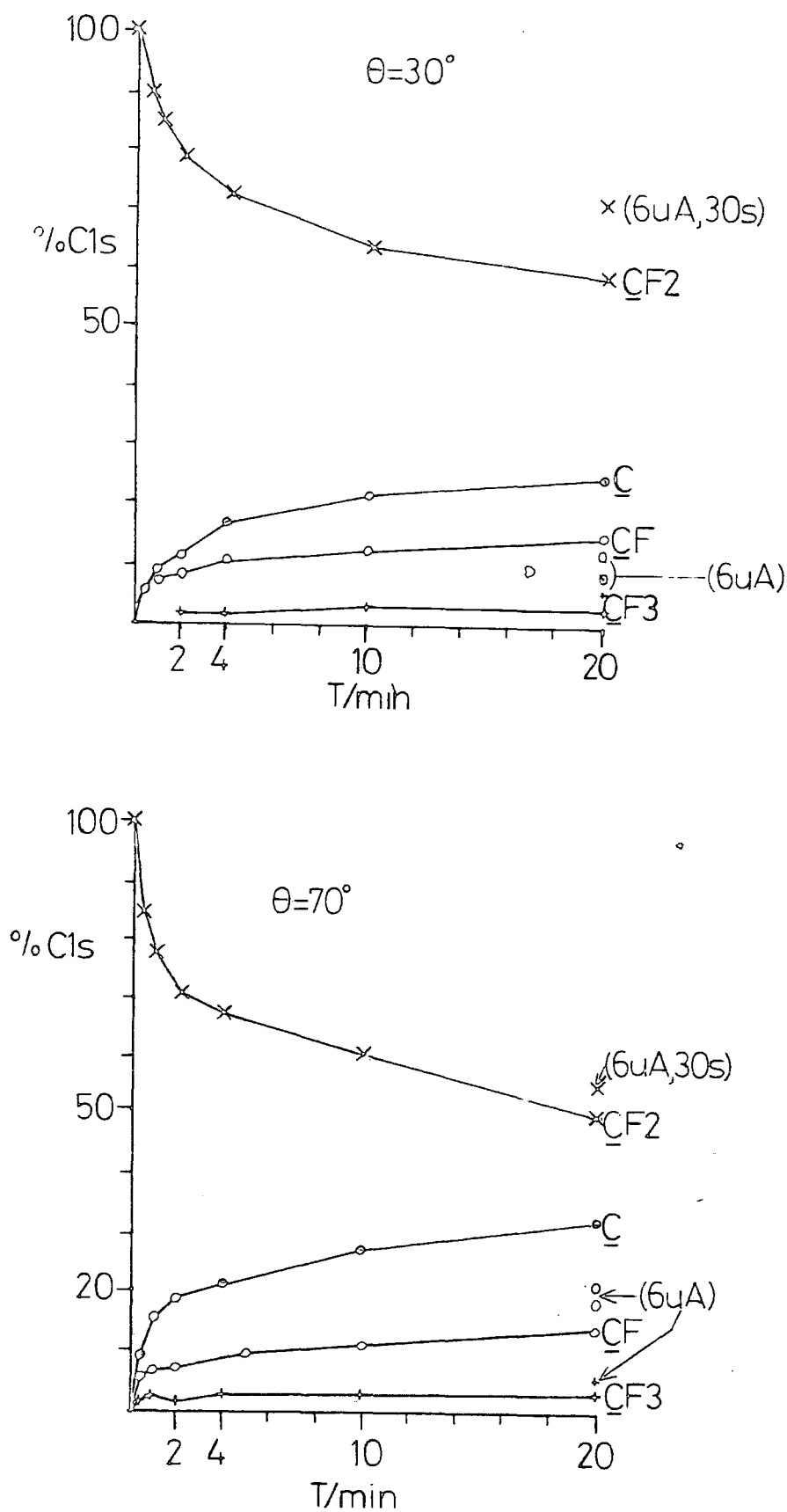


Figure 4.14 Variation of components of spectra shown in Fig.4.13

during irradiation will be higher therefore favouring a re-combination reaction to occur enhancing the relative proportions of $\underline{\text{CF}}_2$ and $\underline{\text{CF}}_3$ groups at higher current but equivalent dose.

In spite of the secondary processes occurring the abstraction of rate data has been attempted from the F_{1s} levels and the CF_2 component of the C_{1s} level. The F_{2s} levels in addition provide greater insight into the depth of the reaction. For ESD processes of monolayers,^{146,157} the concentration of undamaged species within the detection region at any one time, $N(t)$ has been found to follow a first order relation,

$$N(t) = N_0 \exp\left(\frac{-I_e Q_0 \cdot t}{A\epsilon}\right) \quad (\text{eqn. 4.4})$$

where Q_0 is the effective cross section of the desorption process, N_0 is the initial undamaged material concentration within the analysis region, I_e is the total beam current, A is the irradiated area and ϵ is the electronic charge.

Thus a straight line whose gradient varies with I_e should be given, if ESD is the only process occurring, in a first order plot of $\frac{N}{N_0}$. Departure from linearity indicates that a simple ESD process is not occurring for a variety of incident beam currents at 2kV, at take-off angles of 30° . Plots of $\ln\left(\frac{\text{CF}_2}{\text{C}_{\text{Tot}}}\right)$ versus t and $\ln\left(\frac{\text{F}_{1s}}{\text{C}_{1s}}\right)$ vs. t are shown in Figs. 4.15 and 4.16. Both sets of data show distinct curvature, the data obtained from the CF_2 components being somewhat smoother than from the $\text{F}_{1s}/\text{C}_{1s}$ ratios. The curvature observed could be indicative of several first order processes occurring. However, Hutton²⁰³ has recently shown in a study of the interactions of a hydrogen plasma with PTFE that curvature observed in first order plots may be attributed to a single first order process occurring within separate monolayers of the polymer surface. This point will be

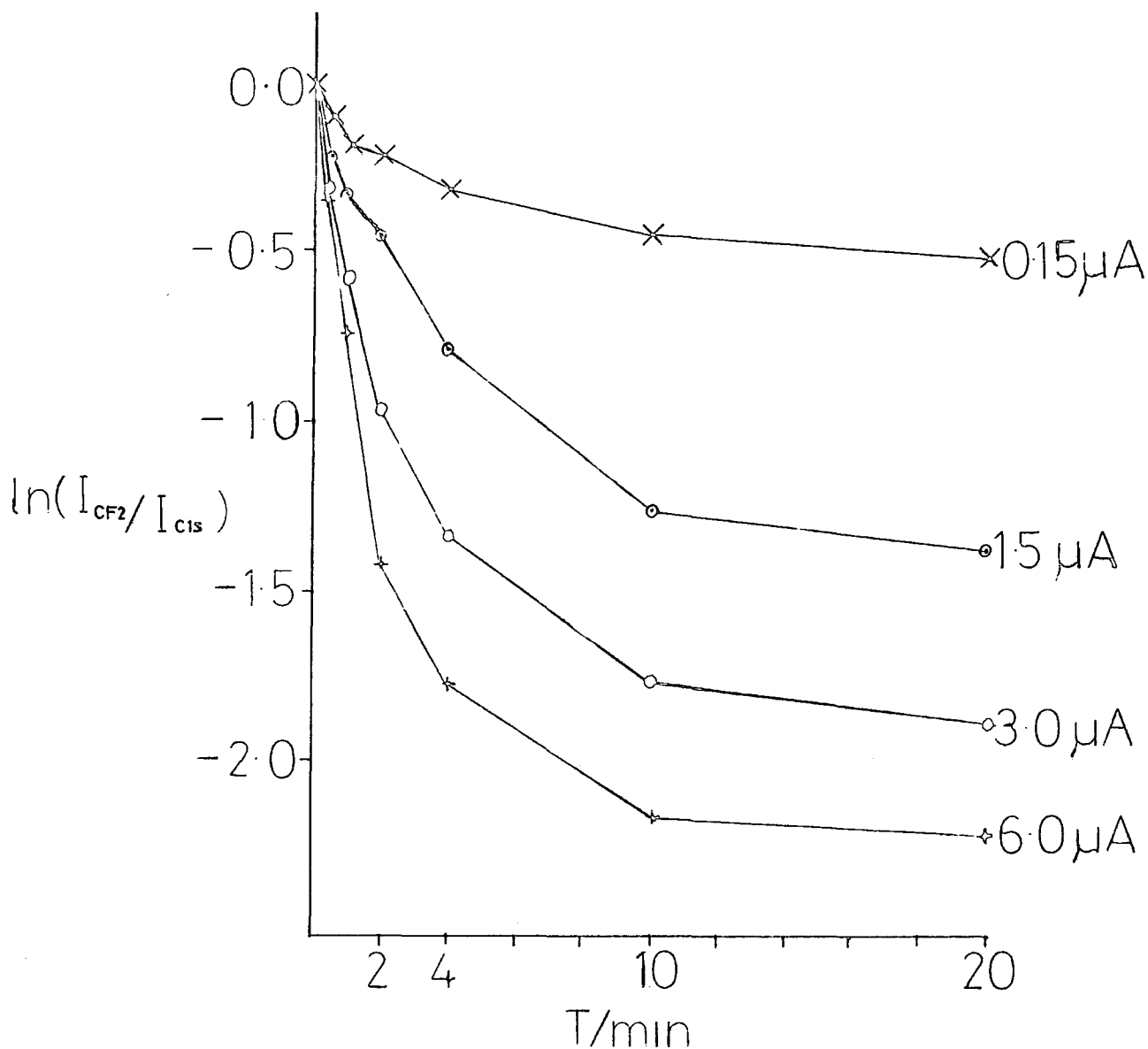


Figure 4.15 First order plot of $\ln(I_{CF_2}/I_{C_{1s}})$ versus bombardment time at various electron beam currents for PTFE

returned to later in the discussion. The initial data points have however been used to obtain an initial first order rate constant for the decay of the CF_2 and F_{1s} signal intensities and the results of this treatment are shown in Table 4.1 together with data obtained from the 70° take-off angle spectra.

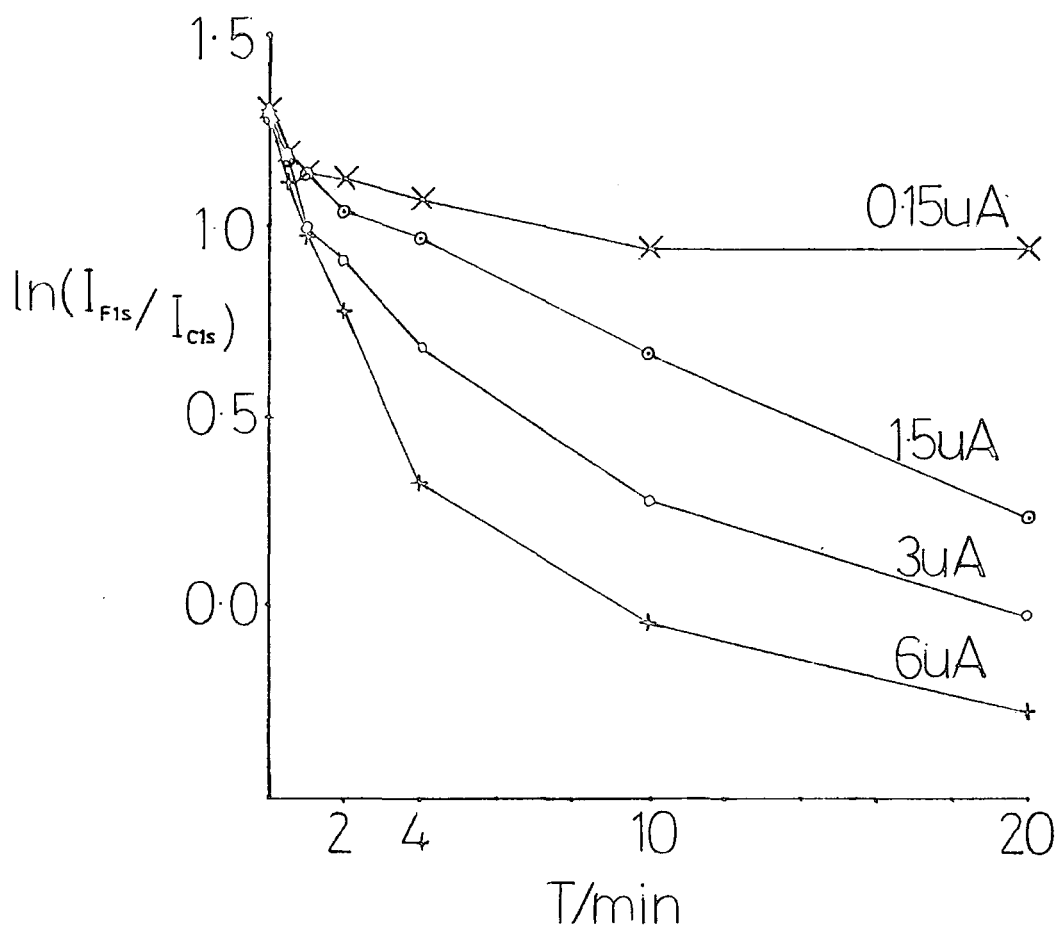


Figure 4.16 First order plot of the variation of the I_{F1s}/I_{C1s} intensity ratios at various electron currents

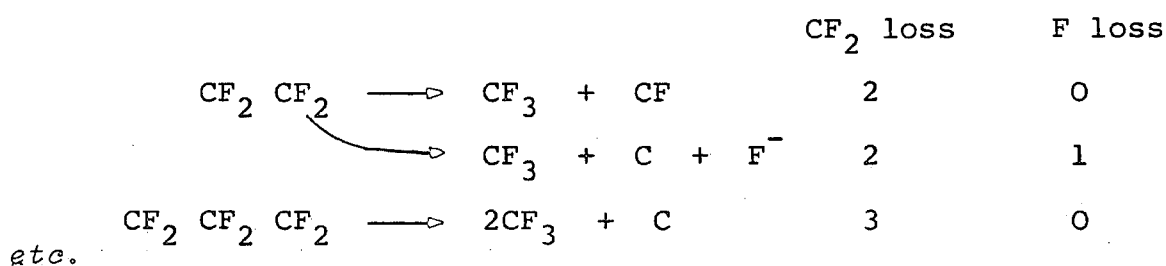
As can be seen from the rate constants determined, reaction occurs at a greater rate in the surface regions than in the subsurface and bulk since rates determined at 70° are consistently greater than those at 30° take-off angle. The relative values for the CF_2 component data are consistently larger, however. For a simple reaction occurring faster at the surface

TABLE 4.1 Pseudo first order rate constants (in units/min⁻¹)
obtained for PTFE

Beam Current/ μA		0.15	1.5	3.0	6.0
Core level					
F_{1s}	{ 30	.08	.11	0.17	0.27
	{ 70	.11	.12	0.21	0.33
CF_2	{ 30	.11	.22	0.34	0.71
	{ 70	.16	.24	0.47	0.73

it would be expected that the rate obtained using the F_{1s} levels, which have a shorter mean free path and are therefore more surface sensitive than the C_{1s} levels, would be greater. Such was the case found in the hydrogen plasma treatment of PTFE. The greater rate of CF_2 loss is in disagreement therefore to the surface enhanced reaction if the mean free paths of the C_{1s} and F_{1s} levels is solely taken into account. However the greater rate constant obtained from the CF_2 component data may be rationalised on consideration of the processes occurring in electron bombardment.

Component analyses have shown that in the initial stages of reaction loss of fluorine is also accompanied by molecular rearrangement giving CF_3 , CF , and C groups in addition to the CF_2 groups initially present. In the initial stages of reaction at $6\mu\text{A}$ incident beam current production of $\sim 10\%$ CF_3 groups occurred, thus stoichiometrically this can have arisen from a variety of schemes, *e.g.*



Loss of CF_2 groups therefore will not mirror the loss of fluorine from the polymer because of side reactions forming a significant proportion of CF_3 groups. This is in marked contrast to the treatment possible on the ESCA data of the hydrogen plasma treatment of PTFE where fluorine loss did mirror the decay in the CF_2 component signal.²⁰³ It may also be shown that formation of a significant proportion of CF groups will also increase the rate determined from the CF_2 levels compared to that from the F_{1s} levels. This added complication seriously hampers even a crude semiquantitative modelling of the reaction but the initial pseudo first order rates obtained do show some interesting features as will become apparent.

Firstly the ratios of the $\text{CF}_2:\text{F}_{1s}$ rate constants at a given take-off angle fall with decreasing beam current. This is consistent with the observation of a smaller proportion of CF_3 functionalities appearing at low beam currents. Similarly the ratios of the rate constants from the CF_2 component data at $30^\circ:70^\circ$ falls with lower beam current for the same reason.

The variation of derived rate constants as a function of beam current is shown in Fig. 4.17. As would be expected the rate of reaction increases with dose rate, the rate of observable damage appears to be a linear function of dose rate. However, on going from $0.15\mu\text{A}$ to $6\mu\text{A}$, *i.e.* a 40X increase in beam current (*i.e.* dose rate) for the 30° data, the CF_2 component rate increases by a factor of only $\sim 7x$; the increase in the F_{1s} rate being even lower at $\sim 4x$.

The formation of active species at a faster rate at higher beam currents is consistent with the variation of derived rate constants; dose rates used in this study represent near to

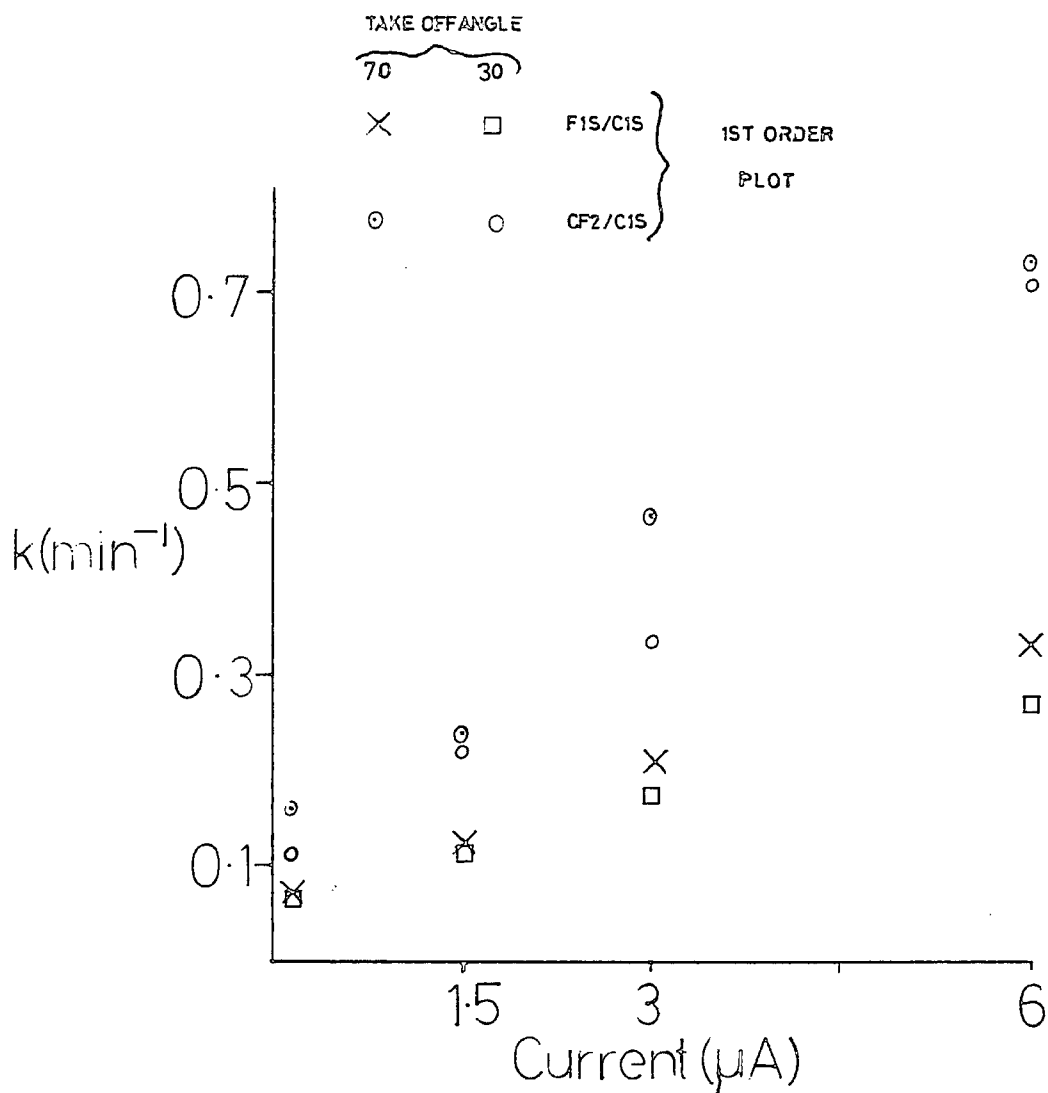


Figure 4.17 Variation of pseudo first order rate constants obtained with electron beam current

saturation in terms of electrons bombarding the polymer surface over the time scale of the measurements.

A desorption cross section for fluorine from PTFE may be estimated from these data, however as has become apparent the processes occurring are not a simple ESD process comparable to, say, CO on W. Estimates of the 'desorption' cross section from the F_{1s} rate data obtained are $\sim 10^{-15}$ – 10^{-16} cm^2 which, for a simple desorption process are unusually large values and are tantamount to the domination of chemical processes over defluorination by a simple ESD mechanism.

Pantano¹⁵⁷ has defined a damage threshold for materials in an attempt to standardise beam effects in Aes of electron sensitive materials as the dose required to cause a 10% detectable change in the material. Using the values for rate constants obtained from the \underline{CF}_2 component data the sensitivity of PTFE is estimated to be $6 \times 10^{-6} \text{ C cm}^{-2}$. This may be compared with typical sensitivities of positive electron beam resists between 10^{-10} and $10^{-6} \text{ C cm}^{-2}$.²³⁸

As a first attempt to model the process occurring the variation in the F_{1s} and F_{2s} intensity ratios was fitted to a substrate-overlayer system as outlined in Chapter One, section 1.3.4 (ii).

The model assumes a modified layer of material on top of a substrate of unmodified material. The intensity of the F_{1s} level, may therefore be written as

$$IF_{1s} = k_1 \left\{ x(1 - e^{-d/\lambda_1 \cos \theta}) + 2e^{-d/\lambda_1 \cos \theta} \right\} \quad (\text{eqn.4.5})$$

where x is the stoichiometry of the altered layer where symbols have their usual meanings.

Likewise the F_{2s} intensity is given by

$$IF_{2s} = k_3 \left\{ x(1 - e^{-d/\lambda_3 \cos \theta}) + 2e^{-d/\lambda_3 \cos \theta} \right\} \quad (\text{eqn.4.6})$$

This model therefore assumes a layer of homogeneous stoichiometry x .

The relative intensity ratio is therefore

$$\frac{IF_{1s}}{IF_{2s}} = \frac{k_1 \{ x(1 - e^{-d/\lambda_1 \cos \theta}) + 2e^{-d/\lambda_1 \cos \theta} \}}{k_3 \{ x(1 - e^{-d/\lambda_3 \cos \theta}) + 2e^{-d/\lambda_3 \cos \theta} \}} \quad (\text{eqn.4.7})$$

The constant $\frac{k_1}{k_3}$ is the bulk sensitivity factor for the F_{1s} to F_{2s} levels derived from consideration of homogeneous materials.

Values of $\frac{IF_{1s}}{IF_{2s}}$ were thus calculated for values of d from 0 to 90\AA and values of x from 0 to 2. Comparison with the experimental data, using a value of x from the F/C ratios showed that with increasing reaction time, particularly at beam currents of 1.5, 3.0 and $6\mu\text{A}$ the F_{1s}/F_{2s} experimental ratio gave a close fit to the theoretical value for values of d which initially increases with increasing bombardment time, but plateaus to a value of $\sim 40\text{\AA}$ at 30° take-off angle. However, although the observation of a moving boundary layer is supported by a similar treatment for the 70° spectra the absolute values determined at the higher take-off angle plateaued at $\sim 20\text{\AA}$. This may be due to a surface roughening effect, which will tend to converge the average take-off angle seen by the analyser to $45^\circ, 150^\circ$ but both values obtained represent a limit beyond the sampling depth for the F_{1s} and C_{1s} levels at each take-off angle. The most likely situation is a modified layer whose fluorine concentration gradually increases with depth rather than a homogeneous overlayer of modified material with a well defined interface with the unmodified material.

Thus a model is needed where a modified surface layer changes in depth as a reaction proceeds as well as composition. Such a model has been used by Hutton²⁰³ in treating data obtained from the modification of PTFE by a hydrogen plasma. An adapted version of the program to synthesise the model has been used here in an attempt to gain insight into the variation of the relative intensities of the core levels under investigation.

The model is similar to those recently published in that it uses a modified version of the simple substrate overlayer model where the surface is split into lateral sections such that the contribution of each to the observed intensity may be calculated. A vertically inhomogeneous reaction is allowed to proceed in each monolayer at a first order rate, the inhomogeneity being introduced by varying the effective concentration of active species with depth.

Relative intensities of the F_{1s} and F_{2s} intensities are given along with component ratios of the C_{1s} group. Again a non-ambiguous fit to the modelled data was not found, the closest fits were found when the reaction was one-tenth that of the surface rate at $\sim 40\text{\AA}$ but that especially in the latter stages of irradiation the relative intensity ratios predicted from a first order process fall too rapidly compared to the experimental data. In fact the data were found to have the best fit assuming a reaction dependent on \sqrt{t} rather than times which may be indicative of diffusion processes. In studies of the inert gas¹⁰² and hydrogen plasma modification of polymers the diffusion of the active species into the polymer was found to be a limiting factor on the depth of modification, in the present context it is not unreasonable to assume that the reverse process, *i.e.* diffusion of an active species (*e.g.* F^\cdot or F^-) out of the polymer does have a role to play.

These attempts do tend to imply that the reaction is too complex to follow using a simple model, since side reactions in the model are completely ignored, as is an increase in the number density of the carbon atoms which, as will become apparent, increases greatly during the period of bombardment.

The behaviour of the absolute total intensities of the C_{1s} envelope during irradiation is worthy of further mention. It was found that for both 30° and 70° spectra, at whatever beam current used the C_{1s} total intensity rose to a maximum value of 1.4 times that of its initial value, Fig.4.18 being a typical example.

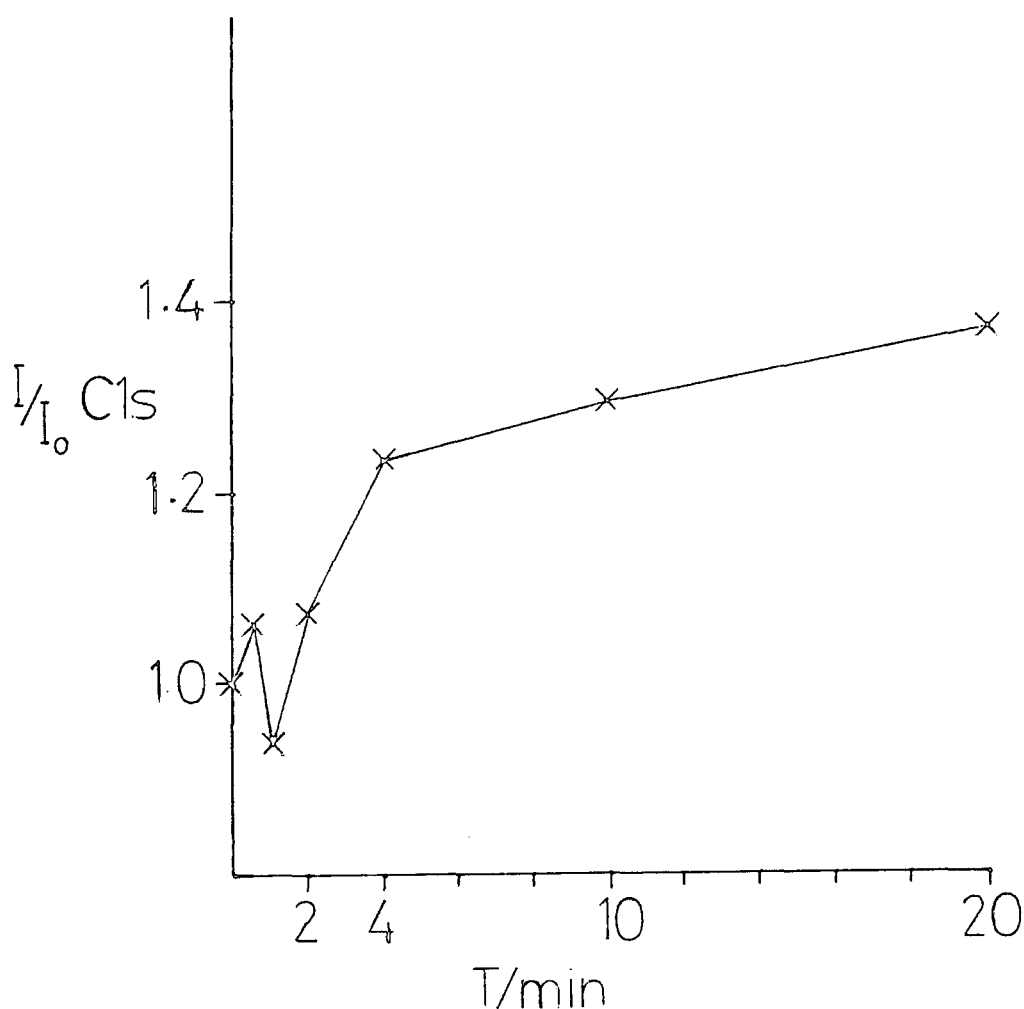


Figure 4.18 Behaviour of the C_{1s} total intensity as a function of bombardment time

The intensity of a given core level in XPS (*c.f.* Chapter One) is proportional to the number density of atoms within the sampling volume. Thus the increases observed are evidence of increased carbon atom density. To what extent this is due to the removal of interchain spacing of the original polymer matrix by either crosslinking or removal of substituent atoms cannot be fully ascertained from the available data. Both the creation of a crosslink, with a C-C bond distance of $\sim 1.5\text{\AA}$ between two chains (which in polyethylene are separated by $\sim 4.7\text{\AA}$), and the loss of fluorine atoms to give chains of conjugated carbon atoms, will increase the number density and it is reasonable to assume that both processes are occurring. PTFE was originally described as a degradable polymer in terms of its radiation chemistry, but evidence for its crosslinking is now available.

(iii) Energy dependence of beam damage in PTFE

A limited study was undertaken to investigate the influence of bombarding electron kinetic energy on PTFE. Instrumental parameters at the time dictated that less than the whole area of the sample was irradiated, thus differential charging effects inhibit a total analysis of the data. However the F_{1s} to C_{1s} intensity ratios obtained indicate that over the range 1kV to 2.5kV kinetic energy has little effect on sample damage within the ESCA sampling depth during the initial stages of reaction. Greatest defluorination appears to be occurring at 1kV electron energy but a general trend in these data is not seen (see Fig.4.19).

This is not surprising when the effective range of the electrons is taken into account. Using values calculated from

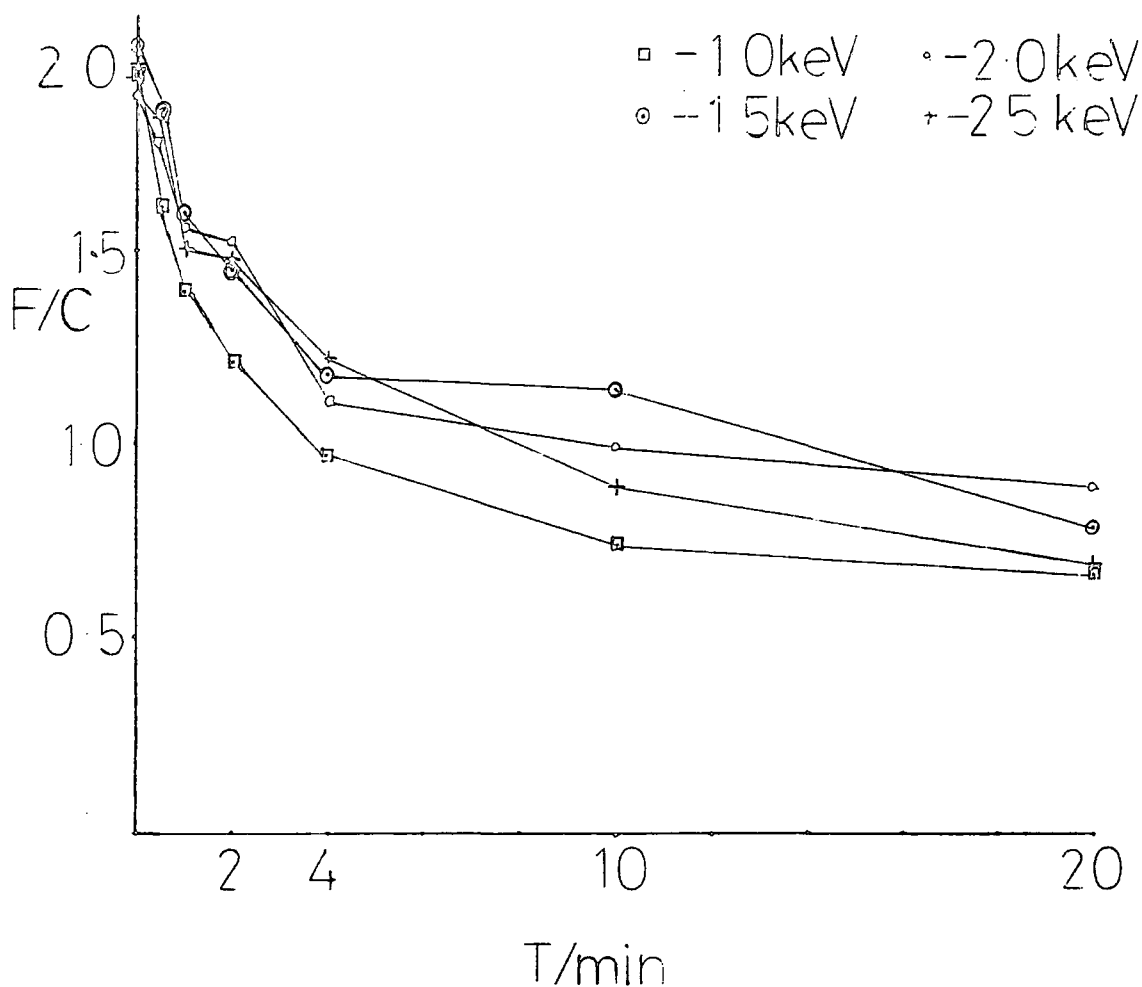


Figure 4.19 Variation of F/C stoichiometries for PTFE at various electron energies

Ashley¹⁶⁸ the ranges for 1 to 2.5keV electrons, in terms of the sampling depth used in this study fluctuations in the range will have no effect on damage observed. This observation is reinforced by an approximate calculation of electron ranges in poly(paraxylylene) using mean free paths extrapolated from the data in Chapter Three. Assuming a square root dependence of mean free path on kinetic energy the track lengths of an electron which undergoes one collision per mean free path travelled with a loss of 20eV is calculated to be $\sim 720, 1280, 1984$ and 2777\AA for incident electron energies of 1.0, 1.5, 2.0 and 2.5keV

respectively. Thus the ranges are all well beyond the sampling depth of ESCA.

4.3.2 Electron beam bombardment of PVF₂

(i) Preliminary observations

Like PTFE, the most directly evident feature of bombardment of poly(vinylidene fluoride) (PVF₂) surfaces by electrons is a marked decrease in fluorine content. As can be seen from the spectra in Fig.4.20. The F_{1s} levels show a gradual decrease in relative intensity compared to the C_{1s} levels. The changes evident in the C_{1s} spectra also point to extensive fluorine loss. The initial spectra consists of two major peaks, corresponding to CF₂ features at 290.8eV and CH₂ features at 286.3. A small amount of hydrocarbon was also evident at ~285eV. Upon irradiation the CF₂ peak decreases in relative intensity while the features due to CH₂ relative to CF₂, and lower binding energy CH₂ and CH functionalities, show an increase. Features of intermediate binding energy, due to CF functionalities grow with bombardment.

The results of component analysis of the C_{1s} levels and grouping together of the carbonaceous components is shown in Fig.4.21. One major departure from the damage observed in irradiated PTFE is the negligible percentage of CF₃ groups present for PVF₂ even at higher doses. PVF₂ is regarded as a crosslinking polymer¹⁷⁸ with regard to its radiation effects and the virtual absence of CF₃ functionalities observed in this study is certainly in agreement with this finding.

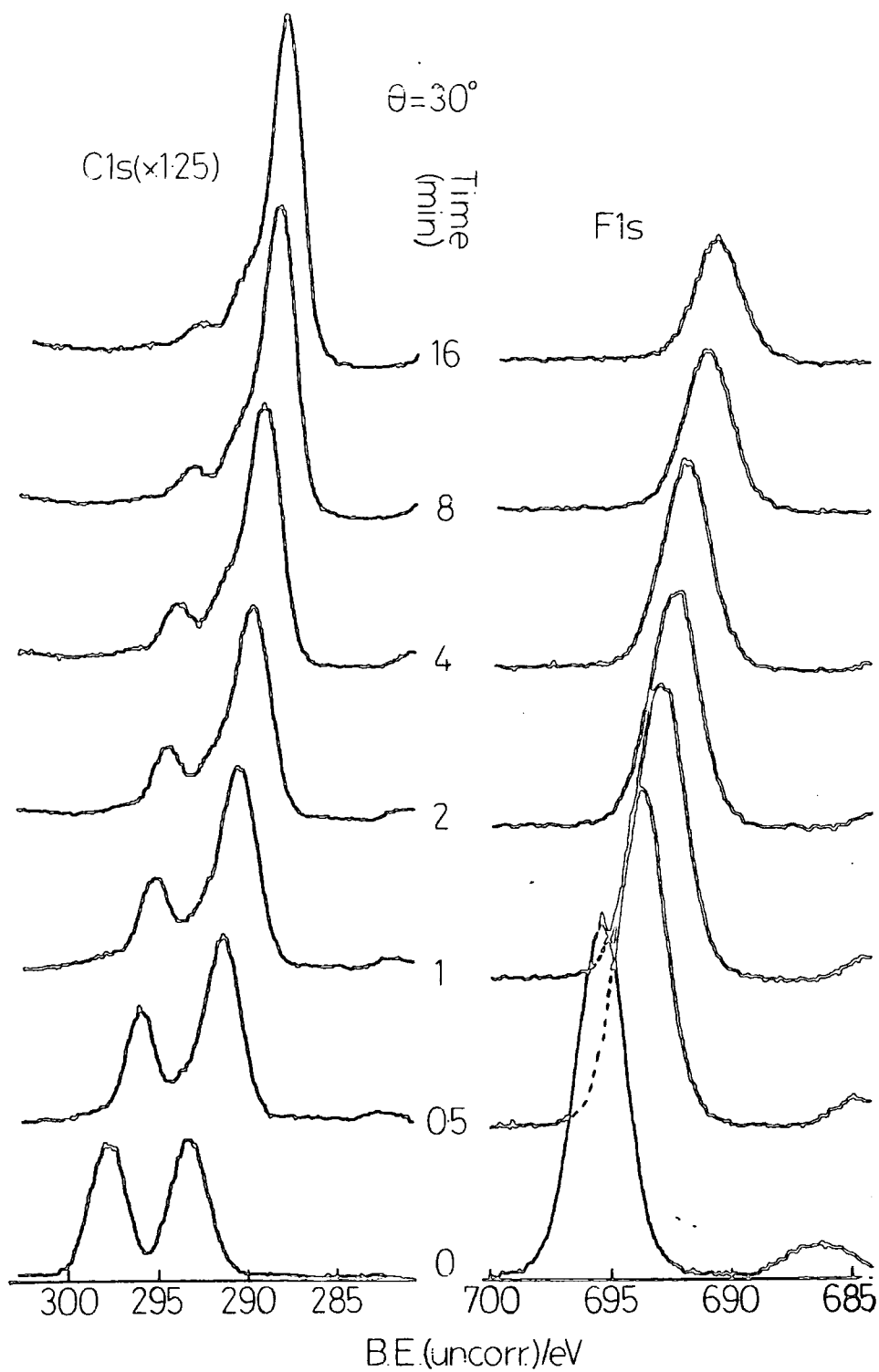


Figure 4.20 Changes in the C_{1s} and F_{1s} spectra of PVF₂ with electron bombardment (3 μ A, 2kV)

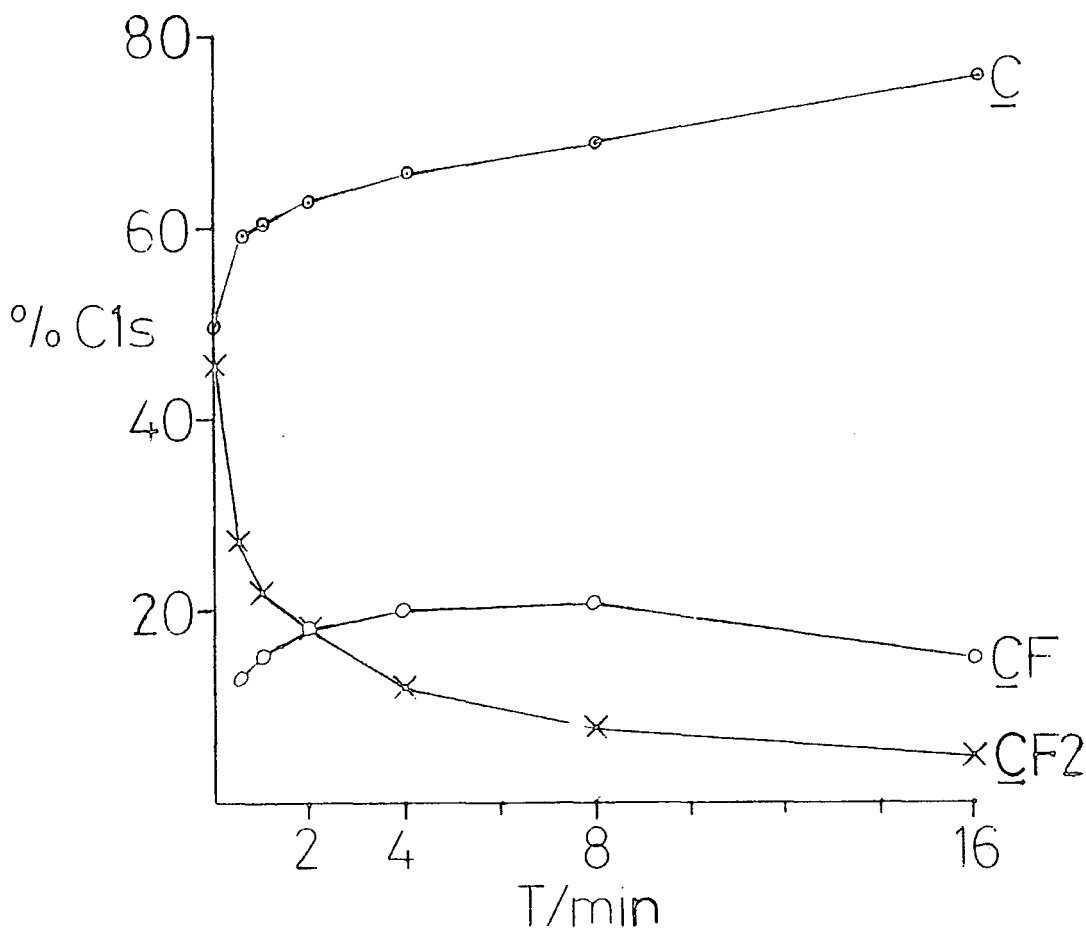


Figure 4.21 Component analysis of PVF₂ C_{1s} spectra

The component analysis shows that initial, rapid loss of CF₂ features occurs such that after a dose of $\sim 6.8 \times 10^{13}$ electrons/cm² (*i.e.* 1 minute's irradiation) the CF₂ intensity has dropped by $\sim 50\%$. This corresponds to the loss of ~ 2 CF₂ groups per incident electron which is greater than was noted for PTFE (1.6 CF₂ groups per electron). The rate of decrease falls with increasing bombardment time such that the next 15 minutes of irradiation brings about a drop in the CF₂ contribution

of 20% of the total C_{1s} envelope. The \underline{CF} functionalities show a maximum growth to ~20% of the C_{1s} envelope and a predominant process occurring must therefore be conversion of CF_2 groups by loss of fluorine (as yet unspecified) to \underline{CF} although the decrease in intensity of the \underline{CF}_2 features is not solely compensated for by an increase in the \underline{CF} features, indicating that loss of fluorine from \underline{CF} functionalities is occurring from the outset, the initial relative growth of these features outweighing their demise. A state is reached however where the reverse case holds and for extended irradiation times therefore the \underline{CF} groups lose intensity.

As was the case for PTFE asymmetry is observed in spectra at extended treatment times, again in the order $F_{1s} < C_{1s} < F_{2s}$, for the reasons given as in the case of PTFE, and so at extended treatment times the formation of a conjugated system is implicit. The crude bromine test also indicated the presence of unsaturation. The bulk irradiation of PVF_2 has also been found to introduce unsaturation over long irradiation times.¹⁷⁸ The decrease in fluorine relative to carbon is illustrated in Fig.4.22, where the F_{1s}/C_{1s} ratios obtained at 30° and 70° take-off angle have been plotted together. The decrease is seen to be uniform with depth since the difference observed in the surface (70) and subsurface (30) spectra are certainly within experimental error negligible. The F_{1s}/F_{2s} ratios do not reveal any general trend and display considerable scatter at longer treatment times. Deeper probing with the $TiK\alpha$ source has therefore been undertaken and C_{1s} spectra recorded for varying treatment times using $MgK\alpha$ and $TiK\alpha$ excitation

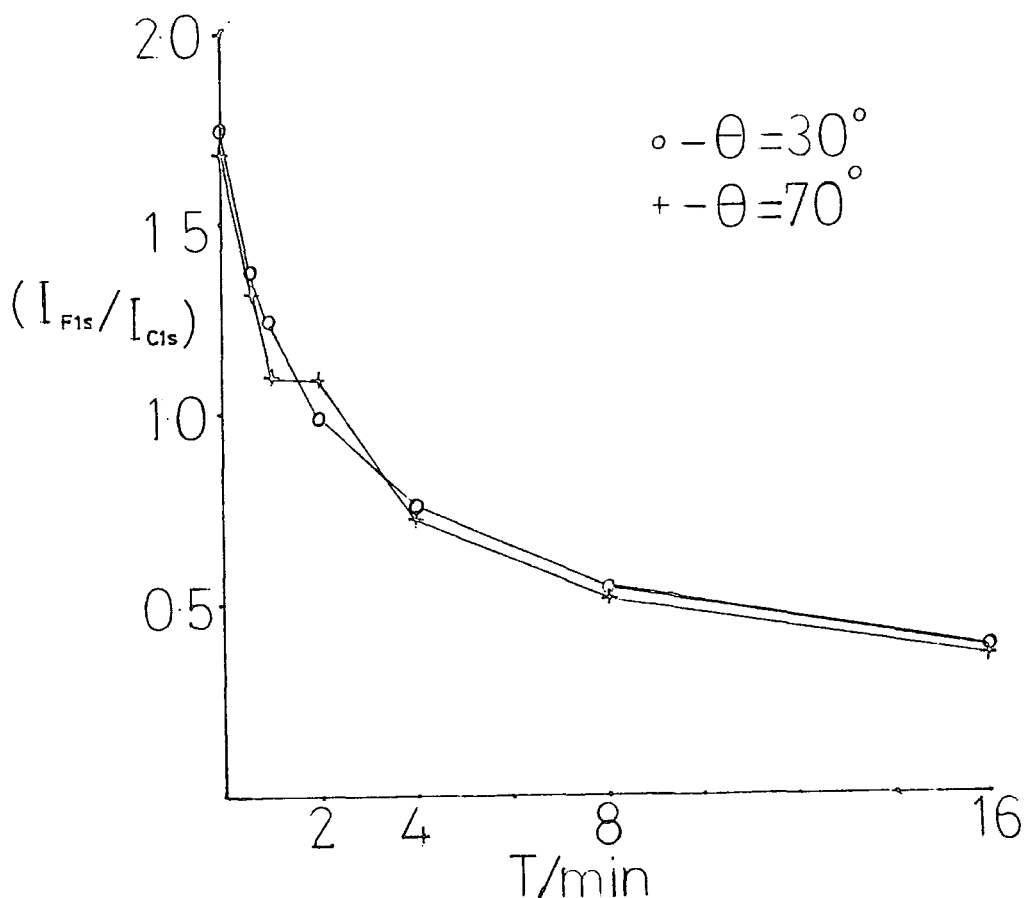


Figure 4.22 Variation of the I_{F1s}/I_{C1s} intensity ratio at 2 take-off angles for PVF₂

are shown in Fig.4.23. Although the $TiK\alpha_{1,2}$ doublet makes fitting virtually impossible it can be seen in these spectra that the growth of C type features in the more surface sensitive $MgK\alpha$ spectra occurs at a faster rate than in the $TiK\alpha$ spectra. Thus in the 16 min. treated sample the $MgK\alpha$ excited C_{1s} spectrum is dominated by carbonaceous material whereas the $TiK\alpha$ spectrum

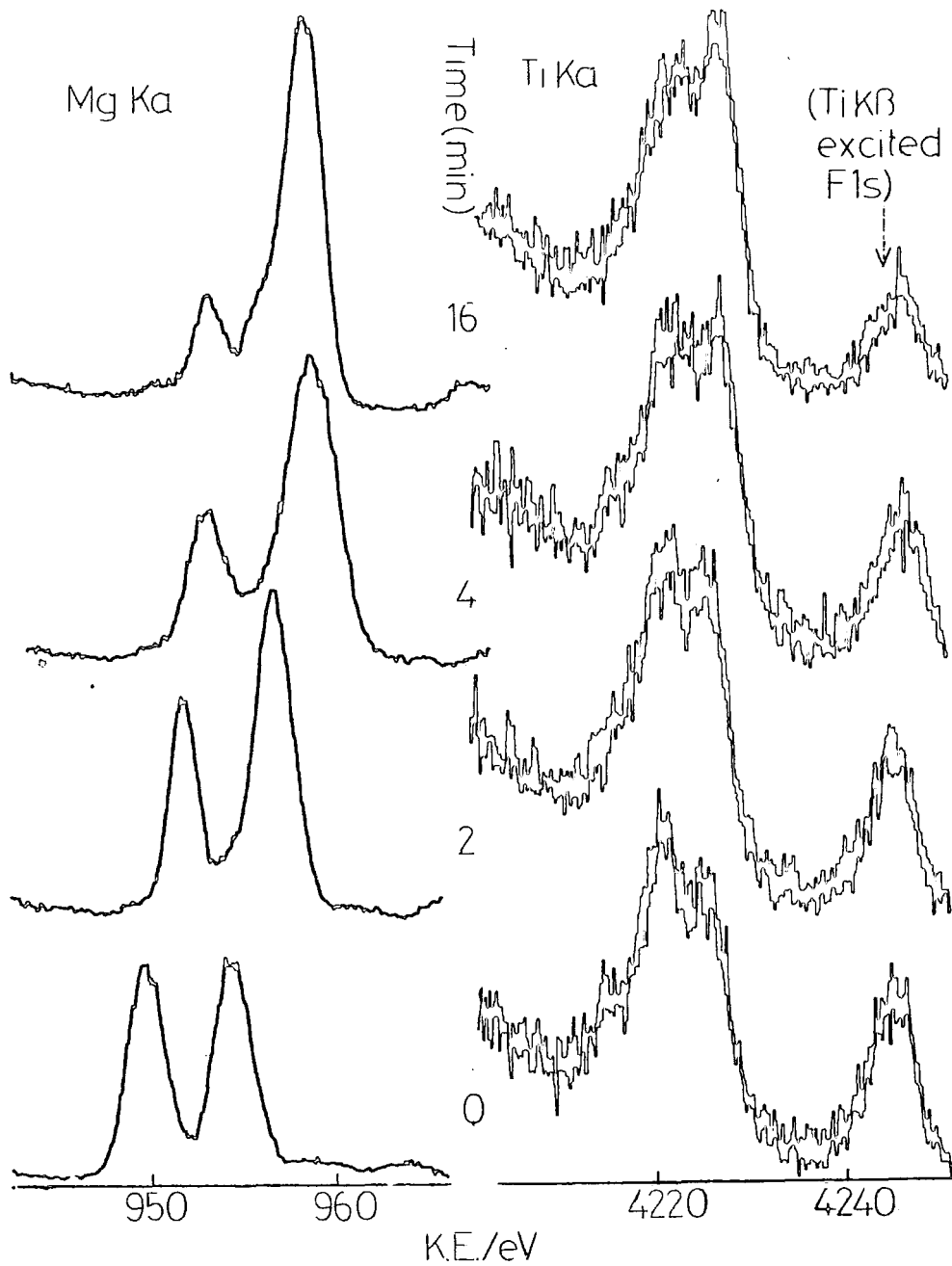


Figure 4.23 Variation of C_{1s} spectra of PVF_2 obtained using $MgK\alpha$ and $TiK\alpha$ X-rays with bombardment time

still has a significant signal arising from fluorinated carbon. The variation is more quantitatively illustrated in the C:F stoichiometries calculated using bulk sensitivity factors for the C_{1s} and F_{1s} levels from the two sources, whereas over the $MgK\alpha$ sampling depth homogeneity of the modified material is indicated earlier a comparison of results from the two X-rays sources indicates inhomogeneity in the top $\sim 120\text{\AA}$ (*i.e.* a sampling depth of the $TiK\alpha$ source for C_{1s} levels at 30° take-off angle). Assuming that the stoichiometry of the modified layer is as given by the $MgK\alpha$ spectra, a simple substrate overlayer treatment of the $TiK\alpha$ data a value of $\sim 45\text{\AA}$ is indicated for the depth of this overlayer.

(ii) Electron energy and dose rate dependence of damage in PVF_2

The influence of dose rate on damage in PVF_2 was studied over a small dose range using a similar treatment as for PTFE. First order plots for the decline in \underline{CF}_2 features at various currents are shown in Fig. 4.24 and the rates obtained were found to be independent of take-off angle, within the error limits of their determination which were considerable compared to those obtained from PTFE. Values for the initial pseudo first order rate constants are shown in Fig. 4.25. Like PTFE the rate obtained from the F_{1s} data is lower than from the \underline{CF}_2 data although the ratios $\frac{k_{CF_2}}{k_{F_{1s}}}$ are not as great as in PTFE due to the absence of \underline{CF}_3 formation in the case of PVF_2 .

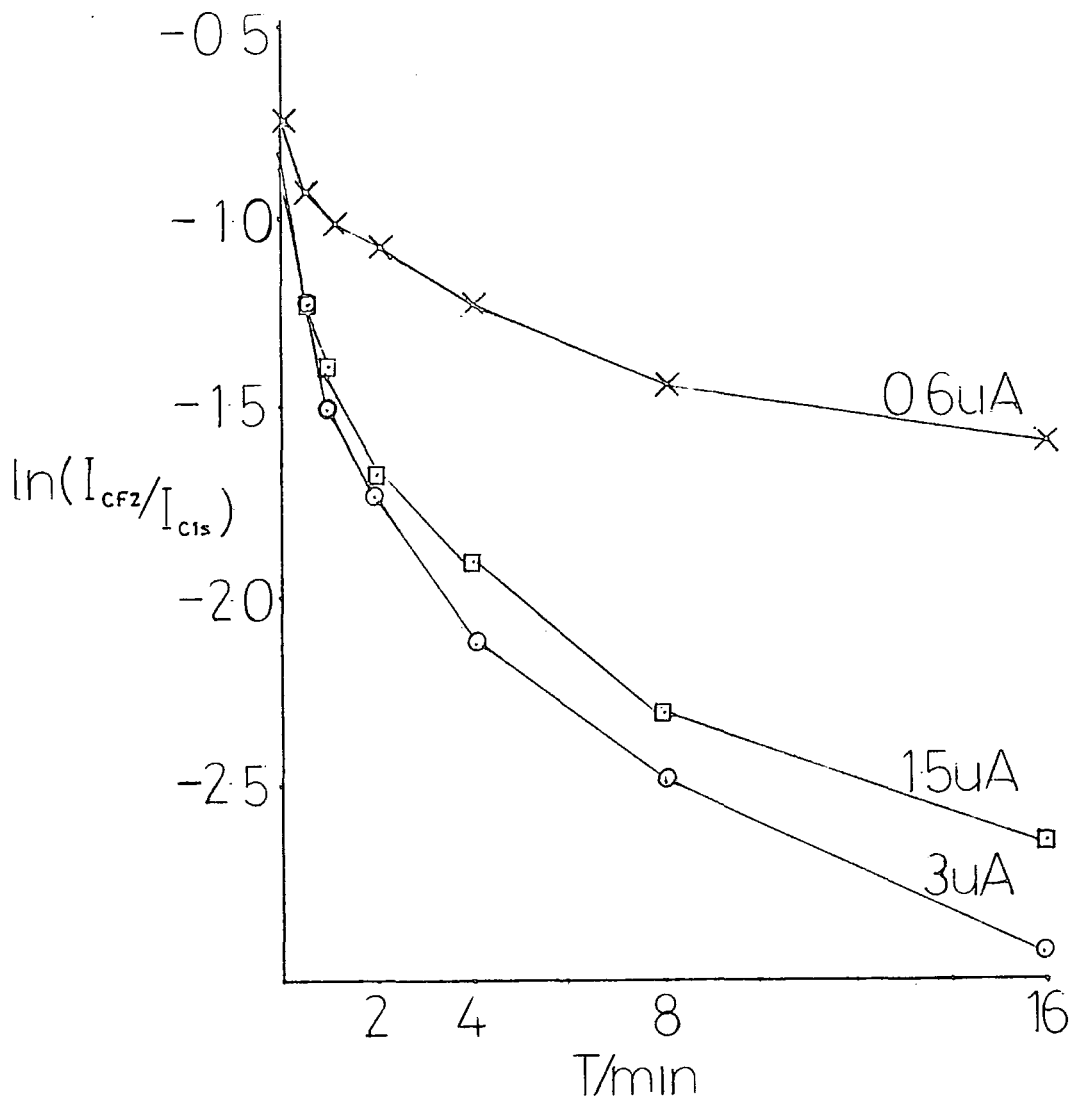


Figure 4.24 First order rate plots of the CF_2 component of PVF_2 with various beam currents

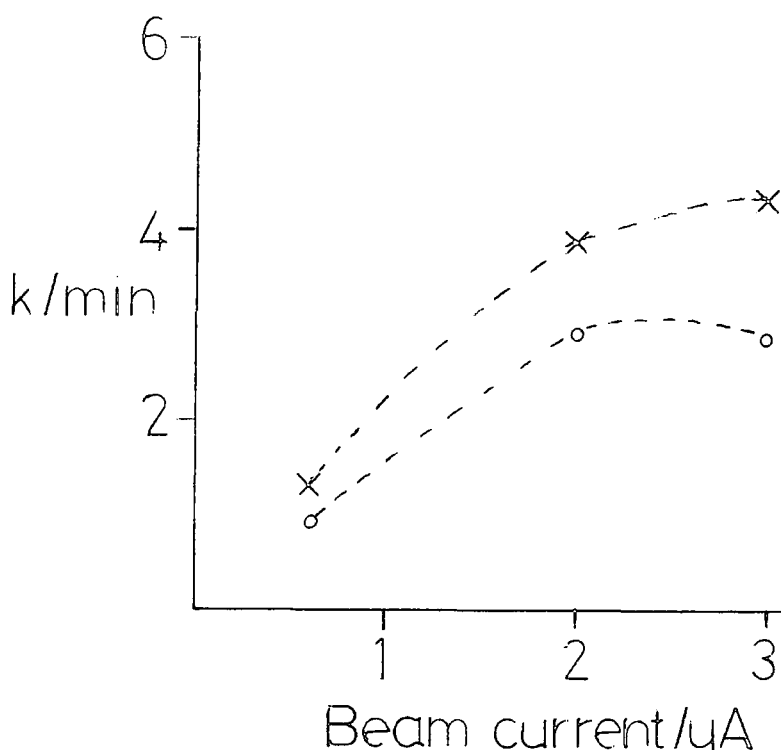


Figure 4.25 Variation of pseudo first order rates obtained from the F_{1s} and CF_2 component data with electron current

Although the rates obtained have somewhat high error limits ($.84 < r^2 < .97$ for the least squares fit) the trend again observable is that a non-linear relationship is evident, with a saturation current reached at lower beam currents than was found to be the case in PTFE. The rate constants for PTFE and PVF_2 are comparable at equivalent beam currents and saturation occurs at lower currents in PVF_2 . Makuuchi²⁴⁶ and coworkers have shown that removal of HF formed during irradiation of PVF_2 does increase the radiation damage observed in the polymer, without HF removal the reaction is presumably showed by reaction of HF with chain radicals.

A limited study has been made of energy dependence of beam modification, the primary electron energies used being 500 and 200eV, at equivalent primary doses of 0.28 A. Alignment of the electron gun, particularly at energies lower than 2000eV was found to be particularly problematical, and limited a full span of energy dependent studies. The spectra obtained at each energy for an equivalent dose were found to be very similar, as can be seen from the plots of the decrease CF_2 signal and the F_{1s} signal shown in Fig.4.26.

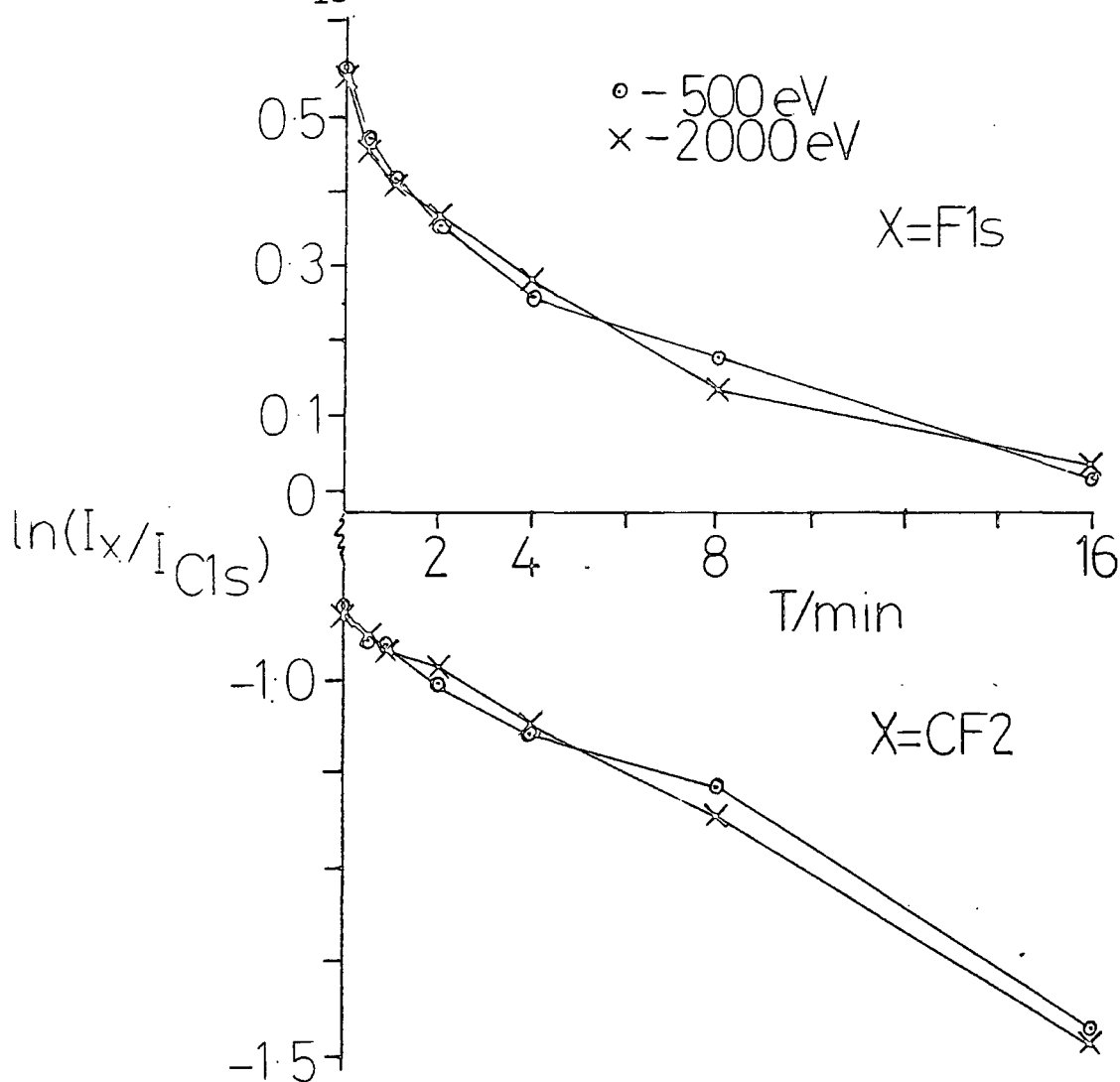


Figure 4.26 Decrease in CF_2 component of PVF_2 at 500 and 2000eV

The pseudo first order rate constants obtained from the two sets of data are found to be very similar, and so can be concluded from this albeit brief study that the damage mechanism is not significantly altered in going from 500 to 2000eV primary energy.

This is a significant result since a primary energy of 500eV is insufficient to cause ionisation of an F_{1s} level (BE ~ 690 eV) and so this mode of excitation of the initial polymer is found to be insignificant in terms of damage caused by the electron beam. Thus electron induced damage *via* Auger de-excitation of the F_{1s} level is not an important process as might be predicted by the Knotek-Feibelman¹⁴⁸ ESD model discussed in Chapter Two. However the cross sections for ionisation of an F_{1s} level by electrons of enough energy is almost an order of magnitude lower (see Fig. 2.7), than for C_{1s} ionisation which are, in turn, lower than valence ionisation cross sections.

Differences in fluorine to carbon stoichiometries however were discernable in $TiK\alpha$ spectra of samples irradiated at the two energies. A substrate overlayer treatment of the results obtained at 500eV gives a depth of the modified layer of about 20\AA (*c.f.* 45\AA for 2kV). Thus for a 4x increase in primary energy the estimated depth of modification increases by a factor of just over 2. This is strongly reminiscent of the square root dependence of electron mean free paths on energy, the depths of modification are, however, estimated at 3 times the mean free path for 500eV electrons and ~ 1.5 times for 2kV electrons. It should again be noted that the model assumes a homogeneous modified layer of polymer on top of an unaltered

substrate, whereas the probable situation is a modified layer whose composition varies with depth.

4.3.3 Mechanistic aspects of electron beam degradation of PVF₂ and PTFE

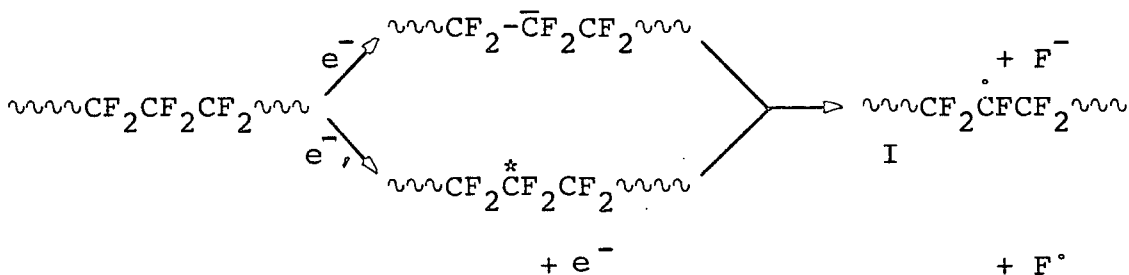
The results presented in the foregoing discussion clearly indicate that the primary effect of electron bombardment is defluorination of the polymer's surfaces to a depth of at least several tens of angstroms. The availability of hydrogen in PVF₂ appears to cause marked differences in observable effects of electron beam bombardment which, as will become apparent, tally with the effects of bulk irradiation of these polymers by high energy radiation. The following discussion presents a likely scenario of events, a full account of the process requires greater investigation.

The primary event in electron beam bombardment is probably excitation or ionisation of a localised section of the polymer chain. Core ionisation has been shown for the F_{1s} levels to be relatively insignificant in terms of observable damage. However ionisation of higher lying, core like levels, *e.g.* the F_{2s} levels, has recently been shown to be significant²⁹ in ESD in yields from condensed organic molecules. Such processes have cross sections of the same order of magnitude as 'true' valence level ionisation. Cross sections for valence ionisation¹²⁷ excitation¹³¹ and electron attachment¹³¹ increase with decreasing electron energy and the role of low energy secondary electrons is likely to be most significant. It is worthy noting that changes observed in this study are similar to those recently reported in an investigation of the

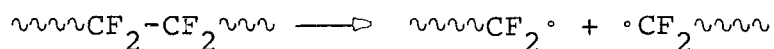
argon ion beam bombardment of fluoropolymer surfaces. The common factor between the two treatments is the copious source of low energy secondary electrons.

Reaction in the cation manifold is probably a minor process, although Briggs¹²⁸ has reported an ESD spectrum of PTFE, positive ion yields are likely to be significantly lower than neutral yields. Thus for both polymers cations formed are likely to be rapidly quenched by the large flux of low energy secondary electrons to leave localised excitations in the polymer chain with energies greater than that required for bond cleavage. (It should be remembered that the per-fluoroalkanes were commonly used as solvents in the early days of vacuum u.v. spectroscopy because of their transparency to light down to wavelengths of 1500\AA ²⁵³ *i.e.* Rydberg states have energies of $\sim 8\text{eV}$ or more). The large slow electron flux will also give rise to electron attached species, dissociation of fluoride ions from which is favoured owing to the high electron affinity of fluorine in relation to the C-F bond energy.^{131,240}

Considering firstly the case of PTFE, dissociative electron attachment or homolytic fission of a C-F bond from a localised excitation could both give rise to the radical I.

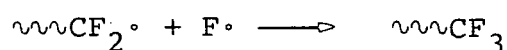


Alternatively main chain scission of a C-C bond, which has a slight energetic preference to C-F fission (in terms of ground state bond energies) can give rise to the radical II.



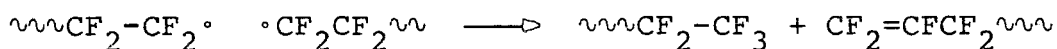
II

Radicals I and II have certainly been detected in the e.s.r. spectra of bulk irradiated PTFE,^{254,255} with an estimate for the ratios of 10/1²⁵⁶ given for the in chain ($\text{CF}_2-\overset{\bullet}{\text{C}}\text{F}-\text{CF}_2$) to the end chain ($\sim\text{CF}_2^\bullet$) in PTFE irradiated *in vacuo*, although these values refer to relatively long lived radicals. Indirect evidence for chain scission is provided in the present study for the formation of terminal $-\text{CF}_3$ groups in the initial stages of bombardment, arising from fluorine atom addition to I,

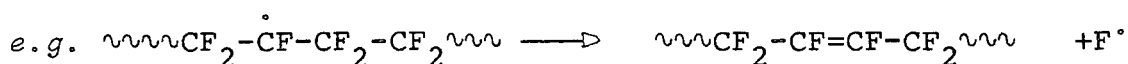


such a reaction being more likely in the subsurface than the surface.

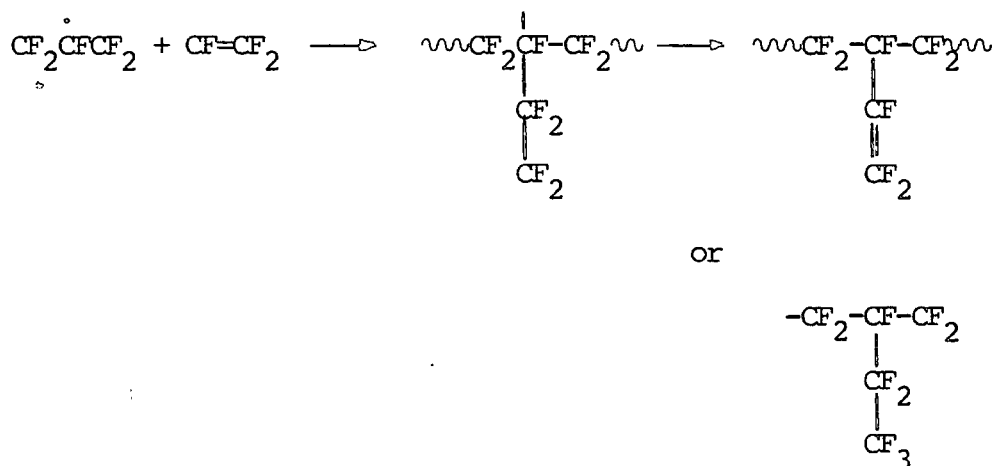
The origin of the fluorine atom could be from formation of I, or disproportionation of two terminal radicals which, due to the cage effect have been kept adjacent to each other



As previously stated conflicting reports^{245,246} have been made on the presence of CF_3 groups in bulk irradiated PTFE, although $\text{CF}_2=\text{CF}-$ ²⁴⁴ groups have been detected by i.r. spectroscopy. The initial stages of irradiation in the present study are also characterised by greater growth of CF and C functionalities. The formation of CF may be rationalised by the disproportionation reaction above and by decay of radical I by elimination of another fluorine atom,



Radical I could conceivably crosslink although this is sterically unlikely and certainly the rise in the absolute intensity of the C_{1s} level occurs when the fluorine content of the polymer has been considerably reduced. The totality of the ESCA data cannot be directly correlated with loss of short chain perfluoroalkanes and alkenes, in the initial stages of bombardment. Evolution of these gases certainly occurs in high energy irradiation of PTFE, with CF_4 in greatest abundance and other alkenes and alkanes being detected up to C_{14} .^{247, 248} Irradiation of PTFE is a patented procedure for synthesis of the short and medium chain fluoroalkenes. Re-reaction of a monomeric unit formed by irradiation could give rise to a branched chain structure,²⁴⁵ e.g.

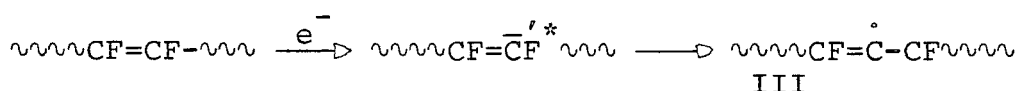


From the onset of irradiation it is clear however that the proportion of carbon not directly attached to fluorine constantly grows, initially corresponding to carbon in a fluorine environment but ultimately with the position of this peak ($BE < 285eV$) corresponding to 'graphitic' or conjugated carbon, and the asymmetry to high binding energy as evident from the raising of the baseline.

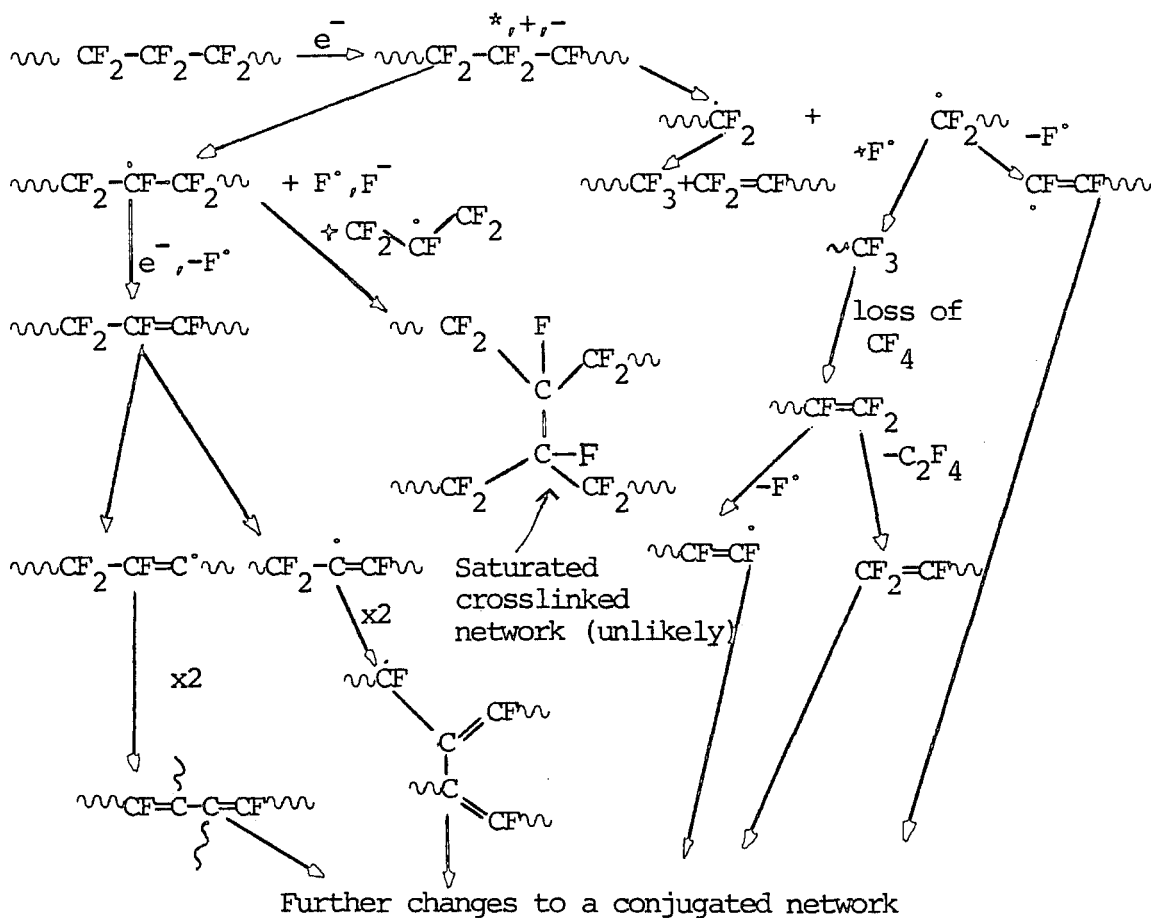
Further, the component analysis as a function of time and higher rate constants obtained from the decrease in

the \underline{CF}_2 peak than from the F_{1s} peak suggests that CF_2 groups are not directly converted to \underline{C} type carbon but *via* \underline{CF} functionality. Abstraction of fluorine by a fluorine atom is unlikely as this reaction is endothermic.²⁵⁷

Thus possible pathways include



The steric hindrance on III due to F groups being absent, crosslinking or branching is now possible and the formation of a complex, carbonaceous network may proceed from such a species. This point will be returned to at a later stage. The preceding discussion may be conveniently summarised in the reaction scheme shown below, which is by no means exhaustive.

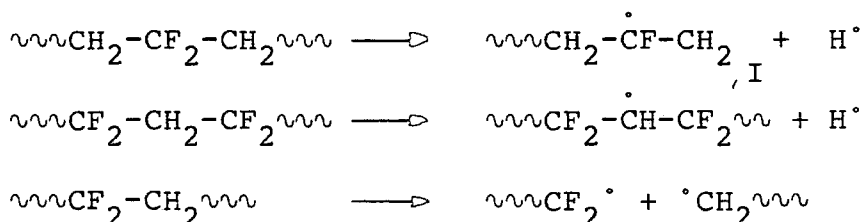


The major difference between bombardment of PVF₂ and PTFE is the higher proportion of $\underline{\text{CF}}_3$ functionalities formed in PTFE and homogeneity within the surface and subsurface regions for PVF₂. These observations can be rationalised on the basis of HF elimination (*i.e.* relatively unreactive compound to F[•]) being the dominant mode of fluorine loss from PVF₂.

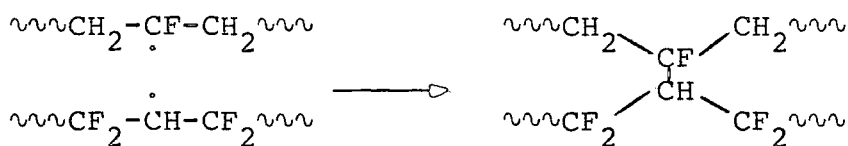
The data presented also indicate that loss of $\underline{\text{CF}}_2$ groups from a chain occurs *via* $\underline{\text{CF}}_2 \rightarrow \underline{\text{CF}}$ processes rather than $\underline{\text{CF}}_2 \rightarrow \underline{\text{C}}$ type processes.

The possibility of crosslinking in PVF₂ is also feasible from the onset of irradiation since the steric hindrance of complete fluorine substitution is removed. The formation of unsaturation in PVF₂ during a radiolysis as revealed by i.r.² and more significantly a detailed EPR and ENDOR²⁵⁸ analysis. The latter study revealed that upon irradiation a polyene network, $\{ \overset{\times}{\text{C}} = \overset{\times}{\text{C}} \}_n$ with an average value from n of ~7, evidence for a polyenic network in the present study is provided by the appearance of asymmetry in the C_{1s}, F_{1s} and F_{2s} peak for extended irradiation times, indicating the presence of a conjugated unsaturated system.

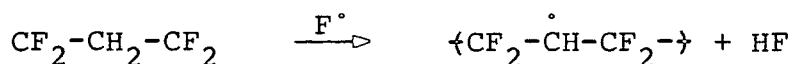
A likely reaction scheme can therefore be envisaged to begin by initial C-C, C-H or C-F cleavage



Crosslinking may occur by combination of chain radicals, *e.g.*



Detailed component analysis of the $\text{C}_{1\text{s}}$ spectra in the initial stages of bombardment does reveal that CF functionalities are predominantly in a non-fluorinated environment, that is, at a BE of $\sim 288\text{eV}$ indicating that the crosslinking reaction above is favoured over the recombination of two radicals of type I. The fluorine and hydrogen atoms generated in the initial reactions may then abstract another hydrogen or fluorine atom propagating the generation of radicals in the chain



The elimination of HF from such a radical may be envisaged as the key reaction which generates unsaturation. Unimolecular elimination of HF from an excited chain segment will also introduce unsaturation. The continued elimination of HF, together with crosslinking reactions will ultimately give a network of polyene structures: the driving force for all these reactions being the favourable heat of formation of HF. Loss of H_2 from the chain, or abstraction of H^\bullet by free H atom may also be occurring, the removal of fluorine as F_2 is again not envisaged to be favourable however.

CHAPTER FIVE

AN ESCA INVESTIGATION OF THE LOW ENERGY
ELECTRON BEAM POLYMERISATION
OF THE FLUOROBENZENES

5.1 Introduction

There is growing commercial interest²⁵⁹ in the use of the electron beam for polymer processing. The automobile^{260,261} industry in particular has examples of electron beam curing plants in daily operation. The advantages offered by electron beam curing over the conventional curing process of stoving include greater curing speed (~ 3 s *versus* several minutes),²⁶¹ less solvent loss,^{262,263} low space requirements and lower energy consumption, (high solid loadings and waste solvent disposal are also added bonuses). There are, however, still problems. The materials to be cured still tend to be more expensive and in some cases can be unpleasant to use.²⁶⁰ Installation costs also tend to be higher than a traditional plant. However uses of high energy electron beams are spreading.

This chapter presents the results of an investigation of polymerisation of organic materials by low energy electron beams. Although processes occurring are similar for high electron energy beams the great difference is the path length of the electrons. Thus these studies were performed *in vacuo* and a thin film was synthesised. To allow comparison with plasma polymerisation the starting materials used were the series of fluorobenzenes, hexafluorobenzene down to fluorobenzene. The plasma polymerisation of these compounds has formed the basis for several detailed investigations with the particular emphasis being the use of ESCA.²¹⁷⁻²²¹ This is the first investigation of the structure and bonding of any low energy electron beam polymers by ESCA. There have been several investigations of low energy electron beam polymerised materials where the elect-

rical properties of materials used were the only form of characterisation. The next section gives a review of this work.

5.1.1 Previous studies of polymers produced by low energy electron beams

The coincidental formation of thin contaminant polymeric films had been observed in several early electron microscopy investigations.²⁶⁵⁻²⁶⁷

Ennos^{268,269} showed that contaminant polymer films originated from the interaction of electrons with organic molecules adsorbed on metallic substrates. The backstreaming of diffusion pump oil was realised to be the source of the organic monomer molecules. Poole²⁷⁰ suggested, from a study of electron bombardment of metals with Apiezon grease in the vacuum system, that film formation proceeds by free radical polymerisation of adsorbed molecules followed by electron beam crosslinking.

Investigation in the field was directed towards prevention of these films until the suggestion that the polymers produced could find a use as electrical thin film insulators for circuit fabrication.²⁷¹ Subsequently several investigations in the 1960s were carried out which concentrated on measurement of electrical properties of films produced by bombardment of substrates in vacuum systems rich in silicone oil vapour; Christy²⁷² studied rates of formation of films produced from DC704 diffusion pump oil as a function of electron beam current, oil pressure and substrate temperature.

On varying the current density from 70 to $\sim 450 \mu\text{A cm}^{-2}$ at a substrate temperature of 25°C the rate of film formation increases from 0.17 \AA s^{-1} to 0.3 \AA s^{-1} , as can be seen from Fig.5.1.²⁷² A saturation rate occurs at higher current

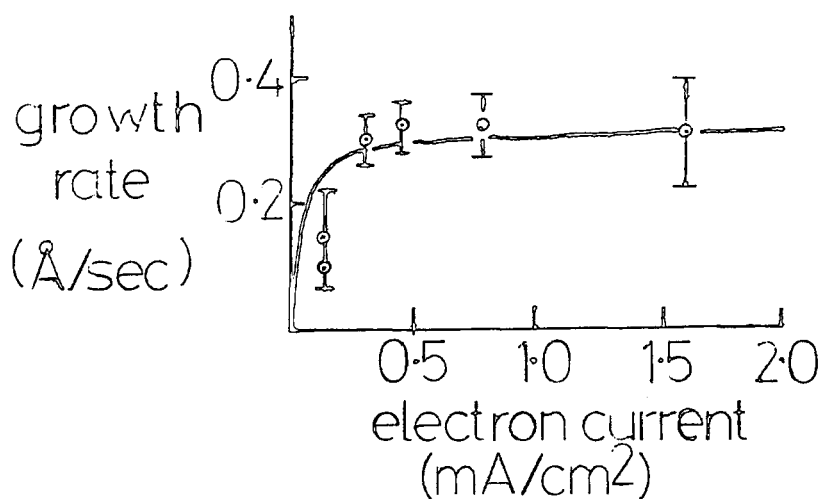


Figure 5.1 Variation of rate of formation of polymer films with bombarding current

densities. The rate also decreases on increasing the substrate temperature, an observation previously observed by Ennos.

A phenomenological theory developed by Christy related the rate of film formation, R , to the current density, f ,

molecular volume of the monomer, v , the cross section for crosslinking electron-molecule collision, σ , the molecular flux at the substrate, F and the effective molecular area, a , by

$$R = \frac{vF}{1 + 1/\sigma\tau f} \quad (\text{eqn. 5.1})$$

at low pressures and

$$R = (c/a)vF \quad (\text{eqn. 5.2})$$

at high pressures, where τ is the mean stay time of the adsorbed molecule.

Christy's measurements did not differentiate between the high energy primary electrons and the lower energy secondaries. An extensive study of the secondary electron emission from growing films of electron beam polymerised DC-704 was however carried out by Mann.²⁷³ Although the nature of the experiments precluded any quantitative information, the growth rate of the polymer film was found to be dependent on secondary emission. This result is consistent with the finding, in a study of polymerisation in electron mirror microscope systems by Mayer,²⁷⁴ that electron energies as low as 6eV could initiate polymer film formation from residual pump oil vapours. It is relevant to note here that glow discharges used in plasma polymerisation are characterised by average electron energies of $\sim 1-10$ eV.²⁷⁶ Although plasma polymerisations occur *via* complicated free radical and ionic mechanisms which are not fully understood, reaction causing polymerisation is predominantly by collision of an electron²⁷⁷ with a monomer molecule.

Subsequent studies on electron beam polymerised DC-704 films have investigated various electrical properties including dielectric constant,²⁷⁸ conductivity (dark current)²⁷⁷⁻²⁸¹ and photoconductivity.²⁸⁰ Dark current measurements indicate

that conductivity increases with bombardment time. On exposure of the films to air, conductivity drops by several orders of magnitude. This latter observation has been taken as evidence of the role of trapped free radicals acting as donors and acceptors in the conduction process, since an electronic rather than ionic conduction mechanism is also inferred from the observation that conductivity remains constant at a fixed voltage. Photoconductivity measurements give a band gap $\sim 2\text{eV}$ with small carrier mobility. These findings altogether indicate that the polymer films are highly crosslinked structures, more akin to an inorganic amorphous semiconductor than a conventional polymer. However i.r. evidence is reported to indicate that methyl and phenyl groups are still present.²⁸²

Electron beam polymerisation of DC704 vapours in the presence of other gases gives films which have unsatisfactory electrical properties in terms of reproducibility.²⁸³ The search for thin films with suitable electrical properties prompted the uses of different starting materials in several investigations. An investigation of the polymerisation of 1,3 butadiene²⁸⁴ vapour indicated that reaction took place at the surface of the substrate rather than in the gas phase. Active sites, formed by electron beam collision of an adsorbed molecule, which propagate the polymerisation process were assigned tentatively as being cationic, with an average lifetime of ~ 3 minutes.

A study of polymerisation of divinylbenzenes²⁸⁵ onto a substrate held at -80°C was found to give very high rates of deposition, which were independent of beam current.

A more recent study does show rates which are dependent on beam current,²⁸⁶ when the substrate temperature is closer to ambient. Retention of unpolymerised material in the former study may be partly responsible for the high rates observed.

Gregor has reported electrical properties of electron beam polymerised epoxy resin²⁸⁷ and epichlorohydrin,²⁸⁸ and published several reviews²⁸⁹⁻²⁹¹ on thin film dielectrics in the late 1960s and early 1970s. His later reviews tended²⁹¹ to neglect electron beam polymers, which reflected the shift in the electronics industry away from research into the use of polymer films as intrinsic components of integrated circuits. (Polymer resists play an essential role however in device fabrication).

Increased interest was at the time shown in the formation of thin organic films by plasma polymerisation,²⁹⁵ Langmuir-Blodgett techniques²⁹⁴ and u.v. photolysis.²⁹² Photopolymerisation at surfaces has been studied in detail by Wright. The technique involves irradiation of a surface in an atmosphere of the starting material. The process is thought to proceed by adsorption of the monomer followed by photochemical excitation. The role of the surface is indicated by negative activation energies of polymerisation. Adsorption tends also to lower the excitation energy since, for example, C_4Cl_6 may be polymerised using light at wavelengths larger ($\sim 1900\text{\AA}$) than its excitation energy. Plasma polymerisation involves some degree of heterogeneous and homogeneous reactions initiated by low energy electrons and involving a variety of species including ions and excited state neutrals and metastables.

The number of publications in the field of low energy electron beam polymerisation has greatly decreased. A

notable exception was the investigation by Frost²⁹³ and co-workers on the structure and mechanism of formation of polymer films formed by bombardment of various monomers including perfluorobutene. Irradiation of monomers in the gas phase gave polymers distinctively different from those produced by polymerisation of the condensed monomer, due to different mechanisms of formation. Gaseous polymerisation proceeds by negative ion fragmentation in the gas phase followed by adsorption whereas for condensed multilayers film growth occurs by electron initiation.

Fritzsche²⁸⁶ has studied the gas phase deposition of thin films by electron beam and ion beam induced polymerisation both experimentally and theoretically.

By assuming a free radical growth mechanism, experimental growth rates were used to determine a cross section for activation of polymerisation of $\sim 2 \times 10^{-4} \text{ cm}^2$. By pulsing the electron beam the lifetime of active centres was found to be about half a second. Ion beam polymerisation was shown to be a more efficient process, in terms of dose yield. However the total charge necessary to deposit a 100nm layer could be 0.15 C/cm^2 .

Most processes involving high energy electrons (*i.e.* 100keV or over) have been recognised for three decades, after the pioneering work led by Charlesby¹⁷⁰ and Chapiro.¹⁷¹ Polymerisation by high energy radiation generally proceeds by free radical chain carriers, although there are specific cases where an ionic mechanism is favoured. Ionic mechanisms have been shown to occur for systems such as isobutylene, butadiene

and isoprene by the observation of greater degrees of polymerisation as the temperature is lowered. The radiation induced polymerisation of isobutylene in particular had a negative activation energy. The occurrence of solid state polymerisations induced by high energy radiation, especially at low temperature, is also taken as evidence for ionic polymerisation. The rationale behind this is that in solids charge neutralization of the ion is slowed down owing to the limited mobility of the ions in a solid. The radiation polymerisation of hexamethylcyclotrisiloxane for example, occurs by an ionic chain process which under optimum conditions consumes 450 molecules per 100eV of ionising radiation adsorbed. In the present study differentiation between ionic and radical mechanisms is not straightforward, since for initially closed shell unsaturated systems the definitions are not mutually exclusive and charged radicals undoubtedly play an important role.

5.2 Experimental

Polymers were prepared by deposition of the appropriate monomer onto a cooled gold substrate and subsequent bombardment of the condensed monomer by 2kV electrons. This was all carried out in the sample preparation chamber directly attached to the ES300 spectrometer described in Chapter One. Typical pressures during bombardment were $\sim 5 \times 10^{-9}$ - 1×10^{-8} T.

Gold was chosen as a substrate because of its chemical inertness and its excellent thermal conductivity properties, essential for uniform coverage of the monomer. The gold sheet (Johnson-Matthey) was cut using scissors to give a rectangle slightly wider and longer than the probe tip which itself was $\sim 20 \times 8$ mm. The gold was thoroughly polished using "Brasso"

followed by a distilled water rinse and was screwed down onto a copper probe tip again to give good thermal contact. After a final rinse with high grade organic solvent (methanol) the gold was placed in an inductively coupled r.f. hydrogen plasma operating at $\sim 50\text{W}$ and $< 0.1\text{T}$ pressure.

The sample was then placed into the analysis position of the spectrometer *via* the sample preparation chamber and $\text{Au}4f_{7/2}$ and C_{1s} spectra were taken to check the cleanliness of the gold.

If clean, the substrate was withdrawn into the preparation chamber to a position, determined earlier, where the electron beam would impinge on an area $10 \times 6\text{mm}$ at the centre of the probe tip.

The cooling for the probe was started and the temperature allowed to gradually decrease to -120°C . Cooling is carried out by drawing liquid nitrogen along the inside of the probe shaft to a stud compressed against the interior of the probe ending. Temperature is fully controllable and determined by a thermocouple in contact with the stud. The cooling was allowed to equilibrate by leaving for $\sim \frac{1}{2}$ hour. Delay is recommended by the manufacturers. Uneven coverage of the substrate was found to occur if the time allowed to elapse was shorter.

A reservoir shaft, shown schematically in Fig. 5.2 was introduced into the preparation chamber so that its end was directed towards the probe tip from a distance of $\sim 4''$.

The monomers used were the series of fluorobenzenes, per-fluorobenzene, pentafluorobenzene, 1,2,3,5 tetra-fluorobenzene, 1,3,5 trifluorobenzene, orthodifluorobenzene and monofluorobenzene all of which were research-grade samples from Bristol

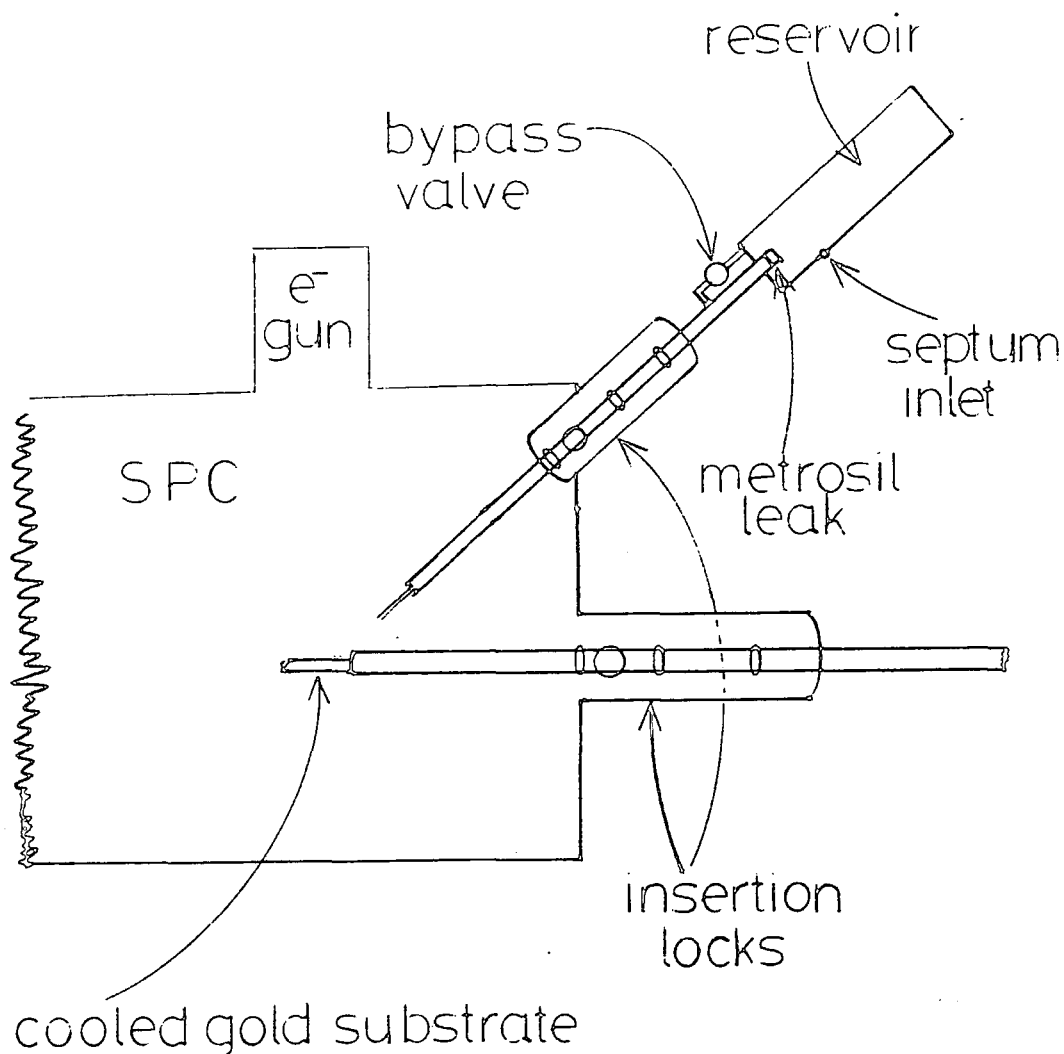


Figure 5.2 Schematic of reservoir shaft

Organic Ltd. These were chosen for several reasons, which may be summarised as follows:

(i) The plasma polymerisation of these compounds has been the subject of several detailed investigations with ESCA as a means of providing the main source of information regarding their

structure and bonding.²¹⁷⁻²²¹

(ii) Fluorine substituents have been shown to give a very wide range of binding energies within the C_{1s} envelope, thus $-CF_3$, $-CF_2$, CF and C functionalities are readily observable from the ESCA data.

(iii) Apart from plasma polymerisation, these compounds are not readily polymerisable by conventional means, giving the electron beam polymerisation of these compounds added novelty.

About 5 μ l of the appropriate monomer was injected into the reservoir shaft *via* a septum using a 10 μ l syringe. In its normal mode of operation, *i.e.* the introduction of liquids into UHV for their ESCA analysis a metrosil leak seal allows a very slow inlet of the sample in the vapour phase so that deposition onto a cooled substrate may be finely controlled. This allows constant removal and replenishment of the sample in monolayer quantities hence obviating X-radiation damage effects. However for its present use a valve by-passing the metrosil leak was opened until a film was clearly visible on the cooled substrate. The reservoir shaft was then withdrawn from the UHV region of the sample preparation chamber. During deposition the pressure in the system rose to $\sim 10^{-5}T$, due to some fluorobenzene not condensing, but on removal of the reservoir shaft dropped to $\sim 10^{-9}T$, with the monomer frozen onto the substrate. The condensed film was then irradiated with 2kV electrons at a known dose ($\sim 5\mu A$) for thirty minutes. The probe was then left to reach ambient temperatures in its original position.

A major pressure rise occurred in all cases at $\sim 100^{\circ}\text{C}$ corresponding to unexposed monomer boiling off, mainly from the end of the probe shaft. This left a clearly visible thin film covering the area on the substrate which had been bombarded by the electron beam. The sample was then pushed through to the analysis position and the C_{1s} , F_{1s} , F_{2s} , $\text{Au}4f$ and O_{1s} spectra taken using $\text{MgK}\alpha$ excitation at two take-off angles. The spectra were recorded on the DS300 data system in digital fashion as described in Chapter One.

In a separate series of experiments condensed hexafluorobenzene was bombarded for varying times, the experimental procedure being identical to that described above except a defocussed beam was rastered over an area of $\sim 0.8 \times 1.5\text{cm}$ with a beam current, as measured on a blank side of the copper probe tip, being $\sim 0.4\mu\text{A}$ using the circuit shown in Fig. 4.3, Chapter Four.

5.3 Results and Discussion

5.3.1 Electron beam polymer composition and gross chemical structure as a function of starting material

(a) Hexafluorobenzene

Before discussion of the ESCA investigation it is worthwhile to discuss some general points arising from the polymerisation of condensed hexafluorobenzene which are also applicable to the rest of the series.

Following irradiation of the monomer some darkening could clearly be seen in the area of the condensed film which had

undergone electron bombardment. By allowing the probe to warm up from -120°C a significant pressure rise in the system (from $\sim 10^{-8}$ to 10^{-4}T) occurred at $\sim 100^{\circ}\text{C}$. This was observed to be due to the evaporation of the residual monomer from areas of the probe tip not treated by the electron beam. On removal of the excess monomer a thin film adhering to the gold substrate could clearly be observed on the bombarded area of the substrate. Thus the monomer had undergone a substantial increase in molecular weight since the solid remaining was stable at UHV pressures of $\sim 10^{-8}\text{T}$. In later experiments where the total electron dose received by the condensed monomer was reduced more than one pressure rise was observed to occur presumably corresponding to the removal of successive oligomers although the temperatures at which these came off were not reproducible from one run to another.

Optical and scanning electron microscopy studies of the films revealed that they were pinhole free, essentially flat surfaces. At its perimeter the polymer formed did not have a sharp cutoff but showed a gradual decrease in thickness. Hutton has noted that for analogous but thinner films formed by argon ion bombardment,²⁰³ rapid warming of the films resulted in the formation of a reticulated structure on the substrate, but in the present study this effect was not observed.

The prime objective of this work was to investigate the gross chemical structures of electron beam polymers and so no direct measurement of film thickness was undertaken. However during the initial deposition of the monomer the developing film displayed variation in colour due to interference of incident light such that the same colour, *e.g.* green was observed

at least four times. Thus the films formed were of the order of at least four times the wavelength of visible light, *viz.* over $2\mu\text{m}$.

The film was also examined in a transmission electron microscope adapted to perform RHEED, (Reflection High-Energy Electron Diffraction). RHEED can give information on the surface atomic arrangement of the sample by measurement of the diffraction pattern formed by a beam of high energy electrons following impingement of the sample surface at grazing incidence. For the samples provided, which were only partially covered by electron beam polymer, a clear sharp diffraction pattern was observed when the beam struck an area of the sample not covered by polymer, but no such pattern was observed on analysis of the polymer covered surface. This indicates that the film was largely amorphous in nature. The dose delivered in the experiment is however very large and during the experiment the film was visibly observed to degrade and so the data should be treated with caution.

A major indication of the crosslinked nature of polymers is provided by the lack of solubility in common solvents. Although the quantity of film synthesised in the current study rules out a quantitative investigation of film solubilities common organic solvents, hexafluorobenzene itself, and water were found to leave the film untouched.

A major problem in the initial stages of the investigation was large quantities of oxygen present in the films. The probable source of this was water particularly present in the Sample Analysis chamber. (The sample preparation chamber where the films were obtained was not subjected to the brusque

treatment the analysis chamber was, where some routinely run samples contained large quantities of water). Frequent baking and the use of a titanium sublimation pump was found to reduce any O_{1s} signal to $\sim 1\%$ of the C_{1s} intensity although earlier films were found to contain varying quantities of oxygen, particularly if the ESCA analysis was carried out with the probe at less than $\sim 0^\circ\text{C}$.

The C_{1s} , F_{1s} and F_{2s} spectra of the polymer recorded at two take-off angles, *viz.* 30° and 70° are shown in Fig. 5.3.

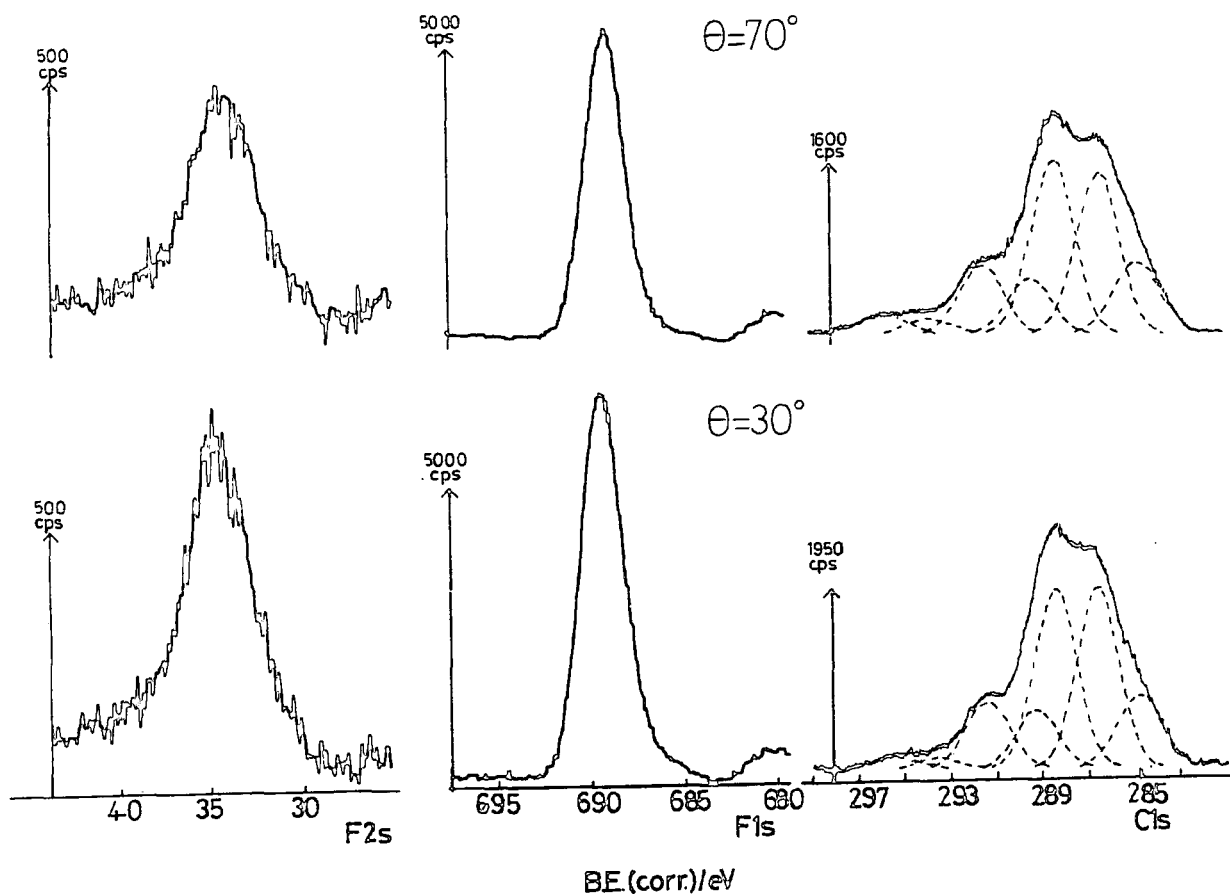


Figure 5.3 C_{1s} , F_{1s} , F_{2s} spectra of the electron beam polymer prepared from hexafluorobenzene

The beam current used was $\sim 0.5\mu\text{A}$ for a total time of 30 minutes.

Visual inspection of the spectra reveals the similarity of the core levels at the two take-off angles. Calculation of the overall film stoichiometry from a knowledge of the instrumental sensitivity factors and the F_{1s} to C_{1s} total intensity ratios gives $C_1F_{0.63}$ and $C_1F_{0.70}$ for the 70° and 30° take-off angle spectra respectively. These values are within experimental error the same and reveal that the film is vertically homogeneous in terms of fluorine to carbon content in the surface and subsurface regions. Component analysis of the C_{1s} spectra has been performed in a manner similar to that previously carried out for spectra obtained from the plasma polymer of hexafluorobenzene. Thus peaks corresponding to $\underline{C}-CF_n$, \underline{CF} , $\underline{CF}-CF_n$, \underline{CF}_2 , \underline{CF}_3 and a $\pi \rightarrow \pi^*$ shakeup satellite of the \underline{CF} peak at binding energies of $\sim 286.8\text{eV}$, $\sim 288.6\text{eV}$, $\sim 289.4\text{eV}$, $\sim 291.7\text{eV}$, $\sim 293.9\text{eV}$ and $\sim 296.0\text{eV}$ have been fitted. In addition a peak at $\sim 285.0\text{eV}$, corresponding to carbon with neither α nor β fluorine atoms present was necessary, the nature of this peak will shortly become apparent. Such a component analysis gives a stoichiometry of $C_1F_{.71}$ and $C_1F_{.73}$ for the 70° and 30° spectra, in excellent agreement with the F_{1s}/C_{1s} calculated stoichiometries. The two sets of data indicate that fluorine loss has occurred to the same degree at both 30° and 70° sampling depths, a further indication of the film's homogeneity is provided by the F_{1s}/F_{2s} intensity ratios, being $\sim 7.2-7.6$ for the two take-off angles, *i.e.* comparable to vertically homogeneous model polymers.

The component analysis indicates that substantial loss of \underline{CF} features has occurred, since in the monomer the \underline{CF} peak at 289.5eV is $\sim 90\%$ of the total C_{1s} envelope, the remaining 10%

being due to a $\pi \rightarrow \pi^*$ shake-up satellite at $\sim 296\text{eV}$. In the polymer the peaks due to $\underline{\text{CF}}$ functionalities have a reduced contribution of $\sim 40\%$, the $\pi \rightarrow \pi^*$ shake-up peak at $\sim 296\text{eV}$ is still present, with an intensity of $\sim 7\%$ of the parent $\underline{\text{CF}}$ peak. Thus retention of unsaturation associated with $\underline{\text{CF}}$ functionalities is indicated although to a lesser degree than in the monomer. Evidence for molecular rearrangement accompanying polymerisation is seen from the presence of $\underline{\text{CF}}_2$ functionalities (which contribute $\sim 12\%$ at both take-off angles) and also from a small ($\sim 2\%$) contribution of features corresponding to $\underline{\text{CF}}_3$ functionalities. The relative contributions of the latter two features are remarkably similar to those observed in the plasma²¹⁷ and argon ion beam²⁰³ polymerisation of hexafluorobenzene, the plasma polymerised films however having greater overall fluorine content than the electron beam and ion beam polymers.²⁰³

The spectra obtained from the electron beam polymer also show a substantial contribution to the C_{1s} envelope of features not directly bonded to fluorine. Line shape analysis allows differentiation of these features into two groups: (a) carbon with fluorine at a β position, and (b) carbon with no fluorine at either the α or β position. In plasma polymerised hexafluorobenzene^{217,218} the latter were shown to be due to hydrocarbon overlayer arising from deposition of residual hydrocarbon in the vacuum system utilised. It is of interest therefore to ascertain whether such is the case in the electron beam polymer using a simple substrate overlayer model.

With uniform coverage of an overlayer, the intensity ratio of the hydrocarbon to the rest of the C_{1s} envelope is given by

$$\left(\frac{I_O}{I_R}\right)_\theta = \frac{1 - e^{-d/\lambda \cos \theta}}{e^{-d/\lambda \cos \theta}} = e^{d/\lambda \cos \theta} - 1 \quad (\text{eqn. 5.3})$$

where d , λ and θ have their usual meanings. For the 70° spectra $\frac{I_O}{I_R} = .15$ giving $d = .67\text{\AA}$. This is less than monolayer thickness ($\sim 5\text{\AA}$) and so coverage if present must be due to a patched overlayer. Modifying eqn. 5.3 to take account of fractional coverage x of overlayer gives

$$\left(\frac{I_O}{I_R}\right)_\theta = \frac{x(1 - e^{-d/\lambda \cos \theta})}{(1-x) + x e^{-d/\lambda \cos \theta}} \quad (\text{eqn. 5.4})$$

By numerically calculating values of $\frac{I_O}{I_R}$ from eqn. 5.4 for a range of values of x and d (in 5\AA steps) comparison may be made with the experimental data.

For the present case best agreement is found for fractional monolayer coverage, *i.e.* $d = 5\text{\AA}$, with $x = 0.2$. The relative intensity ratio $\frac{I_O}{I_R}$ calculated using these values for the 30° take-off angle is ~ 0.07 where the observed contribution is 15%. Thus the C type carbons at $\sim 285\text{eV}$ are not due to overlayer coverage but are incorporated in the polymer film, in marked contrast to the case found for plasma polymerised hexafluorobenzene. This is consistent with the expectations based on the F/C stoichiometries for the two films. Thus whereas for the electron beam polymer the stoichiometry is lower in fluorine than for the starting material for the plasma polymer under most conditions it remains the same.

In Chapter Four it was shown that at room temperature electron beam bombardment of clean gold causes a small increase in the intensity of the C_{1s} peak occurring in the $\sim 285\text{eV}$ region

showing that a low level of electron beam induced adsorption or polymerisation of residual vacuum gases was occurring even at these very low ($\sim 10^{-9}$ Torr) pressures and beam doses.

Fluorine loss was also shown to occur to a much greater degree than adsorption on electron beam bombardment, with CF_2 groups in PTFE and PVF_2 gradually losing fluorine and giving a surface predominantly of carbonaceous nature. It would appear that the latter process accompanies the electron beam polymerisation, electron stimulated adsorption being insignificant.

Some molecular rearrangement does appear to be occurring in the electron beam process, evident from the appearance of peaks arising from CF_2 ($\sim 12\%$ of the total C_{1s} envelope) and CF_3 ($< 2\%$) groups. The C_{1s} spectra of plasma polymerised perfluorobenzene also revealed²¹⁸ evidence for extensive molecular^{217,218} rearrangement with components appropriate to CF_3 and CF_2 groups of increased intensity.

(b) Pentafluorobenzene

Bombardment of condensed pentafluorobenzene under the same conditions as for hexafluorobenzene (*viz.* 2kV beam energy; 5 μ A beam current as measured on the probe tip; sample cooled at constant -120°C) produced a polymer where C_{1s} , F_{1s} and F_{2s} spectra recorded at two take-off angles ($30^\circ + 70^\circ$) are shown in Fig. 5.4.

The stoichiometries of the films calculated from $\text{C}_{1s}/\text{F}_{1s}$ ratios are found to be $\text{C}_1\text{F}_{0.56}$ for the 30° spectra and $\text{C}_1\text{F}_{0.49}$ for the 70° spectra. These data are indicative of the homogeneity of the film within the different sampling depths

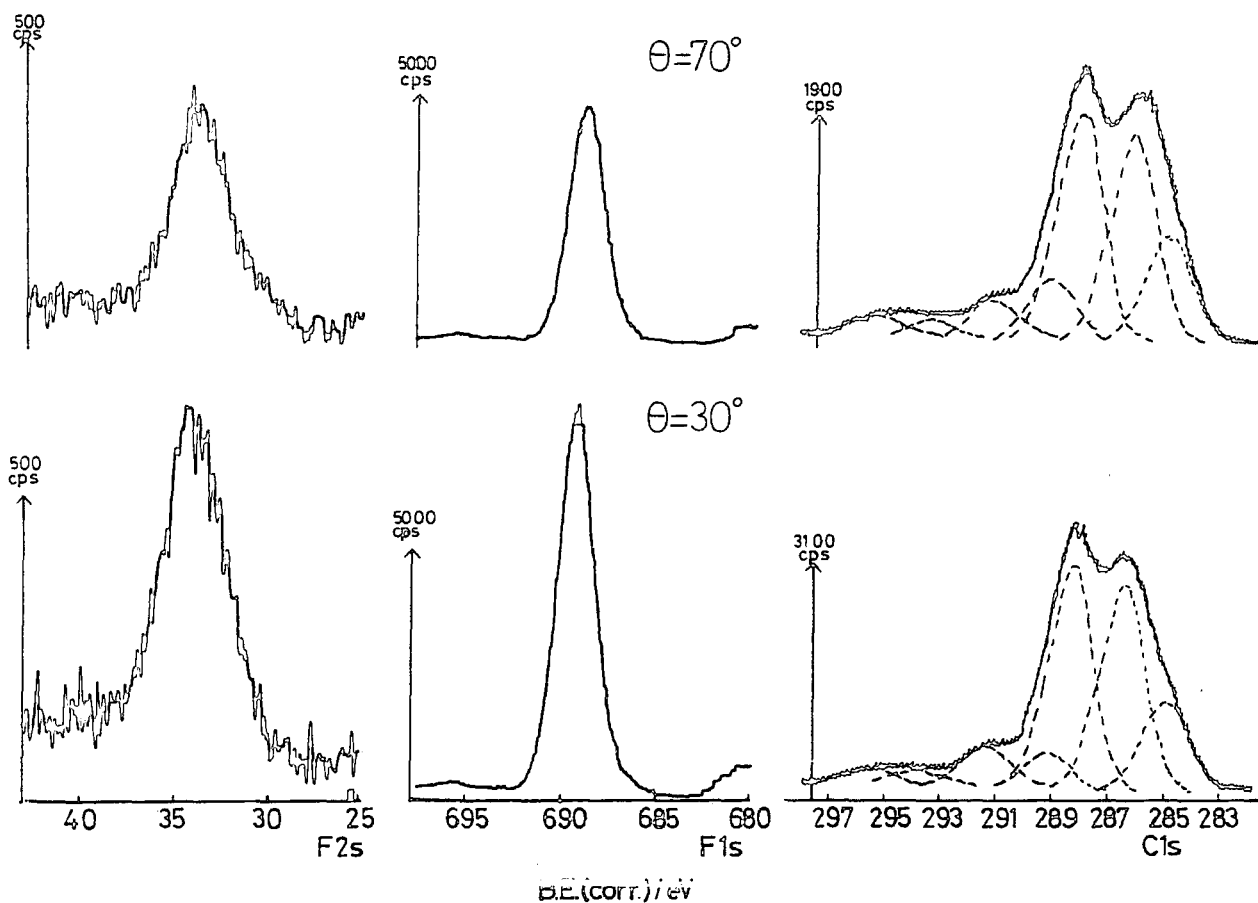


Figure 5.4 C_{1s} , F_{1s} , F_{2s} spectra of the electron beam polymer prepared from pentafluorobenzene

of the two take-off angles, also revealed by the F_{1s}/F_{2s} ratios at both 30° and 70° which are close to those derived for homogeneous polymers. Line shape analysis of the C_{1s} spectra has been carried out using the same philosophy as that for the hexafluorobenzene polymers, with peaks assigned initially, in order of increasing binding energy, as \underline{CH} , $\underline{C-CF}_n$, \underline{CF} , $\underline{CF-CF}_n$, \underline{CF}_2 , \underline{CF}_3 and a $\pi \rightarrow \pi^*$ shake-up satellite of the \underline{CF} peak. The stoichiometries calculated from this analysis are $C_1F_{0.63}$ and $C_1F_{0.70}$, in relatively poor overall agreement with the data

calculated from the F_{1s}/C_{1s} intensity ratio. If the peak at $\sim 293.5\text{eV}$, originally assigned as arising from CF_3 structural features, and having a relative intensity of $\sim 3.5\%$ of the total C_{1s} envelope, is alternatively assigned as being due to a $\pi \rightarrow \pi^*$ satellite of the C-CF_n component centred at $\sim 286.3\text{eV}$, the stoichiometries as calculated from C_{1s} contributions become $\text{C}_1\text{F}_{0.56}$ and $\text{C}_1\text{F}_{0.58}$ for 30° and 70° . A schematic of the peak fitting procedure is shown in Fig. 5.5.

The major difference between these spectra and the spectra obtained for the perfluorobenzene electron beam polymer is the significant drop in the contribution of CF_2 components to the C_{1s} spectra (a drop from $\sim 12\%$ to 6%). Also evident from inspection of the C_{1s} spectra is the apparent shift of the peak at ~ 286.3 , corresponding to carbons not directly bonded to fluorine but with an adjacent CF group, to lower binding energy. This is consistent with the lower fluorine content of the films. The binding energy of the centroid of the F_{1s} peak shows a decrease of $\sim 4\text{eV}$ in binding energy²⁹⁷ corresponding also to the lesser degree of fluorination.

Comparison with the pentafluorobenzene plasma polymers²¹⁸ reveals differences similar to those observed between the hexafluorobenzene polymers prepared by the two techniques. The fluorine content of the electron beam polymers is again lower than the plasma polymers (which had typical stoichiometries $\sim \text{C}_1\text{F}_{0.75}$). The uniformity in terms of vertical homogeneity in the plasma polymers is also observed in the electron beam polymer. The C_{1s} spectra of the electron beam polymer do not reveal the same extent of molecular rearrangement as was the case in the pentafluorobenzene plasma polymer,²¹⁸ since relative contributions

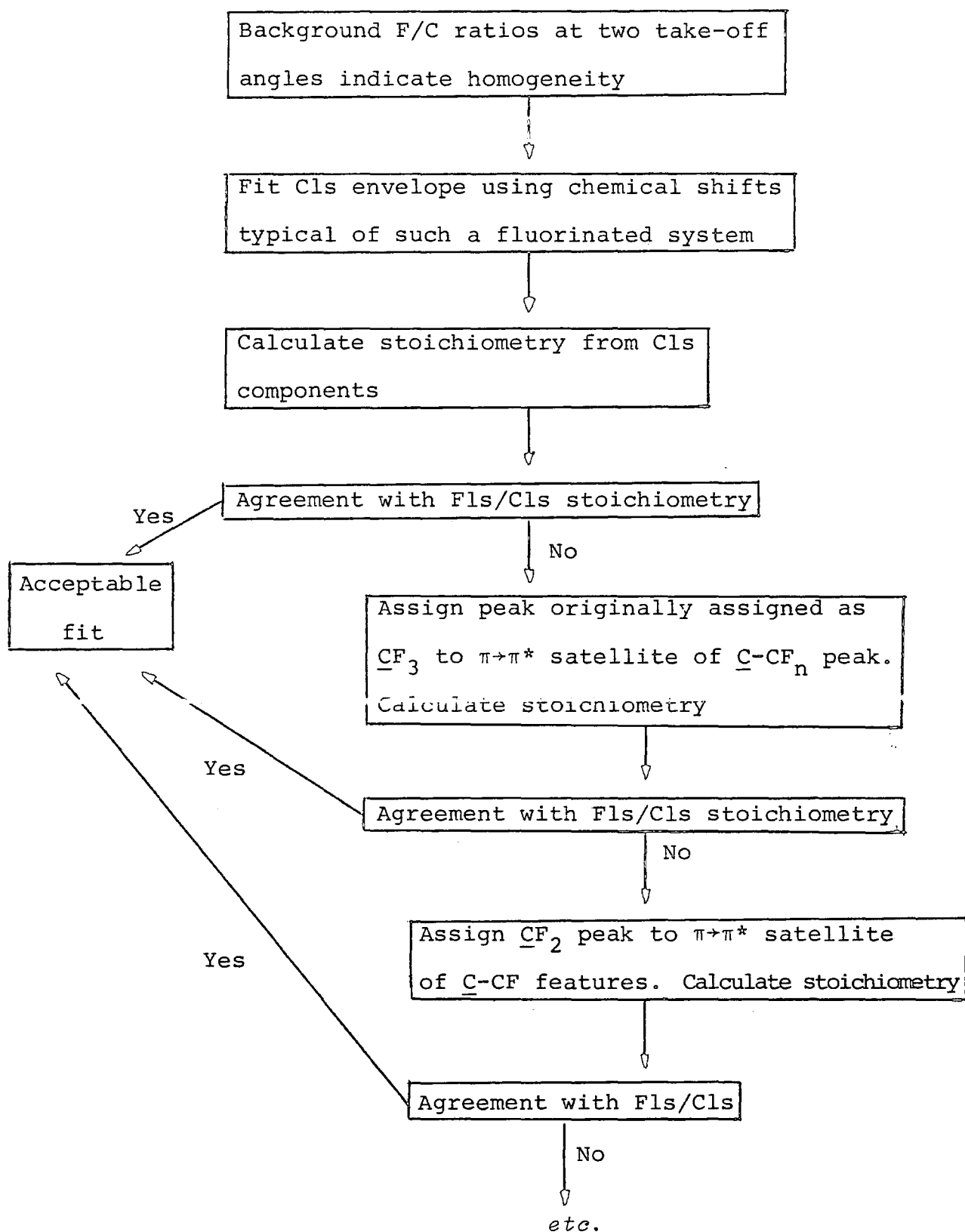


Figure 5.5 Schematic of the peak fitting routine used

arising from CF_2 and CF_3 functionalities are lower in the electron beam polymer. However less CF_3 and CF_2 groups may be indicative also of defluorination of the initially rearranged product.

Substrate overlayer calculations detailed in section 5.3.1(a) also reveal that C type features giving the peak at $\sim 285\text{eV}$ are incorporated in the polymer film and are not due to a hydrocarbon overlayer. Thus again electron beam irradiation has produced a significant proportion (15%) of carbonaceous material not present initially in the monomer.

(c) Tetrafluorobenzene

The 1,2,3,5 isomer of tetrafluorobenzene, bombarded under the same conditions as hexa- and pentafluorobenzene yielded a polymer whose C_{1s} , F_{1s} and F_{2s} spectra are shown in Fig.5.6. Inspection of the C_{1s} core level spectra immediately reveals less contribution of components due to CF_2 and CF functionalities than that observed in the perfluorobenzene and pentafluorobenzene cases: stoichiometries derived from the $\text{F}_{1s}/\text{C}_{1s}$ ratios being $\text{C}_1\text{F}_{0.47}$ at 30° and $\text{C}_1\text{F}_{0.45}$ at 70° . Peak fitting of the C_{1s} envelope was performed as previously described for the perfluorobenzene and pentafluorobenzene electron beam polymers, however assignment of the peak at 293.6eV to CF_3 functionalities again causes severe discrepancy to occur between stoichiometries calculated by consideration of the $\text{F}_{1s}/\text{C}_{1s}$ intensity ratios and those from component analysis of the C_{1s} envelope at both take-off angles. Assignment of this peak to the $\pi \rightarrow \pi^*$ shake-up satellite of the C-CF_n peak at $\sim 286.6\text{eV}$ brings the stoichiometries calculated by the two methods to close agreement, as can be

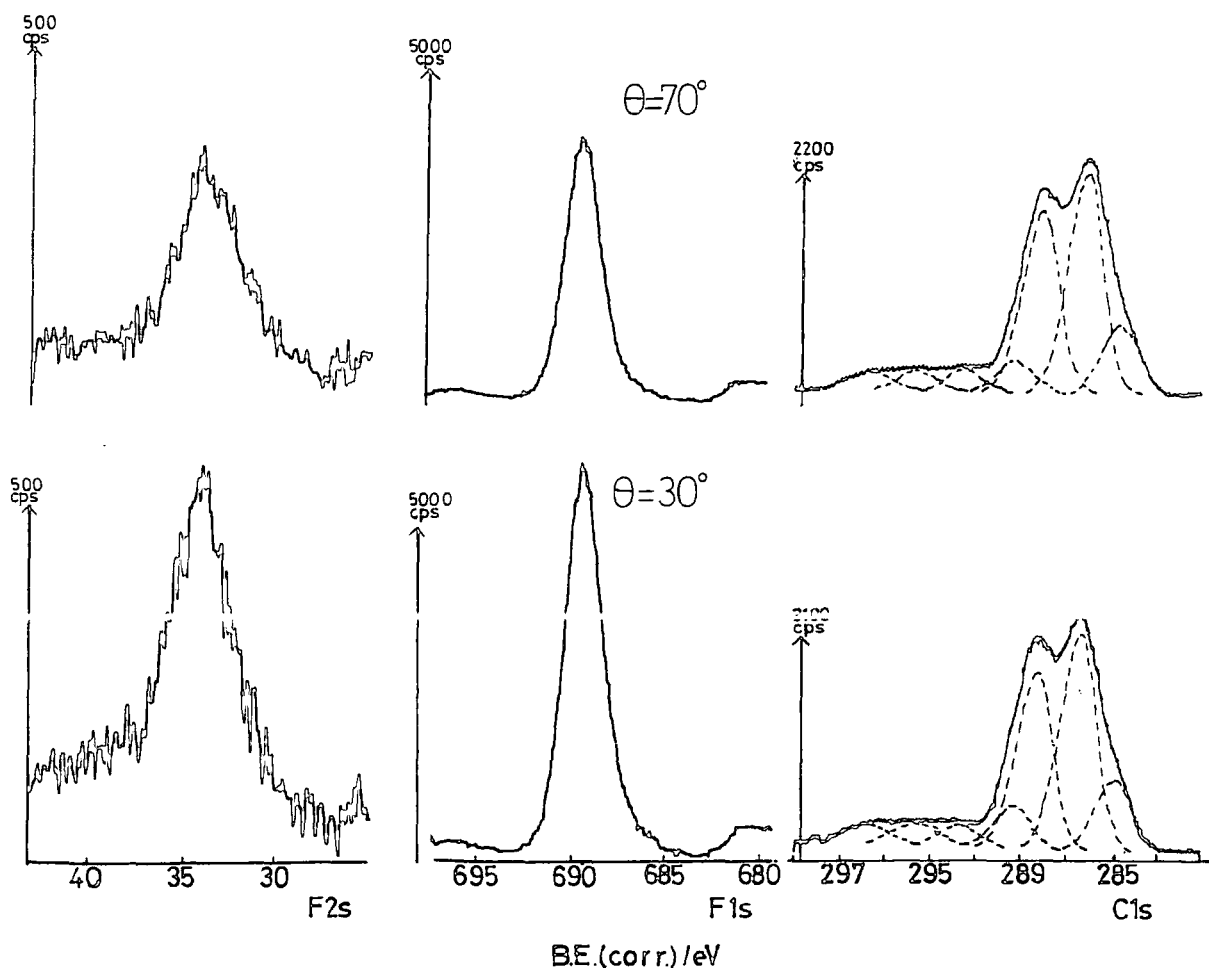


Figure 5.6 C_{1s} , F_{1s} and F_{2s} spectra of electron beam polymerised tetrafluorobenzene

seen from Fig.5.6. Such an assignment however gives an unusually high intensity, $\sim 13\%$, of the shake-up transition compared to its parent peak. Thus features at $\sim 293.6\text{eV}$ are probably attributable to both CF_3 and $\pi \rightarrow \pi^*$ shake-up transitions but to what extent each contributes cannot be accurately assigned.

The proximity of stoichiometries calculated from the 70°

and 30° data reveals that the films formed are again vertically homogeneous. This is confirmed by close inspection of the component analysis of the C_{1s} spectra where intensities due to various structural features are very similar at the two take-off angles, and also by the proximity of the F_{1s}/F_{2s} ratios.

Comparison with the data reported for the polymer prepared by plasma polymerising 1,2,3,5 tetrafluorobenzene²¹⁹ indicates again that there is less fluorine incorporation in the electron beam polymer, since the former had derived stoichiometries very close to that of the starting monomer ($C_1F_{0.67}$) whereas the electron beam polymer has ~33% less fluorine. A smaller proportion of CF_2 groups in the electron beam polymer compared to plasma polymers is again shown to be the case, indicative of less rearrangement occurring in the electron beam polymerisation process.

(d) Trifluorobenzene

The polymer formed by bombardment of condensed 1,3,5 trifluorobenzene under the same conditions as the other fluorobenzenes yielded C_{1s} , F_{1s} and F_{2s} spectra shown in Fig. 5.7. The stoichiometries derived from the F_{1s}/C_{1s} ratios at the two different take-off angles are within experimental error, the same, *viz.* 0.30 at 30° and 0.31 at 70° , indicative of the vertically homogeneous nature of the film, also confirmed by the F_{1s}/F_{2s} ratio. The stoichiometries show that the trifluorobenzene electron beam polymer is lower in fluorine content than polymers prepared from the tetra-, penta- and hexa-fluorobenzenes. This may also be seen by inspection of the C_{1s} envelopes, which reveal a much lower contribution to the band profile from \underline{CF} components and deconvolution of the C_{1s} envelope, in a manner

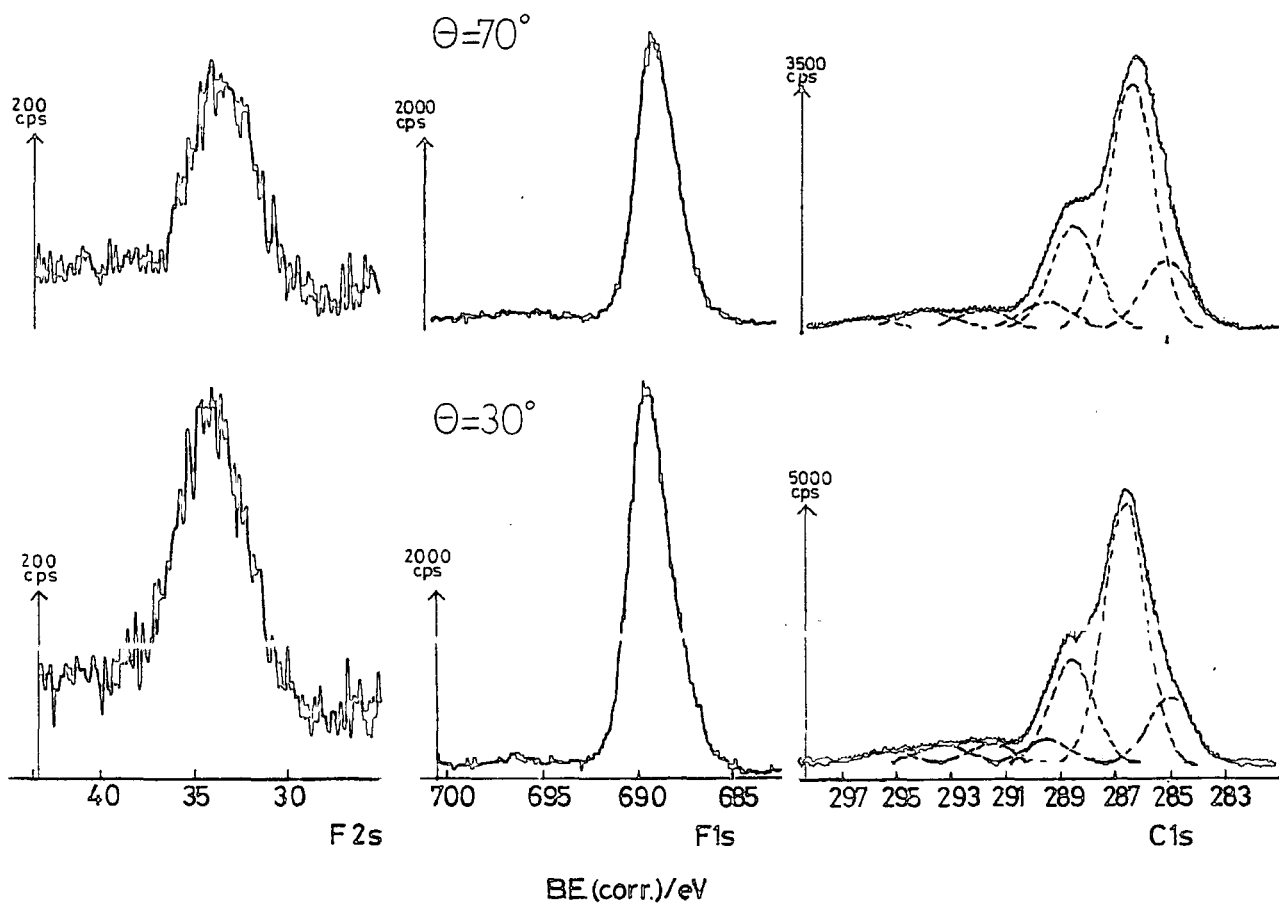


Figure 5.7 C_{1s} , F_{1s} and F_{2s} spectra of electron beam polymerised trifluorobenzene

consistent with that used in fitting C_{1s} spectra of the hexa-, penta- and tetra-fluorobenzene electron beam polymers, indicates this trend in a more quantitative fashion. However even assuming that all of the signal assigned to CF_3 components is due to $\pi \rightarrow \pi^*$ shake-up transitions, the fluorine content as calculated from the C_{1s} envelope is slightly higher than the F_{1s}/C_{1s} computed stoichiometry. This indicates that some of the

signal intensity originally assigned to $\underline{\text{CF}}_2$ features may be due to a $\pi \rightarrow \pi^*$ shake-up satellite peak of $\underline{\text{C}}\text{-CF}$ features (which themselves have not been explicitly taken into account). Thus the data reveal some retention of conjugative features, but to what extent cannot be accurately judged. The F_{1s} spectrum at 30° take-off angle indicates some retention of conjugation at $\underline{\text{CF}}$ functionalities.

A previous investigation of the plasma polymers produced from trifluorobenzene²²¹ gave a polymer stoichiometry, as determined by both ESCA and bulk analysis, of $\text{C}_1\text{F}_{0.4}$, thus the electron beam polymer is again less fluorinated than its analogous plasma polymer.

(e) Difluorobenzene

The ortho isomer of difluorobenzene was polymerised under the standard conditions used for the rest of the series and the C_{1s} , F_{1s} and F_{2s} level spectra of the product are shown in Fig.5.8. The low fluorine content of the films is immediately evident, with the peak due to -CF at $\sim 288\text{eV}$ now just appearing as a broadening asymmetry to the high binding energy side of the main peak.

The low fluorine content of the film necessitates a change in the line shape analysis for the C_{1s} envelope. The reason for this is the large contribution from C-CF functionalities occurring at $\sim 0.6\text{eV}$ to higher binding energy to the CH_2 peak at 285eV . Thus the spectra were peak fitted assuming the functionalities contributing to the overall C_{1s} profile were $\underline{\text{CH}}_2$, $\underline{\text{C}}\text{-CF}$, $\underline{\text{C}}\text{-CF}_n$, $\underline{\text{CF}}$, $\underline{\text{CF}}\text{-CF}_n$, $\underline{\text{CF}}_2$ at binding energies of $\sim 285\text{eV}$, 285.7eV , $\sim 286.6\text{eV}$, $\sim 288\text{eV}$, 288.9eV and 291eV . Shake-up peaks due to $\pi \rightarrow \pi^*$ shake-up transitions for the C-CF , C-CF_n were also

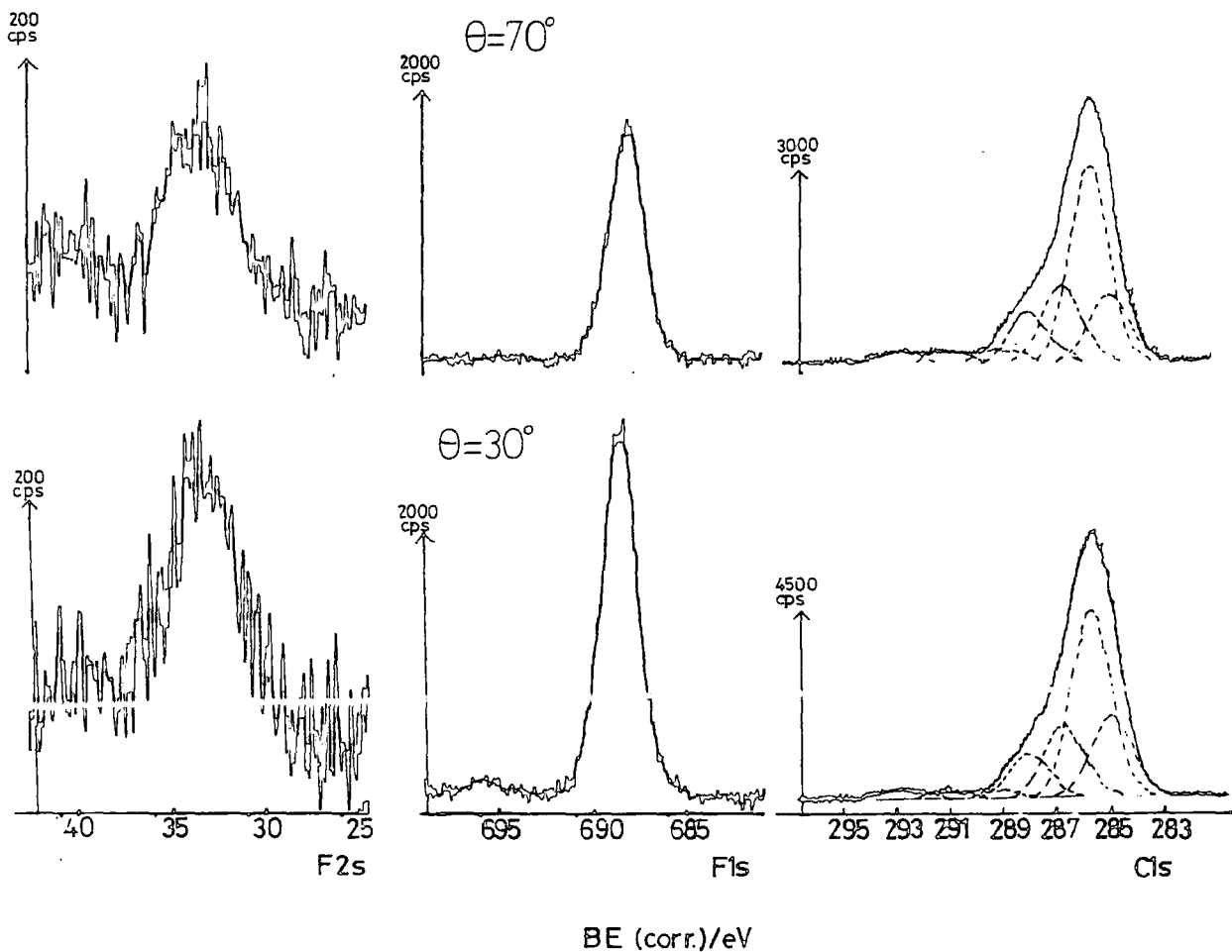


Figure 5.8 C_{1s} , F_{1s} and F_{2s} spectra of electron beam polymerised difluorobenzene

fitted assuming a transition energy of $\sim 7\text{eV}$.

The stoichiometry calculated from the C_{1s} component contributions at both take-off angles ($C_1F_{0.15}$ at 30° , $C_1F_{0.19}$ at 70°) are close to that calculated from the F_{1s}/C_{1s} ratios ($C_1F_{0.16}$ at 30° and $C_1F_{0.18}$ at 70°). The stoichiometry indicates that extensive fluorine loss has occurred, the stoichiometry changing from $C_1F_{0.33}$ for the starting material to $C_1F_{0.18}$ *v.e.*

a decrease of approximately 45%. The plasma polymerisation²²¹ of orthodifluorobenzene involved a ~20% decrease in fluorine content, so again the electron beam polymerisation process involves greater fluorine loss.

The electron beam polymer of orthodifluorobenzene, like the plasma polymer, is shown by the angular dependent data to be vertically homogeneous. This is considerably emphasised by the proximity of the relative intensities of the C_{1s} components, evident from Fig.5.8. Additional evidence of homogeneity is provided by the F_{1s}/F_{2s} intensity ratio at 30° , however the 70° ratio is relatively unreliable because of the low intensity of the F_{2s} peak giving poor counting statistics.

The $\pi \rightarrow \pi^*$ shake-up peaks, being relatively free from other (e.g. CF_3 , CF_2) groups, may be used as a test of conjugation in the system. For both 70° and 30° take-off angles the $\pi \rightarrow \pi^*$ component contributes ~6% of the major component at ~285.7eV. The shake-up component of the $C-CF_n$ peak has a corresponding value of ~9%. Both these figures are indicative that a large degree of unsaturation was retained by the electron beam polymer, since typical intensities for $\pi \rightarrow \pi^*$ peaks are ~11% of the parent peak for monomeric perfluorobenzene. Evidence for unsaturated CF features may also be taken from the small $\pi \rightarrow \pi^*$ shake-up transition ~7eV to the higher binding energy side of the F_{1s} peak.

(f) Monofluorobenzene

As would be expected, the polymer prepared by electron bombardment of monofluorobenzene, under the same conditions as the other fluorobenzenes, has the least amount of fluorine as revealed by the F_{1s} , F_{2s} and C_{1s} spectra shown in Fig. 5.9. The

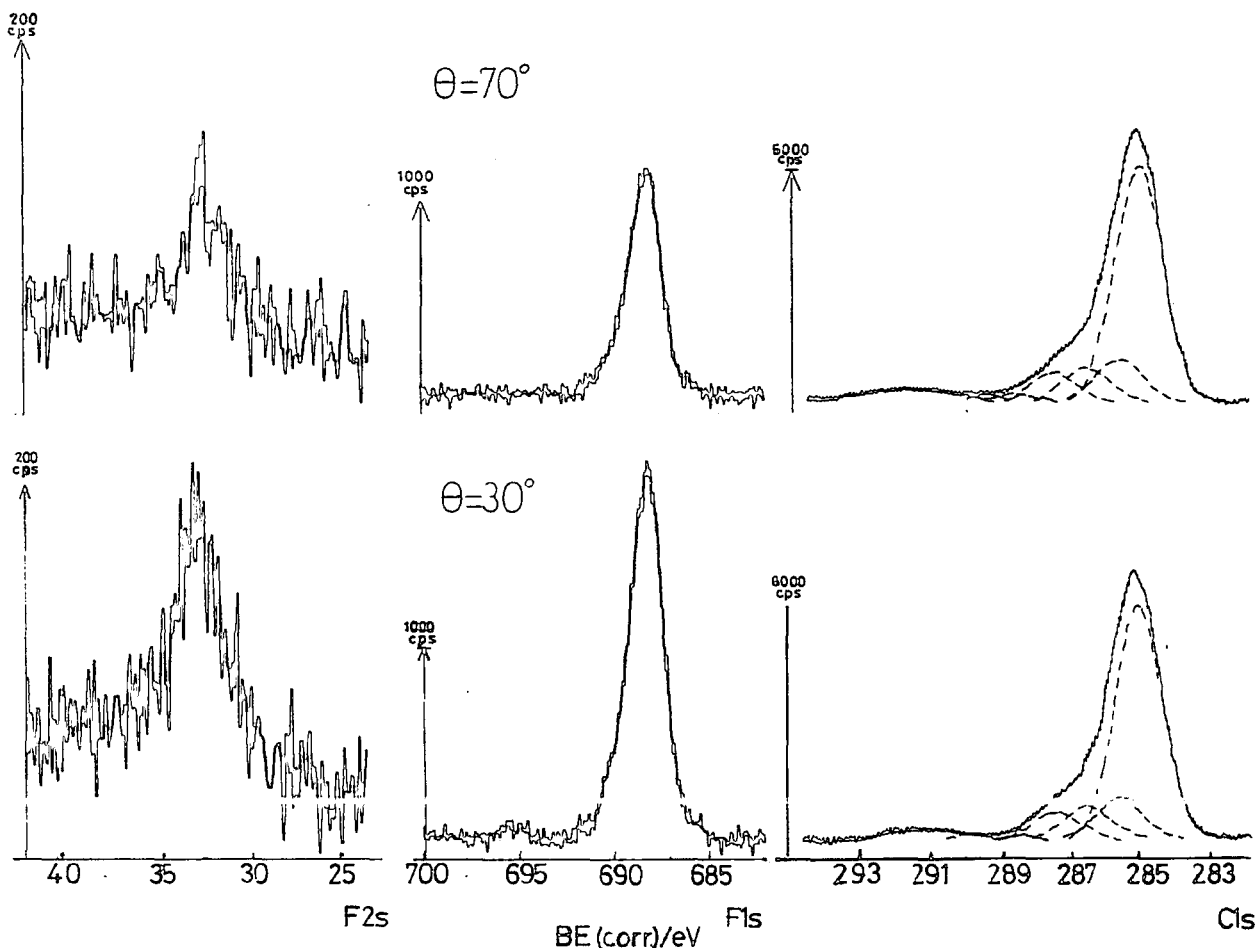


Figure 5.9 C_{1s} , F_{1s} and F_{2s} spectra of electron beam polymerised monofluorobenzene

F_{2s} spectrum, of poor quality in terms of signal to noise ratio, is particularly affected by the low fluorine content, which, coupled with the relatively low cross section for photoionisation by $MgK\alpha_{1,2}$ X-rays, yields a low intensity peak.

Analysis of the C_{1s} spectra was performed using peaks corresponding to $\underline{C}H_2$, $\underline{C}-CF$, $\underline{C}-CF_n$, \underline{CF} , $\underline{CF}-CF_n$ structural features at binding energies of $\sim 285\text{eV}$, 285.7eV , 286.6eV , 287.6eV and 288.5eV respectively. The broad peak centred around $\sim 292\text{eV}$ has

been fitted as corresponding to two $\pi \rightarrow \pi^*$ shake-up satellites, of the C-CF and CH_2 peaks. The average stoichiometry, $\text{C}_1\text{F}_{0.9}$ shows again that significant fluorine loss is occurring. However in marked contrast to the rest of the series the fluorine content of the electron beam polymer is significantly higher than in the plasma polymerised monofluorobenzene.

Homogeneity of the electron beam polymer is shown again by the great similarity of the 30° and 70° take-off angle data. The intensity of the shake-up components is about 5% of their parent peaks, indicative of substantial retention of conjugative features. Such retention was only observed in the plasma polymerisation of monofluorobenzene under mild conditions,²²¹ viz. low power and, more critically, higher pressure. Evidence for $=\text{CF}$ structural features can be seen from the slight $\pi \rightarrow \pi^*$ shake-up transition peak $\sim 6\text{eV}$ to higher binding energy of the main F_{1s} peak in the electron beam polymer.

(g) Overall Comparison of Polymers Produced

The data presented in the previous sections indicate that electron beam polymer composition is a function of the initial starting material, in contrast to the majority of gas phase electron beam deposition reactions where the polymer was envisaged to be largely independent of starting material. However for all the polymers carbonaceous material, evident by a peak at $\sim 285\text{eV}$ was incorporated in the film and not due to an extraneous hydrocarbon overlayer. The fluorine content of the electron beam polymers also indicate that significant fluorine loss had occurred. The structures of the polymer films produced from electron bombardment of the isomeric fluorobenzenes indicate

a complex relationship to those of the starting "monomers". However the structures are distinctive in each case although at high beam current and extended bombardment times the ultimate structures will inevitably tend to be similar for all of these starting materials.

The variation of C:F stoichiometries relative to initial 'monomer' composition is shown in Fig.5.10, which emphasises that substantial fluorine loss has occurred. The greatest relative decrease occurs in the less fluorinated starting materials.

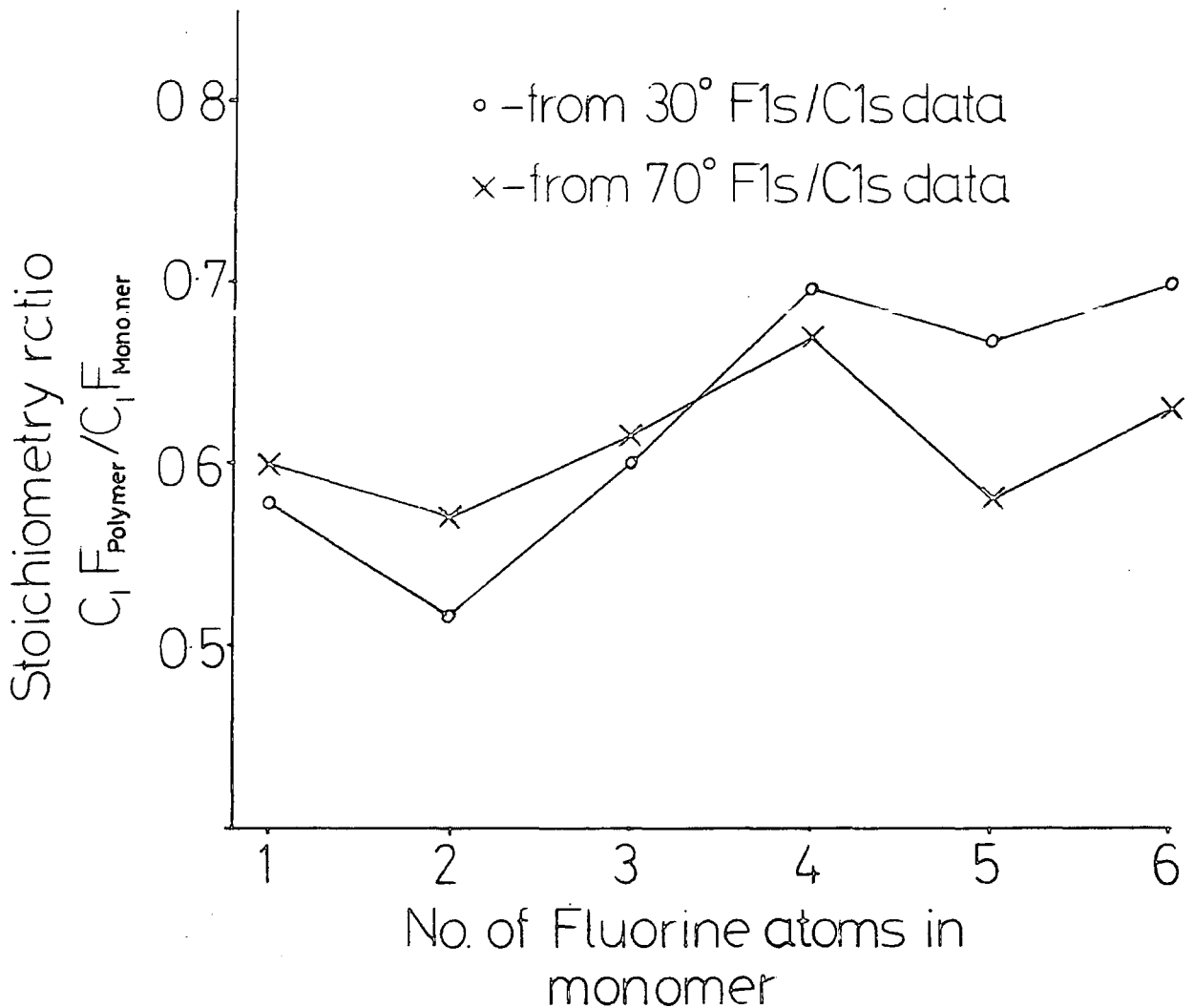


Figure 5.10 Polymer:monomer stoichiometry ratios as a function of starting monomer

This is similar to the trend observed for the plasma polymers of the fluorobenzenes²²¹ where the starting material to polymer stoichiometry ratios did vary over a large range, *viz.* from 1 for hexafluorobenzene to 0.3 for monofluorobenzene. Defluorination in both treatments therefore is favoured with greater hydrogen content of the starting material, which indicates that HF elimination aids defluorination. The loss of HF from the starting material to yield a benzyne has been shown by MNDO SCF calculations^{219,221} in the case of tetrafluorobenzene, to be less favourable energetically than isomerisation reactions, *via* valence isomers and hexadienyne formations *via* fulvene. Separate calculations indicate that hydrogen substitution for fluorine does not show any trend in stabilising or destabilising the benzyne with respect to the parent fluorobenzene. Fluorine elimination as HF may however occur in fulvene/hexadienyne structures formed in the initial stages of polymerisation.

Fluorine loss was significantly greater in the electron beam polymerisation of the higher fluorinated systems with the concomitant appearance of carbonaceous features.

The change in relative contributions of $\underline{\text{C}}$, $\underline{\text{CF}}$, and $\underline{\text{CF}}_2$ functionalities of the electron beam polymers as a function of starting monomer may clearly be seen from Fig.5.11. Thus as would be expected $\underline{\text{C}}$ functionalities increase and $\underline{\text{CF}}$ decrease with decreasing fluorine content of the starting monomer. The greater fluorine content of the perfluorobenzene compared to pentafluorobenzene is seen to be due solely to an increase in $\underline{\text{CF}}_2$ functionalities, indicative of greater rearrangement taking place in the perfluorobenzene polymer.

The vertical homogeneity of the electron beam polymers was in general shown to be uniform for the lower fluorinated

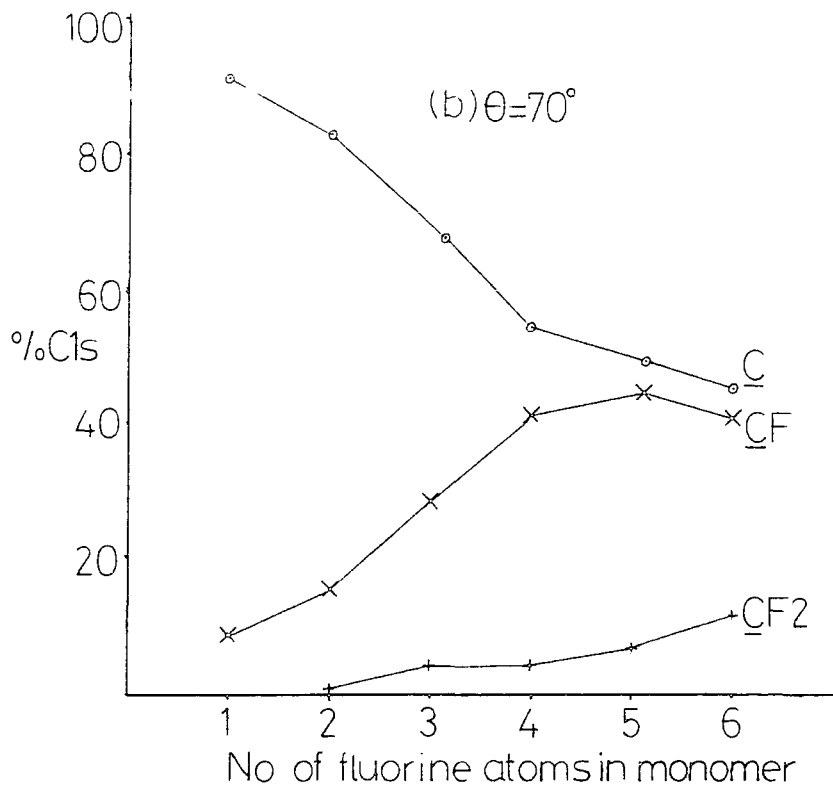
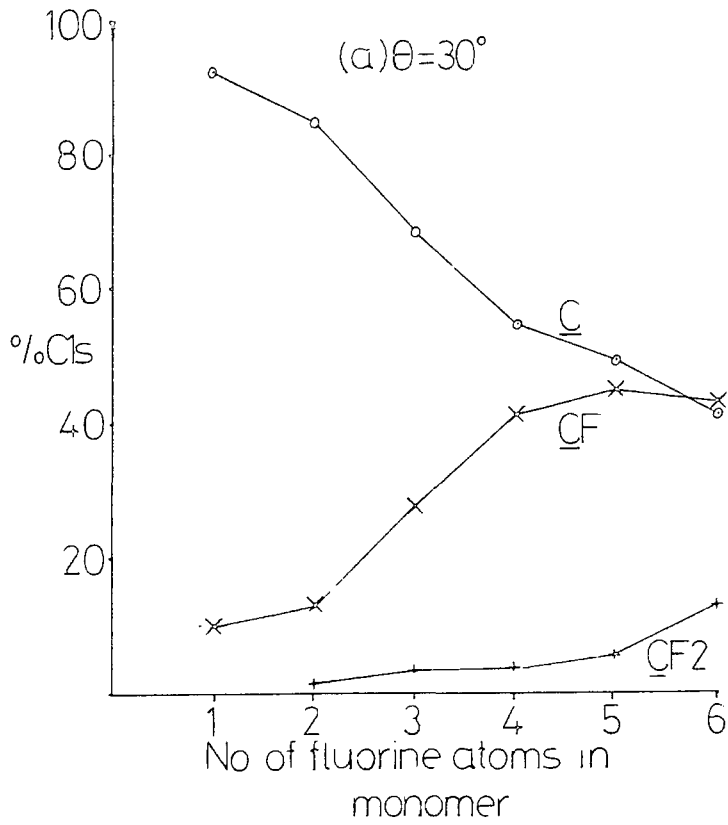


Figure 5.11 Variation of summed relative component contributions to the C_{1s} envelope

members but greater fluorine loss was seen to occur at the absolute surface of the penta- and per-fluorobenzene series. Retention of some conjugated features is observed for all the electron beam polymers by the presence of $\pi \rightarrow \pi^*$ shake-up peaks for both the C_{1s} and F_{1s} spectra.

These polymers showed very low levels of oxygen, typically $\sim 1\%$ of the carbon. This again is due to the UHV mode of preparation. On exposure of the samples to air however the oxygen level changed significantly; to $\sim 5\%$ of the carbon. This phenomenon was also observed in the plasma polymers where oxygen content of *in situ* polymerised films was far lower than those made in free standing reactors, which necessitated exposure of the sample to air prior to ESCA analysis. The position of the broad O_{1s} signal . . . encompassing . . . a wide range of functionalities, and a "blurring" of the C_{1s} peak indicates that the oxygen present in the exposed samples has chemically reacted with the electron beam polymer surface as opposed to uptake by a physisorption process.

5.3.2 The Effect of Bombardment time on final polymer structure

In order to gain insight into possible processes occurring in electron beam polymerisation a series of experiments was carried out where the time of electron bombardment of the condensed fluorobenzene was varied. The substrate used in all cases was again gold. The electron beam however was now rastered over a greater area of the probe tip ($\sim 1.0 \text{ cm}^{-2}$). Hexafluorobenzene was chosen as the starting material since in the previous sections it was found that -

(i) The mode of fluorine loss in hexafluorobenzene may be considered unique to the electron beam process. Fluorine loss in the other isomers appears to be complicated by a convolution of processes which also occur in plasma polymerisation and those which are inherent in the electron beam processes.

(ii) The relative intensity of the $-CF_2$ signal was highest for the perfluorobenzene electron beam polymer. Occurrence of CF_2 functionalities is evidence of molecular rearrangement processes occurring.

Separate experiments were therefore carried out on condensed multilayers of perfluorobenzene with electron beam bombardment times of 1, 3, 7.5, 15 and 30 mins. In all cases the beam current ($\sim 4\mu A$ as measured on the probe tip) and energy (2kV) used were the same.

The C_{1s} spectra at two take-off angles for the resulting polymer are shown in Fig.5.12. As can be seen from Fig.5.12 substantial changes to the line shape are occurring, with growth of features to the low binding energy side of the main CF peak at $\sim 288.5eV$. The treatment after 1 minute appears to be anomalous, and substrate overlayer calculations indicate that the peak at $\sim 285eV$ is not incorporated in the film but is due to an overlayer of, presumably, hydrocarbon material. For the rest of the series the model calculations show that the C peak is incorporated in the film. On removal of the effects of the $-CH_2$ peak at $285eV$ binding energy it is found to follow a definite trend. Line shape analysis of the C_{1s} peaks has been carried out along the lines of that described in section 3(i)(a) of this chapter. Stoichiometries obtained from such fits were found to be in agreement with those calculated from the F_{1s}/C_{1s}

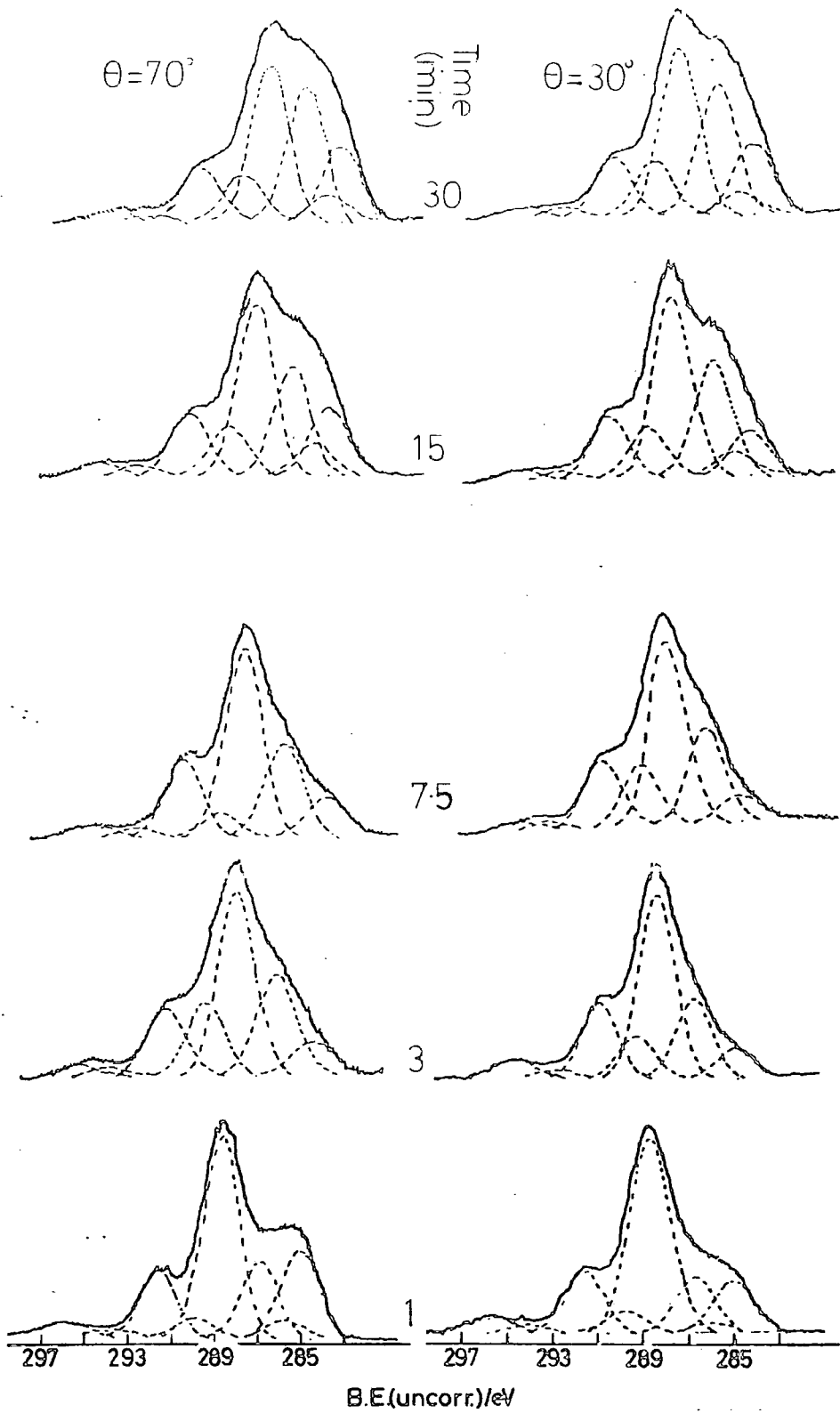


Figure 5.12 C_{1s} spectra of electron beam polymerised hexafluorobenzene as a function of bombardment time

ratio. These are shown in graphical form in Fig.5.13. Fig.5.13 shows a definite trend of lower fluorine content with increased bombardment time. Thus for low treatment times the polymer stoichiometry is very close to the monomer. This is quite logical since extrapolation to zero treatment time should give a polymer of the identical stoichiometry to the monomer, the yield would, however, be 0%.

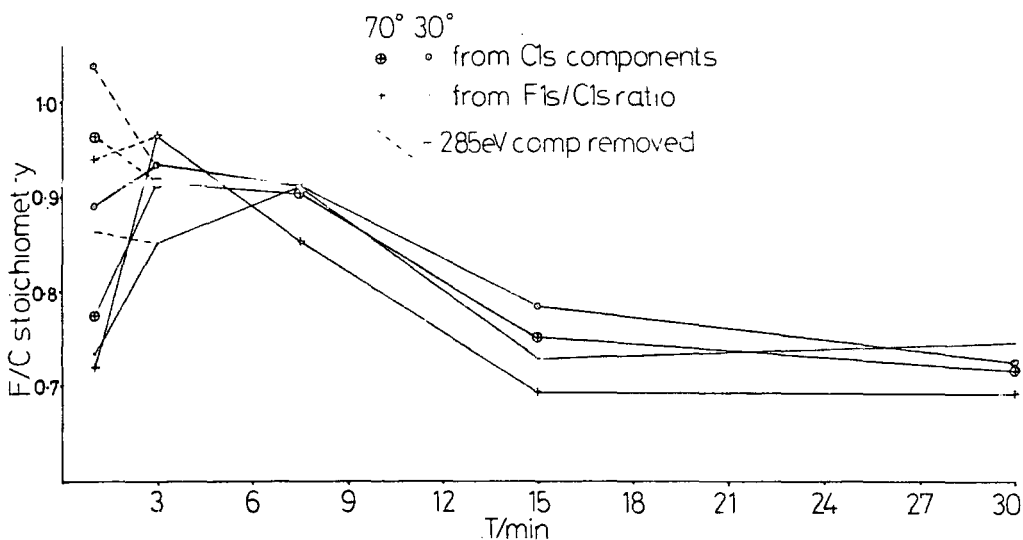


Figure 5.13 Effect of bombardment time on measured stoichiometry

The component data may be grouped together to give contributions arising from \underline{C} , \underline{CF} , \underline{CF}_2 and \underline{CF}_3 functionalities and these data are displayed in Fig. 5.14.

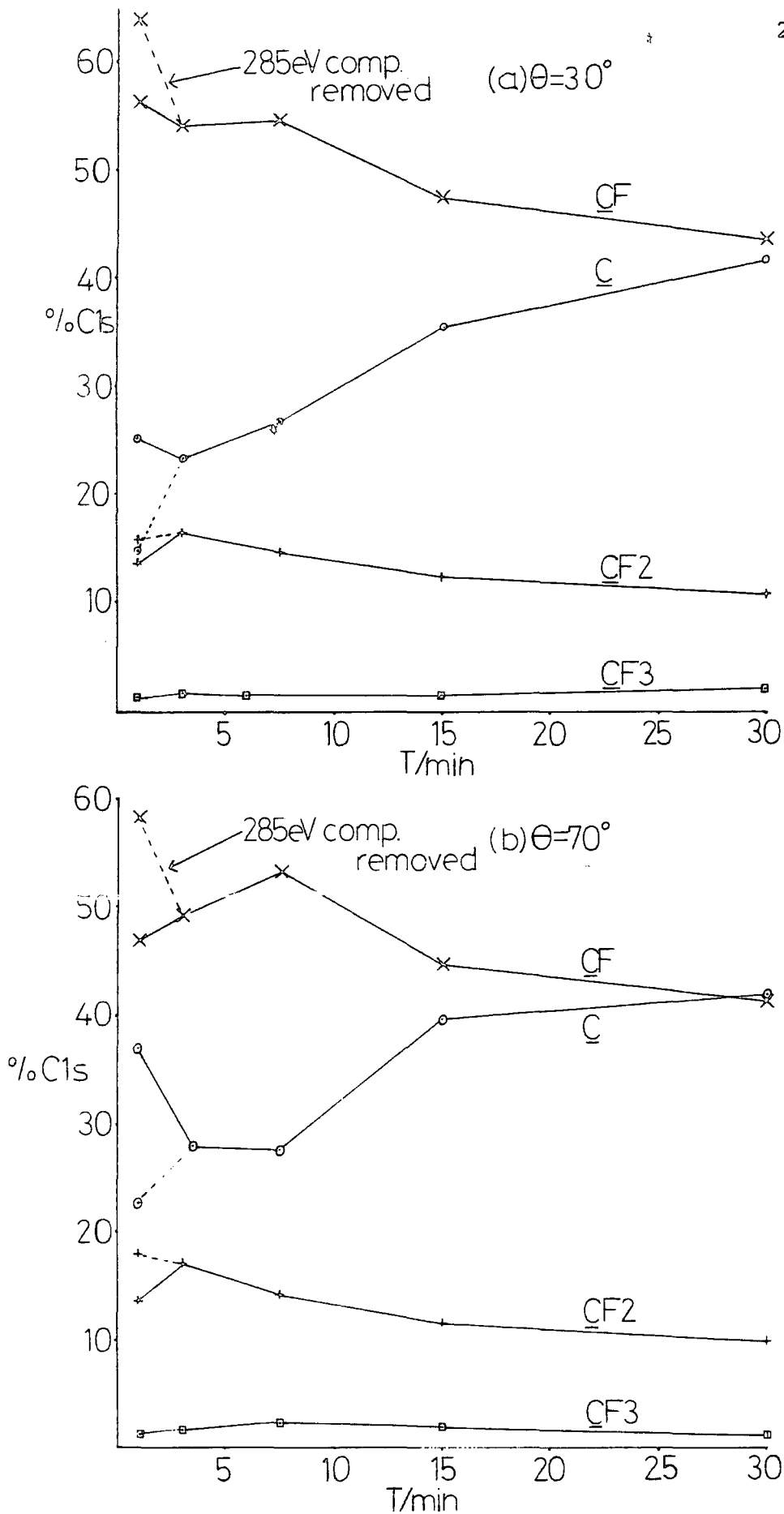


Figure 5.14 Effect of bombardment time on component contributions to C_{1s} spectra (a) 30° and (b) 70°

It may be seen from Fig.5.14 that there is an initial formation of $\underline{\text{CF}}_2$ and $\underline{\text{CH}}$ groups with a concomitant decrease in $\underline{\text{CF}}$ up until a treatment time of 3 minutes. After this $\underline{\text{CF}}_2$ functionalities show a decreasing signal.

The initial formation of $\underline{\text{CF}}_2$ functionalities is evidence for significant molecular rearrangement. The $\underline{\text{C}}$ peaks contribute about the same as the $\underline{\text{CF}}_2$ after 1 min. treatment time, and the overall stoichiometry is about the same as the starting material. The $\pi \rightarrow \pi^*$ peak has also decreased to some extent. Initially therefore fluorine migration accompanied by chain formation is occurring. From the available data the linkages could be between any one of the $\underline{\text{C}}$, $\underline{\text{CF}}$ or $\underline{\text{CF}}_2$ groups. There is also an initial formation of $\underline{\text{CF}}_3$ groups but to a much smaller extent than $\underline{\text{CF}}_2$ functionalities.

After 1 minute bombardment time there is still conversion of $\underline{\text{CF}}$ to $\underline{\text{CF}}_2$ groups but at a much slower rate than initially. Eventually a stage is reached where fluorine migration to give $\underline{\text{CF}}_2$ groups will not be feasible because of the lower concentration of $\underline{\text{CF}}$. Under the constant bombardment of the beam, however, defluorination is occurring from both $\underline{\text{CF}}_2$ and $\underline{\text{CF}}$ groups but, as Fig.5.14 indicates, defluorination of $\underline{\text{CF}}_2$ groups to $\underline{\text{CF}}$ functionalities between 3 and 7.5 min. bombardment time cancels the effect of $\underline{\text{CF}}$ defluorination, since the % of $\underline{\text{CF}}_2$ functionalities decreases whilst the $\underline{\text{CF}}$ component remains virtually constant and the amount of carbon not bonded to fluorine increases.

Prolonged treatment time (*i.e.* 15-30 minutes) causes the fluorine loss to continue, evident by the drop off in the $\underline{\text{CF}}$

peak contribution and the increase of C type carbon.

Thus initial polymerisation is achieved in ~ 1 minute and thereafter a combination of beam effects occur with defluorination predominating which would ultimately lead to a defluorinated carbonaceous network similar to that envisaged to occur in the electron beam irradiation of PTFE and PVF₂ discussed in Chapter Four. Plasma polymerisation is also thought²⁹⁸ to occur *via* competing processes of polymerisation and ablation. Although a study of chemical composition of films prepared from hexafluorobenzene²²⁰ at various r.f. powers did reveal an inverse relationship between fluorine content and power the films were found to have stoichiometries of between C₁F₁ and C₁F_{0.89} *i.e.* a smaller range than that observed in the electron beam process.

The similarity of films produced by electron beam, ion beam and plasma processes points to a common polymerisation mechanism, which probably involves initiation by low energy electrons, since these are present in all three treatments.

It is worthwhile to estimate the average yield, in terms of chemical events, per primary electron bombarding the condensed hexafluorobenzene. To achieve this some measure of the number of chemical events per molecule is needed, and an estimate may be given by changes in the C_{1s} envelope. For example at 30° take-off angle and one minute treatment time the features corresponding to CF:C:CF₂ functionalities are in the ratio 4:1:1. Thus each molecule may be assumed to have undergone at least 2 events, since originally 6 CF groups are present in the starting material.

The total number of events may be calculated by consideration of the number of molecules which are being investigated by ESCA examination. This calculation is straightforward since the number of molecules present in a layer of thickness d , area A , density ρ is given by

$$NL = \frac{\rho}{M} \times A \times d \times N,$$

where N is Avogadro's number and M is the molecular weight. Taking ρ as $\sim 1.61 \text{ g cm}^{-3}$ and d as the effective sampling depth at angle θ , then the total number of events is given by

$$\begin{aligned} NE &= \frac{\rho}{M} \times A \times 3\lambda \cos\theta \times N. \times 2 \\ &= 1.893 \times 10^{15} \end{aligned}$$

The dose *viz* $4\mu\text{A}$ over $\sim 1 \text{ cm}^2$ for one minute corresponds to 1.5×10^{14} electrons bombarding the target hence the yield at 1 min. bombardment time is ~ 25 events per primary electron. A similar calculation for the 70° spectra gives a yield of ~ 12 events per primary electron. So the electron beam clearly initiates a whole series of events whose nature is at present uncertain. The large difference between the values obtained at 30° and 70° is understandable considering the large mean free path of the impinging electrons compared to the sampling depth. Assuming a mean free path of $\sim 30\text{\AA}$ for 2keV electrons then the total proportion of electrons passing through the layer corresponding to 70° take-off angle sampling depth with no energy loss is given by

$$N_{el} = \exp\left(\frac{-14.6}{30}\right) = 0.619.$$

The implication of this figure is that $\sim 38\%$ of the original beam flux has undergone energy loss on passage through the layer

effectively observed at 70° take-off angle. A yield may therefore be constructed corresponding to the number of events caused by electrons which have undergone energy loss, and its value at 70° is 32. A corresponding yield for the 30° take-off angle is 36.

Similar values for the spectra after 3 minutes are 15 and 13 for 30° and 70° spectra respectively.

It is clear from these values that an electron beam is a very efficient chemical initiator. The large yields obtained are indicative of the complex series of events occurring. The lower yield values obtained for the 70° spectra may be indicative of the role of secondary electrons in the polymerisation process. At the 30° C_{1s} sampling depth less secondary electrons, produced by ionisation caused by the primaries, will be able to leave the surface without themselves causing further ionisation or excitation events to take place. This assumes that the number of secondaries produced is constant over the 30° and 70° sampling depths. This is not unreasonable since (i) secondary electron emission studies of polymers indicate that the number of secondaries produced at a depth x is independent of x ,¹²⁴ (ii) semi-empirical theories of secondary electron emission are based on the assumption that the depth dependence of secondary production is proportional to the rate of energy loss of the primary.¹⁶³ The stopping power of polystyrene for 2keV electrons is about 0.827eV \AA^{-1} *i.e.* constant over a 36\AA distance.¹⁶⁷

As mentioned earlier, the role of secondary electrons in electron beam polymerisation has previously been reported,²⁷³ as has the observation that electron energies as low as 6eV could initiate a gas phase polymerisation process.²⁷⁴

Low energy electrons are also the initiating agent in the plasma polymerisation process, and it is worthy of note that the initial (*i.e.* 1 min. treatment time) electron beam polymer is the nearest to the plasma polymers of hexafluorobenzene in terms of stoichiometry (when the effects of extraneous H/C are taken into account), indicating similarity in their respective formation processes.

As was the case in electron beam bombardment of solid polymer surfaces the internal secondary electron distribution increases with lowering electron energy.^{110,122} The nature of the initiation process is not certain, however electron attachment, excitation and ionisation are probable. Consideration of typical cross sections and the internal electron distribution¹³¹ gives a likely ordering of the occurrence of such processes as: attachment >> excitation > ionisation although such an ordering is necessarily speculative. Electron attachment negative ion states of hexafluorobenzene for electron energies 0 to 3eV have been studied in detail by Christophorou and coworkers¹⁴⁴ with states observed corresponding to the attached electron occupying one of the three antibonding π molecular orbitals of hexafluorobenzene. Lifetimes of such states are estimated to be between 10^{-9} s and 10^{-6} s. An E.s.r. study of γ radiolysis of hexafluorobenzene²⁷⁵ has also indicated the presence of anionic $C_6F_6^-$. The fate of such negative ions may be detachment of fluoride ions leaving a pentafluorophenyl radical or electron loss leaving the molecule in an excited state.

Electron impact excitation studies of the fluorobenzenes have been carried out by Kuppermann²⁹⁹ and coworkers where various states with energies between 4-8eV have been found.

Such excited states, formed either by decay of an electron attached species or by direct electron excitation possess enough energy to undergo rearrangement reactions *via* structural isomers such as fulvenes, Dewar benzenes, benzvalenes and prismanes.

Polymerisation of benzene *via* fulvenes and hexadienyne is thought to occur under u.v. irradiation and such a route in the present case would yield 1 $\underline{\text{C}}\text{F}_2$ group per 6 carbon atoms which is close to that derived from the C_{1s} envelope. Involvement of these two species would also account for the retention of $\pi \rightarrow \pi^*$ shake-up peaks observed in the electron beam polymers. After the initial polymerisation process the polymer is susceptible to radiation damage evidenced by the decrease in fluorine content of the films for greater bombardment times.

Eventually a carbonaceous network would be given more akin to the films formed in early studies outlined in the introduction to this chapter where doses used tended to be of the order of mA rather than μA .

CHAPTER SIX

AN MNDO SCF MO INVESTIGATION OF SOME
STRUCTURAL ISOMERS OF THE PERFLUORO DIAZINES
(PYRIMIDINE, PYRAZINE AND PYRIDAZINE)
OF RELEVANCE TO THEIR PLASMA POLYMERIZATION

6.1 Introduction

The formation of thin films by electron beam bombardment of the fluorobenzenes reported in Chapter Five gave polymers whose structural features as determined by ESCA resemble those of films produced by the plasma polymerisation²¹⁷⁻²²¹ of these compounds. In addition the argon ion beam bombardment²⁰³ of condensed perfluorobenzene has also been shown to give structurally similar polymers. All three processes are copious sources of low energy electrons whose role is probably initiation of the polymerisation process by either electron attachment, excitation or ionisation of the 'monomer'. Therefore structural features in ion beam-, electron beam- or plasma-polymers are closely related for a given 'monomer' system.

The acquisition of structural data for electron beam- (and ion beam) produced polymers is however in its initial stages and at present variation of formation parameters involves time consuming experiments. The investigation of structural features and rates of formation of plasma polymers by means of ESCA involves relatively quick experiments in comparison. It is also over seven years since a programme was instigated in Durham with the specific task of amassing such data for a variety of systems. Thus in a series of papers²¹⁵⁻²²⁴ the investigation of the major structural features and rates of formation of plasma polymers produced from the excitation of low power "cool" plasmas in a range of alkenes,^{215,216} aromatics,²¹⁷⁻²²¹ heterocyclic,²²² heteroaromatic^{223,224} and alicyclic²²⁶ "monomers" has been reported. In the particular case of the benzenes for the more highly fluorinated members the overall C:F stoichiometry of the plasma polymers has been found to be essentially

the same as for the starting monomers. For the isomeric tetrafluorobenzenes²¹⁹ the component structural features elaborated by means of ESCA provide evidence of substantial rearrangement, however, the gross structure and the rates of deposition are essentially the same for all 3 isomers and this has been taken as evidence of their interconversion during the plasma process. The contrast with fluorinated alkenes where the structure but not the composition depends strikingly on the substitution pattern, as does the rate of deposition is interesting since in the alkene series elimination seems to be a dominant route compared with rearrangement. MNDO SCF computations²¹⁹ on valence isomers of the tetrafluorobenzenes indicates facile routes for ring scrambling dominantly *via* the prismane and benzvalene manifolds whilst elimination leading to benzyne type intermediates is energetically much more expensive. Evidence in the literature on plasma processing of substituted benzenes has provided *prima facie* evidence for ring scrambling²²⁷ since it is possible to recover positional isomers from the material passing through the reactor under the appropriate conditions. The nature of the rearranged plasma polymer has suggested the importance of reactions at the substrate-plasma interface arising from the fulvene²²⁷ ring structure and indeed the SCF MO computations show that in the neutral, cation and excited state manifolds the fulvene structure is the closest in energy to the parent benzenoid system.

The well known influence on the chemistry of fluorinated systems consequent upon substitution of ring carbon for nitrogen²²⁸ extends also to the plasma polymers which may be made from nitrogen heterocycle analogues of the fluorobenzenes. It has

recently been shown²²⁵ that the rates of plasma polymer formation are distinctively different for the isomeric perfluorodiazines suggesting that equilibration and ring scrambling is of less importance for this series than for the homocyclic analogues. It is also known experimentally that introduction of ring nitrogens strongly influences the relative energies of the various valence tautomers of the heterocyclic systems.²²⁹⁻²³¹ Thus relatively stable benzvalene, prismane and Dewar benzene analogues are known in the perfluoroalkylated diazine systems.

In this chapter some aspects of the relative energetics of the neutral and cationic species of the isomeric perfluorodiazines are considered. For comparison purposes consideration has been given to acyclic as well as heterocyclic structures; the emphasis being on the potential explanation of differences in plasma behaviour with respect to the corresponding benzenes, but which may be equally well applied to the electron beam polymerisation of both sets of compounds.

6.2 Computational Details

Geometry optimisations of the ground states of all the species in Figure 6.1 have been performed using the MNDO method²³² incorporating the DFP optimisation routine.²³³ Initial geometries were estimated from standard bond lengths and angles²¹² where possible.

Single SCF calculations using the optimised ground state geometries were carried out for the cation, first excited singlet and first excited triplet states for one of each of the isomers containing nitrogens at 1,3 positions.

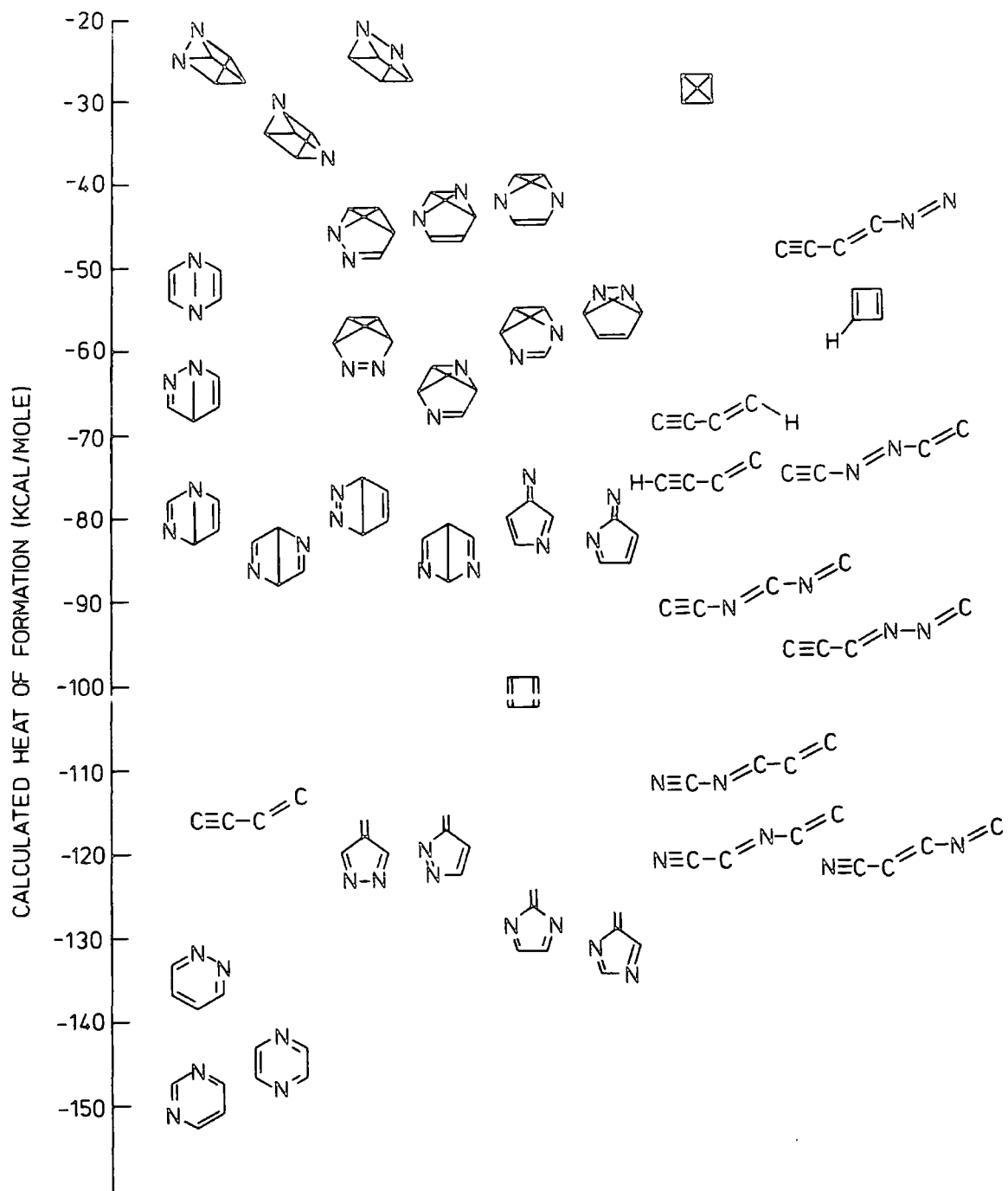


Figure 6.1 Heats of formation of the perfluorodiazines, some of their structural isomers and related compounds

The calculations were carried out on a CDC7600 at UMRCC. Typically the C.P.U. time for a complete geometry optimisation was about 300 seconds. Full details of the optimised geometries are not essential to the discussion presented but salient features will be pointed out.

6.3 Results and Discussion

6.3.1 Ground States

It is convenient in discussing the data to consider briefly the overall energetics (and where appropriate comments on the geometries) for each of the aza substituted isomers of a given structural type.

(i) Parent perfluoro heteroaromatics

Although there have been a number of theoretical studies at a variety of levels of sophistication of the parent ring systems of pyrazine, pyrimidine and pyridazine^{232,300} there have been no previous studies of the relative energies for the geometry optimised perfluorinated derivatives. For the hydro series the relative heats of formation fall in the order 1,4 \approx 1,3 > 1,2 diazine, the pyrimidine (1,3) and pyrazine (1,4) being the more stable by \approx 20 kcal/mole.²⁹⁶ The data displayed in Figure 6.1 indicate a relative stabilizing effect of fluorine substitution (with respect to the pyrimidine) for the pyridazine and a relative destabilizing effect for the pyrazine; the predicted stability order therefore being pyrimidine > pyrazine > pyridazine.

As expected the optimised geometries give planar

systems in all three cases; the computed bond lengths in each case closely following those that might have been anticipated on the basis of tables of standard bond lengths.²¹²

(ii) Diazafulvenes

For fluorinated benzenes the valence isomer closest in energy terms to the planar aromatic system is that appropriate to the fulvene structure.²¹⁹ In the particular case of the tetrafluorofulvenes MNDO SCF MO computations indicate that the various possible isomers have closely similar energies.²¹⁹ In this respect the introduction of nitrogens into the system provides a striking contrast. In this study we have investigated 6 of the possible diazafulvenes and the results are displayed in Figure 6.1. It is clear from this that structures involving N-F bonds are thermodynamically unstable with respect to isomers having nitrogen as part of the five membered ring system; the energetic preference typically being ~ 40 -50 kcal/mole. For structures involving ring nitrogen there is again a small energetic preference for the 1,3 disposition.

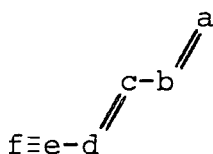
The optimised structures were planar with C-C and C=C bond lengths where appropriate of $\sim 1.49\text{\AA}$ and 1.37\AA indicating a degree of conjugation in these isomers.

(iii) Diazadienynes

A previous investigation of isomers of the tetrafluorobenzenes²¹⁹ indicated that fluorodienynes were at higher energy than the fulvene valence isomers but lower in energy than the Dewar benzene, prismane and benzvalene isomers. The data in Figure 6.1 reveal that the energies of the diazadienynes are strongly dependent on the position of nitrogen substitution with

particular preference being for structures encompassing $-C\equiv N$. By contrast the structure involving N-F bonds is destabilized whilst structures involving N-N bonds also tend to be relatively unfavourable. The net effect is that for the isomers involving the thermodynamically favourable $-C\equiv N$ group the energies are comparable with those for the most favourable fulvene structures.

The most interesting feature arising from the optimisation of these isomers is the non-planarity of 3 of the 7 structures considered. The relevant twist angle, $abcd$ (180° in the planar isomers) was found to be $\sim 147^\circ$ when b and f are nitrogen, and $\sim 40^\circ$ when either b and d or d and f are nitrogen.



Heats of formation calculated for five values of this twist angle indicate that there is a balance of two main factors. The loss of conjugation energy caused by deviation from planarity, is balanced by a decrease in repulsive interaction of non-bonded atoms, predominantly fluorine-fluorine and nitrogen-fluorine. A plot of these interactions and the variation of heat of formation with twist angle is shown for one of the isomers in Figure 6.2. In this case a twist angle of 180° is clearly unfavourable since the F-F interatomic distance is only 2.58\AA , significantly lower than twice the crystallographically determined Van der Waal's radius for F_2 ($1.5 - 1.6\text{\AA}$). However, the potentially favourable conformation, in terms of F-F interactions and conjugative stabilisation, with zero twist angle, involves an N-F distance of 2.78\AA , again, lower than would be expected from Van der Waal's radii. Thus the twist angle of

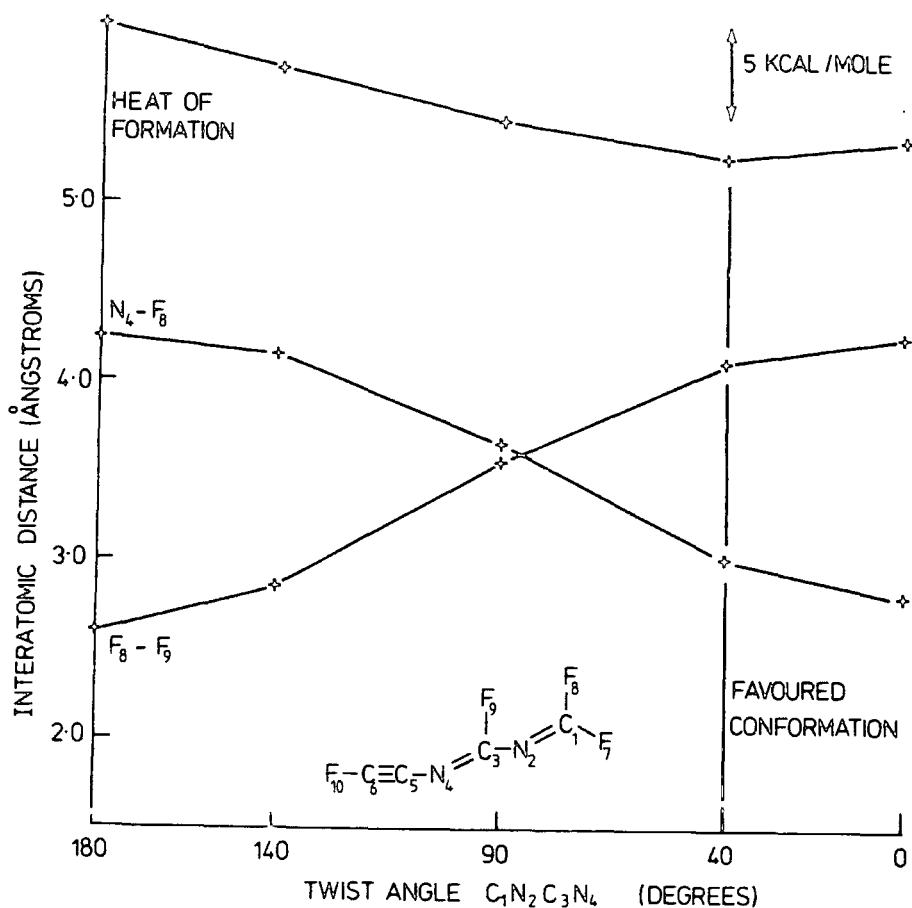
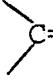


Figure 6.2 Effect of varying twist angle in a hexadienyne system

40° in the fully optimised geometry can be rationalised, since the N-F interatomic distance is 3.02\AA , the F-F distance is still favourable, and the conjugation energy is not significantly decreased.

(iv) Diaza Dewar benzenes

In the tetrafluorobenzene series the valence isomers next in energy after the hexadienyne are the Dewar benzenes.²¹⁹ As might have been anticipated whilst the various positional isomers for the tetrafluoro derivative span a very small energy range, the introduction of the nitrogen substituents has a sub-

stantial influence on the overall pattern. Structures involving C=N tend to be energetically favourable with respect to those which involve nitrogen in a bridgehead position. It is interesting to note that there is again a preference for structures involving nitrogen in a 1,3 disposition with respect to those involving a 1,2 arrangement, however, the preference is small. For the most favourable cases the total span in energy for 1,2, 1,3 and 1,4 substitution patterns is only 6 kcal/mole which is substantially less than for the heteroaromatic ring systems themselves.

The optimised structures for the Dewar benzenes have an average carbon-carbon bridgehead bond length of $\sim 1.64\text{\AA}$ which seems large until compared with the experimentally determined value of 1.63\AA for the hexamethyl Dewar benzene.²⁷⁶ The dihedral angle in these systems is also close to the experimental value of 117.7° .³⁰¹

(v) Diazabenzvalenes

Seven positional isomers have been studied and their heats of formation are shown in Figure 6.1. A straightforward correlation between the positions of nitrogen substitution and the heats of formation is not apparent, though there appears to be preference for nitrogen at the bridgehead position joining the two cyclopropyl rings, the bond angles of about 60° at this strained position being less unfavourable to nitrogen where lone-pair-bond pair repulsions are involved, rather than the bond pair-bond pair repulsions of a C-F unit.

The range spanned by these nitrogen substituted isomers is again greater than the tetrafluorobenzvalene analogues.

In all the isomers the C-C or C-N bond common to the two cyclopropyl rings is shorter than the others involved in the bicyclobutyl ring system overall. This was also found for the tetrafluorobenzvalenes, but of course contrasts with the result for bicyclobutane itself. The dihedral angle of the bicyclobutyl ring was found to increase with increasing nitrogen substitution of that ring, which reflects the increasing bond lengths along the series N=N, C=N, C=C, involved in the "pendant group".

(vi) Diazaprismanes

The 1,3 substituted isomer is again energetically preferred by ~ 9 kcal/mole. This again emphasises the fact that a ring nitrogen substituent gives rise to a greater spread in energies for a given structural isomer than fluorine substitution.

The optimised structures for the prismanes indicate a highly strained system with all interatomic distances corresponding to regular single bonds.

(vii) Summary

Although there is a spread in the heats of formation for each isomer, the general trend of parent < Dewar benzene < benzvalene < prismane is the same as that observed experimentally for the hexamethyl³⁰² and perfluoromethyl³⁰³ homocyclic analogues, and observed in various theoretical treatments of the parent benzene isomers.^{304,300(d)} This ordering was also found for the MNDO study of the tetrafluorobenzenes²¹⁹ in which the difference between the most and least stable isomers was ~ 100 kcal/mole compared to ~ 125 kcal/mole in the present investigation. Relative to the parent aromatic systems the diaza Dewar benzenes

and benzvalenes are destabilised by ~ 10 kcal/mole compared to the tetrafluorobenzene series, whilst for the prismanes the destabilisation is ~ 20 kcal/mole. However, the heats of formation of the diazafulvene isomers show a slight stabilisation compared to the tetrafluorofulvenes. The greatest difference between the results of Figure 6.1 and the tetrafluorobenzenes is the large range of energies spanned by the diazahexadienyne, the origin of which was discussed in section (iii).

6.3.2 Excited States

(i) Cations

First ionisation potentials calculated by Koopmans' Theorem,²⁵ hence corresponding to a 'frozen' final state, for the heteroaromatic systems tend to be over estimated by about 0.4 eV compared to experimentally determined UPS values.³⁰⁵ Heats of formation have been calculated for the 1,3 isomers in the cation manifold using ground state optimised geometries which for the perfluoro-pyrimidine gives a Δ SCF relaxation energy of 0.3 eV. The data displayed in Figure 6.3 show that although the ordering is the same as for the neutral species, the energy separation between the isomers is different. In particular, the fulvene is stabilised with respect to the heteroaromatic system compared to the ground state manifold. This observation is consistent with UPS data for homocyclic benzene and fulvene³⁰⁶ where the ionisation potential of fulvene is ~ 0.7 eV lower than benzene, indicating an increased stability of fulvene in the cation manifold.

Of the other isomers whilst the prismane, Dewar benzene and benzvalene are destabilised by about 25 kcal/mole by cation

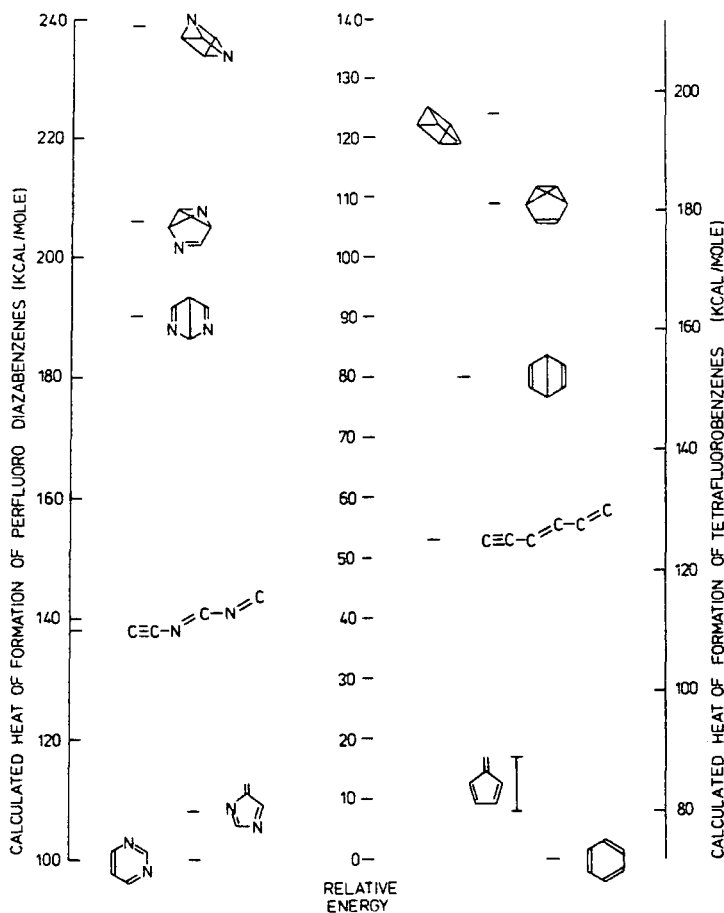


Figure 6.3 Heats of formation of the cations of the perfluoro 1,3-diazabenzene and some of the tetrafluorobenzene structural isomers

formation, the hexadienyne, significantly, is stabilised by 18 kcal/mole, with respect to the parent. It is interesting to compare these results with those for the tetrafluorobenzene analogues (Figure 6.3) where the cation heats of formation calculated by Koopmans' Theorem show destabilisation of ~25 kcal/mole for prismane and benzvalene cations, ~16 kcal/mole for the Dewar isomer and no significant change for the hexadienyne, compared with the parent. The stabilisation for the fulvene system is comparable with that noted above for the heterocyclic system.

(ii) Singlet and triplet states

First excited singlet and triplet state heats of formation were calculated for the same 1,3 isomers as were investigated in the cation manifold, and the results are shown in Figure 6.4. Singlet-triplet splittings of about 50 kcal/mole

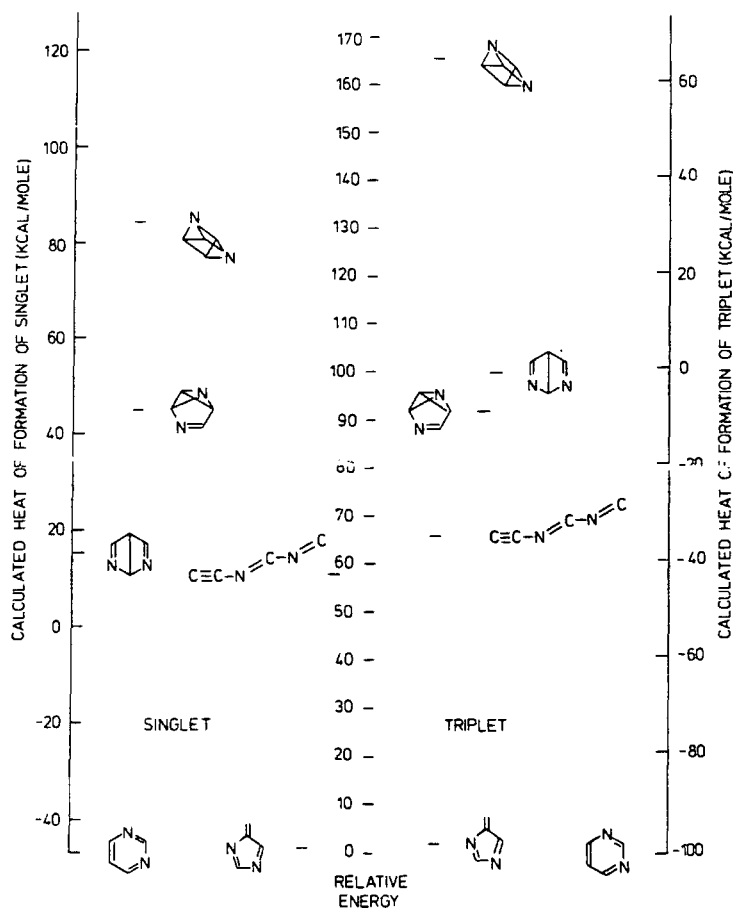


Figure 6.4 The heats of formation of the singlet and triplet excited states of the perfluoro 1,3-diazabenzene isomers

and wave function analysis for the two singly occupied MO's indicate that the MNDO SCF procedure has locked onto a $\pi \rightarrow \pi^*$ configuration for the aromatic, fulvene, hexadienyne and benzvalene isomers. In contrast for the prismane and Dewar benzene the lower singlet-triplet splitting and σ - π inseparability means

that the nature of the excited state cannot be assigned in a clear cut manner. The singlet and triplet $\pi\pi^*$ states of perfluoropyrimidine are calculated to be 4.45 and 2.07 eV above the ground state respectively. The experimentally observed band maximum for the $\pi\rightarrow\pi^*$ transition involving singlet states is at 241 nm³⁰⁷ corresponding to an energy separation of 5.14 eV, in tolerable agreement with that calculated theoretically.

The calculation on perhydropyrimidine again gives the first excited singlet as $^1\pi\pi^*$ whereas it is well known to be $^1n\pi^*$.³⁰⁸ Similarly MNDO predicts the first triplet to be $^3\pi\pi^*$, some 2.7 eV above the ground state, whereas the first triplet is known to be $^3n\pi^*$ at 3.6 eV,³⁰⁹ with the $^3\pi\pi^*$ being some 0.1 - 0.2 eV higher still.³¹⁰

The benzvalene is found to be slightly destabilised with respect to the heteroaromatic (~ 8 kcal/mole) in both singlet and triplet manifolds. The hexadienyne is similarly destabilised in the triplet state, but in the singlet its relative energy is the same as that in the ground state. Thus these two isomers are useful markers by which to identify the relative changes in energy of the others. The major difference between the ground and excited state manifolds is the stabilisation (by 15-20 kcal/mole) of the fulvene isomer with respect to the heteroaromatic, in both the singlet and triplet states, bringing it to within 2 kcal/mole in the latter case, *i.e.* certainly within the error limits of MNDO.²³² The Dewar benzene on the other hand, whilst having the same relative energy in the ground and singlet states, is considerably destabilised in the triplet state (~ 35 kcal/mole), so that its energy becomes comparable with that of benzvalene.

The prismane is destabilised in both excited states, but the effect is much greater in the triplet (~ 49 kcal/mole) than in the singlet (~ 14 kcal/mole).

Thus the overall pattern in the excited states is a destabilisation of the prismane and a stabilisation of the fulvene structures, whilst the other isomers are relatively unchanged.

6.3.3 Application to Plasma Polymerisation of these Compounds

The object of these calculations is to attempt to rationalise experimental data obtained on the structure and composition of plasma polymers obtained from the isomeric perfluorodiazines in comparison with the isomeric tetrafluorobenzenes.

It is important to consider that the electron energy distribution in a cool plasma is typically Maxwellian³¹¹ with an average electron energy of ~ 2 eV and a tail extending beyond the ionisation potential of these systems. The electron flux will interact with the monomer flux in three primary ways giving rise to electron attachment, excitation and ionisation. From the typical distribution pattern of electron energies the typical electron flux involved in each of these 3 processes is approximately in the ratio 60:40:0.4²¹⁹ respectively. However, for purposes of comparison we will consider only the ground state manifold in our discussion of the relative energetics of the perfluorodiaza- (Figure 6.1) and tetrafluorobenzene (Figure 6.5) isomers relevant to the plasma polymerisation of these compounds.

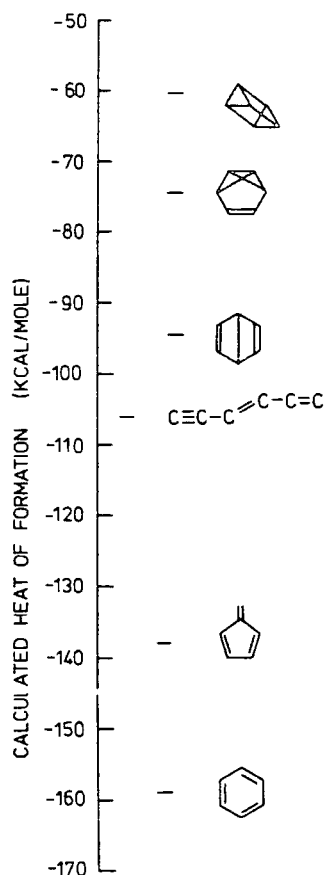


Figure 6.5 The heats of formation of some of the tetrafluorobenzene structural isomers²¹⁹

6.3.3 (i) Interconversion of parent isomers

Table 6.1 details the energetics of the most favourable routes of interconversion between the parent isomers,³¹² shown schematically in Fig.6.6. The value of ΔH_{eb} is simply the difference between the calculated heats of formation of the starting compound and the least stable isomer involved in the conversion. Similarly ΔH_R is the energy separation of the initial and final isomers thus, a

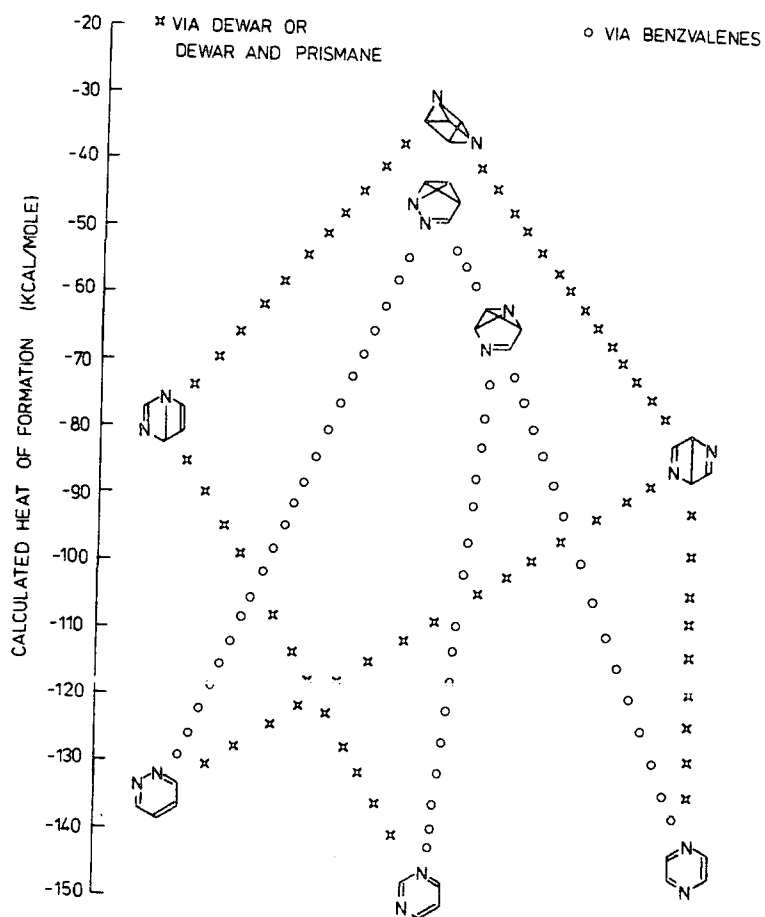


Figure 6.6 Energetically most favourable routes of parent isomerisation

TABLE 6.1 Energetics of Parent Isomerisation (kcal/mole)

TETRAFLUOROBENZENES		ΔH_{eb}	ΔH_{R}
<i>via</i>	Dewar	+ 64.5	0
<i>via</i>	Dewar and prismane	+ 98.5	0
<i>via</i>	Benzvalene	+ 84.5	0
DIAZABENZENES		ΔH_{eb}	ΔH_{R}
1,2 - 1,3	<i>via</i> Dewar and prismane	+103	-14
	<i>via</i> Benzvalene	+ 89	-14
1,2 - 1,4	<i>via</i> Dewar	+ 51	-10
	<i>via</i> Benzvalene	+ 89	-10
1,3 - 1,4	<i>via</i> Dewar and prismane	+117	+ 4
	<i>via</i> Benzvalene	+ 91	+ 4

value of ΔH_{eb} for the reverse process is formed from ΔH_{eb} (forward) - ΔH_{R} . Comparison with the tetrafluorobenzene data is facilitated by taking an average of the ΔH_{eb} values for the forward and reverse processes of the diaza series. This indicates that the interconversion of the parent isomers *via* the prismane (which also involves Dewar benzene intermediates) is approximately 14 kcal/mole less favourable for the diaza-compounds, compared with the corresponding tetrafluorobenzene positional isomerisation. Similarly, interconversion involving just benzvalenes is of the order of 10 kcal/mole less favourable. The 1,2 - 1,4 diaza transformation, the only one to involve Dewar benzenes alone, is seen to be more facile (~ 10 kcal/mole) than the equivalent process in the homocyclic series, a result which is not surprising when one considers the large body of literature

concerning the mechanism of this process for the diazabenzene case.²²⁸ Thus in general formation of isomers which would be expected to be involved in ring scrambling is energetically more favourable in the case of the tetrafluorobenzene series. However, isomers which are not involved in ring scrambling processes, *viz.* the fulvenes and hexadienyne, are predicted to be formed more easily in the diaza- series as can be seen from the ΔH_R values in Table 6.2, the formation of the diazahexadienyne isomers being more favourable by an average of ~ 20 kcal/mole.

TABLE 6.2 Energetics of Polymer-Precursor Formation (kcal/mole)

TETRAFLUOROBENZENES		ΔH_R
	to fulvene	+21
	to hexadienyne	+53
DIAZABENZENES		ΔH_R
1,2	to fulvene	+15
	to hexadienyne	+39
1,3	to fulvene	+17
	to hexadienyne	+37
1,4	to fulvene	+16
	to hexadienyne	+24

(ii) Polymerisation

Plasma polymerisation has previously been considered to involve cycloaddition of parent and valence isomer systems.²¹⁹ Using this idea our data suggest cycloaddition of the parent isomer with the fulvenes and hexadienyne is comparatively

favourable energetically for the diaza compounds. This is consistent with the experimental observation of substantially higher levels of CF_2 groups present in the perfluorodiaza-benzene plasma polymers than even plasma polymerised perfluorobenzene polymers, since this group only arises from the participation of fulvene and hexadienyne in the cycloaddition reactions. The proximity of the ΔH_{eb} values (about 20 kcal/mole) of the hexadienyne and Dewar benzene/benzvalene isomers in the tetrafluorobenzenes contrasts with the larger separation (about 50 kcal/mole) in the diaza analogues. This supports the experimental evidence concerning the rates of plasma polymerisation since it shows the relative unimportance of interconversion of the diaza-parent isomers in comparison with hexadienyne formation. For the homoaromatics on the other hand the energetics of interconversion are favourable, thus giving rise to similar rates of deposition and structures.

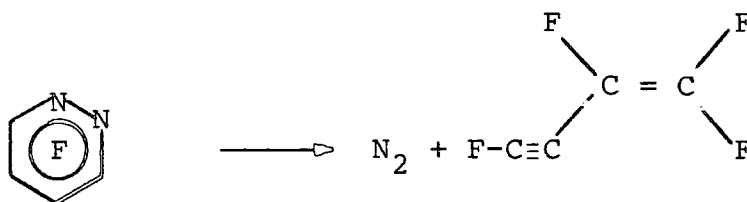
Consideration of the cation manifold gives a similar trend. Fulvene formation especially is greatly eased in both homoaromatic and heteroaromatic systems, but particularly so in the latter case where it is within ~ 3 kcal/mole of the parent.

(iii) Elimination

It is of interest to consider the possibility of the elimination of a small stable molecule from these compounds, since plasma polymerisation of fluoroethylene was shown to be accompanied by elimination of HF. However, in the tetrafluorobenzene case, experiment showed that HF elimination was not significant, a fact interpreted theoretically by the high energy of the resulting benzyne.²¹⁹

On this basis the equivalent elimination (of F_2) has not been considered here. However, the possibility of nitrogen elimination from the diaza series and analogous elimination of acetylene from the tetrafluorobenzenes has been investigated.

Elimination of N_2 from a $C_4N_2F_4$ molecule yields a C_4F_4 fragment for which there are three structural isomers, *viz* the tetrahedrane, the cyclobutadiene and the tetraenyne. The most stable of these is the perfluorotetraenyne (see Figure 6.1). It is readily apparent that pyridazine could eliminate nitrogen without any other rearrangement with a heat of reaction of 27 kcal/mole.



Conversely elimination of N_2 from the 1,3 and 1,4 diazines must occur *via* either a Dewar benzene, prismane or benzvalene thus making N_2 loss as unfavourable as interconversion of the parent systems.

Bulk and surface N/C ratios determined for the plasma polymers of the diazines³¹³ support the prediction of greatest N_2 loss from the 1,2 diazine. By comparison the elimination of a similar stable molecule from the tetrafluorobenzenes yields heats of reactions of ~ 98 kcal/mole for fluoroacetylene and ~ 100 kcal/mole for acetylene.

APPENDIX ONE

PLATES SHOWING THE ES300 SPECTROMETER

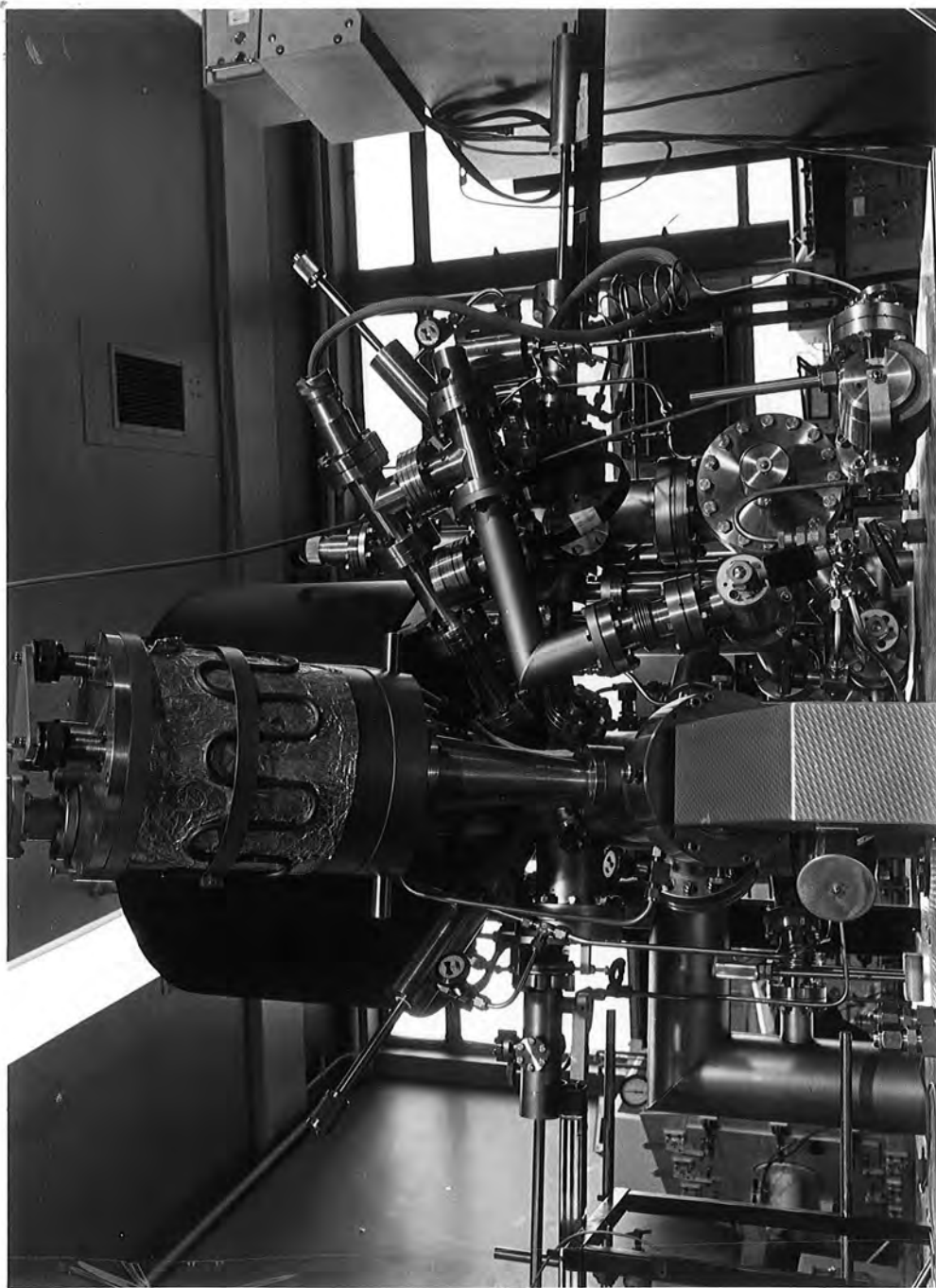
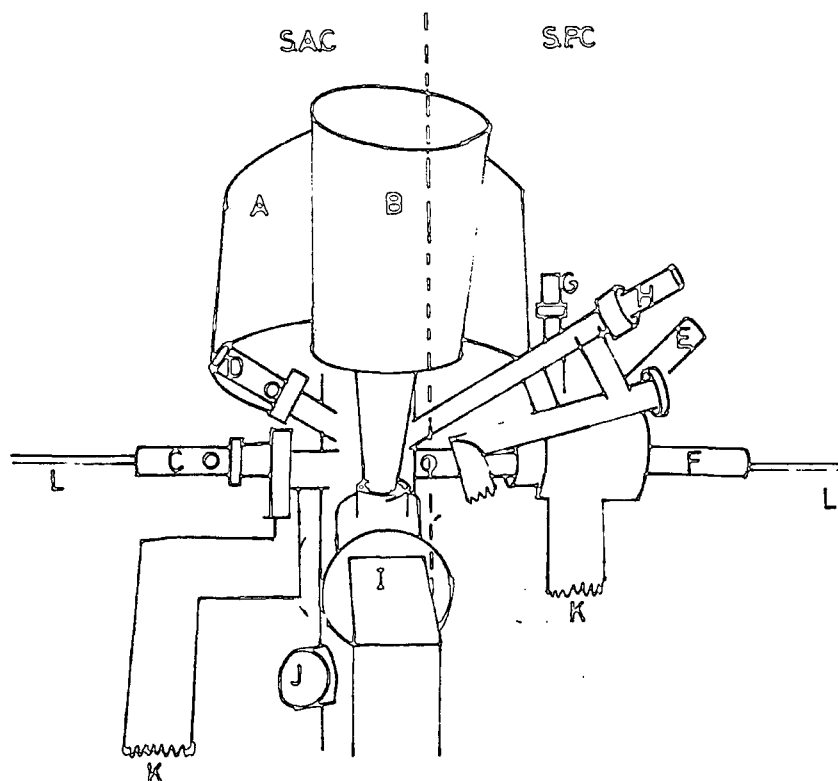


Plate 1.1(a) The ES300 Spectrometer



- A - Analyser
- B - Monochromator
- C - Insertion lock 1
- D - Insertion lock 2
- E - Insertion lock 4
- F - Insertion lock 3
- G - Electron gun
- H - Ion gun
- I - Al X-ray gun
- K - To pumping
- J - Ion gauge

Key to Plate 1.1(a)

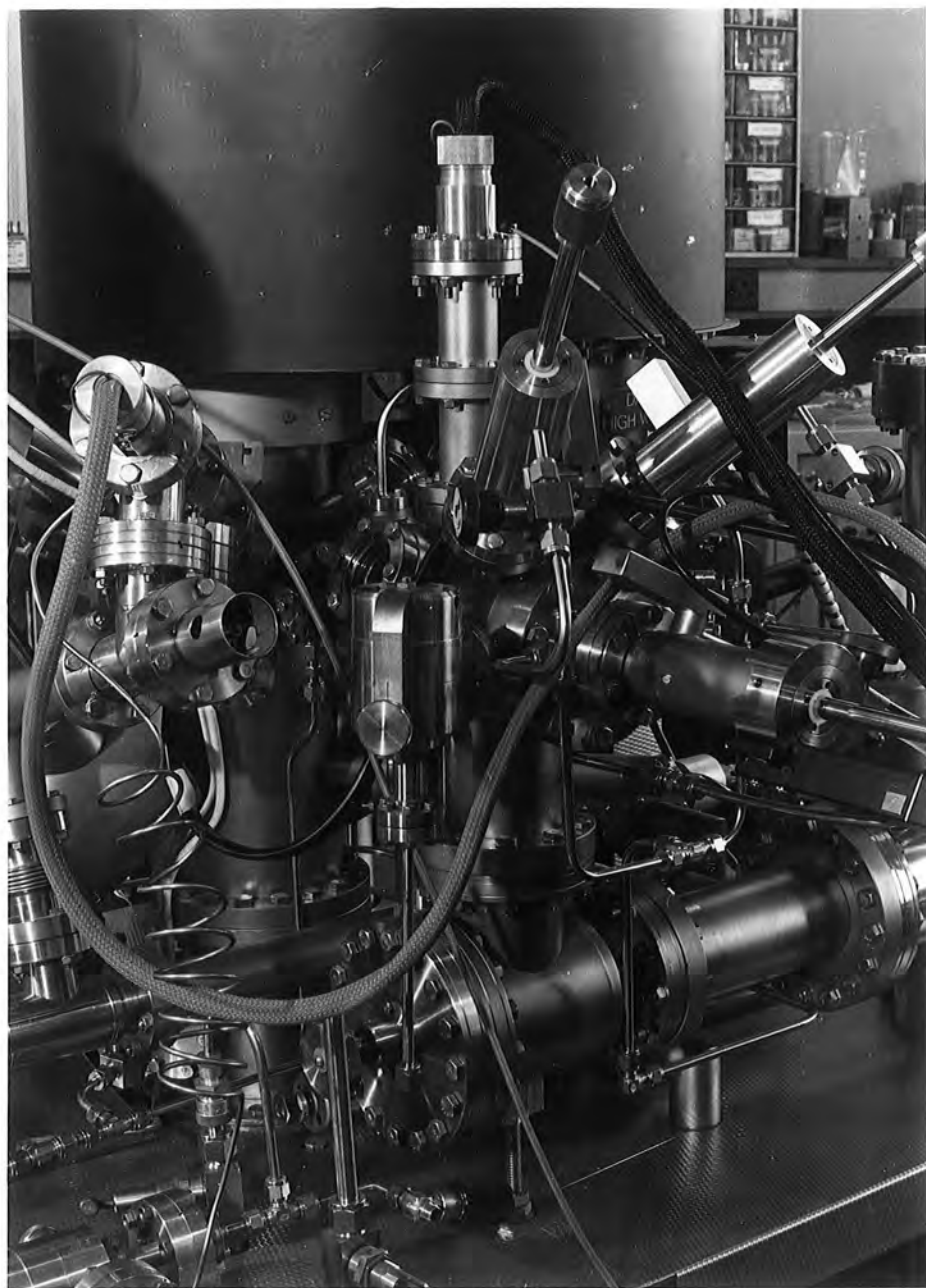
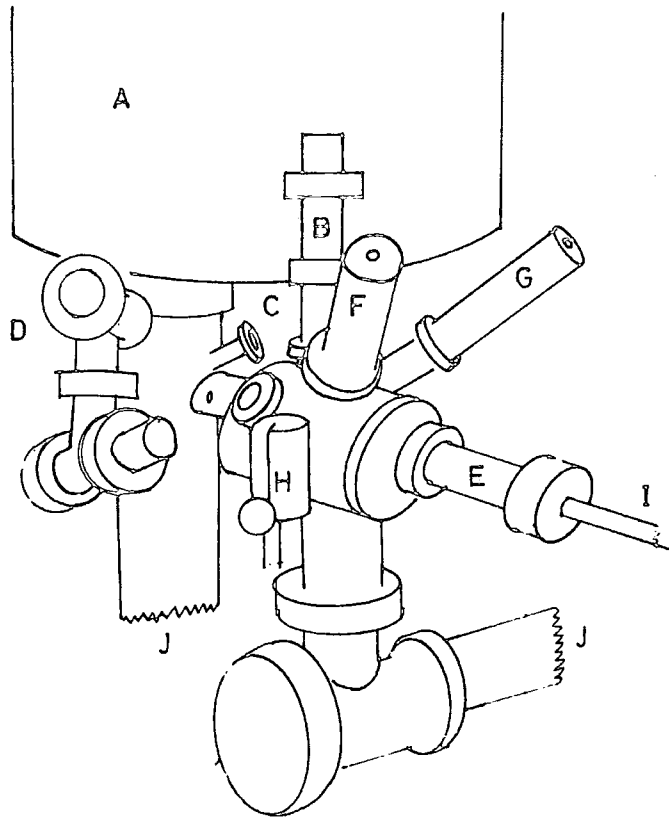


Plate 1.1(b) The sample preparation chamber



- A - Analyser
- B - Electron gun
- C - View ports
- D - Ion gun
- E - Insertion lock 3
- F - Insertion lock 4
- G - Insertion lock 5
- H - Leak valve
- I - Probe
- J - To pumping

Key to Plate 1.1(b)

APPENDIX TWORESEARCH COLLOQUIA, SEMINARS, LECTURES AND CONFERENCES

The Board of Studies in Chemistry requires that each postgraduate research thesis contains an appendix listing all research colloquia, seminars and lectures by external speakers held in the department as well as all conferences attended by the author, during the period of research.

Lectures held October 1980 - July 1983

- Dr. D. Mass (Salford Univ.) - 'Reactions a Go-Go', 16 Oct. 1980.
 Prof. T.M. Sugden (Cambridge Univ.) - 'Chemistry in Flames', 23 Oct. 1980.
 Prof. N. Grassie (Glasgow Univ.) - 'Inflammability Hazards in Commercial Polymers', 30 Oct. 1980.
 Prof. A.G. Sykes (Newcastle Univ.) - 'Metallo-proteins: An Inorganic Chemist's Approach', 6 Nov. 1980.
 Dr. M. Gerloch (Cambridge Univ.) - 'Magnetochemistry is about Chemistry', 12 Nov. 1980.
 Prof. N.N. Greenwood (Leeds Univ.) - "Metalloborane Chemistry", 13 Nov. 1980.
 Dr. T. Gilchrist (Liverpool Univ.) - 'Nitroso-olefins as Synthetic Intermediates', 19 Nov. 1980.
 Rev. R. Lancaster - 'Fireworks', 4 Dec. 1980.
 Dr. R. Evans (Brisbane Univ., Australia) - 'Some Recent Communications to the Editor of the Australian Journal of Failed Chemistry', 18 Dec. 1980.
 Prof. E.A. Dawes (Hull Univ.) - 'Magic and Mystery through the Ages', 22 Jan. 1981.
 Mr. H.J.F. Maclean (I.C.I.Ltd.) - 'Managing in the Chemical Industry in the 1980s', 29 Jan. 1981.
 Prof. F.G.A. Stone (Bristol Univ.) - 'Chemistry of Carbon to Metal Triple Bonds', 5 Feb. 1981.
 Dr. I. Fleming (Cambridge Univ.) - 'Some Uses of Silicon Compounds in Organic Synthesis', 12 Feb. 1981.
 Prof. S. Kettle (Univ. of East Anglia) - 'Variations in the Molecular Dance at the Crystal Ball', 18 Feb. 1981.
 Dr. K. Bowden (Essex Univ.) - 'The Transmission of Polar Effects of Substituents', 25 Feb. 1981.
 Dr. J.F. Stoddart (I.C.I. Ltd.) - - Stereochemical Principles in the Design and Function of Synthetic Molecular Receptors', 11 Mar. 1981.
 Prof. W.P. Jencks (Brandell Univ., Mass) - 'When is an Intermediate not an Intermediate?', 17 Mar. 1981.
 Dr. J.P. Smith (Int. Tin Research Institute) - 'Organotin Compounds - A Versatile Class of Organometallic Compounds', 18 Mar. 1981.
 Dr. W.H. Meyer (RCA, Zurich) - 'Properties of Aligned Polyacetylene' 9 Apr 1981.
 Prof. M. Gordon (Essex Univ.) - 'Do Scientists have to Count?', 7 May 1981.
 Dr. J. Rose (ICI Plastics) - 'New Engineering Plastics', 10 Jun.1981.
 Dr. P. Moreau (Montpellier Univ.) - -Recent Results in Perfluoro-organometallic Chemistry', 17 Jun. 1981.
 Dr. P. Plimmer (Du Pont) - 'From Conception to Commercialization of a Polymer', 21 Sept. 1981.

- Prof. E. Kluk (Univ. of Katowice) - 'Some Aspects of the Study of Molecular Dynamics', 14 Oct. 1981.
- Dr. P.J. Corrish (Dunlop Ltd.) - 'What would Life be like without Rubber?', 22 Oct. 1981.
- Dr. W. Moddeman (Monsanto Ltd.) - 'High Energy Materials' 6 Nov. 1981.
- Prof. A.I. Scott (Edinburgh Univ.) - 'An Organic Chemist's View of Life in the n.m.r. tube', 12 Nov. 1981.
- Dr. W.O. Ord (Northumbrian Water Authority) - 'The Role of the Scientist in a Regional Water Authority', 26 Nov. 1981.
- Dr. R.E. Hester (York Univ.) - 'Spectroscopy with Lasers', 3 Dec. 1981.
- Prof. I. Fells (Newcastle Univ.) - 'Balancing the Energy Equations', 28 Jan. 1982.
- Dr. D. Pethnick (Strathclyde Univ.) - 'Conformational Dynamics of Small and Large Molecules', 10 Feb. 1982.
- Dr. D.W. Turner (Oxford Univ.) - 'Photoelectrons in a Strong Magnetic Field', 17 Feb. 1982.
- Prof. R.K. Harris (Univ. of East Anglia) - 'N.m.r. in the 1980s', 18 Feb. 1982.
- Prof. R.O.C. Norman, FRS (York Univ.) - 'Turning Points and Challenges for the Organic Chemist', 25 Feb. 1982.
- Dr. P. Banfield (I.C.I. Organics) - 'Computer Aided Synthesis Design: A view from Industry', 3 Mar. 1982.
- Dr. R. Whyman (I.C.I. Ltd.) - 'Making Metal Clusters Work', 4 Mar. 1982.
- Prof. D.J. Burton (Iowa Univ.) - 'Some Aspects of the Chemistry of Phosphonium Salts and Phosphates', 28 Jun. 1982.
- Prof. Neidlein (Heidelberg Univ.) - 'New Aspects and Results of Bridged Annulene Chemistry', 13 Sept. 1982.
- Dr. W.K. Ford (Xerox, New York) - 'The Dependence of the Electronic Structure of Polymers on their Molecular Architecture', 27 Sept. 1982.
- Prof. H. Suhr (Univ. of Tübingen) - 'Preparative Chemistry in Non Equilibrium Plasmas', 14 Oct. 1982.
- Mr. F. Shenton (County Analyst, Durham) - 'There is Death in the Pot', 14 Oct. 1982.
- Dr. C.E. Housecroft (Notre Dame Univ.) - 'Bonding Capabilities of Butterfly-shaped Fe_4 Units', 27 Oct. 1982.
- Prof. M.F. Lappert, FRS (Susses Univ.) - 'Approaches to Asymmetric Synthesis and Catalysis using Electron-rich Olefins and some of their Metal Complexes', 28 Oct. 1982, and 'The Chemistry of some Unusual Subvalent Compounds of Group IV and V Elements', 28 Oct. 1982.
- Dr. D.H. Williams (Cambridge Univ.) - 'Studies on the Structures and Modes of Action of Antibiotics', 4 Nov. 1982.
- Dr. J. Cramp (I.C.I. Ltd.) - 'Lasers in Industry', 11 Nov. 1982.
- Dr. G. Bertrand (Paul Sabatier Univ., Toulouse) - 'Curtius Rearrangement in Organometallic Series: A Route for New Hybridized Species', 15 Nov. 1982.
- Prof. F.R. Hartley (R.M.C.S., Shrivenham) - 'Supported Metal Complex Hydroformylation Catalysts', 24 Nov. 1982.
- Dr. D.R. Richards, (P.E.R.M.E.) - 'Terminally Functional Polymers - their Synthesis and Uses', 25 Nov. 1982.
- Dr. G. Wooley (Trent Poly.) - 'Bonds in Transition Metal Cluster Compounds', 8 Dec. 1982.
- Dr. D.C. Sherrington (Strathclyde Univ.) - 'Polymer Supported Phase Transfer Catalysts', 12 Jan. 1983.
- Prof. D.W.A. Sharp (Glasgow Univ.) - 'Some Redox Reactions in Fluorine Chemistry', 27 Jan. 1983.

- Dr. P. Moore (Warwick Univ.) - 'Mechanistic Studies in Solution by Stopped Flow F.T. N.m.r. and High Pressure N.m.r. Line Broadening', 9 Feb. 1983.
- Sir G. Allen, FRS (Unilever Ltd.) - 'U.K. Research Ltd.', 10 Feb. 1983.
- Prof. A.G. MacDiarmid (Pennsylvania Univ.) - 'Metallic Covalent Polymers: (SN)_x and (CH)_x and their Derivatives', 17 Feb. 1983.
- Dr. D. Bloor (Queen Mary College) - 'The Solid State Chemistry of Diacetylene Monomers and Polymers', 2 Mar. 1983.
- Prof. A.C.T. North (Leeds Univ.) - 'The Use of a Computer Display System in Studying Molecular Structures and Interactions', 3 Mar. 1983.
- Prof. D.C. Bradley, FRS (Queen Mary College) - 'Recent Developments in Organo-Imido Transition Metal Chemistry', 8 Mar. 1983.
- Prof. H.G. Viehe (Univ. of Louvain, Belgium) - 'Oxidations on Sulphur', 11 Mar. 1983 and 'Fluorine Substitution in Radical and Biradical Addition Reactions', 11 Mar. 1983.
- Dr. I. Gosney (Edinburgh Univ.) - 'New Extrusion Reactions: Organic Synthesis in a Hot Tube', 16 Mar. 1983.
- Prof. J. Passmore (Univ. of New Brunswick) - 'Novel Selenium - Iodine Cations', 21 Apr. 1983.
- Prof. P.H. Plesch (Keele Univ.) - 'Binary Ionisation Equilibria between two Ions and two Molecules. What Ostwald never thought of', 4 May 1983.
- Prof. K. Berger (Munich Univ.) - 'New Reaction Pathways to Partially Fluorinated Heterocyclic Compounds', 10 May 1983.
- Dr. N. Isaacs (Reading Univ.) - 'The Applications of High Pressures to the Theory and Practice of Organic Chemistry', 11 May 1983.
- Dr. T.D. Marder (U.C.L.A.) - 'The Chemistry of Metal-Carbon and Metal-Metal Multiple Bonds', 13 May 1983.
- Dr. J.M. Vernon (York Univ.) - 'New Heterocyclic Chemistry involving Lead Tetra-Acetate', 25 May 1983.
- Dr. A. Pietrykowski (Warsaw Univ.) - 'Synthesis Structure and Properties of Aluminoxanes', 15 Jun. 1983.

Conferences Attended

- (a) SCF X_α Calculations in Inorganic Chemistry, a One-day Symposium, Queen Mary College, London, November 1980.
- (b) Advances in Polymer Characterisation, an International Symposium, Durham, July 1981.
- (c) Two Graduate Symposia at Durham University, April 1982 and 1983.
- (d) S.E.R.C. Graduate Summer School, Guildford, July 1982.

REFERENCES

1. D.T. Clark, 'Chemical Aspects of ESCA in Electron Emission Spectroscopy', Eds. W. Dekeyser and D. Reidel, D. Reidel Publishing Co., Dandrecht, Holland, 373 (1973).
2. H. Hertz, *Ann.Physik*, 31, 983 (1887).
3. W. Hallwachs, *Ann.Physik*, 33, 301 (1888).
4. J. Elster, and H. Geitel, *Ann.Physik*, 38, 40 (1889).
5. J. Elster, and H. Geitel, *Ann.Physik*, 38, 497 (1889).
6. P. Lenard, *Ann.Physik*, 8, 149 (1902).
7. A. Einstein, *Ann.Physik*, 17, 132 (1905).
8. M. Robinson, *Phil.Mag.*, 50, 241 (1925).
9. M. de Broglie, *Compt.Rend.*, 172, 274 (1921).
10. J.A. Van der Akker, and E.C. Watson, *Phys.Rev.*, 37, 1631 (1931).
11. K. Siegbahn and K. Edvarson, *Nucl.Phys.*, 1, 137 (1956).
12. C. Nordling, E. Sokolowski and K. Siegbahn, *Phys.Rev.*, 105, 1676 (1959).
13. C. Nordling, S. Hagstrom and K. Siegbahn, *Z.Physik*, 178, 423, (1964).
14. S. Hagstrom, C. Nordling and K. Siegbahn, *Phys.Lett.*, 9, 235 (1964).
15. R. Steinhardt, E.J. Serfass, *Anal.Chem.*, 25, 697 (1953).
16. R.G. Steinhardt, F.A.D. Granados and G.I. Post, *Anal.Chem.*, 27, 1046 (1955).
17. K. Siegbahn, C. Nordling, A. Fahlman, R. Nordberg, K. Hamrin, J. Medman, G. Johansson, T. Bergmark, S.E. Karlsson, I. Lidgren and B. Lindberg, "ESCA, Atomic, Molecular

17. (contd.) and Solid State Structure Studied by Means of Electron Spectroscopy", Alinquist and Wiksells, Uppsala (1967).
18. K. Siegbahn, C. Nordling, G. Johansson, J. Medman, P.F. Meden, K. Mamrin, U. Gelius, T. Berkmark, L.D. Werme, R. Manne and Y. Baer, "ESCA Applied to Free Molecules", North Holland Publishing Co., Amsterdam (1969).
19. (a) K. Siegbahn, Rev.Mod.Phys., 54, 709 (1982).
(b) K. Siegbahn, Science, 217, 111 (1982).
20. J.G. Jenkin, R.C.G. Leckey and J. Liesegang, J.Electron. Spectrosc., Rel.Phenom., 12, 1 (1977); 14, 477 (1978).
21. J.H. Scofield, J.Elect.Spectros. Rel.Phen., 8, 129 (1976).
22. D.W. Turner, C. Baker, A.D. Baker and C.R. Brundle, Eds., "Molecular Photoelectron Spectroscopy", Wiley, N.Y., 1970.
23. L.S. Cederbaum, and W. Demcke, J.Electron.Spectros. Rel. Phenom., 13, 161 (1978).
24. C. Kittel, "Introduction to Solid State Physics", 4th Ed., Wiley, New York, (1971).
25. T.A. Koopmans, Physica, 1, 104 (1933).
26. P.S. Bagus, Phys.Rev., 139A, 619 (1965).
27. M.O. Krouse, A. Carlson and R.D. Dismukes, Phys.Rev., 37, 170 (1968).
28. R. Manne, and T. Aberg, Chem.Phys.Lett., 7, 282 (1970).
29. D.A. Shirley, Adv.Chem.Phys., 23, 85 (1973).
30. L.C. Synder, J.Chem.Phys., 55, 95 (1971).
31. D.B. Adams and D.T. Clark, Theoret.Chim.Acta, 31, 171 (1973).

32. I.H. Hillier and J. Kendrick, *J. Electron. Spectrosc., Rel. Phen.*, 6, 325 (1975).
33. U. Gelius and K. Siegbahn, *Farad. Disc. Chem. Soc.*, 54, 257 (1972).
34. D.T. Clark, I.W. Scanlan and J. Muller, *Theoret. Chim. Acta.*, 35, 341 (1974).
35. D.T. Clark, & I.W. Scanlon, *J. Chem. Soc., Farad. Trans. II*, 70, 1222 (1974).
36. W.R. Saleneck, *Solid State Commun.*, 27, 685 (1978).
37. U. Gelius, *J. Electron. Spectrosc. Relat. Phenom.*, 5, 985 (1974).
38. D.T. Clark, D.B. Adams, A. Dilks, J. Peeling and H.R. Thomas, *J. Electron. Spectrosc. Rel. Phenom.*, 8, 51 (1976).
39. D.T. Clark and A. Dilks, *J. Polym. Sci. Polym. Chem. Edn.*, 14, 533 (1976).
40. D.T. Clark and A. Dilks, *J. Polym. Sci. Polym. Chem. Edn.*, 15, 15 (1977).
41. D.C. Frost, C.A. McDowell and A. Ishitani, *Rev. Mod. Phys.*, 24, 861 (1972).
42. D.C. Frost, C.A. McDowell and B. Wallbank, *Chem. Phys. Lett.*, 40, 189 (1976).
43. T. Ohta, T. Fukitawa and H. Furoda, *Chem. Phys. Lett.*, 32, 369 (1975).
44. S. Doniach, & M. Sunjic, *J. Phys.*, C3, 285 (1970).
45. P.H. Citrin, *Phys. Rev.*, B12, 5545 (1973).
46. S. Hufner, and G.K. Wertheim, *Phys. Rev.*, B11, 678 (1975).

47. G.K. Wertheim and P.H. Citrin, *Topics in Applied Phys.*, 26, 197 (1978).
48. R. Manne, & T. Åberg, *Chem. Phys. Lett.*, 7, 282 (1970).
49. P. Auger, *Compt. Rend.*, 65, 180 (1925).
50. D. Coster, R. de L. Kronig, *Physica*, 2, 13 (1935).
51. E.H.S. Burhop, Ed. "The Auger Effect and Other Radiationless Transitions", Cambridge University Press, 1952.
52. J.C. Fuggle in "Electron Spectroscopy: Theory Techniques and Applications, Vol.4, Ed. C.R. Brundle, & A. Baker, Academic Press, London, 1980.
53. C.J. Todd in "Electron Spectroscopy: Theory Techniques and Applications", Vol.4, Ed. C.R. Brundle and A. Baker, Academic Press, London, 1980.
54. C.D. Wagner and P. Biloen, *Surf. Sci.*, 35, 82 (1973).
55. C.D. Wagner, *Anal. Chem.*, 44, 967 (1972).
56. C.D. Wagner, *Chem. Soc. Far. Disc.*, 60, 291 (1975).
57. S.P. Kowalczyk, L. Ley, F.R. McFeely, R.A. Pollak and D.A. Shirley, *Phys. Rev.*, B9, 381 (1974).
58. C.D. Wagner, *J. Electron Spectrosc., Rel. Phenom.*, 10, 305 (1977).
59. C.D. Wagner, L.H. Gale, and R.H. Raymond, *Anal. Chem.*, 51, 466 (1979).
60. A.E. Sandstrom in "Handbook of Physics", Vol. XXX, 'X-rays', 164 Ed. S.F. Flugge, Springer Verlag (1977).
61. R. Jenkins, R.W. Gould and D. Gedke in "Quantitative X-ray Spectrometry", Dekker, New York (1981).

62. D.T. Clark, 'Chemical Aspects of ESCA', in "Electron Emission Spectroscopy", Eds. W. Dekeyser, D. Reidal, D. Reidal Publishing Co., Dordrecht, Holland, 373 (1973).
63. C. Nordling, Arkiv. Physik, 15, 397 (1959).
64. C. Johansson, J. Hedman, A. Berudtsson, M. Klasson and R. Nilsson, J. Electron Spectrosc. Rel. Phenom., 2, 295 (1973).
65. C.J. Powell, N.E. Erickson and T.E. Madey, J. Electron Spectrosc., Rel. Phenom., 17, 361 (1979).
66. H. Siegbahn and L. Karlsson in 'Photoelectron Spectroscopy' in "Encyclopaedia of Physics", Vol. XXXI, ed. S. Flugge, Springer Verlag, New York, 1982.
67. U. Gelius and K. Siegbahn, Farad. Disc. Chem. Soc., 54, 257 (1972).
68. W.L. Jolly, & D.N. Hendrickson, J. Amer. Chem. Soc., 92, 1863 (1970).
69. D.B. Adams and D.T. Clark, J. Electron Spectrosc., Rel. Phenom, 2, 201 (1974).
70. W.J. Hehre, R. Ditchfield and J.A. Pople, J. Chem. Phys., 54, 724 (1971).
71. W.J. Hehre, R.F. Stewart and J.A. Pople, J. Chem. Phys., 51, 2657 (1969).
72. M.E. Schwartz, Chem. Phys. Lett., 6, 631 (1970).
73. D.A. Shirley, Chem. Phys. Lett., 15, 325 (1972).
74. J.N. Murrell and B.J. Ralston, J. Chem. Soc. Farad. Trans., II, 68, 1393 (1972).

75. O. Goscincki, B. Pickup and G. Purvis, *Chem.Phys.Lett.*, 22, 117 (1973).
76. J.W.D. Connolly, H. Siegbahn, U. Gelius and C. Nordling, *J.Chem.Phys.*, 58, 4265 (1973).
77. C.S. Fadley, 'Basic Concepts of X-ray Photoelectron Spectroscopy', in "Electron Spectroscopy, Theory, Techniques and Applications", Vol.2, Ed.C.R. Brundle and A.D. Baker, Academic Press, London, 1978.
78. T. Novakov and J.M. Hollander, *Bull.Am.Phys.Soc.*, 14, 524 (1969).
79. T. Novakov and J.M. Hollander, *Phys.Rev.Lett.*, 21, 2133 (1968).
80. B.E. Watson and A.J. Freeman in "Hyperfine Interactions", A.J.Freeman and R.B. Frankal, Academic Press, N.Y., 1967.
81. C.S. Fadley, D.A. Shirley, A.J. Freeman, P.S. Bagus and J.V. Mallow, *Phys.Rev.Lett.*, 23, 1397 (1969).
82. M. Mehta and C.S. Fadley, *Phys.Lett.*, A55, 59 (1975).
83. J. Cooper and R.N. Zare, *J.Chem.Phys.*, 48, 942 (1968).
84. F.O. Ellison, *J.Chem.Phys.*, 61, 507 (1974).
85. J.H. Scofield, UCRL Report No. 51326.
86. R.F. Reilman, A. Msezane and S.T. Manson, *J.Electron. Spectrosc., Rel.Phenom.*, 8, 389 (1976).
87. D.T. Clark in "Advances of Polymer Science", Ed.H.J.Cantow, Springer Verlag, Berlin, 24, 125 (1977).
88. P.H. Van Cittert, *Z. Phys.*, 69, 239 (1931).
89. H.F. Carley and A.J. Joyner, *J.Electron.Spectrosc.Rel. Phenom.*, 16, 1 (1979).

90. G.K. Wertheim, J. Electron Spectrosc., Rel. Phenom, 6, 239 (1975).
91. A. Eisberg, "Fundamentals of Modern Physics", Wiley, New York (1961), Chap. 14.
92. K. Yates, A. Barrie and F.J. Street, J. Phys., E6, 130 (1973).
93. B.L. Henke, Adv. X-Ray Anal., 13, 1 (1969).
94. E.M. Purcell, Phys. Rev., 54, 818 (1958).
95. J.E. Castle and R.H. West, J. Electron Spectrosc., Rel. Phenom., 19, 409 (1980).
96. C.D. Wagner, W.M. Riggs, L.E. Davis, J.F. Moulder and G.E. Muiltenberg, "Handbook of X-Ray Photoelectron Spectroscopy", Perkin-Elmer Corp., U.S.A., (1979).
97. M.F. Ebel, & M. Ebel, J. Electron Spectrosc. Rel. Phenom, 3, 169 (1974).
98. J.F. McGilp and I.G. Main, J. Electron Spectrosc., Rel. Phenom, 6, 397 (1975).
99. D.A. Huchital and R.T. McKeon, Appl. Phys. Lett., 20, 158 (1972).
100. D.T. Clark, H.R. Thomas, A. Dilks and D. Shuttleworth, J. Polym. Sci., Polym. Chem. Edn., 17, 627 (1979).
101. D.T. Clark, A. Dilks and H.R. Thomas, J. Polym. Sci., Polym. Chem. Edn., 16, 1461 (1978).
102. D.T. Clark and A. Dilks, A.C.S. Centennial Meeting, New York, April 1976, 'International Symposium on Advances in Characterisation of Polymer Surfaces', 101, Ed. L.H. Lee, Academic Press, N.Y. (1976).

103. D.T. Clark and A. Dilks, J.Polym.Sci., Polym.Chem.Edn.,
16, 791 (1978).
104. D.T. Clark and A. Dilks, J.Polym.Sci., Polym.Chem.Edn.,
16, 911 (1978).
105. D.T. Clark and A. Dilks, J.Electron. Spectrosc. Rel.Phenom,
11, 225 (1977).
106. H. Siegbahn, L. Asplund, P. Kelfre, & K. Siegbahn,
J.Electron Spectrosc., Rel.Phenom, 5, 1059 (1974).
107. H. Fellner-Feldegg, H. Siegbahn, L. Asplund, P. Kelfre
and K. Siegbahn, J.Electron.Spectrosc. Rel.Phenom,
7, 421 (1975).
108. H. Siegbahn, S. Svensson and M. Lundholm, J.Elec.Spectrosc.,
Rel.Phenom, 24, 205 (1981).
109. L.S. Cederbaum and W. Domcke, Adv.Chem.Phys., 36, 265 (1977).
110. J.C. Tracey, 'Auger Electron Spectroscopy' in "Electron
Emission Spectroscopy", W. Dekeyser and D. Reidal, Eds.,
Reidel Pub. Co., Dordrecht, (1973).
111. *c.f.* D.T. Clark in 'Handbook of Electron Spectroscopy',
D. Briggs, Ed., Heyden, London, (1977).
112. J.J. Ritsko in "Photon, Electron and Ion Probes of Polymer
Structure and Properties", eds. D.W. Dwight,
T.J. Fabish and H.R. Thomas, A.C.S. Ser.Symp.No.162 (1980).
113. J.J. Ritsko, J.Chem.Phys., 70, 5349 (1979).
114. L.A. Harris, J.Appl.Phys., 39, 1419 (1968).
115. J.J. Lander, Phys.Rev., 91, 1382 (1953).
116. H.D. Hagstrum, Phys.Rev., 96, 325 (1954).

117. R.W. Weber and W.T. Peria, *J.App.Phys.*, 38, 4355 (1967).
118. P.W. Palmberg, G.K. Bohn and J.C. Tracy, *Appl.Phys.Lett.*, 15, 254 (1969).
119. W.E. Moddemann, T.A. Carlson, M.O. Krause, B.P. Publen, W.E. Bull and G.K. Schweitzer, *J.Chem.Phys.*, 55, 2317 (1971).
120. L. Austin and H. Starke, *Ann.Physik*, 9, 271 (1902).
121. H. Bruining, "Physics and Applications of Secondary Electron Emission", McGraw-Hill, New York, (1954).
122. A.J. Dekker, *Solid St. Phys.*, 6, 251 (1958).
123. R. Kollath, "Secondary Electron Emission of Solids Induced by Electron Bombardment" in 'Encyclopaedia of Physics', Vol.21, p.232, Springer, Berlin, (1956).
124. E.A. Burke, *IEEE Trans.Nucl.Sci.*, NS-27, 1760 (1980).
125. R.F. Willis and D.K. Skinner, *Sol.State.Comm.* 13, 685 (1973).
126. H. Salow, *Z.Tech.Physik*, 21, 8 (1940).
127. M. Gryzinski, *Phys.Rev.*, A138, 336 (1965).
128. D. Briggs and D. Wootton, *Surf.Inter.Anal.*, 4, 109 (1982).
129. A. Joshi and L.E. Davis, *J.Vac.Sci.Technol.* 14, 1310 (1977).
130. J.C. Fuggle, 'High Resolution Auger Spectroscopy' in "Electron Spectroscopy, Theory, Techniques, Applications" Eds. A.D. Baker and C.R. Brundle, Vol.4, p.93, Academic Press, London, (1981).
131. L.G. Christophorou and M.W. Grant, *Adv.Chem.Phys.* 36, 413 (1977).
132. A. Kuppermann, W. Flicker and O.A. Mosher, *Chem.Rev.*, 79, 77 (1979).

133. I. Sauers, L.G. Christophorou and J.G. Carter, *J.Chem.Phys.*, 71, 3016 (1979).
134. E.N. Lassetre, and M.E. Krasnow, *J.Chem.Phys.*, 40, 1240 (1964)
135. J.R. Oppenheimer, *Phys.Rev.*, 32, 361 (1928).
136. M. Matsuzawa, *J.Chem.Phys.*, 51, 4705 (1969).
137. P.N. Sen and S. Basu, *Int.J. Quantum.Chem.*, 1, 591 (1967).
138. N. Swanson and C.J. Powell, *J.Chem.Phys.*, 39, 630 (1963).
139. J.J. Ritsko and R.W. Bigelow, *J.Chem.Phys.*, 69, 4162 (1979).
140. J.J. Ritsko, L.J. Brillson, R.W. Bigelow and T.J. Fabish, *J.Chem.Phys.*, 69, 3931 (1978).
141. R.W. Ditchfield, D.T. Grubb and M.J. Whelan, *Phil.Mag.*, 27, 1267 (1973).
142. M.K. Barbarez, D.K. Das Gupta and D. Hayward, *J.Phys.D.*, 10, 1789 (1977).
143. L.G. Christophorou, *NATO Adv. Sci. Inst. Ser.*, Ser.B., 89, 133 (1983).
144. L.G. Christophorou and K.S. Gant, *J.Chem.Phys.*, 65, 2977 (1976).
145. J.R. Frazier, L.G. Christophorou, J.G. Canter and H.C. Schweinter, *J.Chem.Phys.*, 69, 3807 (1980).
146. T.E. Madey and J.T. Yates, *J.Vac.Sci.Tech.*, 8, 255 (1971).
147. (a) D. Menzel and R. Gamer, *J.Chem.Phys.*, 41, 3311 (1964).
(b) P.A. Redhead, *Con.J.Phys.*, 42, 886 (1964).
148. M.L. Knotek and P.J. Feibelman, *Phys.Rev.Lett.*, 40, 964 (1978).
149. D. Menzel, *J.Vac.Sci.Tech.*, 20, 538 (1980).
150. C.S. Fadley, *J.Electron.Spectrosc.*, *Rel.Phenom*, 5, 725 (1974).

151. T.A. Carlson in "Desorption Induced by Electronic Transitions" p.169, eds. N.H. Tolk, M.M. Traum, J.C. Tully and T.E. Madey, Springer Series in Chemical Phys. 24, Springer-Verlag, Berlin, (1982).
152. T.A. Carlson and R.M. White, J.Chem.Phys., 44, 4510 (1966).
153. T.A. Carlson, and M. Krause, J.Chem.Phys., 56, 3206 (1972).
154. D.E. Ramaker in "Desorption Induced by Electronic Transitions" eds. N.H. Tolk, M.M. Traum, J.C. Tully, and T.E. Madey p.70, Springer Series in Chemical Physics, Vol.24, Springer-Verlag, Berlin, 1982.
155. J. Kelber and M.L. Knotek, Surf.Sci., 121, L499 (1982).
156. J.A. Kelber and M.L. Knotek, J.Vac.Sci.,Technol., A1, 1149 (1983).
157. C.G. Pantano and T.E. Madey, Appl.Surf.Sci.,7, 115 (1981).
158. P.H. Holloway, T.E. Madey, C.T. Campbell, R.R. Rye and J.E. Houston, Surf.Sci., 88, 121 (1979).
159. N.J. Chou, C.M. Osburn, Y.J. van der Meulen and R. Hammer, Appl.Phys.Lett., 22, 380 (1973).
160. L.G. Pittaway, Br.J.Appl.Phys., 15, 967 (1964).
161. From results of an ASTM Questionnaire on sample damaging during Aes. cited in ref. 56.
162. H.A. Bethe, Ann.Physik, 5, 525 (1933).
163. H.A. Bethe, in "Handbook of Physics", vol.24, p.273, Springer, Berlin, (1933).
164. J.I. Goldstein "Electron Beam - Specimen Interactions" in 'Scanning Electron Microscopy and X-Ray Microanalysis', eds. J.I. Goldstein, D.E. Newbury, P. Echlin, D.C. Joy, C. Fiori, and E. Lifslin, Plenum Press, N.Y., (1981).

165. K. Kanaya, and S. Okayama, *J.Phys.D.*, 5, 45 (1972).
166. L.R. Painter, E.T. Arakawa, M.W. Williams and J.C. Ashley, *Radiat.Res.*, 83, 1 (1980).
167. J.C. Ashley, C.J. Tung, & R.H. Ritchie, *IEEE Trans.Nuc.Sci.*, NS25, 1566 (1978).
168. J.C. Ashley, *IEEE Trans.Nuc.Sci.*, NS27, 1454 (1980).
169. J.C. Ashley and M.W. Williams, *Rad.Res.*, 81, 364 (1980).
170. A. Charlesby, "Atomic Radiation and Polymers", Pergamon Press, New York (1960).
171. A. Chapiro, "Radiation Chemistry of Polymeric Systems", Interscience, New York (1962).
172. A.A. Miller, E.J. Lawton, and J.S. Balwit, *J.Polym.Sci.*, 14, 503 (1954).
173. A. Charlesby, *Radiat.Phys.Chem.*, 15, 393 (1980).
174. C. David, "High Energy Degradation of Polymers", in "Comprehensive Chemical Kinetics", Vol.14, p.175, eds. C.H. Bamford, C.F.H. Tipper, Elsevier, Amsterdam, (1975).
175. D. Turner, *J.Polym.Sci., D. Macromolecular rev.*, 5, 229 (1971).
176. D.T. Grubb, *J. Mater.Sci.*, 9, 1715 (1974).
177. S.W. Shalaby, *J.Pol.Sci., D.Macromolecular Rev.*, 14, 419 (1979).
178. R.E. Florin in 'Fluoropolymers', ed. L.A.Wall, Wiley, N.Y. (1972).
179. M. Tsuda and S. Oikawa, *J.Polym.Sci., Polym.Chem.Edn.*, 17, 3759 (1979).
180. J. Weiss, *J.Polym.Sci.*, 29, 245 (1959).
181. W. Moreau and N. Viswanathan, *ACS Series Symp.* 25, 107 (1976).

182. J.M. Benyon, R.A. Saunders and A.E. Williams, *Anal.Chem.*, 33, 221 (1961).
183. M. Dole and C.D. Keeling, *J.Amer.Chem.Soc.*, 75, 6082 (1953).
184. H. Hiraoka and W. Lee, IBM Research Report RJ2155(29568) 12/19/17.
185. H.H. Madden, *J.Vac.Sci.Technol.* 18, 677 (1981).
186. P.H. Holloway, *Adv.Electron. Electron Phys.* 54, 241 (1982).
187. J.E. Houston and R.R. Rye, *Comm.Sol.St.Phys.*, 10, 233 (1983).
188. R.R. Rye, D.R. Jennison & J.E. Houston, *J.Chem.Phys.*, 73, 4867 (1980).
189. J.A. Kelber, R.R. Rye, G. Nelson and J.E. Houston, *Surf.Sci.*, 116, 148 (1982).
190. J.E. Houston and R. R. Rye, *J.Chem.Phys.*, 74, 71 (1981).
191. S.W. Gaarenstroom, *J.Vac.Sci.Technol.*, 16, 600 (1979).
192. D.T. Clark "The Investigation of Polymer Surfaces by Means of ESCA" in "Polymer Surfaces", eds. D.T. Clark and W.J. Feast, Ch.16, J. Wiley and Sons. N.W., (1978).
193. D.R. Penn, *J.Elec.Spectrosc.Relat.Phenom*, 9, 29 (1976).
194. M.P. Seah and W.A. Dench, *Surf.Inter.Anal.*, 1, 2 (1979).
195. D.T. Clark and H.R. Thomas, *J.Polym.Sci.Polym.Chem.*, Edn., 15, 2843 (1977).
196. D.T. Clark and D. Shuttleworth, *J.Polym.Sci.Polym.Chem.Edn.*, 16, 1093 (1978).
197. B.L. Henke, *Adv.X-Ray Anal.*, 13, 1 (1970).
198. D.T. Clark, Y.C.T. Fok, and G.G.Roberts, *J.Electron.Spectrosc., Relat.Phenom*, 22, 173 (1981).

199. M. Klasson, J. Hedman, A. Bendtsson, R. Nilsson, C. Nordling and P. Melnik, *Phys.Ser.*5, 93 (1972).
200. M. Klasson, A. Berndtsson, J. Hedman, R. Nilsson, R. Nyholm and C. Nordling, *J.Electron.Spectrosc. Rel.Phenom*, 3, 427 (1974).
201. Kratos Application note.
202. D.T. Clark in "Photon, Electron and Ion Probes of Polymer Structure and Properties", eds. D.Wright, T.J. Fabish, H.R. Thomas, *ACS Ser.Sym.*182, (1981).
203. D.R. Hutton, Ph.D. Thesis, University of Durham (1983).
204. Vacuum Generators Ltd., Applications note.
205. J.E. Castle, L.B. Hazell, and R.H. West, *J.Electron Spectrosc. Rel.Phenom*, 9, 247 (1979).
206. H.S. Munro, Ph.D. Thesis, University of Durham (1982).
207. R. Wilson, Ph.D. Thesis, to be submitted.
208. P.J. Stephenson, Ph.D. Thesis, University of Durham, 1981.
209. (a) W.F. Gorham, *J.Polym.Sci.*, A4 (1966).
(b) W.F. Gorham, *Encyc.Polym.Sci.& Tech*, vol.15
210. C.J. Powell, *Surf.Sci.*, 44, 29 (1974).
211. D.R. Penn, *Phys.Rev.B.*, 13, 5248 (1976).
212. L.E. Sutton (Ed.), *Tables of Interatomic Distances*, Chem. Soc.Special Publication No.18, Chemical Society, London, (1958).
213. S. Evans, R.G. Pritchard and J. Thomas, *J.Phys.*, 10. 2483 (1977).
214. N. Samoto, & R. Schimizu, *J.Appl.Phys.*, 54, 3855 (1983).

215. D.T. Clark and D. Shuttleworth, *J. Polym. Sci. Polym. Chem. Ed.*, 17, 1317 (1979).
216. D.T. Clark and D. Shuttleworth, *Eur. Polym. J.*, 15, 265 (1979).
217. D.T. Clark and D. Shuttleworth, *J. Polym. Sci. Polym. Chem. Ed.*, 18, 27 (1980).
218. D.T. Clark and M.Z. AbRahman, *J. Polym. Sci. Polym. Chem. Ed.*, 19, 2129 (1981).
219. D.T. Clark and M.Z. AbRahman, *J. Polym. Sci. Polym. Chem. Ed.*, 19, 2689 (1981).
220. D.T. Clark and M.Z. AbRahman, *J. Polym. Sci. Polym. Chem. Ed.*, 20, 1717 (1982).
221. D.T. Clark and M.Z. AbRahman, *J. Polym. Sci. Polym. Chem. Ed.*, 20, 1729 (1982).
222. D.T. Clark and M.Z. AbRahman, *J. Polym. Sci. Polym. Chem. Ed.*, 20, 691 (1982).
223. D.T. Clark and M.M. Abu-Shbak, *J. Polym. Sci. Polym. Chem. Ed.*,
in press.
224. D.T. Clark and M.M. Abu-Shbak, *J. Polym. Sci. Polym. Chem. Ed.*,
in press.
225. D.T. Clark and M.M. Abu-Shbak, *J. Polym. Sci. Polym. Chem. Ed.*,
in press.
226. D.T. Clark and D. Shuttleworth, *J. Polym. Sci. Polym. Chem. Ed.*, 18, 407 (1980).
227. H. Suhr, in *Techniques and Applications of Plasma Chemistry*¹
T.R. Hollahan and A.T. Bell, Eds., Wiley, New York,
(1974), Chap. 2.

228. R.D. Chambers, Fluorine in Organic Chemistry, Interscience Monographs on Organic Chemistry, Wiley, New York, (1973).
229. R.D. Chambers, R. Middleton and R.P. Corbally, J.C.S. Chem.Comm., 731 (1975).
230. R.D. Chambers, W.K.R. Musgrave and K.C. Srivastava, J.C.S. Chem.Comm., 264 (1971).
231. R.D. Chambers and C.R. Sargent, J.C.S.Chem.Comm., 446 (1979).
232. M.J.S. Dewar and W. Thiel, J.Amer.Chem.Soc., 99, 4899,4907 (1977).
233. R. Fletcher and M.J.D. Powell, Comp.J., 6, 163 (1963),
W.C. Davidson, Comp.J., 10, 406 (1968).
234. W.L. Davidson and I.G. Geib, J.Appl.Phys., 19, 427 (1948).
235. A. Charlesby, Proc.Roy.Soc., A215, 187 (1952).
236. Raychem Ltd., Technical literature.
237. R. Thornley and T. Sun, J.Electrochem.Soc., 112, 1151 (1965).
238. H.S. Cole, D.W. Skelly, and B.C. Wagner, IEEE Tran.Electron Dev., ED-22, 417 (1975).
239. J. Gambier, J. Physique et. Rad., 1937, 278 (1937).
240. D.T. Clark, W.J. Feast, M. Modena, I. Ritchie, W.K.R. Musgrave, & M. Raggazini, J. Polym.Sci.Polym.Chem.Edn., 12, 1049 (1974).
241. D.B. Adams, Ph.D. Thesis, University of Durham (1973).
242. D. Shuttleworth, Ph.D. Thesis, University of Durham, (1978).
243. M. Dole, "Fluoropolymers" in 'Radiation Chemistry and Macromolecules', Vol.1, ed. M. Dole, Interscience, N.Y. (1972).
244. N.A. Slovokhatova in "Ionising Radiation Effects on Organic and Inorganic Systems", Moscour (1958).

245. W.K. Fisher, & J.C. Corelli, *J. Polym. Sci. Polym. Chem. Edn.*, 19, 2465 (1981).
246. K. Makuuchi, M. Asano and T. Abe, *J. Polym. Sci. Polym. Chem. Edn.*, 14, 617 (1976).
247. R. Hambeck, *Nucl. Sci. Abstr.*, 14:3528 (1960).
248. A.R. Schultz, "Chemical Reactions of Polymers", ed. E.M. Fettes, Interscience, N.Y. (1964).
249. G. Johansson, J. Hedman, A. Berndtsson, M. Klanson, & R. Nilsson, *J. Electron Spectrosc. Rel. Phenom.*, 2, 295 (1975).
250. R.W. Ryan, *Modern Plastics*, 31, 152 (1953).
251. K. Siegbahn, *J. Electron Spectrosc. Rel. Phenom.*, 5, 3 (1974).
252. M. Barber, E.L. Evans and J.M. Thomas, *Chem. Phys. Lett.*, 18, 423 (1973).
253. D.W. Turner in "Determination of Organic Structure by Physical Methods", Vol. 2, Ed. F.C. Naehod and W.D. Phillips, Academic Press, New York (1962).
254. E.E. Schneider, *J. Chem. Phys.*, 23, 978 (1955).
255. H.N. Rexroad and W. Gordy, *J. Chem. Phys.* 30, 399 (1959).
256. S. Siegel and H. Hedgpath, *J. Chem. Phys.*, 46, 3094 (1967).
257. W.M.D. Bryant, *J. Polym. Sci.*, 56, 277 (1962).
258. J.N. Helbert, B.E. Wagner, E.H. Poindexter and L. Levan, *J. Polym. Sci., Polym. Phys. Ed.*, 13, 825 (1975).
259. R. Bradley, *Chem. Tech.*, 1981 234 (1981).
260. S.V. Nabler, and E.P. Tripp, *Radiat. Phys. Chem.*, 9, 325 (1977).

261. E. Haering, Proc. IXth International Conference in Organic Coatings Science and Technology, p.47, (1983).
262. T.J. Miranda, T. J. Huemmer, J. Paint.Technol.41,118 (1969).
263. R. Makuuchi, Proc. IXth International Conference in Organic Coatings Science and Technology, p.97, (1983).
264. S.E. Young, Prog.Org.Coatings, 4, 225 (1976).
265. H. König, and G. Helwin, Z.Physik, 129, 491 (1951).
266. J.H.L. Watson, J.Appl.Phys., 18, 153 (1947).
267. R.L. Stewart, Phys.Rev., 45, 488 (1934).
268. A. Ennos, Brit.J.Appl.Phys., 4, 101 (1953).
269. A. Ennos, Brit.J.Appl.Phys., 5, 27 (1954).
270. K.M. Poole, Proc.Phys.Soc., B66, 542 (1953).
271. D.A. Buck and K. Shoulders, Proc.Eastern Joint Computer Conference, 1958, AIEE Spec.Publ.T-114, p.55 (1959).
272. R.W. Christy, J.Appl.Phys., 31, 1680 (1960).
273. H.T. Mann, Electrochem.Technol., 2, 287 (1963).
274. L. Mayer, J.Appl.Phys., 34,2088 (1963).
275. O.A. Anisimov, V.M. Grigoryants and Y.N. Molin, Chem.Phys. Lett., 74, 15 (1980).
276. M.J. Cardillo and S.H. Bauer, J.Amer.Chem.Soc., 92, 2399 (1970).
277. J.M. Tibbitt, R. Jensen, A.T. Bell and M. Shen, Macromolecules, 10, 647 (1977).
278. H.T. Mann, J.Appl.Phys., 35, 2173 (1964).
279. R.W. Christy, J.Appl.Phys., 35, 2179 (1964).
280. R.H. Colburn and R.W. Christy, J.Appl.Phys., 40, 3958 (1969).

281. P.R. Emtage and W. Tantapron, *Phys.Rev.Lett.*, 8, 267 (1962).
282. L.E. Babcock and R.W. Christy, *J.Appl.Phys.*, 43, 1423 (1972).
283. L. Holland and L. Laurenson, *Vacuum*, 14, 325 (1964).
284. I. Haller, and P. White, *J.Phys.Chem.*, 67, 1784 (1963).
285. E.M. Da Silva and E. Klokhol, *Electrochem.Soc.Mtg.*, Electric Insulation Div., Abs.No.14, San Francisco (1965).
286. C.R. Fritzsche, *J.Appl.Phys.*, 53, 9053 (1982).
287. A. Brennemann and L.V. Gregor, *J.Electrochem.Soc.*, 112, 1194 (1965).
288. L.V. Gregor and L.H. Kaplan, *Th.Sol.Films*, 2, 95 (1968).
289. L.V. Gregor "Gas Phase Deposition of Insulating Films" in 'Physics of Thin Films', Vol.3, Eds. G. Hass and R.E. Thun, Academic Press, New York (1966).
290. L.V. Gregor, *IBM J.Res.Dev.*, 12, 140 (1968).
291. L.V. Gregor, *Proc. IEEE*, 59, 1390 (1971).
292. A.N. Wright in "Polymer Surfaces", ed. D.T. Clark and W.J. Feast, J. Wiley and Sons, New York (1978).
293. S. Frost, W.J. Murphy, M.W. Roberts, J.R.H. Ross and J.H. Wood, *Farad.Spec.Disc.Chem.Soc.*, 2, 198 (1972).
294. G.L. Gaines, Jr., *Insoluble Monolayers at Liquid - Gas Interfaces*, Interscience, New York (1966).
295. M. Millard, in "Techniques and Applications of Plasma Chemistry", eds. J. Hollahan and A.T. Bell, Wiley, New York (1974).
296. J.D. Cox and G. Pilcher, *Thermochemistry of Organic and Organometallic Compounds*, Academic Press, N.W., (1970).

297. D.T. Clark, D. Kilcast, D.B. Adams and W.K.R. Musgrave,
J.Electron Spectrosc. Rel.Phenom, 1, 227 (1973).
298. H. Yasuda and T. Hsu, Surf.Sci., 76, 232 (1978).
299. R.P. Frueholz, W.M. Flicker, O.A. Mosher and A.J. Kuppermann,
J.Chem.Phys., 70, 3057 (1979).
300. (a) W. Nieseën, W. Kraemer and G. Diecksen, Chem.Phys.,
41, 113 (1979).
- (b) J. Almlöf, B. Roos, U. Wahlgren and H. Johansen,
J.Electron Spectrosc., Rel.Phenom, 2, 51 (1973).
- (c) R. Wagner, P. Hockman and M. El-Bayoumi, J.Mol.Spec.,
54, 167 (1975).
- (d) R.C. Bingham, M.J.S. Dewar and D.H. Lo, J.Amer.Chem.Soc.,
97, 1294 (1975).
301. B. Andersen, H.M. Seip and B. Beagley, Acta Chem.Scand.,
1837 (1969).
302. J.F.M. Oth, Recl.Trav.Chim., Pays-Bas, 87, 1185 (1968).
303. D.M. Lemal and L.H. Dunlap, J.Amer.Chem.Soc., 94, 6562 (1972).
304. (a) M.D. Newton, J.M. Shulman and M.M. Manus, J.Amer.Chem.
Soc., 96, 17 (1974).
- (b) N.C. Baird and M.J.S. Fewar, J.Amer.Chem.Soc., 91,
352 (1969).
305. R. Suffolk, J.Electron Spectrosc. Rel.Phenom, 3, 53 (1974).
306. E. Heilbronner, R. Gleiter, H. Hopf, V. Hornung and
A. de Meijee, Helv.Chim.Acta, 54, 783 (1971).
307. R.D. Chambers, J.A.H. MacBride and W.K.R. Musgrave,
unpublished results.
308. S.F. Mason, J.Chem.Soc., 1247 (1959).

309. K.K. Innes, J.P. Byrne and I.G. Ross, *J.Mol.Spectrosc.*, 22, 125 (1967).
310. R.M. Hochstrasser and C. Morzzacco, *J.Chem.Phys.*, 49, 971 (1968).
311. A.T. Bell, *Techniques and Applications of Plasma Chemistry*, J.R. Hollahan and A.T.Bell, Eds., Wiley, New York, 1974, Chap.1.
312. For general discussions of the rearrangement of these isomers see
D. Bryce-Smith and A. Gilbert, *Tetrahedron*, 32, 1309 (1976).
J.A. Barltrop and J.D. Coyle, *Excited States in Chemistry*, Wiley, New York, 1975.
I. Haller, *J.Chem.Phys.*, 47, 1117 (1967).
L.T. Scott and M. Jones, *Chem.Rev.*, 72, 183 (1972).
313. M.M. Abu-Shbak, Ph.D. Thesis, University of Durham, (1983).
314. M. Sunjic and C. Lucas, *J.Electron Spectrosc. Rel. Phenom.*, 5, 963 (1974).
315. Y.M. Cross and J.E. Castle, *J.Electron.Spectrosc.*, *Rel. Phenom.*, 22, 53 (1981).

